

# Development of a Prototype Synthetic Diamond Detector for Radiotherapy Dosimetry

A thesis submitted in partial fulfilment  
of the requirements for the Degree of

Doctor of Philosophy  
in Medical Physics

by

Gregory T. Betzel

Department of Physics and Astronomy

University of Canterbury

Christchurch, New Zealand

2010





# Abstract

---

This thesis details an investigation of the suitability of commercially-available single crystal and polycrystalline diamond films made via chemical vapor deposition (CVD) that were not studied previously for use in radiotherapy dosimetry. Novel sandwich-type detectors were designed and constructed to investigate the dosimetric response of diamond films under clinical conditions. Relatively inexpensive diamond films were obtained from three manufacturers: Diamonex, Diamond Materials GmbH and Element Six. Spectrophotometry, Raman spectroscopy and bulk conductivity studies were used to characterize these films and correlate crystalline quality with detector performance. Novel detectors were designed and constructed to investigate detectors under clinical conditions, including Perspex encapsulations and PCBs to minimize fluence perturbations. The dosimetric response of these diamond detectors was examined using a 6 MV beam from a Varian Clinac 600C linear accelerator. Diamond detectors were evaluated by measuring a number of response characteristics.

Polycrystalline CVD diamond films from Diamonex (100, 200, 400- $\mu\text{m}$  thicknesses) were considered unsuitable for dosimetric applications due to their lack of stability, low sensitivity, high leakage currents, high priming dose and dependence on dose rate. High-quality polycrystalline diamond films from Diamond Materials (100, 200, 400- $\mu\text{m}$  thicknesses) displayed characteristics that varied with film thickness. A 100- $\mu\text{m}$  film featured slow response dynamics and high priming doses. Thicker films featured suitable dosimetric characteristics, e.g. negligible leakage currents, low priming doses, fast response dynamics and good sensitivity with small sensitive volumes. Element Six single crystal CVD diamond films (500- $\mu\text{m}$  thicknesses) with small sensitive volumes (0.39  $\text{mm}^3$ ) exhibited suitable characteristics for dosimetry. These films showed negligible leakage currents ( $< 1.25 \text{ pA}$ ), low priming doses (1–10 Gy), quick response dynamics, high sensitivity (47–230  $\text{nC Gy}^{-1}$ ) and were weakly dependent on dose rate and directional dependence ( $\pm 1\%$ ).

A relatively inexpensive single crystal CVD diamond film from Element Six that exhibited high sensitivity (230  $\text{nC Gy}^{-1}$  at 0.5 V  $\mu\text{m}^{-1}$ ), amongst other favourable characteristics, was selected for further analyses. An appropriate operating voltage was determined before further

clinically relevant measurements could be conducted. This included how changes in an applied electric field affected detector response, and determined whether an optimal operating voltage could be realized within the parameters of conventional instrumentation used in radiation therapy. The results of this study indicated a preference towards using 62.5 V (at  $\sim 0.13 \text{ V } \mu\text{m}^{-1}$ ) out of a range of 30.8–248.0 V for temporal response as required for modulated beams due to its minimal rise time (2 s) and fall time (2 s) yet sufficient sensitivity ( $37 \text{ nC Gy}^{-1}$ ) and weak dependence on polarity ( $\pm 1.5\%$ ).

Investigations were then performed on the same diamond detector to evaluate its performance under more clinically relevant conditions. Repeatability experiments revealed a temporary loss in sensitivity due to charge detrapping effects following irradiation, which was modelled to make corrections that improved short-term precision. It was shown that this detector could statistically distinguish between dose values separated by a single Monitor Unit, which corresponded to 0.77 cGy. Dose rate dependence was observed when using low, fixed doses in contrast to using stabilized currents and higher doses. Depth dose measurements using this detector compared well with ion chambers and diode dosimeters. Comparisons of initial measurements with values in the literature indicate encouraging results for fields sizes  $< 4 \times 4 \text{ cm}^2$ , but further measurements and comparisons with Monte Carlo calculations are required. Using this detector to make off-axis measurements in the edge-on orientation reduced perturbation of the beam due to its sandwich configuration and thin 150 nm Ag contacts. This diamond detector was found to be suitable for routine dosimetry with conventional radiotherapy instrumentation with a materials cost of  $< \text{NZ\$}200$ .

# Acknowledgments

---

The success of this project was due to the kind and generous support of many people.

I would first like to sincerely thank Dr. Lou Reinisch for his mentorship and support that started across the world via email nearly four years ago, who encouraged me to pursue my doctoral studies at the University of Canterbury. Thank you to Dr. Stuart Lansley for daily mentoring and interesting discussions about diamond. I kindly thank Dr. Jürgen Meyer who provided valuable guidance and insight for the majority of my studies.

Thank you to everyone in the Department of Physics and Astronomy for all their support: Dr. Scott Choi, Graeme Kershaw, Stephen Hemmingsen, Geoff Graham, Graeme MacDonald, Ross Ritchie, John Turner, Rhondda Sullivan, Rosalie Reilly and Xuefeng Liu. Thanks to Helen Devereux and Gary Turner from the Department of Electrical and Computer Engineering for their help in the Nanofabrication Laboratory.

Thank you to the group of medical physicists at Christchurch Hospital for providing assistance and helpful discussions despite their busy schedule with the commissioning of new machinery: Mark Bird, Dr. Deloar Hossain, Wen Long and Ben Wilder. Special thanks to Florentina Baluti for her kind support and many evenings helping make our research a success.

Thank you to Education New Zealand, the New Zealand Cancer Society and Sigma Xi for supporting my research.

Sincere thanks to my family and friends who have supported me unequivocally, in whichever hemisphere I may be. I especially thank my loving parents, who have always encouraged me to explore and discover with no bounds. With sincere gratitude, I thank my wonderful wife Amycla, who has supported and motivated me through love, understanding and laughter.



# Contents

---

<b>Abstract</b> .....	<b>i</b>
<b>Acknowledgments</b> .....	<b>iii</b>
<b>Contents</b> .....	<b>v</b>
<b>List of Figures</b> .....	<b>ix</b>
<b>List of Tables</b> .....	<b>xiii</b>
<b>Glossary</b> .....	<b>xv</b>
<b>1. Introduction</b> .....	<b>1</b>
1.1 Motivation.....	1
1.2 Outline.....	3
<b>2. Background</b> .....	<b>5</b>
2.1 Properties .....	5
2.2 Synthesis: Development and Principle .....	7
2.3 Historical Developments of Radiation Detection with Diamond.....	10
2.4 Radiation Dosimetry with Diamond.....	12
2.5 Material Studies .....	15
2.6 Radiotherapy Dosimetry.....	16
2.7 Dosimeter Comparisons.....	17
2.8 Concluding Remarks .....	20
<b>3. Materials &amp; Experimental Details</b> .....	<b>21</b>
3.1 Diamond films .....	21
3.2 Diamond Film Characterization.....	26
3.2.1 Spectrophotometry.....	27
3.2.2 Raman Spectroscopy.....	27
3.2.3 Surface and Bulk Conductivity .....	28
3.3 Electrodes .....	29
3.3.1 Surface Preparation .....	30
3.3.2 Metallization .....	30
3.4 Detector Designs and Fabrication .....	32
3.4.1 Large PCB Detector.....	32
3.4.2 “Thick Perspex” Detector.....	35

3.4.3	“Thin Perspex” Detector.....	37
3.5	Experimental Setup.....	41
3.5.1	Source of X-rays.....	41
3.5.2	Setup for “Thick Perspex” Detectors .....	42
3.5.3	Setup for “Thin Perspex” Detectors.....	43
3.6	Concluding Remarks.....	45
<b>4.</b>	<b>Results of Diamond Film Characterization.....</b>	<b>47</b>
4.1	Spectrophotometry .....	47
4.2	Raman Spectroscopy.....	50
4.3	Bulk Conductivity.....	53
4.4	Concluding Remarks.....	56
<b>5.</b>	<b>Initial Dosimetric Analysis.....</b>	<b>57</b>
5.1	Experimental Details .....	57
5.2	Initial Response .....	57
5.3	Priming .....	61
5.4	Post-priming Response .....	64
5.5	Dose Rate Dependence.....	68
5.6	Directional Dependence .....	71
5.7	Concluding Remarks.....	74
<b>6.</b>	<b>Operating Voltage.....</b>	<b>77</b>
6.1	Experimental Details .....	78
6.2	Current-Voltage Characteristics .....	78
6.3	Response Dynamics.....	80
6.4	Sensitivity.....	83
6.5	Dependence on Dose and Dose Rate.....	86
6.6	Concluding Remarks.....	90
<b>7.</b>	<b>Clinical Investigations.....</b>	<b>91</b>
7.1	Setup.....	91
7.2	Repeatability.....	91
7.3	Dose Rate Dependence: Fixed Dose Analysis.....	96
7.4	Tissue Phantom Ratios.....	98
7.5	Output Factors .....	99
7.6	Beam Profiles.....	102
7.7	Concluding Remarks.....	105
<b>8.</b>	<b>Conclusions and Future Work.....</b>	<b>107</b>



8.1	Conclusions .....	107
8.2	Future Work .....	109
	<b>Bibliography .....</b>	<b>111</b>
	<b>Appendix A : Surface Preparation Procedures .....</b>	<b>137</b>
	<b>Appendix B : Encapsulation Drawings.....</b>	<b>139</b>
	<b>Appendix C : Raman Spectra – Other Films.....</b>	<b>143</b>
	<b>Appendix D : List of Papers .....</b>	<b>147</b>



# List of Figures

---

2.1.	The diamond cubic crystal structure with characteristic cubic edge length $a_0$ of pure diamond with natural isotope content at room temperature [71].	6
2.2.	Schematic of the principal components of the CVD process [86].	9
2.3.	Regions of relative predominance of the three primary interactions of photon with matter [174].	13
2.4.	Schematic of a diamond detector where (●) are electrons and (○) are holes.	13
2.5.	An example of priming effects in a CVD diamond detector.	14
3.1.	A $5 \times 5 \times 0.2 \text{ mm}^3$ Diamonex polycrystalline diamond film.	24
3.2.	A $10 \times 10 \text{ }\mu\text{m}$ AFM scan of a Diamonex film.	25
3.3.	Element Six films. (a) E6SC1b; (b) E6SCP2, E6SCPL; (c) E6PC250; (d) E6TM100; (e) E6TM180 and (f) E6OP. [212]	25
3.4.	Diamond Materials (square wafers were used in this thesis) [209].	26
3.5.	A $10 \times 10 \times 0.2 \text{ mm}^3$ Diamonex sample with four different metal electrodes on (a) the growth surface and (b) the opposing substrate surface.	31
3.6.	Board image of the large PCB detector used for manufacture.	33
3.7.	Photos of the ends of large PCB detector #1. (a) Sensing end of the detector; (b) Threaded BNC coaxial end of the detector.	34
3.8.	Schematic of thick Perspex detector [168].	35
3.9.	Thick Perspex detector without encapsulation.	36
3.10.	Thin Perspex detector using free air wire attachment.	37
3.11.	Schematic of thin Perspex detector [217].	38
3.12.	Thin Perspex detector with PCB (top) with close-ups of the diamond showing the Ag electrode (middle) and a side view (bottom).	39
3.13.	Varian 600C linear accelerator and phantom.	42
3.14.	Setup for thick Perspex detectors with an SDD = SAD = 100 cm.	43
3.15.	Thin Perspex detector setup using Solid Water slabs.	44
4.1.	Absorbance as a function of wavelength for (a) single crystal CVD (E6SCPL) and (b) thermal grade pCVD (E6TM180) diamond films.	48

4.2.	Absorbance as a function of wavelength for two single crystal CVD (E6SCIb) diamond films. ....	48
4.3.	Absorbance as a function of wavelength for several diamond films (from high to low absorbance as shown with the arrow): E6SCP2, E6EL200, E6EL500, E6OP, and DM100, DM200 and DM400. ....	49
4.4.	Raman spectrum for Dx200. ....	51
4.5.	Raman spectra for Diamond Materials samples (a) DM200, (b) DM100 and ....	51
4.6.	Raman spectra for Element Six samples (a) E6SCP2 and (b) E6SCPL. ....	52
4.7.	Raman spectra for two E6SCIb samples. ....	52
4.8.	Leakage current vs. applied field for various diamond films.....	55
4.9.	Leakage current as a function of voltage for several Diamonex films. ....	55
4.10.	Leakage current as a function of voltage for E6 and Diamond Materials films.....	56
5.1.	Un-primed response for Diamonex films Dx100 (□) and Dx200-1 (■).....	59
5.2.	Un-primed response for Diamonex films Dx400m (Δ), Dx400-1 (▼) .....	59
5.3.	Un-primed response for Diamond Materials films DM200 (▲), DM100 (■) and DM400 (●).....	60
5.4.	Un-primed response for Element Six films E6SCP2 (●) and E6SCPL (○).....	60
5.5.	Additional priming dose for Dx200-1. Exponential fits are plotted for average current measured while the x-ray beam (250 MU min <sup>-1</sup> dose rate) was on (□) and off (■). ....	62
5.6.	Priming response for DM100 (▲), DM200 (Δ) and DM400 (▼). ....	62
5.7.	Priming response for E6SCPL (●) and E6SCP2 (○).....	63
5.8.	Priming response using dose rates of 50, 100, 150, 200 and 250 MU min <sup>-1</sup> for Dx200-1 (Δ, top) and Dx200-2 (□, bottom). ....	66
5.9.	Response to dose rates of 50, 100, 150, 200 and 250 MU min <sup>-1</sup> (from left to right) for DM100 (▲), DM200 (■) and DM400 (●). ....	66
5.10.	Response to dose rates of 50, 100, 150, 200 and 250 MU min <sup>-1</sup> (from left to right) for E6SCPL (●) and E6SCP2 (○). ....	67
5.11.	Photocurrent vs. dose rate for Dx100 (●) and Dx200-1 (○). Films are shown with power law curve fits. ....	69
5.12.	Photocurrent vs. dose rate for DM100 (▲), DM200 (▼) and DM400 (◄). Films are shown with power law curve fits. ....	70
5.13.	Photocurrent vs. dose rate for E6SCP2 (□) and E6SCPL (■). Films are shown with power law curve fits. ....	70

5.14.	Variation in current vs. incident angle of irradiation for the Dx200 film for ( $\Delta$ ) 50 and ( $\blacktriangle$ ) 250 MU min <sup>-1</sup> .....	72
5.15.	Variation in current vs. incident angle of irradiation for the DM400 film for ( $\nabla$ ) 50 and ( $\blacktriangledown$ ) 250 MU min <sup>-1</sup> .....	73
5.16.	Variation in current vs. incident angle of irradiation for the E6SCPL film for ( $\circ$ ) 50 and ( $\bullet$ ) 250 MU min <sup>-1</sup> .....	73
5.17.	Variation in current vs. incident angle of irradiation for the E6SCP2 film for ( $\square$ ) 50 and ( $\blacksquare$ ) 250 MU min <sup>-1</sup> .....	74
6.1.	Leakage current vs. operating voltage for the E6SCP2 detector using the Keithley ( $\blacksquare$ ) and Farmer ( $\blacktriangle$ ) electrometers. Data are represented with error bars (obscured by data points) as $I_{\text{avg}} \pm \sigma$ . The lines are power law fits to the data as described in the text. ....	79
6.2.	Total charge over 4-s intervals for output rates of 50, 100, 150, 200 and 250 MU min <sup>-1</sup> (left to right) for 248, 125, 62.5 and 30.8 V.....	81
6.3.	Sensitivity vs. operating voltage over the available ranges of positive voltages and nominal dose rates. Horizontal lines illustrate the range of sensitivities within one group.....	85
6.4.	Sensitivity vs. absolute voltage. A straight line is drawn for comparison. Horizontal lines illustrate the difference in sensitivity when polarity is reversed when measuring delivery rates of 250 MU min <sup>-1</sup> . ....	86
6.5.	Charge vs. dose using a dose rate of 1.95 Gy min <sup>-1</sup> at 100, 150 and 200 V over (a) 0–7.7 Gy and (b) 0–1.95 Gy. Lines represent hundreds of data points. Error bars are only shown at several chosen intervals for clarity. ....	87
6.6.	Photocurrent vs. dose rate for 30.8, 62.5, 125 and 248 V. ....	89
7.1.	Total charge per fixed dose measurements of 98, 99, 100, 101 and 102 MU.....	92
7.2.	Total charge per fixed output measurement. Error bars are plotted for $n = 9$ ( $\bullet$ , thick bars) and $n = 10$ ( $\square$ , thin bars). ....	93
7.3.	Sensitivity per fixed dose measurement.....	93
7.4.	Sensitivity vs. time intervals between irradiations. An exponential curve fit is plotted.....	95
7.5.	Total charge from a fixed dose of 0.77 Gy vs. dose rate.....	97
7.6.	Average current vs. dose rate using fixed doses of 0.77 Gy.....	97
7.7.	Tissue-maximum ratios for E6SCP2 ( $\square$ ) with error bars and a Farmer ion chamber ( $\circ$ ).....	99

<b>7.8.</b>	Comparison of Output Factors for E6SCP2 (■, with error bars) and a Farmer ion chamber (○). A best fit line for normalization is shown. ....	<b>101</b>
<b>7.9.</b>	Off axis profile comparison at 10 cm depth for E6SCP2 detector in the face-on (□) and edge-on (■) orientations and a diode detector (Δ).....	<b>104</b>
<b>7.10.</b>	Off axis profile for a 1 × 1 cm <sup>2</sup> using the E6SCP2 detector in the edge-on orientation.....	<b>105</b>
<b>B.1.</b>	Drawing of the thick Perspex encapsulation. ....	<b>139</b>
<b>B.2.</b>	Drawing of the thick Perspex encapsulation mid-section.....	<b>140</b>
<b>B.3.</b>	Drawing of the thin Perspex encapsulation sleeve.....	<b>141</b>

# List of Tables

---

<b>2.1.</b>	Comparison of diamond and Si properties at 293 K. ....	<b>7</b>
<b>3.1.</b>	Summary of diamond films. ....	<b>22</b>
<b>5.1.</b>	Summary of priming data for several diamond films. ....	<b>63</b>
<b>5.2.</b>	Summary of sensitivity data for several diamond films. ....	<b>67</b>
<b>5.3.</b>	Summary of curve fitting data for dependence on dose rate. ....	<b>71</b>
<b>5.4.</b>	Comparison of reported $\Delta$ for different types of material. ....	<b>71</b>
<b>6.1.</b>	Rise time estimates for different voltages and dose rates [s]. ....	<b>81</b>
<b>6.2.</b>	Summary of fitting parameters $\Delta$ and $R^2$ for dose rate dependence. ....	<b>89</b>
<b>6.3.</b>	Summary of findings for the operating voltage analysis. ....	<b>90</b>
<b>A.1.</b>	List of material and wet etchants. ....	<b>138</b>





# Glossary

---

AFM	Atomic Force Microscopy
CVD	Chemical Vapor Deposition
DM	Diamond Materials
Dx	Diamonex
E6	Element Six
FWHM	Full-Width at Half-Maximum
HPHT	High-Pressure High-Temperature
IMRT	Intensity Modulated Radiation Therapy
MOSFET	Metal Oxide Semiconductor Field Effect Transistor
MPCVD	Microwave Plasma CVD
MU	Monitor Unit
MV	Megavolt(age)
OAR	Off-Axis Ratio
OF	Output Factor
PCB	Printed Circuit Board
pCVD	Polycrystalline CVD
PDD	Percent Depth Dose
PTW	Physikalisch-Technische Werkstätten
SAD	Source-to-Axis Distance
scCVD	Single Crystal CVD
SDD	Source-to-Detector Distance
SRS	Stereotactic Radiosurgery
SSD	Source-to-Surface Distance
TAR	Tissue-Air Ratio
TLD	Thermoluminescent Dosimeter
TMR	Tissue-Maximum Ratio
TPR	Tissue-Phantom Ratio



# 1. Introduction

---

## 1.1 Motivation

As of 2007, one in eight deaths worldwide was due to cancer, causing more deaths than AIDS, tuberculosis and malaria combined [1]. Estimates of new cancer cases in the same year totalled 12 million. By 2050, the global burden is expected to be as much as 18 million deaths and 27 million new cases simply due to population growth and ageing [1]. Prevention, early detection and treatment are therefore crucial to its control. One of the three principal modalities used to treat cancer is radiation therapy; this is also called radiotherapy, therapeutic radiology or radiation oncology. Advances in radiation therapy have proven to be vital to cancer treatment; over 50% of all cancer patients, in countries such as the United States, New Zealand and Australia, are now treated with radiation in combination with other modalities such as surgery and chemotherapy [2,3].

As new techniques to deliver radiation to patients become increasingly complex and innovative, e.g. three-dimensional conformal radiotherapy, intensity-modulated radiotherapy (IMRT) and stereotactic radiosurgery [4-6], so must the instrumentation to assure their accuracy and precision [7-9]. Unlike conventional radiotherapy, these techniques may deliver treatment fields  $\leq 4 \times 4 \text{ cm}^2$ . Small field dimensions result in substantial uncertainty in the accuracy of clinical dosimetry due to the resulting nonequilibrium conditions in phantom as well as their comparable dimensions to the target volume [7]. In addition, the radiation detector itself may introduce perturbations in the radiation field that are difficult to quantify. Reasons for this include an unmatched equivalence of the absorption and scattering properties of the sensing and encapsulation material to the medium that surrounds it, as well as complex geometries that create asymmetries in the detector response.

Radiation detectors come in many types (air or liquid-filled ionization chambers, solid-state detectors, diode, scintillator, thermoluminescent, Fricke and film) shapes (parallel-plate, cylindrical and spherical) and sensitive volumes (sub-mm<sup>3</sup> to cm<sup>3</sup>) [10-12]. Existing dosimeters each have their own advantages and disadvantages, and many have been evaluated

and compared for small field dosimetry, e.g. [13-25]. However, improvements must be made to assure accurate dose measurements by minimizing perturbations due to detector geometry and non-tissue equivalence, which lead to dependence on energy, dose and dose rate.

Requirements for modern radiation dosimeters include high sensitivity, small dimensions, fast response, energy and dose rate independence and tissue equivalence [26]. A promising material for dosimetry that may fulfil these requirements is diamond [27-31]; it is a near-tissue equivalent or tissue substitute, chemically inert, non-toxic and highly resistant to radiation. However, the scarcity and variability of *natural* diamonds with suitable dosimetric properties make it impractical for widespread use commercially. Recent progress in growing *synthetic* diamond by the use of chemical vapor deposition (CVD) [32,33] poses to eliminate such shortcomings, where specific properties may be controlled and reproduced at a relatively low cost. In addition, a major advantage of a solid state dosimeter such as diamond is that the high mass density paired with a low ionization potential enables effective detection within a small volume. Diamond can therefore be used as a near-tissue-equivalent dosimeter with a small sensitive volume that enables dosimetry with good spatial resolution, especially in small fields.

Under the influence of an applied electric field, diamond acts as a radiosensitive resistor whose response to irradiation is proportional to absorbed dose. The use of diamond as counters of radiation such as alpha particles and gamma rays has been studied since the late 1940s [27,34,35], when Cotty first mentioned the advantages of diamond for use in medicine. Natural diamond dosimeters were first fabricated and tested for clinical applications in the late 1970s by Planskoy [29] and Burgemeister [30]. More recent studies have evaluated a variety of diamond for radiotherapy applications: hand-selected natural diamond gems, e.g. [36-38] and synthetic diamond films made via high-pressure-high-temperature, e.g. [39,40], polycrystalline CVD, e.g. [41-44] and single crystal CVD, e.g. [45-49].

Although a natural diamond detector for clinical applications exists on the market [11], there are limitations that prevent widespread commercialization of detectors made with either natural or synthetic diamond. The primary obstacle has been optimizing dosimetric properties in the presence of crystalline impurities and imperfections, or defects, e.g. [50-52], which may impede (or benefit) detector behaviour. Other problems that hinder dosimetric performance also originate from interface phenomena, perturbation effects and device encapsulation as investigated extensively in detectors using Si as a sensing material, e.g. [53-58]. Recent studies have also begun investigating these effects in detectors that use diamond [59-61].

The majority of synthetic diamond detector studies have focused upon testing and characterization using locally-grown CVD diamond films. Coupled with material studies, current research is focused upon performing dosimetry for advanced radiotherapy techniques using detector quality single crystal or polycrystalline diamond detectors.

## 1.2 Outline

The overall aim of this project was to investigate the suitability of commercially-available CVD diamond films for use in radiotherapy dosimetry.

Chapter 2 gives a description of diamond, including properties and their advantages and disadvantages for dosimetry, and the processes behind diamond synthesis. A brief history of radiation detection with diamond and its principles are also given, as well as a description of the properties of diamond and their advantages and disadvantages with respect to other dosimeters.

In Chapter 3, materials and experimental details are provided. First, commercially available single crystal and polycrystalline CVD diamond films from three manufacturers that had not been previously studied for their potential use in radiation therapy dosimetry are described in detail. The methods by which these diamond films were characterized are also presented. Details of three detector designs and their fabrication are provided, followed by the experimental setups used for two of these detector packages.

Chapter 4 presents the results and discussion of the material characterization of a number of diamond films, including spectrophotometry, Raman spectroscopy and bulk conductivity investigations. These studies were performed to verify and compare material quality to help correlate film quality with device performance.

Preliminary dosimetric experiments to evaluate detector response under clinical conditions are presented in Chapter 5. This chapter presents and discusses characteristics used to evaluate the suitability of these diamond films for use as dosimeters for use in clinical radiotherapy. Detectors were evaluated for their initial response, priming, response dynamics, sensitivity, dependence on dose, dose rate and incident angle of irradiation.

Chapter 6 presents an investigation into determining an optimal operating parameter of a selected single crystal CVD diamond detector before further clinically relevant measurements could be conducted. This included investigations on how changes in applied electric field affect detector performance, and sought to determine whether an optimal operating voltage can be found within the limits of available dosimetry equipment. Performance as a function

of voltage was evaluated by investigating current-voltage characteristics, response dynamics, sensitivity and dependence on dose and dose rate.

In Chapter 7, more clinically relevant investigations were performed with the same single crystal CVD diamond detector that was used in Chapter 6. This chapter evaluates some of its clinical advantages and limitations. This includes a closer look at repeatability and dose rate dependence, and comparing it with other dosimeters with respect to depth dose measurements as well as output factors and off-axis profiles, where the detector may outperform other dosimeters in small fields due to its near-tissue equivalence, small volume and high sensitivity.

Concluding remarks and ideas for future work are presented in Chapter 8.

## 2. Background

---

In this chapter, a review of diamond properties, diamond synthesis and radiation detection is presented, followed by a review of literature and status on the use of diamond in radiation therapy dosimetry.

Sections 2.1 and 2.2 describe diamond properties the development and principle of diamond synthesis, respectively. Section 2.3 gives an overview of the historical developments of detecting radiation with diamond, and Section 2.4 describes their principles. Material studies of diamond are summarized in Section 2.5. Radiotherapy dosimetry and a description of the requirements of a dosimeter are given in Section 2.6 before a comparison of existing dosimeters used in radiotherapy dosimetry including diamond in Section 2.7.

### 2.1 Properties

Diamond has been known to exist for over two millennia. Along with a few other minerals, it serves as both a gemstone and a tool. Once used for beautification or an abrasive, its application for modern society now extends from markets of wear-resistant coatings and cutting tools to electronics, optics and thermal management. Twenty-first century applications of diamond are being pursued in fields such as biotechnology, quantum computing, high-energy particle detection and micro-electromechanical systems.

Physically, diamond is the hardest known natural material, the stiffest and least compressible. It works well as a thermal conductor - four times the thermal conductivity of copper - and has an extremely low thermal expansion. It is chemically inert to all acids and alkalis at room temperature [62-64].

The diamond lattice is made up of tetrahedrally bonded ( $sp^3$ ) carbon atoms, which create a variation of the face centred cubic (fcc) crystal structure as shown in Figure 2.1. The crystal is actually two interpenetrating fcc lattices with each carbon atom forming four covalent bonds. This arrangement makes this allotrope of carbon extremely stable.

Despite the fact that diamond is an electrical insulator at room temperature, many of its physical, thermal and electrical properties make it a strong candidate for semiconductor applications. Electrically, it has high electron and hole mobilities, high breakdown field strength, low dielectric constant and a wide bandgap - most of which are superior to other well known semiconductor materials. Table 2.1 compares selected properties of diamond with Si, a well-known material that is also used in radiation dosimetry. More details regarding diamond and comparisons with other semiconductor materials such as Si, GaAs, GaN and Ge can be found in the literature [62,65-70].

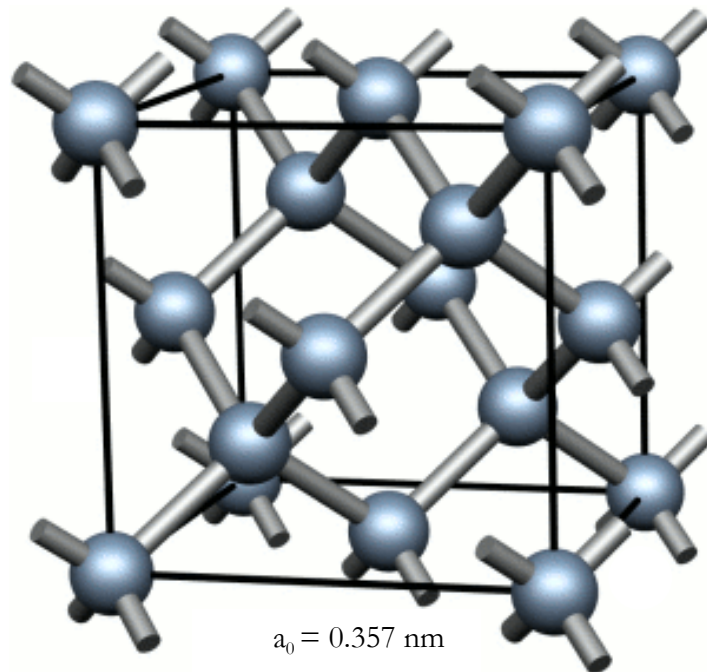


**Figure 2.1.** The diamond cubic crystal structure with characteristic cubic edge length  $a_0$  of pure diamond with natural isotope content at room temperature [71].



**Table 2.1.** Comparison of diamond and Si properties at 293 K.

Property	Diamond	Silicon
Density [ $\text{g cm}^{-3}$ ]	3.52	2.33
Bandgap [eV]	5.47	1.12
Resistivity [ $\Omega \text{ cm}$ ]	$> 10^{12}$	$2.5 \times 10^5$
Breakdown voltage [ $\text{V cm}^{-1}$ ]	$10^7$	$3 \times 10^5$
Electron mobility [ $\text{V cm}^2 \text{ s}^{-1}$ ]	2400	1350
Hole mobility [ $\text{V cm}^2 \text{ s}^{-1}$ ]	2100	480
Saturation velocity [ $\text{cm s}^{-1}$ ]	$2.2 \times 10^7$	$8.2 \times 10^6$
Dielectric constant	5.7	11.9
Energy to form e-h pair [eV]	13	3.6
Thermal conductivity [ $\text{W m}^{-1} \text{ K}^{-1}$ ]	$\sim 2000$	150

## 2.2 Synthesis: Development and Principle

As early as 1880, attempts were made to synthesize diamond once it was known that diamond was a high pressure, high temperature form of carbon. Differences between the different forms of carbon—diamond, graphite and coal—were not even known until the advent of x-rays and their analyses, where the discovery of x-ray diffraction by Max von Laue was applied by Sir William Henry and Sir William Lawrence Bragg and other authors to diamond and graphite [72-75]. Although many claims were made previously, it was not until the 1950s that researchers began publishing studies on undisputed synthesis of diamond in a laboratory. Bundy *et al.* at General Electric Laboratories [76] announced in 1955 the synthesis of diamond via a high-pressure high-temperature process; this gets notoriety as the study that marked the beginning of the present synthetic diamond industry<sup>1</sup>. Successful synthesis by any method, however, was achieved by W. G. Eversole of the Union Carbide Corporation in 1952 using via low-pressure deposition on pre-existing diamond seeds [78]. B. Deryagin *et al.* of the Russian Physical Chemistry Institute in Moscow also made significant contributions during the same period [78,79]. The major achievement of the Soviet group was the use of atomic hydrogen during the growth process; this allowed much higher growth rates and the nucleation of diamond on non-diamond substrates [78].

<sup>1</sup> It is interesting to note that some of the authors discovered almost 40 years later that the very first diamond grown by their technique was not synthetic after all, but a fragment of a natural diamond that somehow made its way into the experiment. The technique, however, was sound [77].

The field of diamond and subsequent applications were limited to natural and high-pressure-high-temperature (HPHT) diamond up until the development of CVD in the late 1970s and early 1980s by a team from the National Institute for Research in Inorganic Materials in Japan. The key to these discoveries in CVD were due to the use of atomic hydrogen during the growth phase [79]. Following these developments, exaggerated claims were made regarding diamond replacing Si in a number of markets, which resulted in a significant amount of funding from government agencies in the 1990s to commercialize diamonds for electronic devices but resulted in limited success. Diamond related research slumbered as other wide band gap semiconductors dominated. There has since been resurgence in research and development of CVD diamond for electronic devices, sensors and other applications in the last decade, which has been reviewed recently in literature, e.g. [80-84]. Developments of the CVD diamond process itself were reviewed extensively by Goodwin and Butler [85] and recently by Butler *et al.* [32,33]. Improvements are being pursued to make single crystal CVD diamond relatively inexpensive with quicker CVD processing times on larger substrates that can be tailored for electronic devices and sensor applications.

Chemical vapor deposition is a process by which a solid material is deposited from a gas or a gas mixture onto a substrate. To synthesise diamond with this technique, particular growth conditions are required (see Figure 2.2). The reactor chamber pressure is typically between 1 to 400 torr, below atmospheric pressure (1 atm = 760 torr). A suitable energy source with which to ionize or decompose the gas mixture is also required, such as resistive, radiant or inductive heating or lasers. The gas mixture consists mainly of hydrogen and a hydrocarbon such as methane. The dissociated hydrogen gas then plays a vital role in the deposition of diamond on the substrate; the hydrogen gas suppresses the formation of graphitic  $sp^2$  bonds thereby allowing the deposition of  $sp^3$  bonds, which form the diamond lattice. Hydrocarbon is the source of carbon and typically is only 1 to 5% of the total mixture.

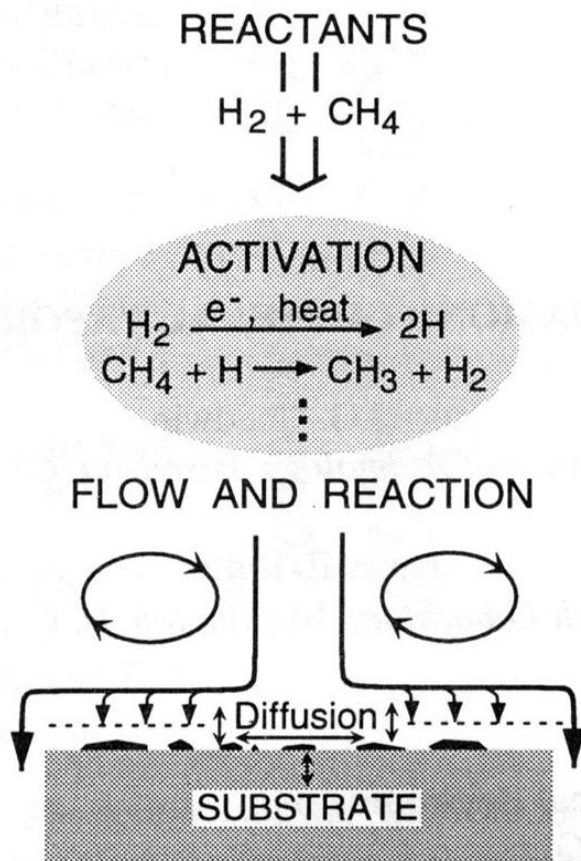


**Figure 2.2.** Schematic of the principal components of the CVD process [86].

A number of methods have been used to synthesize diamond in low-pressure conditions: microwave plasma-assisted CVD (MPCVD), direct-current plasmas CVD, hot-filament CVD, plasma-assisted CVD, combustion flame CVD, etc. [63,74,80]. The primary method used currently for growing homoepitaxial diamond films, or film grown on a substrate or film of the same material, is MPCVD. To create single crystal CVD diamond, the substrate is also single crystal diamond (typically HPHT), which has the same lattice structure and orientation. The growth of diamond on a non-diamond substrate, or heteroepitaxy, is done via materials such as cubic boron nitride (c-BC), Si and SiC, Ni, Co, Pt and Ir [80]. Polycrystalline diamond is grown on such substrates.

## 2.3 Historical Developments of Radiation Detection with Diamond

Developments initiated in the fields of nuclear and high energy physics have had significant spin offs in various areas of life sciences, such as medical imaging, scientific experiments in space and material science. The use of diamond electronics in radiotherapy is but one such example.

The use of diamond as a pinpoint counter of radiation has been studied since the 1940s. P. J. van Heerden is given recognition as the inspiration in early publications for his 1945 thesis work at Utrecht on silver chloride crystals where he observed conductivity induced by alpha particle bombardment [87]. However, more importantly, he attempted the same with natural diamond but was unsuccessful [34,35]. In 1947, Wooldridge, Ahearn and Burton at Bell Labs discovered that diamond could successfully detect alpha particles at room temperature [34]. Curtiss and Brown reported a response from  $\gamma$ -rays later that year [35]. Many studies followed [88-105] especially as reports of reproducible experiments of man-made diamonds were being published [76]. Many reports of using natural diamond as nuclear radiation detectors were published in the late 1960s to 1970s mainly by Koslov, Konorova and colleagues [28,106-112].

Large research facilities have also been interested in using synthetic diamonds for detection so that relatively large-scale detectors at a low cost could be achieved for long-term applications. The RD42 diamond detector collaboration at CERN [113] consists of dozens of researchers whose interests in high energy physics, heavy ion physics and solid state physics are combined to develop diamond tracking detectors for high luminosity experiments at the Large Hadron Collider including the ATLAS and CMS detectors [114-120] and synchrotron x-rays [121-125]. Another collaboration is NoRHDia (Novel Radiation Hard CVD Diamond Detectors for Hadron Physics), which involves groups from CVD diamond research with expertise in single crystal CVD diamond growth, defect spectroscopy and transport properties measurements to create diamond detector applications that address future demands of European research [126]. Some of the same researchers in these groups have also taken interest in using diamond detectors for radiation therapy applications.

Although W. F. Cotty first reported the advantages of diamond for use in medicine in 1956 [27], it was not until the late 1970s that natural diamond dosimeters were first fabricated and tested specifically for clinical applications by Planskoy [29] and Burgemeister [30]. The use of synthetic diamond soon followed in the 1980s by work reported by

Burgemeister [127,128] and Schouten, Schipper and Burgemeister [129] and later by Nam *et al.* [130]. The first commercial diamond dosimeters for radiotherapy made from natural diamond gems were created by a collaboration between PTW of Freiburg [11] and Khrunov *et al.* of the Soviet Union in the late 1980s [38]. The ADII-33 natural diamond detector manufactured (or funded) briefly by UralAlmazInvest Co. of Russia was also tested in the literature [131] but its development and commercialization was apparently unsuccessful.

A number of studies have since evaluated or compared the PTW diamond detector in dosimetric techniques that involve conventional electron and photon beams [132-142] but also proton beams [38,143-146], IMRT [17,147] and stereotactic radiosurgery [148]. Studies focused on characteristics such as energy, dose and dose rate dependence, calibration factors, polarization effects, I-V characteristics, sensitivity and stability. Comparisons between PTW detectors themselves and CVD diamond detectors have also been reported, e.g. [44,149]. Although these detectors work under an acceptable range of beam qualities and applications, their properties have been shown to vary such that each detector must be calibrated individually [150]. This is besides the fact that the nature of manufacturing of these detectors, such as the selection and testing of suitable natural diamonds, makes them rather expensive ( $> \text{AU}\$18,000$ ) [151] and susceptible to long waiting times ( $> 1$  year) [151-153]. No other diamond detector to date has been commercialized for use in radiotherapy dosimetry.

Collaborative efforts have also pursued diamond research in radiation therapy. The *Istituto Nazionale di Fisica Nucleare* (INFN, Italy) Research and Development Program created CANDIDO, an Italian collaboration created over a decade ago to develop diamond dosimeters for applications in radiotherapy [41,149]. The European Integrated Project MAESTRO (Methods and Advanced Treatments and Simulations for Radio Oncology) [154] also includes diamond dosimeter research in their development goals [49,50,155,156].

Outside of these established partnerships, many other researchers have also taken interest in primarily CVD diamonds and their use in radiotherapy dosimetry. The majority of research as mentioned previously has come out of mostly Europe. The focus of many published works has been manufacturing and testing locally grown polycrystalline diamond films, which are more economical than their single crystal counterparts are. However, polycrystalline films inherently contain defects, which can create unpredictable electronic behaviour due to lack of sufficient control over impurity content and crystal defects.

Many publications within the last 16 years have examined diamond films and their detection properties using conventional photon or electron therapy, and have established that they indeed have the potential to be used in radiation therapy [84,157]. Due to its

proven radiation hardness and progress thus far in harsh radiation environments of high energy and nuclear physics, diamond detectors have also been tested in other forms of radiotherapy, e.g. proton therapy [38,143,145,146,155,158-161], neutron and boron capture neutron therapy [162,163] and heavy ion beams including carbon [164-166]. Within the last two years, researchers have been growing CVD diamonds or purchasing commercially-available high-quality single crystal and polycrystalline CVD diamonds to test their suitability for radiotherapy, primarily for modern techniques such as IMRT and small fields [47-49,60,156,162,167-170].

Two books and a proceedings monograph have also recently reviewed diamond detectors and their application in radiotherapy [8,84,157].

## 2.4 Radiation Dosimetry with Diamond

Dosimeters used in radiotherapy are concerned primarily with measuring the absorbed dose from a radiation source that delivers either photons or electrons. The physical processes that enable those measurements are different for either neutral or charged particles. Throughout this thesis, the radiation used was a 6 MV photon beam from a Varian linear accelerator (see Section 3.5.1). Photon and charged particle interactions are well known and described extensively in the literature, e.g. [171-175], and a summary of such interactions in diamond is given below.

Photons may interact with bound electrons via photoelectric or coherent scattering, the field of the nucleus via electron-positron pair production or free electrons via Compton effects. At nominal photon energies of 6 MV in tissue ( $Z_{\text{eff}}$  of soft tissue  $\approx 7.4$  [174]), Compton processes dominate (see Figure 2.3). What follows from the scattering process is the ionizing or excitation of atoms, which promotes electrons to the conduction band while leaving holes in the valence band. In the presence of an applied electric field, these free carriers then drift through the medium towards their respective electrodes (although some electrons and holes may recombine), and thus a change in electrical conductivity is produced. The change in current or total charge can be collected and measured at the electrodes of a detector, which can then be correlated with absorbed dose within the sensitive volume [173,174,176]. Figure 2.4 illustrates these interactions in a simple circuit design used for radiation detection.

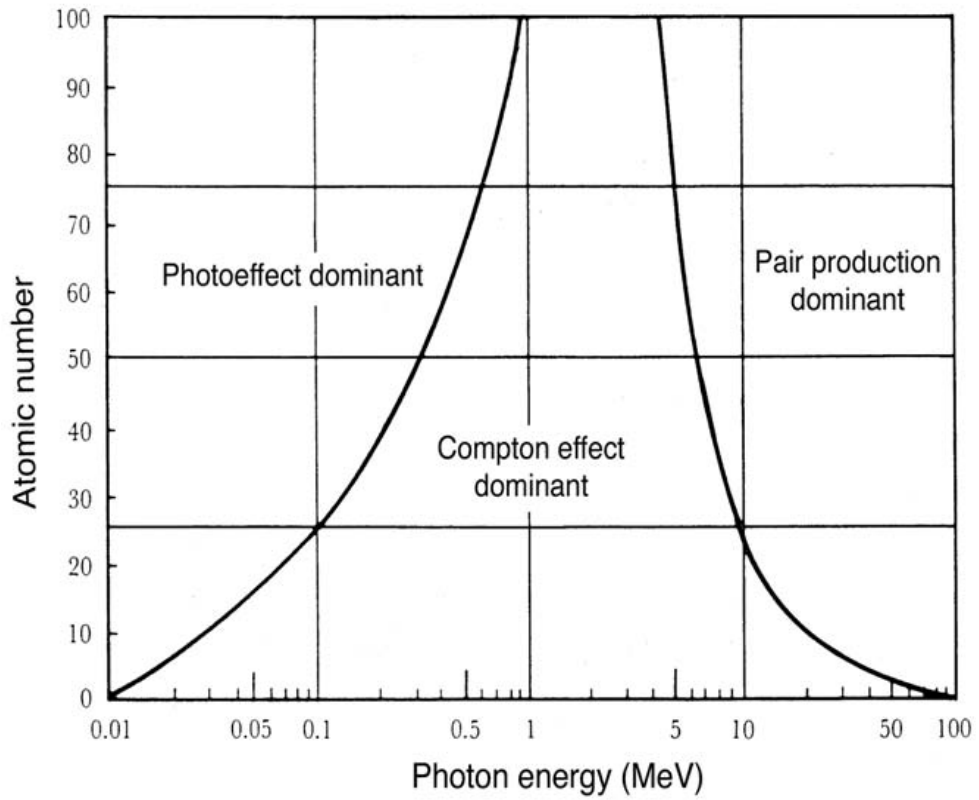


**Figure 2.3.** Regions of relative predominance of the three primary interactions of photon with matter [174].

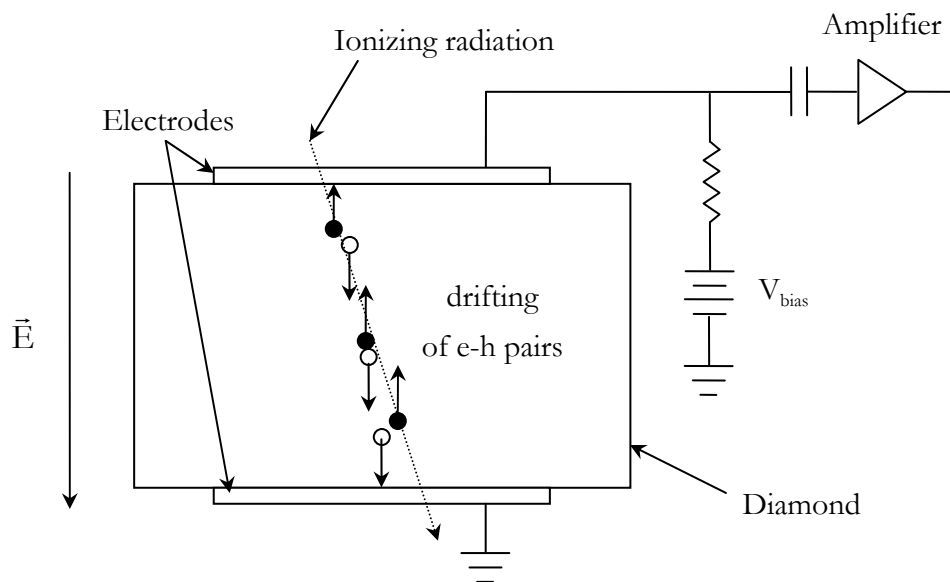


**Figure 2.4.** Schematic of a diamond detector where (●) are electrons and (○) are holes.

In reality, the detection of electron-hole pairs from incident radiation may be reduced by the presence of defects in diamond, which usually leads to a reduction in conductivity. Defects include impurities, point defects, dislocations, grain boundaries, inclusion of graphitic or disordered carbon, etc., which can trap or scatter charge carriers [177]. These defect populations are generally classified as either shallow or deep, depending on the energy or temperature at which they are emptied. For example, the resulting effect of such defects on the temporal response of diamond is illustrated in Figure 2.5. In the figure, a CVD diamond detector was irradiated under clinical conditions (the jitter in the signal was due to noise). From 60–100 s, the gradual increase in the induced current is due to charge carriers becoming more and more detected as they are no longer able to fill traps in the material. After 100 s, the current continues to increase but much more slowly as traps in the material are filled until  $\sim 250$  s. After the beam was turned off at 300 s, a tail appeared that typically corresponds to the detrapping of charge in shallow defects that are released at room temperature. A second irradiation is given at 460 s, which shows that the deep traps are now filled and thus the observed induced current is found to rise to equilibrium more quickly. This filling of traps is defined as the pumping effect or priming. The priming effect varies with diamond types and is investigated in Chapters 5 and 6. The following section describes current developments that aim to correlate material quality, e.g. defects with diamond detector performance.

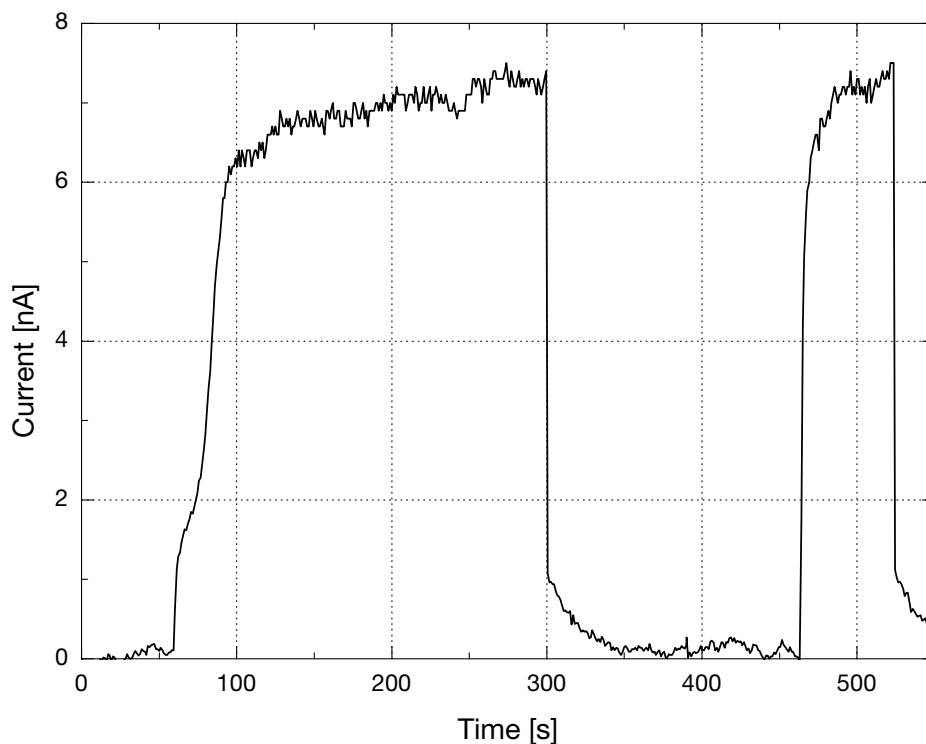


**Figure 2.5.** An example of priming effects in a CVD diamond detector.



## 2.5 Material Studies

As mentioned in Chapter 1, using *natural* diamond as a dosimeter or detector is impractical for commercial widespread use due to the scarcity and variability of suitable dosimetric properties. Dosimeters using diamond made via chemical vapor deposition pose to eliminate such limitations, where specific properties may be controlled and reproduced at a relatively low cost. Fully understanding the material properties of CVD diamond and using them to meet the dosimetric requirements of applications such as radiotherapy is where the main challenge lies. Current developments are focused in the following areas:

1. Non-diamond impurities
2. Deposition parameters
3. Post-deposition preparation
4. Response dynamics
  - i. Priming (or pumping) effects
  - ii. Slow rise and decay times
  - iii. Dose rate dependence

Material studies performed for diamond sensors in general complements radiotherapy diamond detector research. Studies have focused upon correlating crystalline quality, e.g. lattice defects, grain boundaries, quantifying H content and other impurities, shallow and deep trap levels, with electronic properties e.g. polarization effects, charge collection distance and radiative recombination, electron and hole mobility, resistivity and carrier lifetime [178]. Improving sample purity by optimizing deposition parameters or intentionally adding impurities via doping [179-184] and/or ion implantation [179,185,186] is also a focus. Post-preparation of samples also has an effect on electronic properties due to surface contamination and/or H content. To achieve these results techniques that are used include Raman spectroscopy, x-ray diffraction, scanning and transmission electron microscopy, thermal spectroscopy, e.g. thermoluminescence or thermally stimulated currents, photoconductivity, nuclear techniques, e.g. ion beam induction and x-ray microbeam induced current. A few of these techniques were used during this project to characterize and correlate material quality with detector response and are described in Section 3.2.

## 2.6 Radiotherapy Dosimetry

Radiation therapy, or radiotherapy, is the medical use of ionizing radiation to control malignant cells during cancer treatment and is typically combined with surgery and/or chemotherapy. The aim of radiotherapy is to maximize the effective dose that is delivered to the treatment volume while minimizing the dose to the surrounding healthy tissue or organs. Radiation therapy can be delivered to patients via external beam radiotherapy (e.g. x-rays from a linear accelerator) or brachytherapy (e.g. in close proximity to the cancerous tissue using  $^{125}\text{I}$  seeds), depending on the treatment location within the patient. Typical sources or generators of clinical radiation range from low energy kilovoltage or orthovoltage x-rays for contact or superficial therapy to teletherapy such as  $^{60}\text{Co}$  or linear accelerators that produce high energy megavoltage photons or electrons (e.g. 4-25 MV x-rays). Modern conformal techniques such as intensity-modulated radiation therapy, stereotactic radiosurgery and hadron therapy involve using narrow beams with modulated intensities, geometries and energies. New techniques are making real-time monitoring and dose verification challenging, as they put new demands on existing dosimetry systems.

The aim of dosimetry in radiotherapy is to measure the absorbed dose in various tissues of a patient. This involves assessing the deposited dose by means of a radiation detector in a controlled and suitable environment (a phantom). This is then used to predict the dose at any location in the patient by means of mathematical algorithms [187]. For clinical dosimetry, the accuracy of dose delivery using linear accelerators to a patient must be accurate to within  $\pm 2\%$ . It is known that a difference in 5% of the dose delivered to a patient does make a clinically detectable difference [188].

Dose  $D$  and dose rate  $dD/dt$  or  $\dot{D}$  are fundamental quantities in dosimetry and are used throughout this thesis. Absorbed dose  $D$  is defined as the mean energy imparted  $d\bar{\epsilon}$  by the ionizing radiation per mass  $dm$  [189,190]:

$$D = \frac{d\bar{\epsilon}}{dm} \quad (2.1)$$

Absorbed dose is given in units of gray or  $1 \text{ J kg}^{-1}$ .

A radiation dosimeter is a device, instrument or system that is used to directly or indirectly measure the absorbed dose and other various quantities of ionizing radiation. Ideal (or desirable) dosimeter properties can be characterized by the following [157,174,187]:

1. Accuracy and precision – the ability to measure a physical dose correctly and to reproduce results under similar conditions short-term (repeatability) and long-term (reproducibility);

2. Dose response – the measurement should be linearly proportional to the given dose;
3. Dose rate dependence – the dosimeter should be independent of dose rate, although an accurate and precise measurement of dose rate dependence is also desirable;
4. Energy response – the response should be independent of beam quality, which entails that the sensing material match the absorption and scattering characteristics of biological tissue (tissue equivalent)
5. Directional dependence – the dosimeter reading should be independent of the incident angle of radiation and where electrons and scattered photons vary with distance;
6. Spatial resolution – the ability to measure dose in within a well-defined point-like volume;
7. Dynamic response and stability – the dosimeter should have sufficient sensitivity to measure very low to very high doses (in a reasonable amount of time), and be fast and stable.

Existing dosimeters or dosimetry systems all have some limitations in terms of the above properties. Hence, there will be compromises when selecting dosimeters to perform dosimetry for different applications. The following section compares existing dosimeters used in radiotherapy and their limitations with respect to requirements for conventional and small field dosimetry.

## 2.7 Dosimeter Comparisons

Dosimeters can be made from a number of materials (i.e. gas, liquid or solid) and with different sensitive volume or cavity geometries. Dosimeters used in radiotherapy today include air and liquid-filled ionization chambers and counters, film, silicon diodes, thermoluminescent dosimeters (TLD), metal oxide semiconductor field-effect transistors (MOSFETs); recent research using plastic and liquid scintillators also appears encouraging. These dosimeters can be described as either active (online) or passive (offline). Each detector has its advantages and disadvantages for conventional and small field dosimetry.

The most commonly used dosimeter in radiotherapy dosimetry is the gas-filled ion chamber, which has a long history of accuracy and dependability [191]. As local standard dosimeters, ion chambers have high-precision, are well-documented and investigated and have dose rate dependence due to general ion recombination. However, they require a high voltage, have a low sensitivity due to a low density ionizing medium and have a relatively

large volume (typically 0.1–1.0 cm<sup>3</sup> for megavoltage radiotherapy) compared to other dosimeters. The large volume has consequences in small fields where output factors are underestimated due to lateral electron disequilibrium [147]. Micro-ion chambers (0.015 cm<sup>3</sup>) have been designed for relative dose measurements in small field dosimetry. The chamber over-responds to low-energy Compton scatter due to its aluminium electrode [17], and can vary by 0.5% in large-area fields due to stem and polarity effects from its small sensitive volume and cable irradiation [192]. A variety of ion chambers is available depending on their application, e.g. beam quality. Liquid-filled ion chambers improve sensitivity and are therefore smaller than gas-filled chambers. Both chamber types need to be corrected for recombination and temperature effects [193].

Another commonly used dosimeter is radiographic film. Because they are two-dimensional, they can measure dose distributions; they are inexpensive, have almost no angular dependence, are integrative and have very good spatial resolution. However, they require development, are dependent on energy and dose and are not reusable. There can also be variations in film coatings and processing conditions. Radiochromic film, however is self-developing, has tissue equivalence and has very high spatial resolution, but still takes hours or days until the film is ready to be evaluated [187].

Silicon diode detectors have good sensitivity and high signal-to-noise ratios, which allow for small sensitive volumes. However, the high atomic number (and non-water equivalence) of silicon leads to an overestimation of dose at low photon energies as compared to water due to a higher photoelectric cross section [54], although this is not critical [23]. This leads to its use in small fields where compensation for energy dependence is not required. They also display dose rate dependence, and the asymmetry of the diode geometry creates directional dependence by as much as 3%. Interface phenomena and build-up material around the sensing material also create the need for correction factors [187]. Diodes also display a loss in sensitivity over accumulated dose, which requires recalibration [54]. Unshielded diode detectors are also available but corrections for linearity and energy are still required [142,194].

TLDs have been used as x-rays detectors for over 100 years. They are small, are a standalone measurement (no cables), are able to be mailed, and a number of materials are available, e.g. LiF, Li<sub>2</sub>B<sub>4</sub>O, BeO, CaSO<sub>4</sub>, CaF<sub>2</sub> and Al<sub>2</sub>O<sub>3</sub> [187]. Because they are used in a passive or offline mode, there is a delay in the readout, but can be used for personal or in

vivo dosimetry. They are also not as precise as ion chambers and must be handled with care.

A MOSFET is a recent development in radiotherapy dosimetry. They can integrate dose (similar to TLDs) as well as give an immediate readout, have excellent spatial resolution (as small as 10  $\mu\text{m}$  wide), can be used without bias (and hence without cables), are independent of dose rate and their sensitivity can be varied. Their performance appears promising for dose verification [195-199]. However, they have strong nonlinear photon energy dependence below 300 keV and vary in sensitivity as a function of threshold voltage [200].

Plastic fibre scintillators are also a recent development for radiotherapy. They can be tailored to specific physical and electron densities, which can therefore provide near ideal agreement with tissue and water dose responses. They are also independent of dose rate and energy, inexpensive, chemically inert and can be formed into arbitrary shapes and volumes [191,201,202]. Their spatial resolution is also superior to traditional ion chambers, radiographic film and diodes [203]. Their main disadvantage is unwanted stray light in the optical fibre due to Cerenkov radiation, which is negligible in photon beams but not for electron beams [203-205]. These scintillators are also prone to radiation damage over time (2.1 and 7.6% for  $10^3$  and  $10^4$  Gy, respectively) [203]. Although more research is required to address signal collection efficiency and reduction in background, it appears that many advantages and uses of plastic fibre scintillators are comparable to diamond. Several prototypes have been tested in the literature with much of the research performed by Beddar *et al.* [203,206,207].

Diamond is a solid state or semiconductor dosimeter and may act as either an active or a passive<sup>2</sup> dosimeter. In this thesis, diamond films were used as detectors in the active or online mode. As stated in Chapter 1, diamond has a number of advantages that make it an attractive sensing material for radiation dosimetry: it is chemically inert (has little or no ability to react), is radiation hard (highly resistant to ionizing radiation); is a near-tissue equivalent or a tissue substitute with  $Z = 6$  ( $Z_{\text{eff}}$  of tissue  $\approx 7.4$ ,  $Z_{\text{eff}}$  of water = 7.51) and, more importantly, the mass attenuation coefficient ratio and stopping power ratio of water to diamond are nearly constant over a wide range of photon and electron energies (which enables a direct evaluation of dose measurements without additional corrections due to changes in material or energy) [84]; is bio-compatible (non-toxic and can be sterilized); has a

---

<sup>2</sup> Diamond as a thermoluminescent dosimeter (TLD) is also a topic of interest in the literature [48,89-107] but was not within the scope of this thesis. Chapter 8 lists future work regarding diamond as a TLD.

high thermal conductivity at 300 K (these devices are used at room temperature clinically and also negligible temperature dependence); a high carrier (or electron-hole pair) mobility and therefore high sensitivity, short carrier lifetime and high band gap, making it an excellent for devices and sensors. These characteristics allow diamond detectors to be quite attractive for radiotherapy dosimetry, and, as discussed in Section 2.3, a number of studies have compared commercially available PTW natural diamond detectors to other dosimeters for a number of radiotherapy techniques.

Diamond detectors have already proven to be nearly independent of energy and dose, have negligible directional dependence and high sensitivity [157]. A major advantage of a solid state dosimeter such as diamond is that the high mass density paired with a low ionization potential enables effective detection within a small volume. Diamond can therefore be used as a near-tissue-equivalent dosimeter with a small sensitive volume that enables dosimetry with excellent spatial resolution, especially in small fields. However, defect levels in diamond influence device response under irradiation that can affect reproducibility and stability, and can create a dependence on dose rate. The aim of researching CVD diamond for radiotherapy is to not only find an inexpensive alternative to natural diamond detectors, but also improve their response by investigating different CVD diamond qualities whether they are manufactured either commercially or locally.

## **2.8 Concluding Remarks**

This chapter introduced the properties and synthesis of diamond. It also provided an overview of historical developments and principle of detecting radiation with diamond, along with a comparison of existing dosimeters used in radiotherapy dosimetry.

In the next chapter, a detailed description is given for a number of commercially available diamond films that were selected for evaluation and the means by which they were characterized before they were packaged. It then describes several detector designs that were considered including the process of selecting and fabricating electrodes and encapsulation. Finally, it details the experimental setups used for clinical investigations.

# 3. Materials & Experimental Details

---

This chapter describes the diamond films, methods of characterization, detector designs and experimental conditions that were used throughout this thesis.

Every film that was analyzed and/or used in radiation detection experiments is detailed in Section 3.1; this serves as a point of reference for material specifications. The next section (Section 3.2) describes the methods by which films were characterized. The results of this characterization are presented in Chapter 4. The preparation and metallization of films are described in Section 3.3. Detector designs, their improvements and their limitations are covered in Section 3.4. The last section describes the experimental conditions and set-ups used for testing the detectors in a clinical environment (Section 3.5).

Surface preparation and metallization were performed in the Department of Electrical and Computer Engineering and their Nanofabrication Laboratory at the University of Canterbury (UC), Christchurch. Spectrophotometry and Raman spectroscopy as well as most detector fabrication and preliminary testing were performed in the Department of Physics and Astronomy at UC. Experimental setups and dosimetric testing took place in Radiation Oncology at Christchurch Hospital, Christchurch.

## 3.1 Diamond films

A variety of diamond films were characterized and tested for their suitability in radiation dosimetry. Commercially-available free-standing diamond films were purchased from three manufacturers: Diamonex (of Morgan Technical Ceramics, a division of Morgan Crucible Company plc, Allentown, PA, USA) [208], Diamond Materials GmbH (Freiburg, Germany) [209] and Element Six Ltd. (Isle of Man, British Isles) [210]. See Table 3.1. All but one of the commercially available diamond films analyzed during this project was synthesized via CVD.

**Table 3.1.** Summary of diamond films.

Manufacturer	Name	Material	Thickness [ $\mu\text{m}$ ]	Surface	Contact	Sensitive	Price <sup>3</sup>	Manufacturer Details
				Area [ $\text{mm}^2$ ]	$\varnothing$ [mm]	Volume [ $\text{mm}^3$ ]	Approx. NZ\$	
Diamonex	Dx100	pCVD <sup>4</sup>	100	25	2	0.31	10	As-grown finish
	Dx200	pCVD	200	25	2	0.63	14	As-grown finish
	Dx400-1	pCVD	400	25	2	1.26	20	As-grown finish
	Dx400-2	pCVD	400	25	2	1.26	20	As-grown finish
	Dx400m-1	pCVD	400	25	2	1.26	54	Matte finish, both sides
	Dx400m-2	pCVD	400	25	2	1.26	54	Matte finish, both sides
Diamond Materials	DM100	pCVD	100	25	2	0.31	250	Optical quality, polished both sides
	DM200	pCVD	200	25	2	0.63	330	Optical quality, polished both sides
	DM400	pCVD	400	25	2	1.26	450	Optical quality, polished both sides
Element Six	E6EL200	pCVD	200	9	-	-	46	Not available
	E6EL500	pCVD	500	9	-	-	115	Not available
	E6OP	pCVD	500	50 (8 $\varnothing$ )	-	-	490	Thermal conductivity $> 1,900 \text{ W m}^{-1} \text{ K}^{-1}$ , polished both sides to $R_a^5 < 30 \text{ nm}$

<sup>3</sup> As of 7 Jan 2010<sup>4</sup> Polycrystalline CVD<sup>5</sup> Ra is the arithmetic average of the absolute values



**Table 3.1.** Summary of diamond films (cont.)

Manufacturer	Name	Material	Thickness [ $\mu\text{m}$ ]	Surface	Contact	Sensitive	Price	Manufacturer Details
				Area [ $\text{mm}^2$ ]	$\varnothing$ [mm]	Volume [ $\text{mm}^3$ ]	Approx. NZ\$	
Element Six	E6PC	pCVD	250	100	-	-	87	Mechanical grade, one side polished $R_a < 50$ nm, one side lapped $R_a < 250$ nm
	E6PE	pCVD	600	100	-	-	54	Electrochem. grade, $[\text{B}] > 10^{20}$ $\text{cm}^{-3}$ , as-grown surface finish
	E6SC1b	HPHT <sup>6</sup>	500	9	1	0.39	87	Type Ib, $[\text{N}] < 200$ ppm, $[\text{B}] < 0.1$ ppm, one side polished $R_a < 50$ nm, one side lapped $R_a < 250$ nm
	E6SCPL	scCVD <sup>7</sup>	500	9	1	0.39	105	{100} faces, $\langle 100 \rangle$ edges, Typically 100% single sector {100}, $[\text{N}] < 1$ ppm, $[\text{B}] < 0.05$ ppm, one side polished $R_a < 10$ nm, one side lapped $R_a < 250$ nm
	E6SCP2	scCVD	500	9	1	0.39	125	{100} faces, $\langle 100 \rangle$ edges, Typically 100% single sector {100}, $[\text{N}] < 1$ ppm, $[\text{B}] < 0.05$ ppm, both sides polished $R_a < 30$ nm
	E6TM100	scCVD	250	100	-	-	82	Thermal mngmt. grade, thermal conductivity $> 1,000$ $\text{W m}^{-1} \text{K}^{-1}$ , one side polished $R_a < 50$ nm, one side lapped $R_a < 250$ nm
	E6TM180	scCVD	250	100	-	-	160	Thermal mngmt. grade, thermal conductivity $> 1,800$ $\text{W m}^{-1} \text{K}^{-1}$ , one side polished $R_a < 50$ nm, one side lapped $R_a < 250$ nm

<sup>6</sup> High-pressure high-temperature

<sup>7</sup> Single crystal CVD

Polycrystalline CVD diamond films were purchased from Diamonex with nominal thicknesses of 100, 200 and 400  $\mu\text{m}$ . Film sizes of  $5 \times 5$  and  $10 \times 10 \text{ mm}^2$  were used for characterization, but the smaller films were most suitable for irradiation studies. The most noticeable feature of these films was that they were opaque, and appeared graphitic by the looks of their charcoal appearance as shown in Figure 3.1. The as-grown surface of these films was also quite rough compared to other film qualities; Figure 3.2 illustrates the topology of this surface using an atomic force microscope (AFM). They were the least expensive of the films obtained, and the first to be tested for irradiation measurements.

Films purchased from Element Six were categorized by grade: electronic, CVD single crystal, HPHT single crystal, thermal, electrochemistry, mechanical and optical (Figure 3.3). Film thickness and size ranged from 250 to 600  $\mu\text{m}$  and  $3 \times 3$  to  $10 \times 10 \text{ mm}^2$ , respectively. Optical quality pCVD circular diamond with a thickness of 500  $\mu\text{m}$  was also purchased. This manufacturer lists specifications for some of their films online [211]. Several of these films went on to be tested for their suitability detecting clinical x-rays.

Films purchased from Diamond Materials were optical quality polycrystalline made via CVD with nominal thicknesses of 100, 200 and 400  $\mu\text{m}$  and  $5 \times 5 \text{ mm}^2$  in size. The films appeared transparent and colourless. These high quality films were all tested for their suitability for radiation dosimetry. Figure 3.4 shows circular films of the same quality.

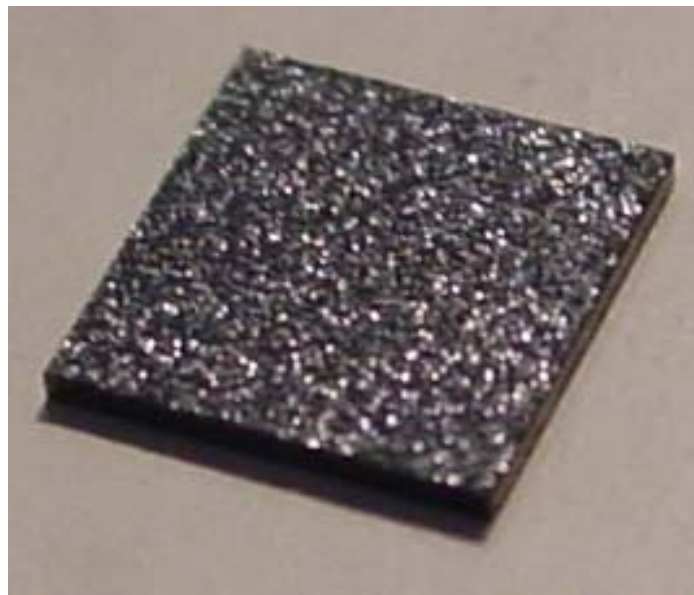


**Figure 3.1.** A  $5 \times 5 \times 0.2 \text{ mm}^3$  Diamonex polycrystalline diamond film.

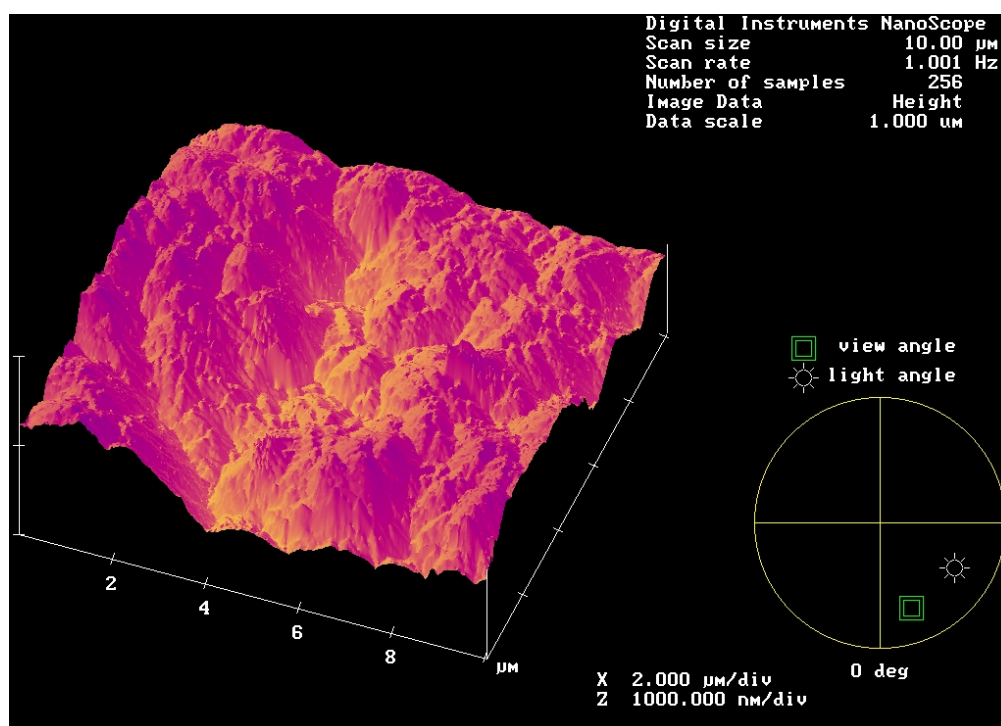


**Figure 3.2.** A  $10 \times 10 \mu\text{m}$  AFM scan of a Diamonex film.

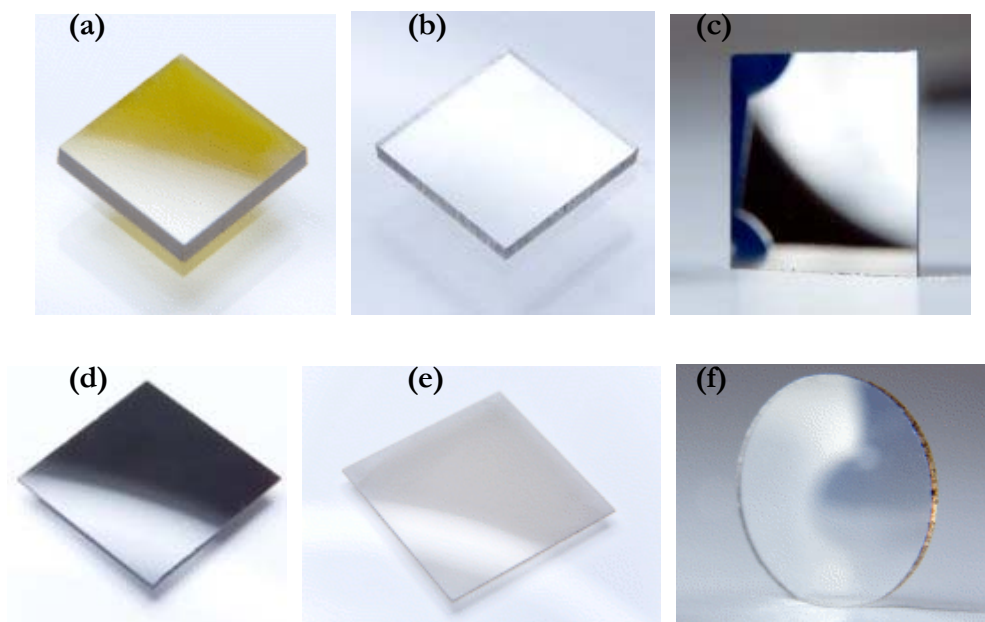


**Figure 3.3.** Element Six films. (a) E6SC1b; (b) E6SCP2, E6SCPL; (c) E6PC250; (d) E6TM100; (e) E6TM180 and (f) E6OP. [212]



**Figure 3.4.** Diamond Materials (square wafers were used in this thesis) [209].

## 3.2 Diamond Film Characterization

Many of the films obtained for these studies came with limited information, parameters or material details. Therefore, it was necessary to characterize them, e.g. identify relative chemical abundances, before they were tested for their suitability as x-ray detectors. This step was required to help correlate material quality with detector performance. A number of techniques have been used to examine films intended for radiation detection, which include photoconductivity, e.g. [183,213-216], Raman spectroscopy, e.g. [182,217-219], thermoluminescence, e.g. [182,220,221], ion beam analysis, e.g. [222-224], scanning electron microscopy, e.g. [225,226] and x-ray diffraction [218,227].

Before any metallization took place, freestanding samples were characterized using spectrophotometry (Section 3.2.1) and Raman spectroscopy (Section 3.2.2). These resources were readily accessible for this project in the Department of Physics and Astronomy. Results and discussion of these investigations are found in Chapter 4.

Contacts (electrodes) were evaporated or sputtered onto the films using facilities in the Department of Electrical and Computer Engineering and their Nanofabrication Laboratory. Films were analyzed for conductivity using either a parameter analyzer or a programmable

remote electrometer (Section 3.2.3). The electrometer was also used to measure leakage current across a range of applied voltages both before and after irradiation experiments.

### 3.2.1 Spectrophotometry

Spectrophotometry is the study of electromagnetic spectra in the near-infrared, visible and near-ultraviolet ranges. Although commonly used in physical chemistry, this technique is also used to identify and evaluate natural diamond gems, e.g. [228]. Previous studies of diamond films or wafers have used this technique to analyze the concentration of impurities in CVD diamond that may be due to defects and/or contaminants in the CVD process, e.g. [229-231]. These impurities have a detrimental effect on the quality required for a number of applications, especially optics. The absorption features of diamond are well known in literature and are referenced in handbooks [63,64]. This was a straightforward method during this project to characterize material before films were bonded and encapsulated for clinical testing.

A GBC Scientific Cintra 40 Double-Beam UV-Visible Spectrometer (GBC Scientific Equipment, Dandenong, Victoria, Australia) [232] was used for this analysis. This instrument scans over a range of 190 to 900 nm wavelengths at a rate of  $1000 \text{ nm min}^{-1}$  ( $39 \text{ steps s}^{-1}$ ), and a variable slit width of 0.2 to 2 nm. Here, a 2 nm slit was used. HPHT, polycrystalline CVD and single crystal CVD diamond films totalling 16 were analyzed, which are listed in Table 3.1. The results of this study can be found in Section 4.1.

### 3.2.2 Raman Spectroscopy

Raman spectroscopy [233-236] is a well-known technique that analyzes the inelastic scattering of radiation from molecules that have been illuminated by monochromatic light. Inelastic, or Raman, scattering is the result of the small probability of incoming light interacting and exchanging energy with the sample in question. This technique has been used extensively to characterize diamond [63,64], especially CVD diamond films, e.g. [216,225,237-244]. Several authors evaluating CVD diamond films for radiation dosimetry have used Raman spectroscopy for characterization [218,227,245,246]. These studies examined relative quantities of dopants or crystal structure and defects to determine their effect on detector performance. This technique was used to investigate crystalline quality of various diamond films before metal contacts were evaporated or sputtered onto the diamond surface.

The light source used in this setup was a Coherent Innova 90 argon laser operating at 514.5 nm ( $19,436 \text{ cm}^{-1}$ ) and with power set at 300 mW (Coherent Inc., Santa Clara, CA, USA)

[247]. Integration time of the scan was set at either 2 or 10 s. The input slit was 0.1 mm. Two gratings were used during this analysis, which yielded ranges of  $\sim 518$  to  $571$  nm and  $\sim 490$  to  $605$  nm. These settings were recommended to achieve satisfactory results with sufficient resolution to observe any non-diamond peaks near the first-order Raman peak of diamond ( $1332\text{ cm}^{-1}$ ) and others caused by nitrogen. Spectra data were then presented in units of wavenumber shifts, which is the difference in wavenumbers between the laser probe and the Raman scatter. The range used gave positive wavenumber shifts, or Stokes shifts.

Raman spectra results from diamond films are presented in Section 4.2.

### 3.2.3 Surface and Bulk Conductivity

The surface of films can have a significant effect on the overall response of the detector, especially at lower energies. Diamond-metal interfaces, surface contaminants, morphology, defects and impurities in the crystal lattice at or near the surface can have an effect on device operation, e.g. [92,248-254]. In this project, surface and bulk conductivity was compared.

After metallization (Section 3.3.2), initial current-voltage measurements of several films were performed on an HP 4155A Semiconductor Parameter Analyzer (Santa Clara, CA, USA) [255]. The analyzer and the associated probe station allowed the measurement of surface and bulk conductivity.

Data were acquired during irradiation experiments using two different instruments, depending on the type of analysis being performed. One instrument used was a 2570/1 Farmer Dosemeter (Thermo Fisher Scientific Inc., Waltham, MA, USA) [256], a standard electrometer that can acquire total charge (in nC) over a user-specified time interval (hereafter referred to as “Farmer electrometer”). Physikalisch-Technische Werkstätten (PTW) threaded triaxial cable was used to connect the detector to this electrometer. The voltages available with this instrument were full, half, quarter and eighth divisions of approx.  $\pm 250$  V; actual settings were measured as  $\pm 248.0$ ,  $\pm 125.0$ ,  $\pm 62.5$  and  $\pm 30.8$  V. Resolutions for low and high settings for collecting charge were  $0.005$  and  $0.05$  nC, respectively. This electrometer was useful for acquiring accurate measurements of total charge, with which average current as a function of time or dose could be found. Note that this electrometer only allowed a maximum total charge of  $204.75$  nC per single measurement performed. Consequently, the high sensitivity of this detector made measurements over long time intervals unfeasible at high voltages such as at  $248.0$  V. Therefore, 4-s intervals were typically used as a convenient way to estimate average current. Maximum continuous current rates ( $6$  and  $60$  nA for low

and high settings, respectively) also limit the use of high voltages with highly sensitive detectors.

A 1 m custom cable was fabricated in-house to connect the detectors to the PTW cable and Farmer electrometer. This cable was required to adapt the 3-lug BNC triaxial bulkhead receptacles on our detectors to the PTW TNC threaded triaxial cable that were used with the Farmer electrometer (TNC threaded triaxial bulkhead receptacles could not be sourced). This custom cable consisted of one Pomona 5218 3-lug BNC triaxial male connector (Pomona Electronics, Everett, WA, USA) [257], one Amphenol RF TNC (threaded) 7/16-28 triaxial connector, Part No. 31-8357-6 (Amphenol RF, Danbury, CT, USA) [258] and 1 m of Belden RG-58A/U triaxial cable (Belden Inc., St. Louis, MO, USA) [259].

A Keithley 6430 Subfemtoamp Remote SourceMeter (Keithley Instruments, Inc., Cleveland, OH, USA) [260] (hereafter referred to as “Keithley electrometer”) is also an electrometer that was used as a high-voltage source with a range from  $-210$  to  $210$  V, and used to measure detector current over time. A remote preamplifier (Keithley Remote Preamp) was required to connect the triaxial connectors of our detectors to the Keithley instrument. This unit was used for its high current sensitivity and temporal resolution, and was useful for analyzing leakage current at pA levels. Voltages from the Keithley electrometer and the Dosimeter were typically applied to the top electrode of the diamond surface as shown in Figure 3.5.

A 10 m (3-lug) triaxial cable, which was fabricated in-house, was required to connect the detectors to the Keithley electrometer. The finished cable consisted of two Pomona 5218 3-lug BNC triaxial male connectors [257] and Belden RG-58A/U triaxial cable [259].

The Keithley electrometer was controlled remotely via computer and LabVIEW 7.1 (National Instruments Corp., Austin, TX, USA) [261]. Virtual instruments were programmed to control operation and data acquisition of the detectors.

### 3.3 Electrodes

A number of suitable materials exist to form electrodes on diamond films, e.g. Au, Ag, Ti and W, or multilayer combinations thereof. Silver (and silver-loaded epoxy adhesive) was chosen for the detectors tested during this study for its high conductivity, relatively small atomic number ( $Z = 47$ ) and low cost compared to gold. This section describes surface preparation required before the sputtering or thermal evaporation of metal electrodes.

Surface preparation and metallization were conducted by the author in the University of Canterbury Nanofabrication Laboratory.

### **3.3.1 Surface Preparation**

Removing contaminants and/or diamond-like carbon species from the surface of diamond films was important for successful sputtering or evaporation of metal electrodes, or contacts. A typical procedure was to degrease the sample, followed by an acid bath and another degrease. This procedure was a simplified version of a more rigorous surface cleaning process used for diamond photodetectors, and described in detail by Lansley [262]; it was also useful for etching contacts when necessary.

The acid bath procedure differed depending on concentrations recommended for wet chemical etching of different metals [263,264]. Note that the time it took for the solution to finish varied depending on the application e.g. thickness of contacts.

These procedures and list of material and wet etchants can be found in Appendix A.

### **3.3.2 Metallization**

Metal electrodes or contacts were required to apply an electric field and measure current through the bulk of the diamond. The application of any number of metals was performed by either sputtering or evaporation. Several elements were considered initially for metallization, although a material with a low atomic number  $Z$  would be ideal as discussed in Section 2.7.

Before metallization, a choice of electrode geometry and corresponding mask was required. Circular electrodes were used, and diameters of 1 and 2 mm were chosen depending on the surface area being  $3 \times 3$  or  $> 5 \times 5$  mm<sup>2</sup>, respectively. An aluminium mask that also served as a sample holder was fabricated to create these shapes. A minimum of 100 nm was found to be sufficient for electrode thickness, but an estimated 150 nm was used as a target for all films. Optimization of electrode thickness and material is one topic for further research; Monte Carlo simulations within our research group have begun to explore this area [61].

Metallization of the majority of electrodes during this project made use of thermal evaporation. Under low pressure ( $\sim 10^{-6}$  torr), the material was vaporized via direct current heating from a MoAl<sub>2</sub>O<sub>3</sub> boat in which it was placed. The vapor then is deposited onto the sample by condensation. The evaporator was made by Balzers (Baltec, Liechtenstein) and equipped with a Sigma Instruments Model QSG201D quartz crystal thin film monitor



(Inficon Holding AG, Bad Ragaz, Switzerland) [265]. More details regarding thermal evaporation can be found in the literature e.g. Sze [266].

Some electrodes were also deposited via sputtering. In this process, the target material is bombarded by energetic ions that release a fraction of the atoms that then condense onto the sample. Using a BOC Edwards Auto 500 DC/RF Magnetron Sputtering System [267], several targets were used to sputter electrodes. See Figure 3.5 for an example of sputtered Al, Cu and Ag contacts and thermally evaporated Au contacts onto a  $10 \times 10 \text{ mm}^2$  Diamonex sample.

Thermal evaporation was the chosen method with which to evaporate Ag contacts onto the diamond films used as detectors in this project.

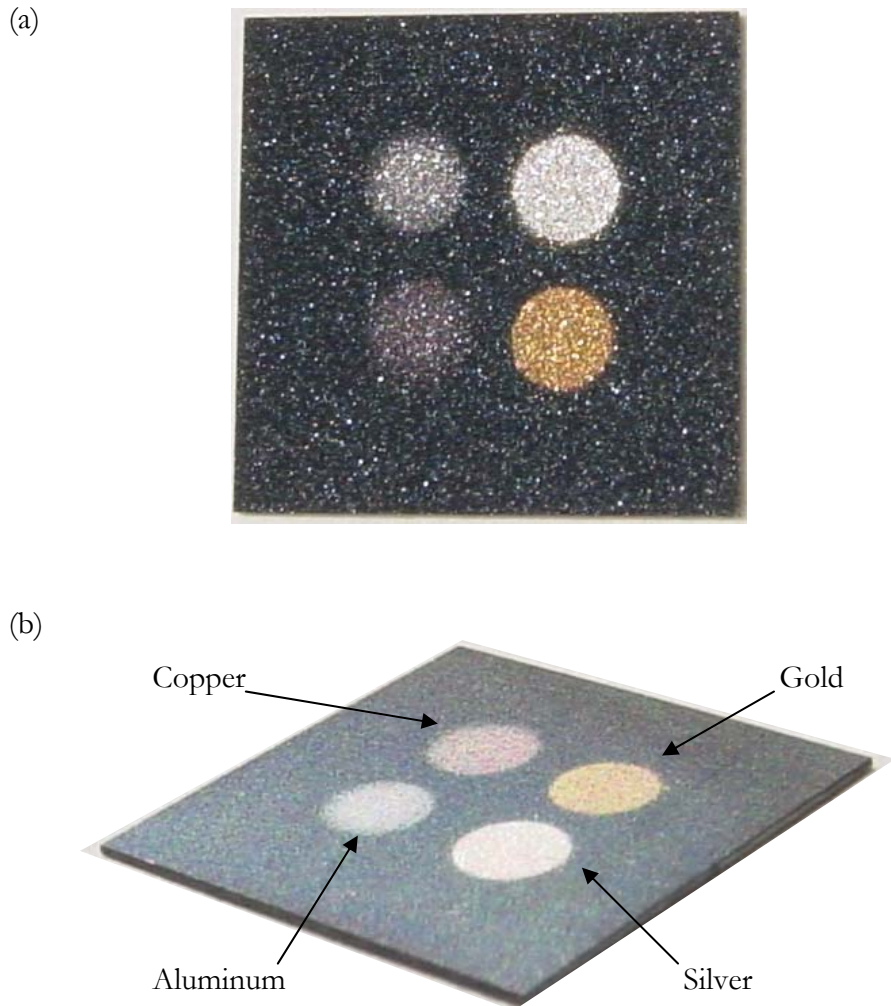


**Figure 3.5.** A  $10 \times 10 \times 0.2 \text{ mm}^3$  Diamonex sample with four different metal electrodes on (a) the growth surface and (b) the opposing substrate surface.

## 3.4 Detector Designs and Fabrication

Enclosures, encapsulations, etc. around a sensing device or detector require appropriate material and geometry to adapt to any number of applications. Detector packaging went through three stages of development during this project, from a relatively large printed circuit board (PCB) design, to a slender, Perspex-encapsulated device that could be used in an existing radiation dosimetry system. The detector design in Section 3.4.2 did not get used under clinical conditions; the detectors in Sections 3.4.3 and 3.4.4 went on to be used for dosimetric investigations.

Circuit design was quite simple, as the main objective was to apply an electric field through the bulk of a diamond film via a sandwich-type configuration (Section 2.4). The result was either to use a PCB and/or wire with which to bond to the diamond film contacts. By adding either a coaxial or a triaxial connector, the sensing material could then be terminated to a voltage and current measurement source; the electrometers used in this project provided both requirements.

### 3.4.1 Large PCB Detector

The first detector design was based upon using a printed circuit board (PCB), with the sensing material (diamond) at one end and a TNC coaxial connector at the opposite end. The slender shape of the PCB (Figure 3.6) was used for two reasons. First, it is important that the sensing material (Figure 3.7(a)) be located sufficiently far from the connector (Figure 3.7(b)). Any scattering of radiation from the connector and cable is therefore greatly reduced. In addition, the long, slender design allowed for placement far into the interior of a phantom for dose measurements. The overall design was by no means optimal, but served as a starting point to acquire meaningful measurements.

The layout was drawn using Easily Applicable Graphical Layout Editor (EAGLE) Version 4.16r1 for Windows (CadSoft Computer, Inc., Penbroke Pines, FL, USA) [268]. This board layout could then be used as a template to manufacture a PCB.

Fabrication of the detectors at first appeared straightforward. A threaded coaxial connector (Pomona Electronics, Everett, WA, USA) [269] was soldered to the PCB as shown in Figure 3.7. Attaching the diamond films, however, was not so easy. First, it was attempted to attach both electrodes to the copper tracks of the PCB via soldering and thin copper wire. To maximize the available electrode surface area for irradiation, wire bonding the top electrode was then attempted, but the surface of these particular diamonds were too rough

and hard to bond to the relatively thin Au electrode. Diamond films were finally glued with Ag loaded epoxy adhesive (RS 2410 Conductive Epoxy Resin and Hardener #186-3616; RS Components NZ, Auckland, NZ) [270].

This detector was designed and used with equipment that used coaxial connections, as it did not have the requisite triaxial connections necessary to be used with the electrometers mentioned in Section 3.2.3. It was first sought to determine if these diamond films, as inexpensive as they were, could respond to clinical x-rays with sufficient sensitivity. However, there were issues even before the detectors could be measured under irradiation.

Two functioning large PCB detectors were measured for their I-V characteristics using a 1000 V regulated high voltage supply and a Trade Quip hand-held sub-microampere digital multimeter (ISL Industrial Ltd., Auckland, New Zealand). The most significant result was that there was too much leakage current. At a polarizing voltage of 100 V, past investigations in literature found leakage current in 100-400  $\mu\text{m}$  thick CVD films to be typically no more than 100 pA. In contrast, these detectors measured 400  $\mu\text{A}$  and 30  $\mu\text{A}$  for the 200- $\mu\text{m}$  film detector (D01) and the 400- $\mu\text{m}$  detector (D02), respectively – three orders of magnitude higher than expected. Resistance measurements of freestanding diamond films using a parameter analyzer (see Section 3.2.3) ruled out the possibility that the CVD diamond itself was to blame (as well as the results of improved designs in the following Sections). A possibility that high leakage current was due to the PCB itself was not feasible since these boards inherently have high resistivities. The most likely problem was the overall design itself that led to challenges soldering and bonding the diamond successfully to the PCB. It was believed that the attempt to successfully solder to the thin Au electrodes only compromised the high resistivity of the circuit, leading to electrochemical effects due to ionic contamination [271] that create paths of lesser resistance around the diamond surface.



**Figure 3.6.** Board image of the large PCB detector used for manufacture.

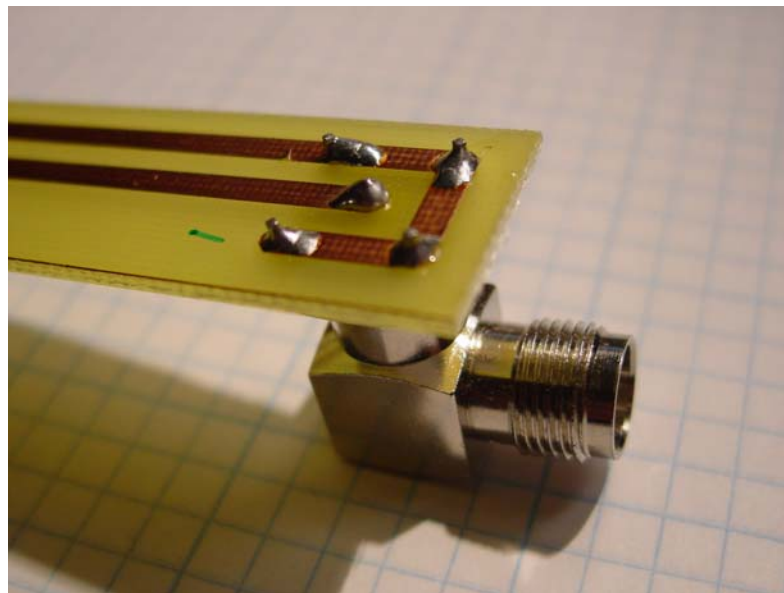
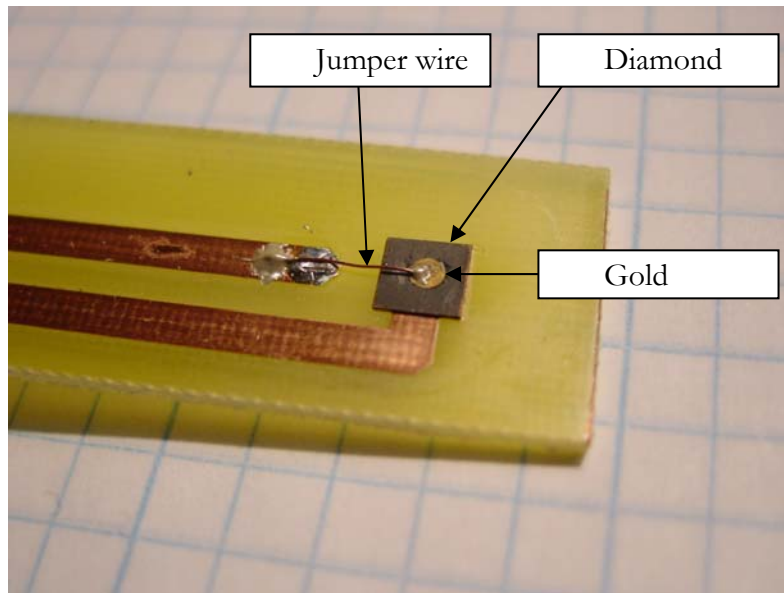


**Figure 3.7.** Photos of the ends of large PCB detector #1. (a) Sensing end of the detector; (b) Threaded BNC coaxial end of the detector.

These detectors were also found to lack stability at reasonable voltages. For example, it was not possible to measure D01 any higher than 150 V, where currents were highly sporadic. At 400 V, D02 was not erratic but still time dependent. It took 10 minutes for the current to stabilize initially from 162  $\mu\text{A}$  to a final steady reading of 174  $\mu\text{A}$ , although stabilization is expected with diamond films.

Design and fabrication was not successful and resulted in too much leakage current. Therefore, the detector was unfit for irradiation experiments due to low ratios of induced currents to leakage currents.

### 3.4.2 “Thick Perspex” Detector

The “thick Perspex” detector design appeared more like a detector for clinical dosimetry than the first design in Section 3.4.1. This detector did not use a PCB, but instead two 0.8 mm thick insulated wires that also functioned as mechanical support (see Figure 3.8). The wires can be seen in more detail in Figure 3.9 where the encapsulation has been removed. Wires were bonded to the center pin and grounded casing of a Pomona 5219 3-lug BNC triaxial bulkhead receptacle (Pomona Electronics, Everett, WA, USA) [269]. The use of triaxial connectors and triaxial cable (triax) provides superior protection against interference over coaxial components. Perspex (Lucite International, Southampton, United Kingdom) [272], which is one of the many trade names of poly(methyl 2-methylpropenoate), was used to encapsulate devices and functioned as a water-equivalent build-up material<sup>8</sup>. Using Perspex allowed for a more sensitive response, although the thickness of the Perspex stock used here (30 mm in diameter, giving a build-up window of 10 mm) was not optimal for electronic equilibrium.

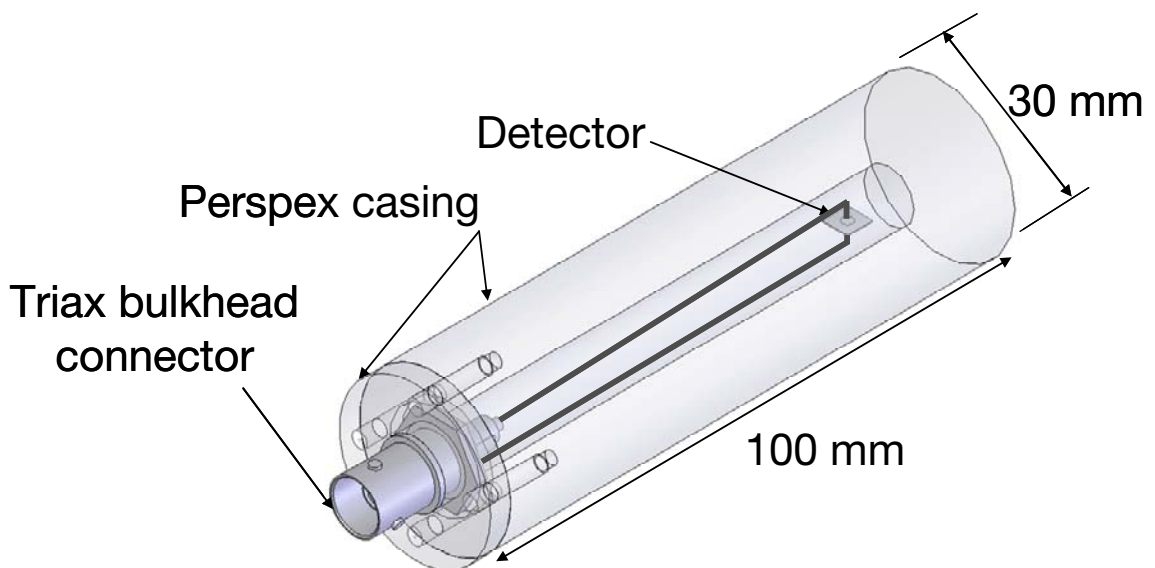


**Figure 3.8.** Schematic of thick Perspex detector [168].

<sup>8</sup> Perspex has been considered for medical dosimetry since the mid-1960s by Orton [273].

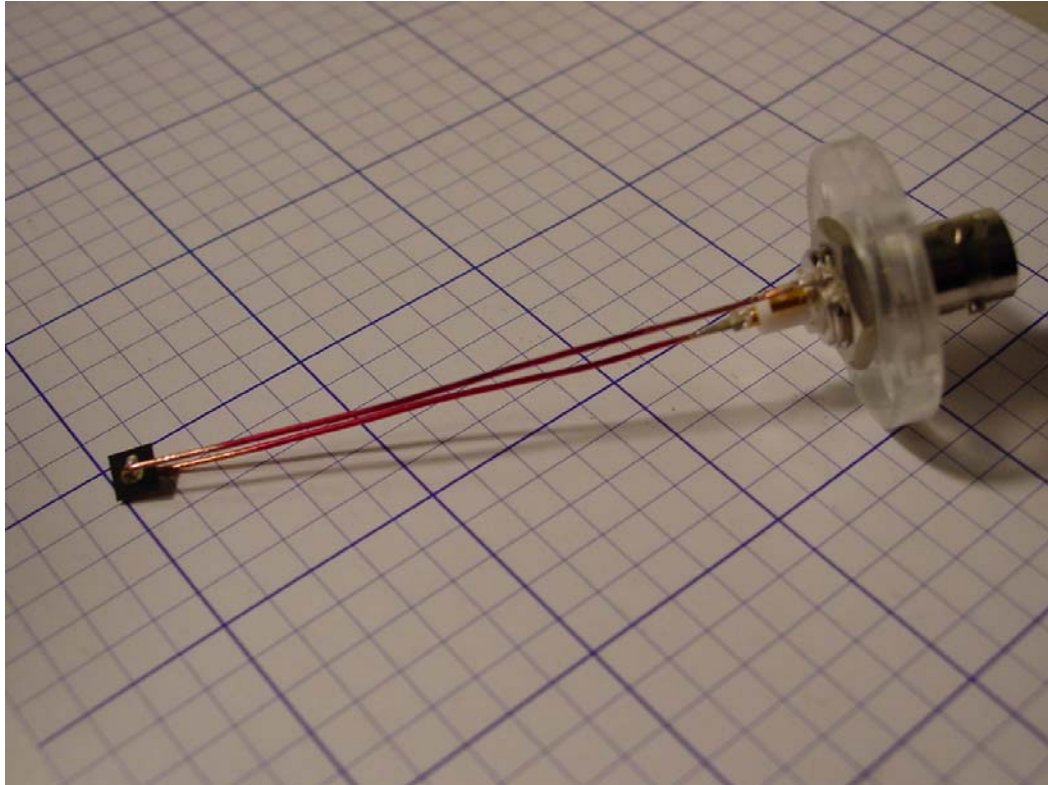


**Figure 3.9.** Thick Perspex detector without encapsulation.

Overall, the design was a simple and cost-effective way to test the first set of diamond films in hospital. It was convenient to find cylindrical Perspex stock that was readily available in the machine shop, although the thickness of the resulting encapsulation was not quite optimal for maximum response at 10 mm. However, the cylindrical design and fixed thickness of build-up material allowed for a complete 360° analysis of angular dependence via accelerator gantry rotation. In addition, the design allowed for removable encapsulation so that thicker Perspex cylinders could be used, or so that other wired diamonds could use the same encapsulation. Using only wires ruled out any problems that might arise from using PCBs. However, fastening wire at any thickness from the triaxial connectors to thin electrodes proved to be challenging, especially at lengths that were used initially for the thin Perspex detectors that again tested Diamonex films in the next section (Section 3.4.3). Using triaxial components here and in future detector designs allows them to be used with existing dosimetry equipment in hospital.

Following satisfactory results of I-V testing, this detector design was used for a number of irradiation measurements that would test the suitability of Diamonex films for detecting 6 MV x-rays [168].

### 3.4.3 “Thin Perspex” Detector

A third detector design was used so that diamond films could be compared to ionization chambers using their corresponding phantoms for dosimetry. The more sophisticated encapsulation shown in Figures 3.10–3.12 takes the shape of the same Perspex sleeve that was designed to protect Farmer ionization chambers. This detector was then capable of being placed in the same Solid Water phantom arrangement used for routine dosimetry measurements. The physical separation of the electrical connections from the sensing material was again used to help reduce interference from x-ray scattering like the PCB detector in Section 3.4.1.



**Figure 3.10.** Thin Perspex detector using free air wire attachment.

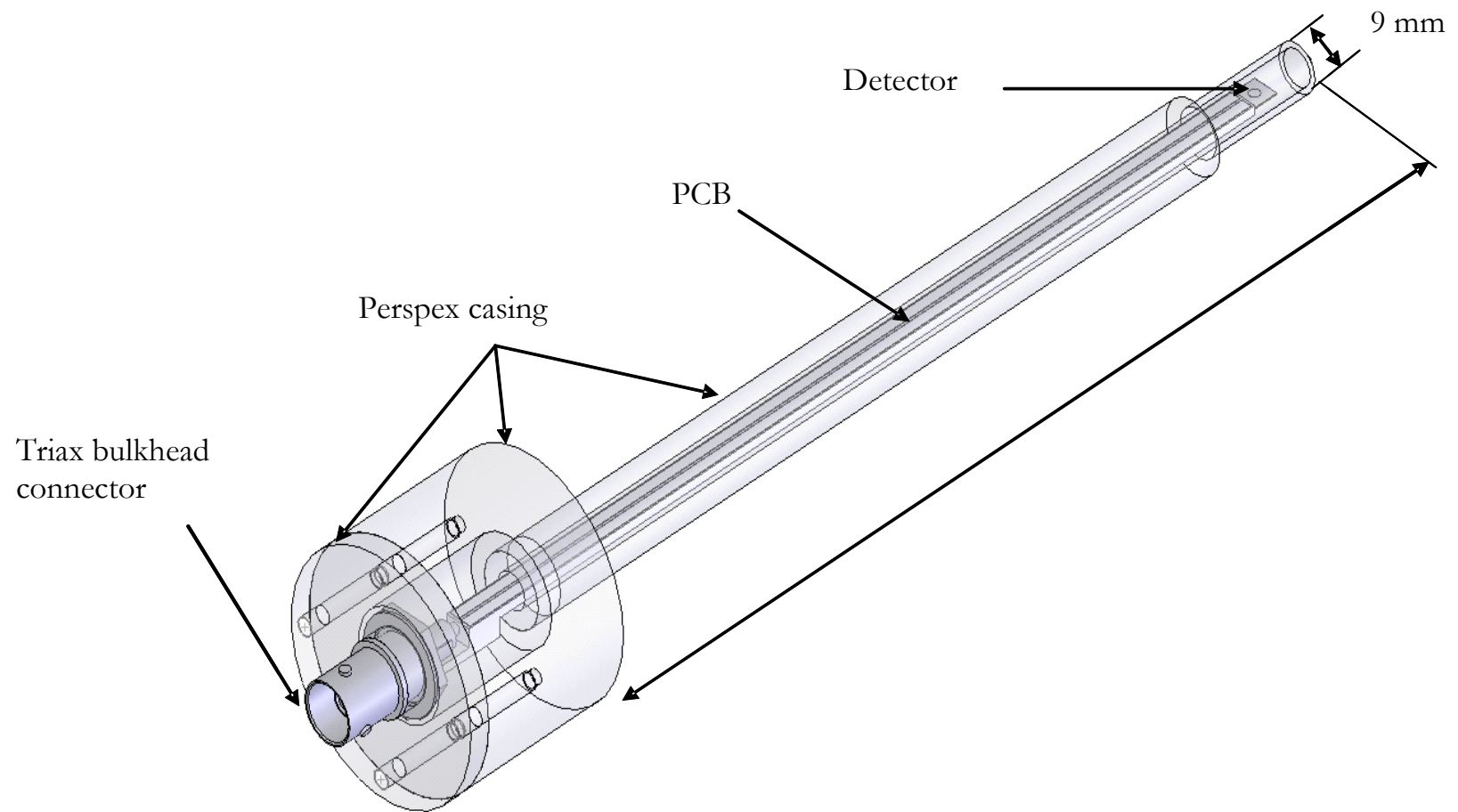


**Figure 3.11.** Schematic of thin Perspex detector [217].



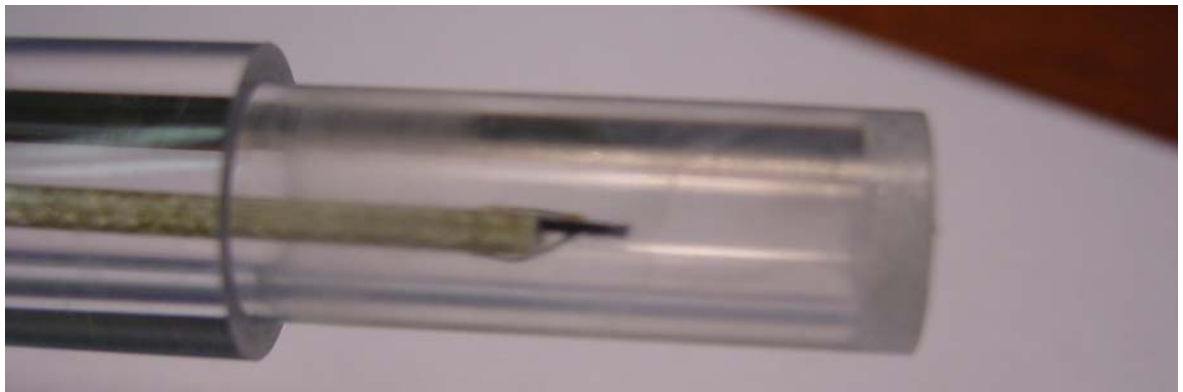
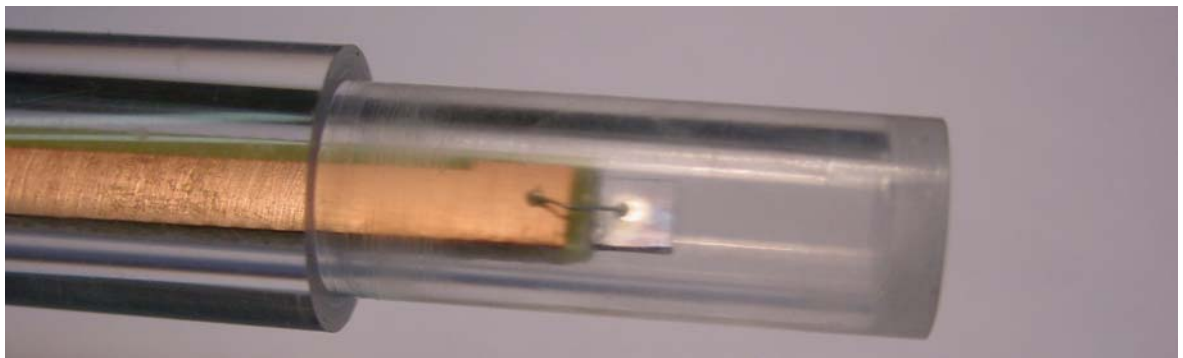
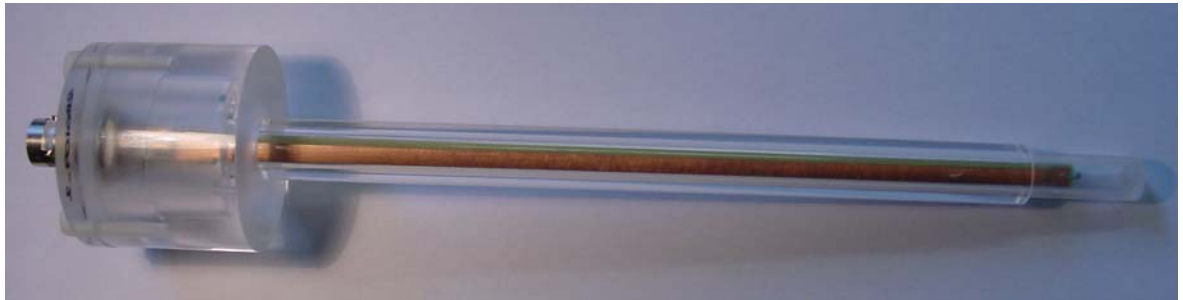


**Figure 3.12.** Thin Perspex detector with PCB (top) with close-ups of the diamond showing the Ag electrode (middle) and a side view (bottom).

The detector consisted of the same materials as used in the two previous designs, except that the geometry was now more optimized for clinical dosimetry. There were two versions of this thin-sleeved detector. The first version used the same wiring design with no PCB as shown in Figure 3.10. It was used in the shorter detector in Section 3.4.2. In the second (and final) version, diamonds were attached with super glue to the end of a narrow  $176 \times 5 \times 1.5 \text{ mm}^2$  PCB with 3-mm wide copper tracks, and then electrically bonded via copper wire and silver loaded epoxy. Both detectors consisted of Perspex encapsulation that comprised of three parts: a thin walled  $12 \text{ mm } \varnothing \times 175 \text{ mm}$  sleeve with a  $6 \text{ mm } \varnothing$  centre, a  $40 \text{ mm } \varnothing \times 40 \text{ mm}$  mid-section and a  $40 \text{ mm } \varnothing \times 4 \text{ mm}$  thick plate (see Appendix B for technical illustrations). The window thickness at the end of one sleeve was machined down to 1 mm as shown in Figure 3.12. The sleeve was then glued to one end of the mid-section. Once the triaxial receptacle was attached to the plate, the PCB was mounted to a triaxial bulkhead receptacle. The mounted detector could then be inserted into the glued Perspex combination. Three or four threaded holes were drilled into the mid-section and plate to use plastic screws, and the receptacle was sealed with super glue to complete construction.

The cavities in some detectors were filled with paraffin-based dental wax (Metrodent, Huddersfield, Yorkshire, UK) [274] to eliminate air around the diamond sensor. This was used to minimize fluence perturbations due to a loss of electron equilibrium at the cavity surface. Wax was inserted and melted inside the Perspex sleeve before insertion of the device. I-V testing was performed before and after wax was inserted into devices and differences were negligible.

Testing of the final design, which included a PCB and optional wax, was successful. Although its fabrication was more labour intensive, this detector could be placed and rotated in an existing phantom, has the potential to be used in water phantoms and uses triaxial connectors that can adapt to either a 3-lug or threaded triaxial connector that can be used with existing dosimetry equipment in hospital. By use of a PCB with three tracks, further noise reduction and/or collimation of the applied electric field could be realized by making use of the centre conductor or guard ring of the triaxial components. This may be tested in future work.

This detector design was used for the majority of measurements performed for dosimetric analysis of diamond films.

## 3.5 Experimental Setup

In this section, the x-ray treatment unit used to investigate detector response and the conditions for irradiation experiments in hospital for the “thick Perspex” and “thin Perspex” detectors are described. The thick Perspex detector was not used in any custom-fitted Solid Water and thus required a fixture. The thin Perspex encapsulation was designed specifically for use in a pre-drilled Solid Water phantom used for routine dosimetry with an ion chamber.

### 3.5.1 Source of X-rays

Irradiation measurements were performed in Oncology Services at Christchurch Hospital, Christchurch, New Zealand, using a fixed 6 MV x-ray beam from a Varian Clinac 600C linear accelerator (Varian Medical Systems, Palo Alto, CA, USA) [275] as shown in Figure 3.13. Available nominal dose rates of 50, 100, 150, 200 and 250 monitor units per minute ( $\text{MU min}^{-1}$ ) were obtained by varying the pulse repetition rate of the linear accelerator (linac). An MU corresponds to the standard unit of output of a machine that is then calibrated with reference setup parameters to relate machine output with absorbed dose ( $\text{Gy MU}^{-1}$ ). The default gantry position ( $0^\circ$ ) is the overhead position as shown in Figure 3.13. The gantry is capable of rotating  $180^\circ$  in either direction from the default position. The accelerator was located in a shielded room, or bunker, with a maze-like exit and an adjacent control area. An access shaft in the concrete wall was used when necessary to feed cable from the experimental setup to a PC in the control area. Linacs at megavoltage x-ray energies of 4–8 MV like this Varian unit are the workhorses of radiation therapy departments, which treat medium to deep seated tumours of the head, neck, extremities and other organs [276].



**Figure 3.13.** Varian 600C linear accelerator and phantom.

### 3.5.2 Setup for “Thick Perspex” Detectors

Measurements involving thick Perspex detectors (Section 3.4.2) did not include an additional phantom or other build-up material. Because of its cylindrical shape and sufficient thickness, this detector was clamped to a fixture on a couch so that the centre of the sensitive volume of the diamond coincided with the isocenter of the accelerator gantry (see Figure 3.14). This setup created a fixed source-detector distance (SDD) and source-axis distance (SAD) of 100 cm and allowed for complete measurements of angular dependence of the detector response. Changes in dose rate were obtained by changing the dose per pulse from the accelerator. With this setup and thickness of build-up material, 1 MU = 0.98 cGy.

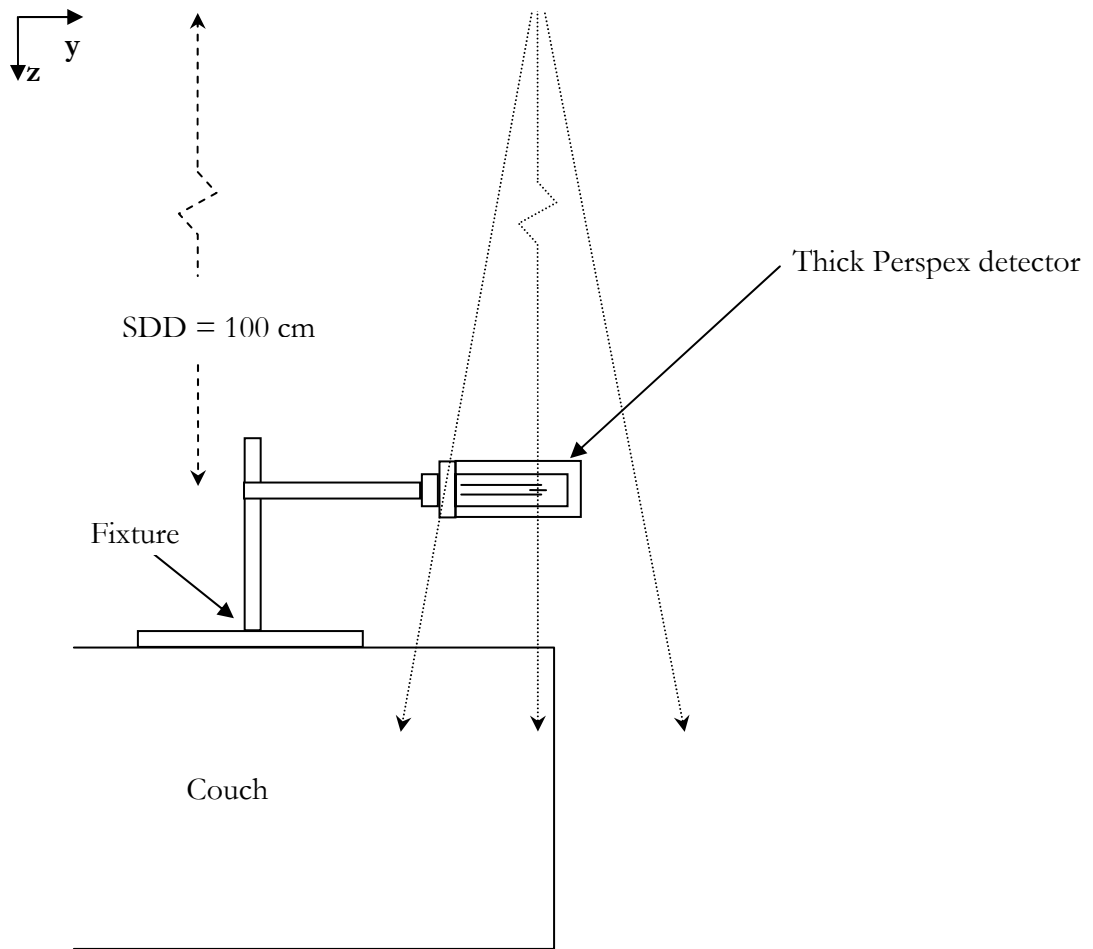


**Figure 3.14.** Setup for thick Perspex detectors with an SDD = SAD = 100 cm.

### 3.5.3 Setup for “Thin Perspex” Detectors

Thin Perspex detectors were first calibrated against a Farmer ionization chamber (PTW, Freiburg, Germany) [277] in a set-up used for routine dosimetry measurements (see Figure 3.15). Reference conditions for the detectors were placed in the central axis of the beam at  $z_{\text{ref}}$  of 10 cm depth in a  $30 \times 30 \times 20 \text{ cm}^3$  Solid Water slab phantom (Gammex, Inc., Middleton, WI, USA) [278] with a source-to-surface distance (SSD) of 90 cm, SAD = 100 cm and a radiation field size of  $10 \times 10 \text{ cm}^2$ . Typical orientation of the diamond film inside the phantom was perpendicular to the direction of radiation or “face-on”; perpendicular orientation was named “edge-on”. Voltages were applied to the top electrode, which typically

faced the source of radiation as shown in the figure. The detectors were fabricated such that the sensitive volume of a diamond film was concentric with the target coordinates in the Solid Water ( $\pm 0.5$  mm for  $3 \times 3$  mm<sup>2</sup> film sizes). The photon beam is locally calibrated such that 100 MU is equivalent to an absorbed dose of  $0.77 \text{ J kg}^{-1}$  or gray (Gy); at an SSD = 98.5 cm and 1.5 cm depth ( $z_{\text{max}}$ ), this corresponds to 1.0 Gy using IAEA TRS-398 Code of Practice [279]. At least 5 cm of Solid Water build-up material was placed between the detector and the couch as required by TRS-398.

This setup was used for a number of measurements including percentage depth dose, tissue-phantom ratios, output factors and off-axis profiles (lateral beam measurements). When necessary, slabs were rearranged to change the depth of the detector, with corresponding changes in SSD, SDD and depth  $z$ . The couch was moved along the  $x$  axis for off-axis profiles.

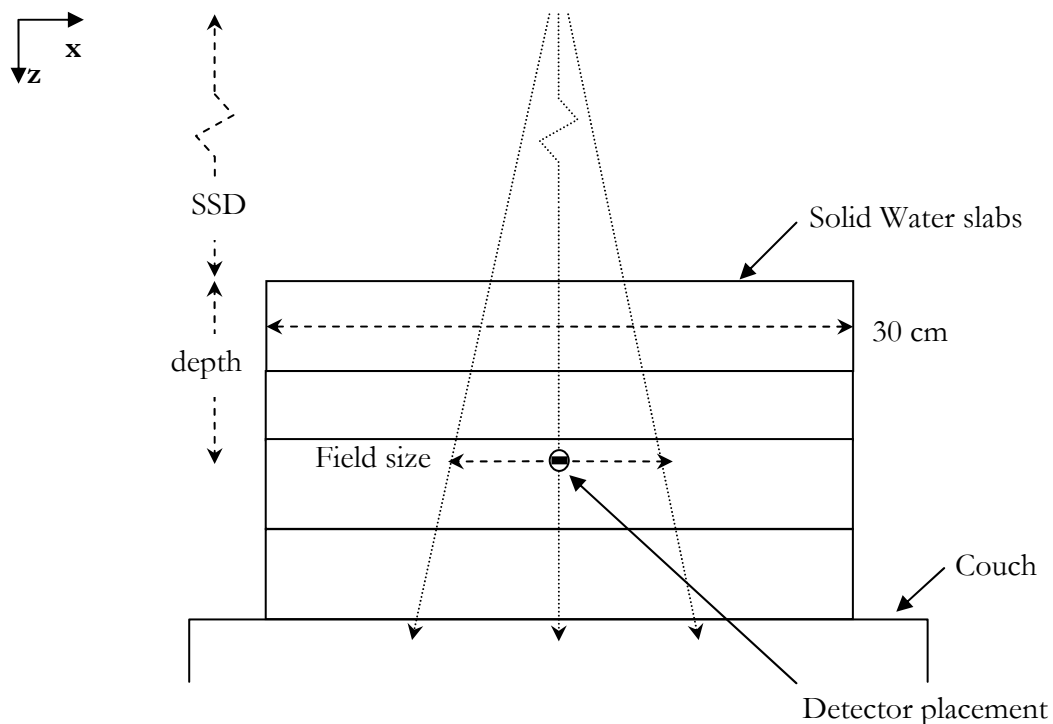


**Figure 3.15.** Thin Perspex detector setup using Solid Water slabs.

## **3.6 Concluding Remarks**

Chapter 3 introduced the diamond films that were involved in this project and the methods by which they were characterized. Different detector designs were presented and detector fabrication was described. The experimental setups used for the “thick” and “thin” Perspex detectors for dosimetric investigations were also presented.

The next chapter provides results and discussion of diamond film characterization as described in Section 3.2 using spectrophotometry, Raman spectroscopy and bulk conductivity studies.





# 4. Results of Diamond Film Characterization

---

Presented in this chapter are the results and discussion of the characterization of several types of diamond films, performed primarily before they were evaluated for their suitability as x-ray detectors. Principles of each method are described in Section 3.2.

The first goal in this research was to examine a range of commercially available synthetic diamond films. To analyze this material, it was helpful to characterize the films before they were metalized and bonded for detection. As stated previously, characterization of these films was performed so that material properties may then be correlated with dosimetric behaviour. These techniques for material analyses were described in Section 3.2. Films were first investigated using spectrophotometry in Section 4.1. Section 4.2 then provides the results and discussion using Raman spectroscopy. Section 4.3 discusses bulk conductivity studies.

## 4.1 Spectrophotometry

Thirteen films sourced from three manufacturers were examined using spectrophotometric analysis, although two did not give satisfactory results. The Diamonex material was not suitable for optical transmission; this was a consequence of their opaqueness. Three absorbance patterns resulted from 11 films as illustrated in Figures 4.1–4.3, where absorbance  $A = -\log(I_0/I)$  and  $I$  is the intensity of radiation at a known wavelength that traversed a sample. In Figure 4.1, the results are similar for (a) the single crystal CVD (E6SCPL) and (b) the thermal grade pCVD (E6TM180). The two HPHT (E6SC1b) diamond films in Figure 4.2 are also quite similar. Figure 4.3 illustrates almost identical absorbance data for single crystal (E6SCP2), electronic quality pCVD (E6EL200 and E6EL500), optical quality pCVD (E6OP), and high quality detector grade polycrystalline CVD (DM100, DM200 and DM400). As shown in Figure 4.1, noise seen at high absorbances is due to the detection limit of the instrument (for example,  $A = 4$  means 0.01% transmittance). Bumps in the signal are due to a change in grating.

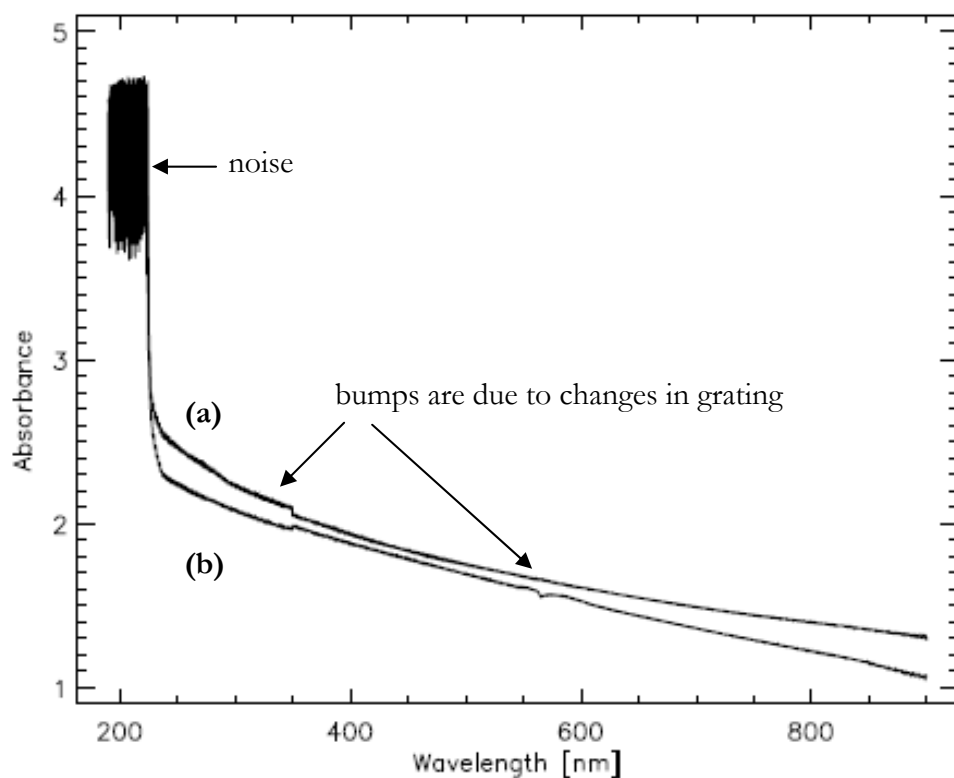


**Figure 4.1.** Absorbance as a function of wavelength for (a) single crystal CVD (E6SCPL) and (b) thermal grade pCVD (E6TM180) diamond films.

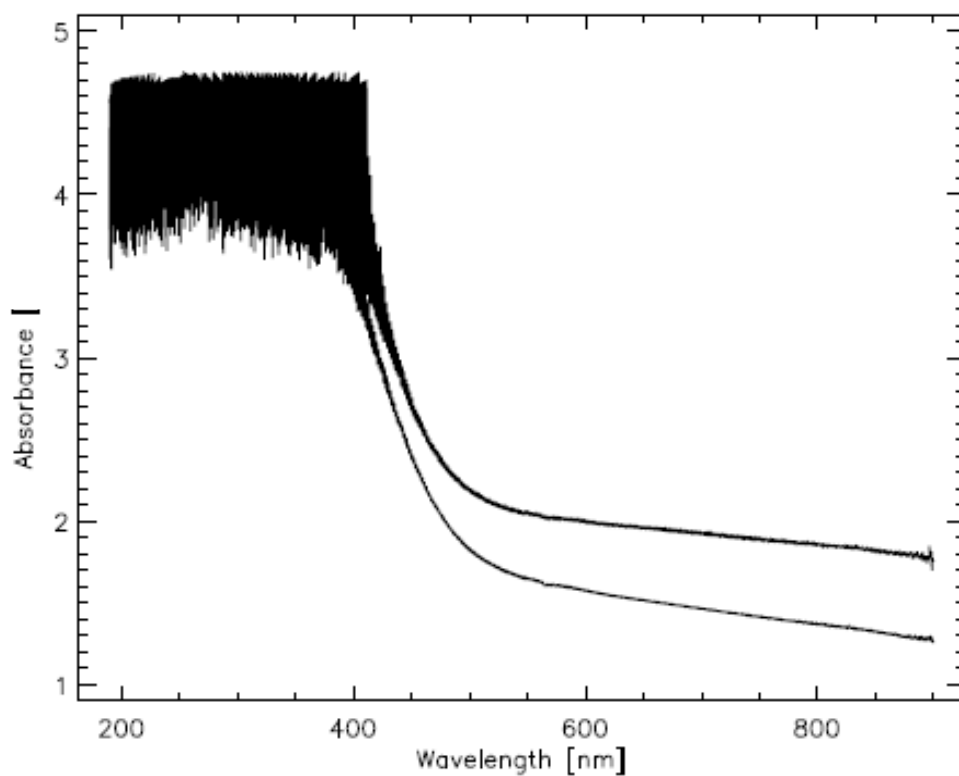


**Figure 4.2.** Absorbance as a function of wavelength for two single crystal CVD (E6SCIb) diamond films.

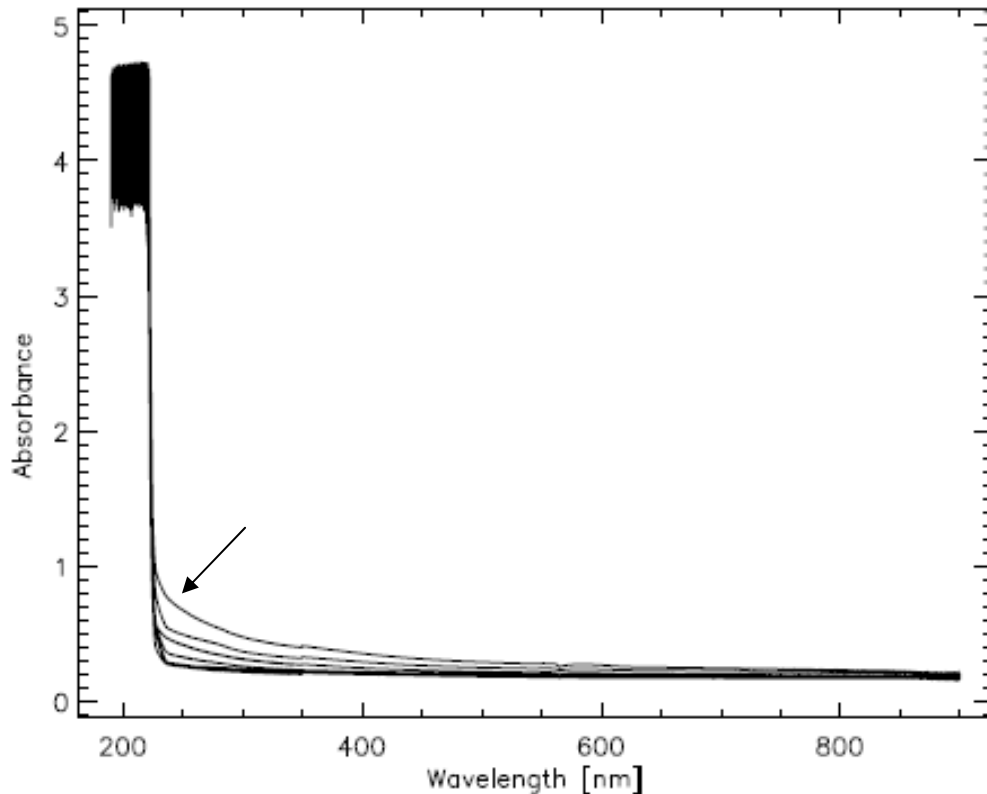


**Figure 4.3.** Absorbance as a function of wavelength for several diamond films (from high to low absorbance as shown with the arrow): E6SCP2, E6EL200, E6EL500, E6OP, and DM100, DM200 and DM400.

The sharp change or cut-off at 225 nm (5.51 eV) seen in Figures 4.1 and 4.3 is the typical diamond absorption edge that is expected for high quality polycrystalline or single crystal diamond [63,230]. From 220 to 6,000 nm, beyond the range of this particular analysis, the general absorption spectrum of diamond is due to the weak absorption of electronic transitions at residual lattice defects [64]. More specifically, most Type IIa (devoid of impurities, colourless) diamonds have a weak continuous absorption “wing” that starts in the far-infrared region and gradually increases towards the absorption edge due to Rayleigh scattering [64]. The wings in Figures 4.1 and 4.2 may indicate increased scattering due to non-diamond inclusions. The results of most films represented in the figures may then illustrate the high quality of those films including the effects of polishing to remove non-diamond inclusions. The increased absorbance in Figure 4.2 is wider in comparison, with a softer absorbance edge, which starts around 400 nm (3.10 eV). The absorption continuum in these HPHT films is the most characteristic feature of both natural and synthetic Type Ib

diamonds. This was reassuring evidence that the HPHT films indeed contained nitrogen. The defining feature of Type Ib diamonds is the N3/N2 centre, which consist of three N atoms (N3) paired with two N atoms (N2) surrounding vacancies [280]. Studies have shown that more optimal dosimetric properties could be obtained with the incorporation of low and precisely controlled nitrogen concentrations [182-184,246,281].

Overall, these results served as a qualitative analysis of the material quality of films before they were tested for irradiation studies. Any concentration of non-diamond inclusions such as nitrogen may have a strong effect on electrical conductivity of the detector.

## 4.2 Raman Spectroscopy

Seventeen diamond films purchased from the three manufacturers were analyzed using Raman spectroscopy before evaporation or sputtering of electrodes. The focus of this section will be on films that were chosen and packaged as detectors. Raman spectra of films that were not used in this thesis but may be used for future work are given in Appendix C.

The quality of films was analyzed using 514.5 nm excitation with a 1-mm spot size (see Section 3.2.2 for more details). Frequency calibration [282] of the data were performed using Ar, Hg and Ne spectra. With a table of known wavelengths [62], a polynomial function was then fit to the observed wavelengths to calculate corresponding wavenumber shifts from the excitation wavelength. As mentioned in Section 3.2.2, Raman spectra are commonly presented not in wavelengths [nm] but in units of wavenumber shift [ $\text{cm}^{-1}$ ].

The ranges used in this analysis allow for observations at room temperature over the range of first and second-order Raman scattering, or 0 to  $2668 \text{ cm}^{-1}$  [64]. The resulting spectra are illustrated in Figures 4.4–4.7. Films were grouped in the figures where possible according to their manufacturer and type. All samples exhibited a sharp absorption band at  $1332 \text{ cm}^{-1}$ , which corresponds to the well-known first-order phonon mode. Data showing this sharp absorption diamond with no other noticeable peaks indicates good quality diamond. The intensity of the first-order phonon peak was relatively small in some polycrystalline samples.

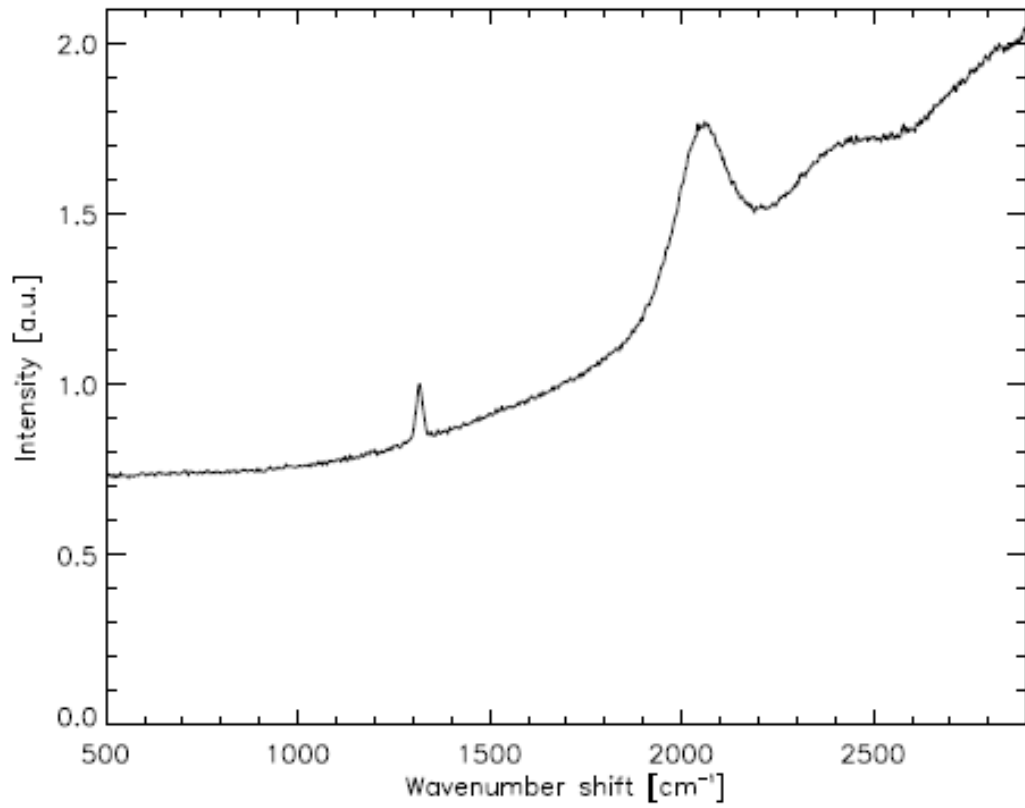


**Figure 4.4.** Raman spectrum for Dx200.

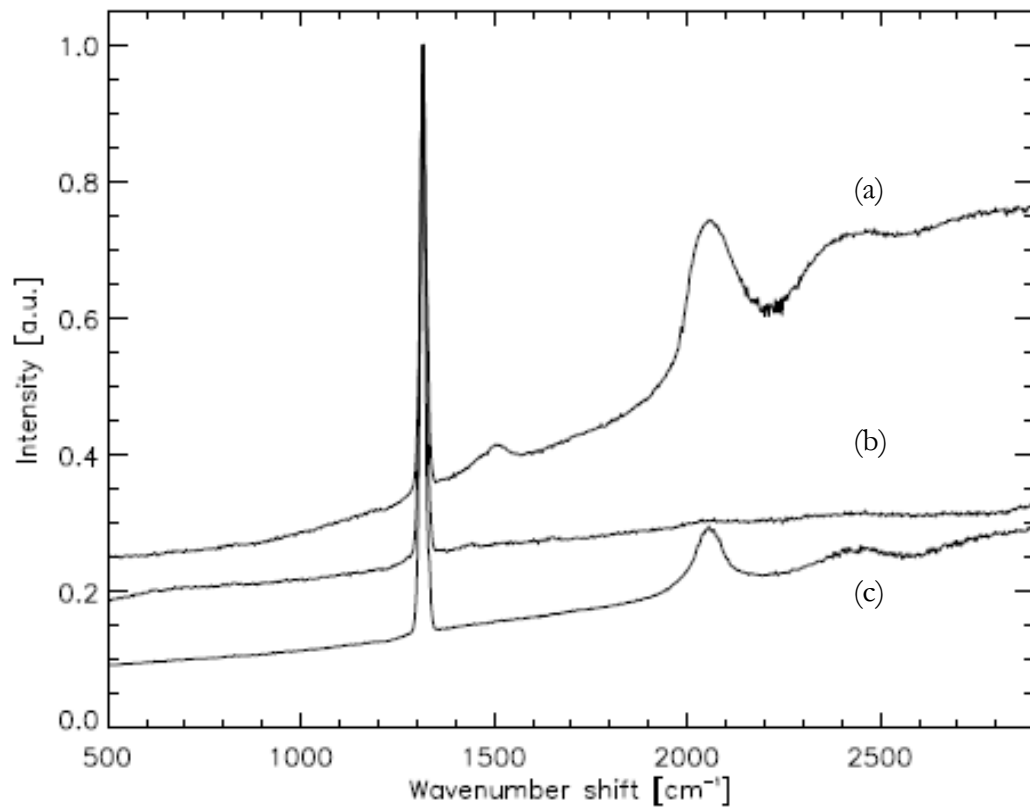


**Figure 4.5.** Raman spectra for Diamond Materials samples (a) DM200, (b) DM100 and (c) DM400.

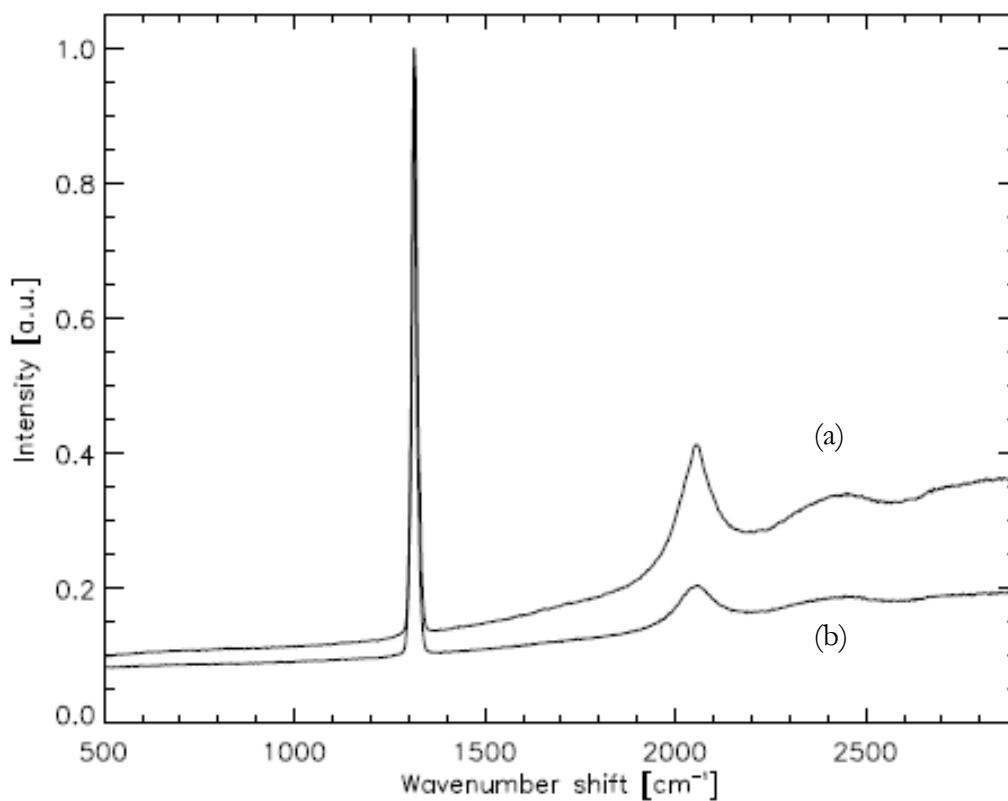


**Figure 4.6.** Raman spectra for Element Six samples (a) E6SCP2 and (b) E6SCPL.

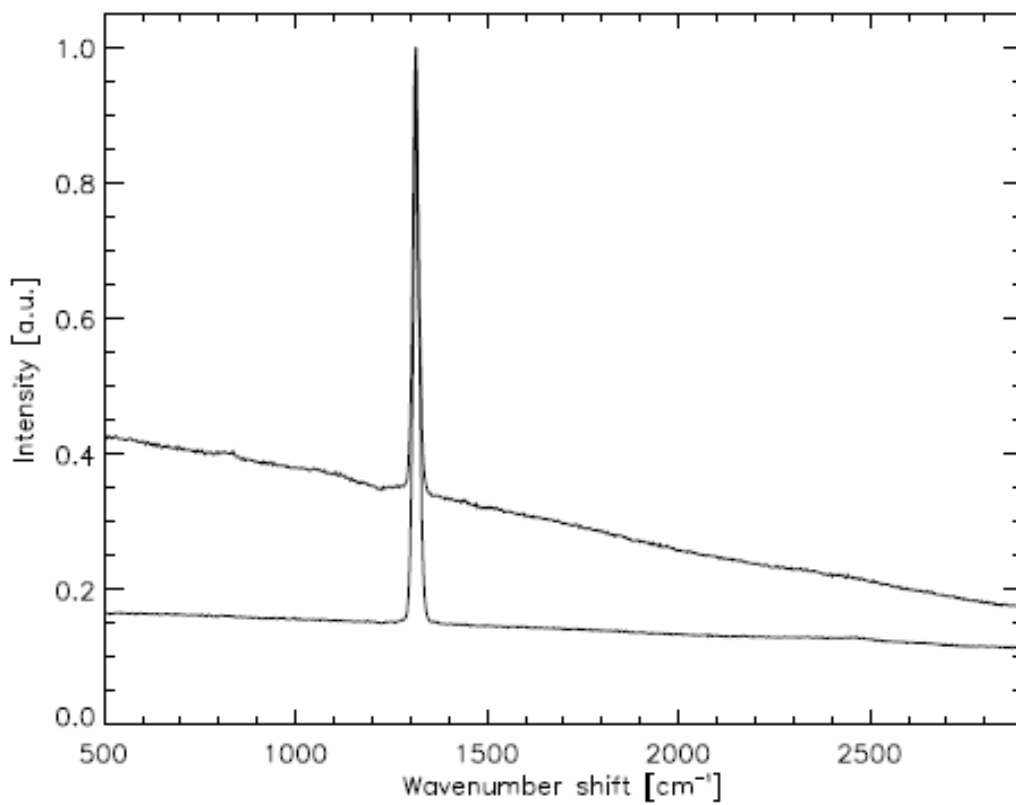


**Figure 4.7.** Raman spectra for two E6SC1b samples.

In Figure 4.4, the spectrum of one 200  $\mu\text{m}$ -thick Diamonex film is plotted, which was typical for all Diamonex films investigated. The weak intensity of the diamond line is due to a decrease in grain size in polycrystalline diamond [64]. The lack of a strong diamond peak also indicates a large concentration of defects, which may increase electrical conductivity. All Diamonex films exhibited peaks at  $\sim 2050$  and  $2400\text{ cm}^{-1}$ , and photoluminescence, which are indicated by broad peaks but at different intensities. These bands all correspond to N vacancy complexes in the crystal [64,182]. The same peaks and background photoluminescence are observed in two Diamond Materials films (DM200 and DM400) in Figure 4.5 and the E6SCPL and E6SCP2 diamonds in Figure 4.6. Figure 4.5, however, illustrates spectra that differ from the same quality of Diamond Materials samples. Although the films were apparently grown under the same conditions, the resulting Raman spectra appear to show the same bands but with different magnitudes. Importantly, the thinnest diamond (DM100) exhibited a clean spectrum, which lacked any non-diamond peaks.

Finally, Figure 4.7 illustrates spectra for two E6 single crystal Type Ib films. Interestingly, they do not exhibit any typical nitrogen peaks as would be expected in these yellowish diamond types. The peaks that indicate the presence of these nitrogen systems were not within the excitation range of the laser. However, these films did exhibit Type Ib characteristics using spectrophotometry in the previous section.

Future work may include a more detailed analysis of the relative quantities of nitrogen or other impurities both between samples and within the same batch from a manufacturer to measure the effect on detector behaviour.

### 4.3 Bulk Conductivity

Data in this section pertain to measurements of conductivity (or resistivity) before detectors were irradiated. By applying a voltage, leakage currents could be measured before and after diamond was irradiated. Applying a voltage sweep could also characterize the type and quality of electrical contacts on the diamond surface.

Bulk measurements were obtained for a number of films using voltage sweeps that were performed with the Keithley electrometer and with different configurations to ensure accuracy. See Table 3.1 for film details. Most films exhibited high average bulk resistivity as expected, although much lower than theory predicts ( $\sim 10^{16}\text{ }\Omega\text{ cm}$ ). Results using the HP Analyzer were up to three orders of magnitude higher than expected. A two-wire clamping fixture that was used with the Keithley electrometer also had similar results. The most

accurate measurements were made using the Keithley electrometer and triaxial connections only after diamonds had been bonded and encapsulated. Measurements during x-ray experiments using the Farmer electrometer (Section 3.2.3) and triaxial connections confirmed the results that were found using the Keithley electrometer before irradiation.

Overall, resistivities of the various materials ranged from  $\sim 10^{10}$  to  $10^{13}$   $\Omega$  cm. Leakage currents for a number of films are plotted as a function of applied field [ $V \mu\text{m}^{-1}$ ] in Figure 4.8. In the figure, the 400  $\mu\text{m}$  Diamonex films show the highest electrical conductivity in this range, followed by the E6 PC250 and TM100 films. Leakage currents, when extrapolated, would be in the tens of nA at a reference field of  $1 V \mu\text{m}^{-1}$ . These results are much lower than typical films ( $> 10^{12}$   $\Omega$  cm) and indicate that they would not be considered suitable for dosimetry. However, the Diamonex films were tested as detectors regardless of their high leakage currents and consequently showed interesting nonlinearities during dose response as discussed in Chapter 5. There is also a notable difference between the Diamonex as-grown film and matte finish, which may indicate a decrease in surface conductivity following mechanical polishing of the as-grown surface. The remaining films in the figure show orders of magnitude less conductivity.

The same leakage currents are also plotted as a function voltage in Figures 4.9 and 4.10. Figure 4.9 illustrates only Diamonex films, where currents illustrate a supra-linear I-V relationship, which indicate typical behaviour of Schottky rectifying electrical contacts. In Figure 4.10, voltage sweeps were performed from  $-210$  to  $210$  V and then from  $210$  to  $-210$  V for each film due to the higher degree of uncertainty involved when measuring the small currents in these films. Five of the films gave showed leakage currents of  $< 10$  pA at  $100$  V.

Leakage current measurements helped characterize the relative differences in electrical conductivity and served as a reference to compare leakage currents after irradiation in other investigations.



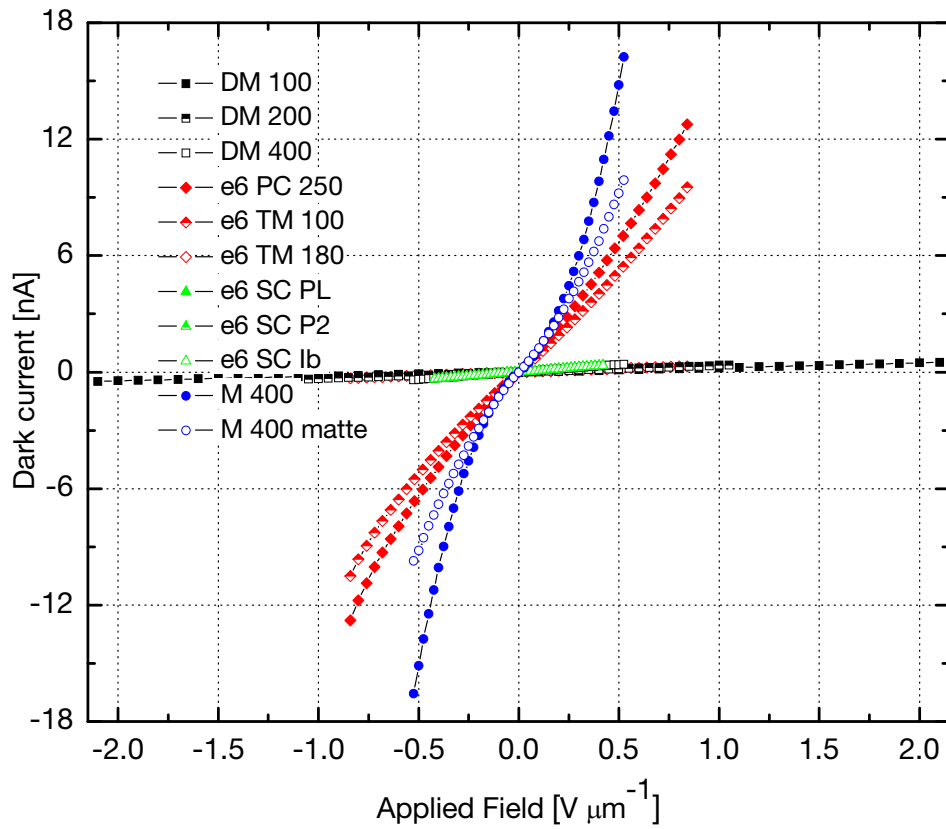


**Figure 4.8.** Leakage current vs. applied field for various diamond films.

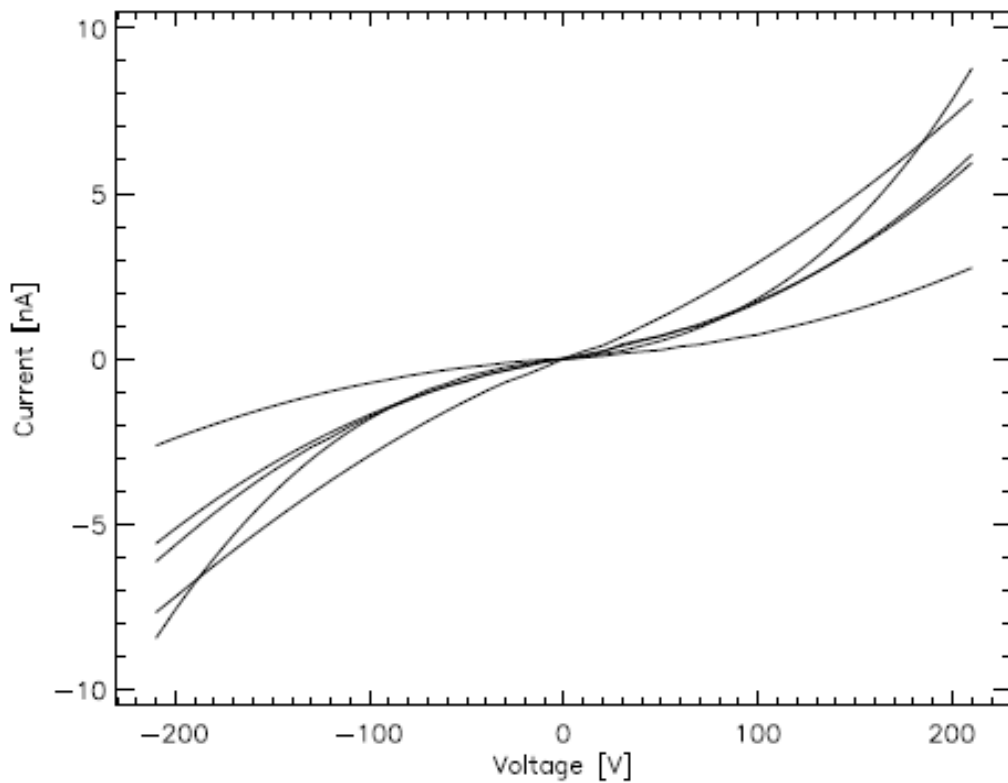


**Figure 4.9.** Leakage current as a function of voltage for several Diamonex films.

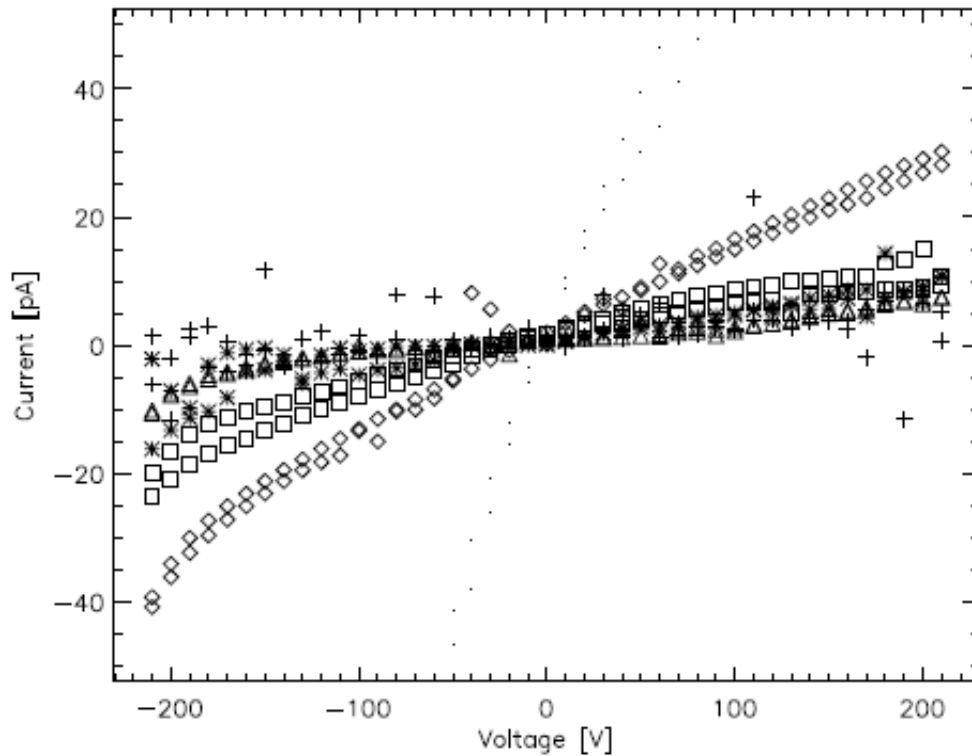


**Figure 4.10.** Leakage current as a function of voltage for E6 and Diamond Materials films.

## 4.4 Concluding Remarks

This chapter presented the results of three investigations into the material properties of diamond films. Each study helped characterize films so that correlations can be made with dosimetric response. Differences were seen between single crystal and polycrystalline diamonds, and impurities have been detected that may affect detector response.

The next chapter presents and discusses dosimetric evaluations of diamond detectors under clinical conditions, which provided a first glimpse at the overall performance and determined what detectors were suitable for detailed clinical dosimetric analyses.

# 5. Initial Dosimetric Analysis

---

This chapter presents preliminary experiments that assessed the overall performance of different diamond films and determined if detectors were suitable for further analyses.

All detectors were first irradiated with a small dose to observe the initial “un-primed” response (Section 5.2). Detectors were then selected to receive a priming dose until currents stabilized (Section 5.3). Once detectors were primed, a series of experiments were performed to observe relative differences in rise times, fall times and sensitivity (Section 5.4), dose rate dependence (Section 5.4) and directional dependence (Section 5.5).

## 5.1 Experimental Details

The 11 detectors chosen for irradiation studies used Diamonex films Dx200-1, Dx200-2, Dx400-1, Dx400-2 and Dx400m, Diamond Materials films DM100, DM200 and DM400 and Element Six films E6SC1b, E6SCPL and E6SCP2. The cavities of most detectors were filled with wax; the DM200 and E6SCP2 detectors were not. Several Diamonex films were irradiated using the thick Perspex encapsulation using the setup in Section 3.5.2 as the more optimal thin Perspex encapsulations were not yet available. All films were evaluated using the thin Perspex detectors that used the Solid Water setup described in Section 3.5.3. The thin Perspex detector setup used an SAD = 100 cm, an SSD = 90 cm and a depth  $z$  of 10 cm. Unless noted otherwise, measurements of average current were performed by integrating charge over 4-s intervals using the Farmer electrometer as described in Section 3.2.3; an interval of 2 s was given between each measurement. All measurements were performed at 248 V using the Farmer electrometer for maximum sensitivity.

## 5.2 Initial Response

The response of a number of diamond detectors were tested with a dose of  $\sim 0.5$  Gy so that they could be compared for differences in initial response. During irradiation, 6 measurements were taken at a dose rate of  $250 \text{ MU min}^{-1}$ . Leakage current was also measured 3 times before and after each dose. Figure 5.1 indicates settings of the x-ray beam

where it was turned on (17 s) and off (53 s) as well as the interval over which measurements were averaged as described in Section 5.1.

All Diamonex films showed high leakage currents ( $> 3$  nA) as shown in Figures 5.1 and 5.2. Despite this, these films exhibited photocurrents between 0.1–0.4 nA. There was no apparent correlation between film thickness  $l$  and leakage current  $I$  as expected using ( $I = AV / \rho l$ ) when combining Ohm's law ( $V = IR$ ) and the definition for resistivity  $\rho$  ( $\rho = AR / l$ ), where  $A$  is area,  $V$  is operating voltage and  $R$  is resistance. After x-ray exposure, leakage currents atypically decreased for the 100 and 200  $\mu\text{m}$ -thick films, which differed from other films. The photocurrent showed an initial spike, or “overshoot”, and then began to settle. Overshoot is seen most clearly for Dx200-1 in Figure 5.1. Ratios of photocurrent to leakage current were  $< 1$ , which were orders of magnitude smaller than the required ratio of 200:1 for reference dosimeters according to IAEA recommendations [283]. The results indicated that these Diamonex detectors required additional corrections and are thus deemed unsuitable for dosimetry.

The response of the three Diamond Materials films is shown in Figure 5.3. All three films exhibited near-zero leakage current before irradiation ( $< 1.25$  pA or below the detection limit of the electrometer), but DM100 showed a short but slow reduction in leakage current following irradiation due to the release of trapped electrons. Although all three films were fabricated under the same conditions, the DM100 response continued to increase over the given dose unlike the other two films that stabilized within the first two measurements of photocurrent. The 200  $\mu\text{m}$ -thick film (DM200) was the most sensitive, which suggests that an optimal combination of electric field and thickness for this material might be around  $1 \text{ V } \mu\text{m}^{-1}$ .

The Element Six material showed slowly rising photocurrents for the duration of their 0.5 Gy irradiations. The slow increase in current was due to the filling of deep electron trap levels, which indicates that a long priming dose may be required before more tests take place. The E6SCPL, E6SCP2 and E6SCIB films exhibited “zero” leakage current over the measured intervals, which equates to  $< 1.25$  pA. The two single crystal CVD films in Figure 5.4 (E6SCPL and E6SCP2) show different sensitivities despite their material similarities. The Type Ib film (E6SCIB, not shown) was found to be more conductive than other films but reached current levels beyond the input current capabilities of the electrometer ( $> 60$  nA) after just one measurement of photocurrent.

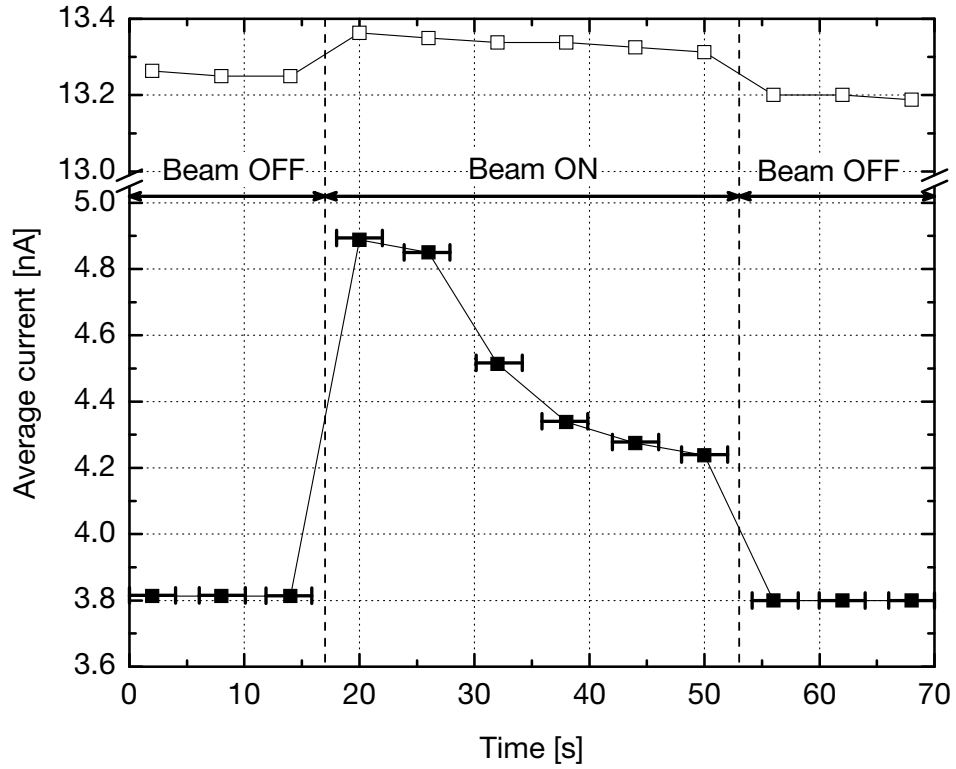


Figure 5.1. Un-primed response for Diamonex films Dx100 (□) and Dx200-1 (■).

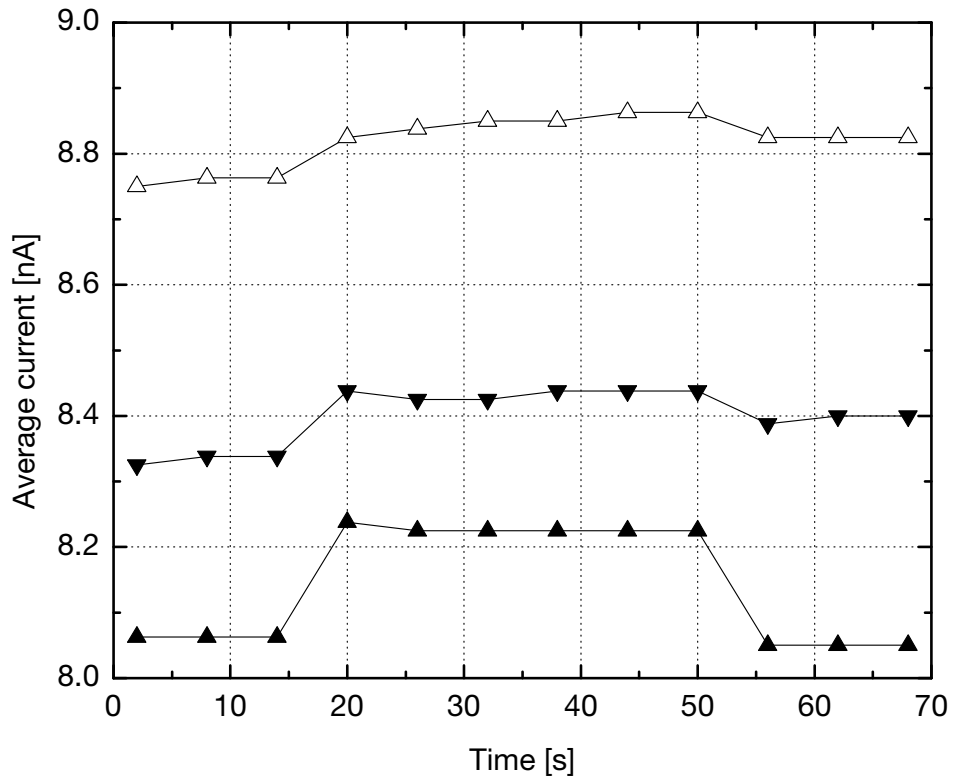


Figure 5.2. Un-primed response for Diamonex films Dx400m (Δ), Dx400-1 (▼) and Dx400-2 (▲).

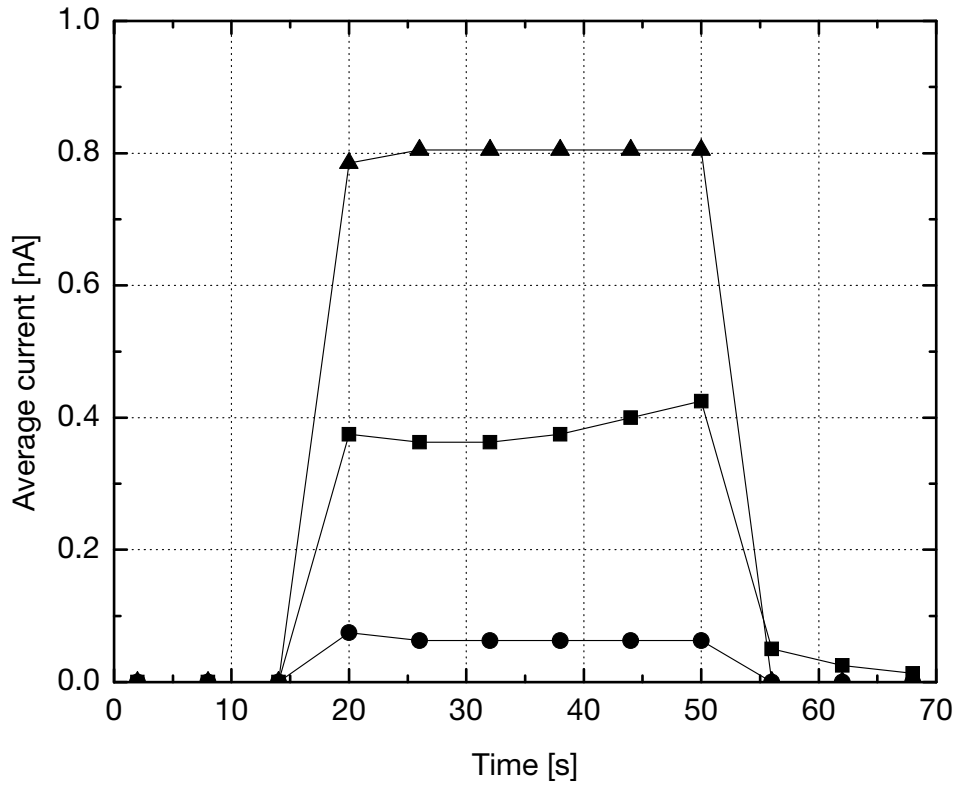


Figure 5.3. Un-primed response for Diamond Materials films DM200 (▲), DM100 (■) and DM400 (●).

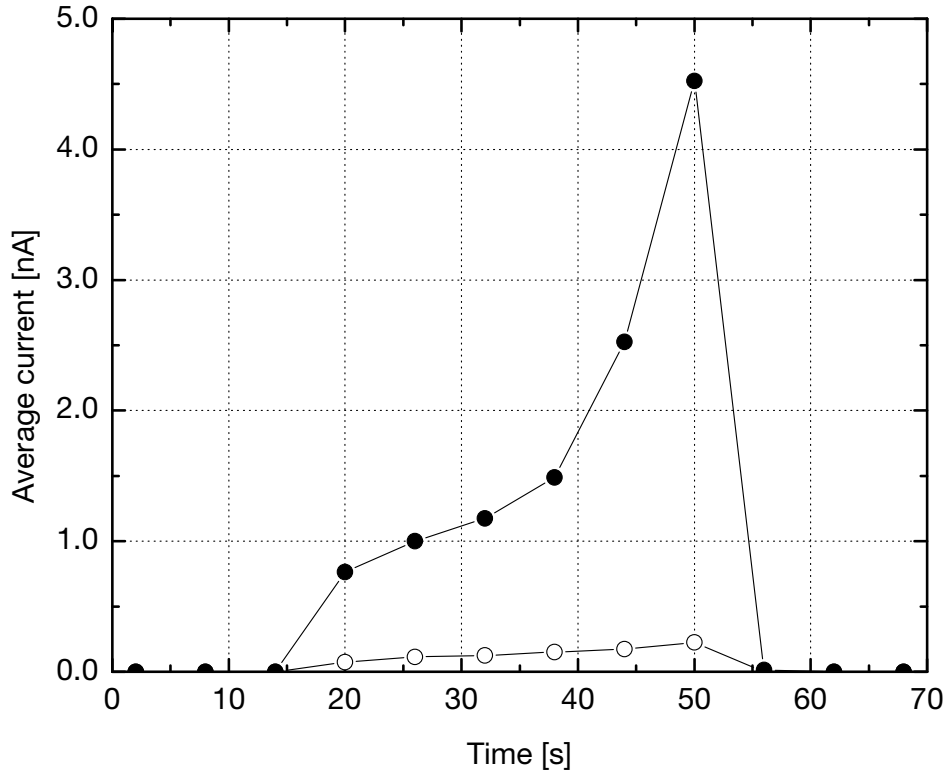


Figure 5.4. Un-primed response for Element Six films E6SCP2 (●) and E6SCPL (○).

## 5.3 Priming

Following an initial dose, films were then given a priming dose, which stabilizes the short-term detector response due to defects as described in Section 2.4. The dose given to each detector varied because irradiation was monitored until response stabilized within a reasonable amount of time. Average current measurements were performed using 1-s intervals. Here, a “reasonable” priming dose was defined as  $< 10$  Gy. A summary of the required priming dose for several films is given in Table 5.1.

To illustrate priming using Diamonex film, Dx200-1 was irradiated at  $250 \text{ MU min}^{-1}$  for  $\sim 100$  Gy as shown in Figure 5.5. Exponential curve functions were fit to both the measured photocurrent (X-rays ON) as well as the leakage current (X-rays OFF) as indicated in the figure. Current levels were monitored during priming with periodic checks of leakage current by turning off the beam for no more than 20 s. When leakage current is subtracted from the photocurrent, the resulting data suggests that after  $\sim 40$  Gy, the average photocurrent, and hence average sensitivity, stabilized but leakage currents continued to decrease over accumulated dose. The high, nonlinear leakage currents along with recurring overshoot of the photocurrent makes it unsuitable for radiation dosimetry. Other Diamonex material also followed similar behaviour when primed.

Average current as a function of priming dose for DM100, DM200 and DM400 are given in Figure 5.6. The requisite dose for each film varied. The DM200 and DM400 films exhibited short priming doses; the DM200 film with a priming dose of  $< 1$  Gy was the most suitable out of any diamond film studied in this project. An actual dose for DM100 that gave a stable current was never reached due to time constraints but was extrapolated to be  $\sim 150$  Gy, which is well above what a reasonable priming dose should be for normal use.

The E6SCPL and E6SCP2 films in Figure 5.7 had short priming doses that would be suitable for dosimetric applications. The E6SCIb film was primed but currents could not be measured because it was too sensitive.

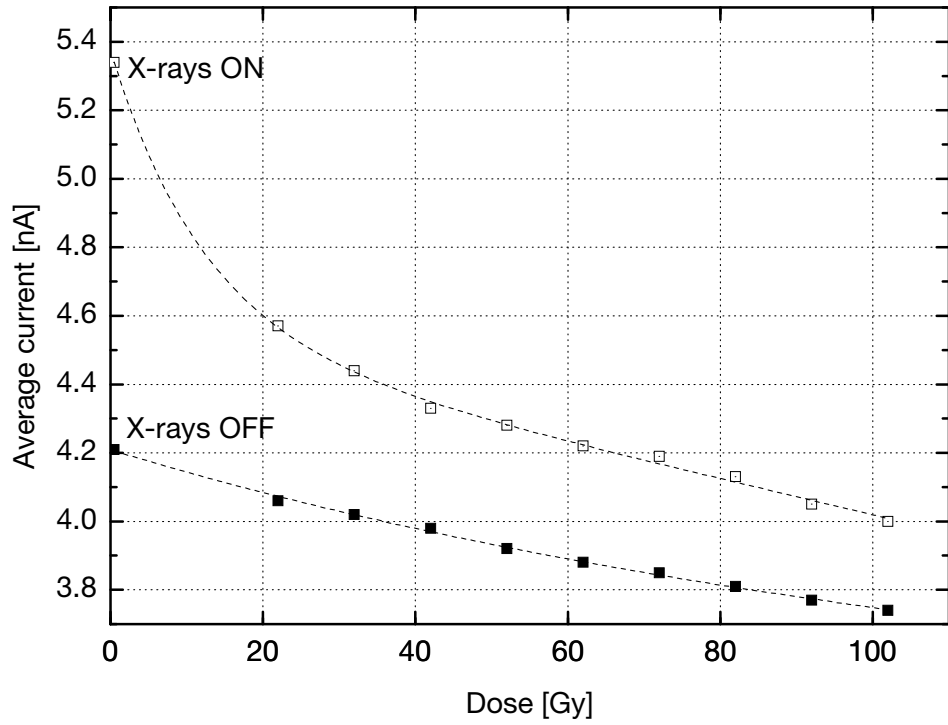


**Figure 5.5.** Additional priming dose for Dx200-1. Exponential fits are plotted for average current measured while the x-ray beam ( $250 \text{ MU min}^{-1}$  dose rate) was on ( $\square$ ) and off ( $\blacksquare$ ).

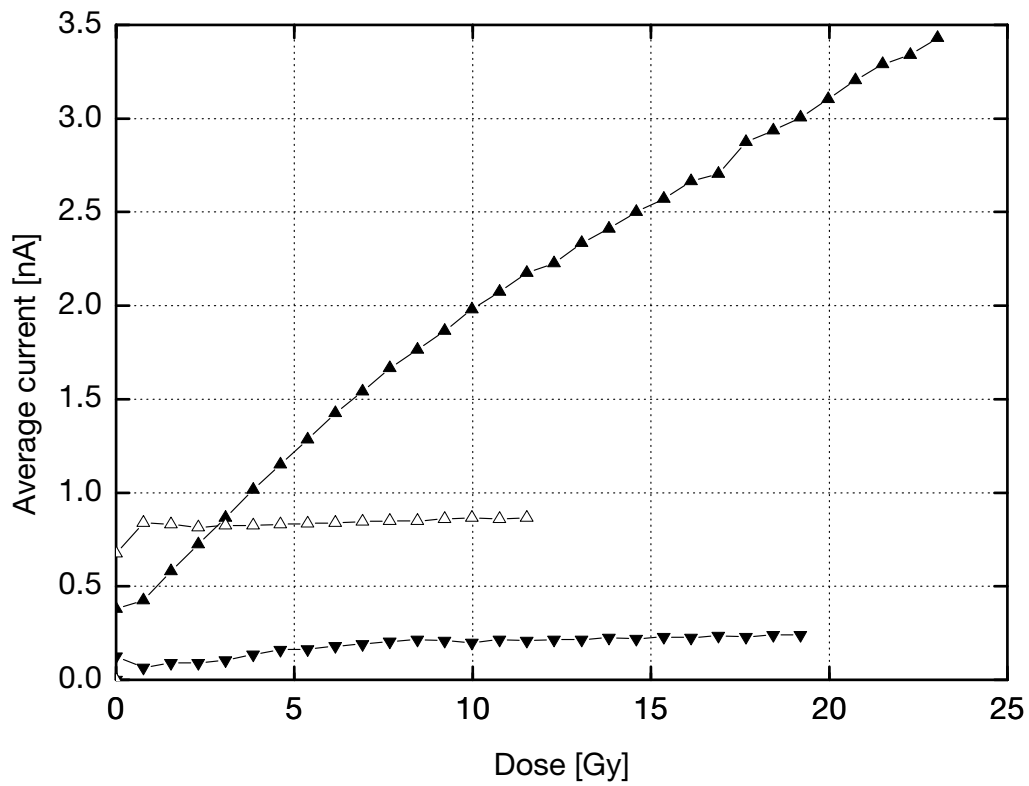


**Figure 5.6.** Priming response for DM100 ( $\blacktriangle$ ), DM200 ( $\triangle$ ) and DM400 ( $\blacktriangledown$ ).



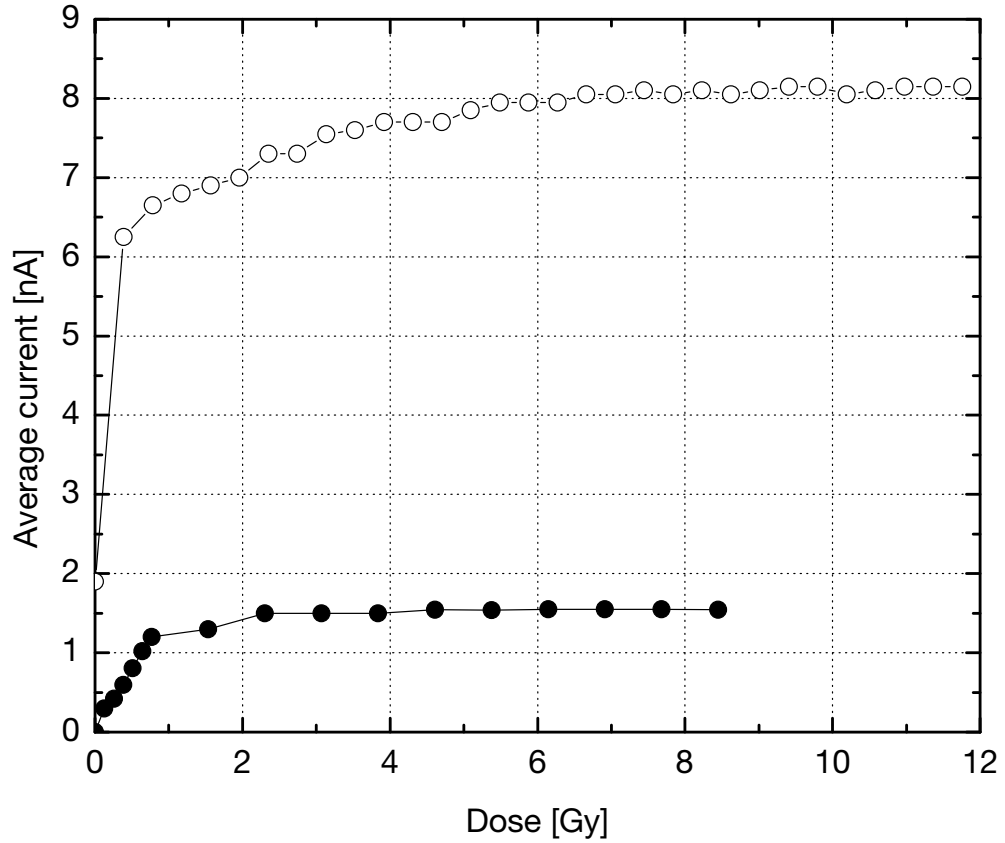


**Figure 5.7.** Priming response for E6SCPL (●) and E6SCP2 (○).

**Table 5.1.** Summary of priming data for several diamond films.

Material	Priming dose	
	[Gy]	[Gy $\mu\text{m}^{-1}$ ]
Dx100	> 70 (~230*)	> 0.7 (~2.3*)
Dx200-1	> 70 (~230*)	> 0.35 (~1.1*)
DM100	> 25 (~150*)	> 0.25 (~1.5*)
DM200	< 1	< 0.005
DM400	< 10	< 0.025
E6SCPL	< 5	< 0.01
E6SCP2	< 10	< 0.02

\* Values in parentheses are extrapolated

## 5.4 Post-priming Response

Once detectors were primed to stabilize detector response, a series of measurements were performed to observe relative differences in rise and fall times, and sensitivity.

Detectors were irradiated with a sequence of different dose rates by varying the pulse repetition rate settings of the linear accelerator, which gave machine outputs of 50, 100, 150, 200 and 250 MU min<sup>-1</sup>. Rise and fall times were defined as the amount of time it took a signal to cross the 10% and 90% thresholds of the calculated mean of stabilized photocurrent [284]. Authors have recommended that rise and fall times be  $\leq 2$  s if a dosimeter is to be used in modern techniques such as IMRT [30,255].

A good illustration of the detector response of the Diamonex film is shown in Figure 5.8, where two Diamonex films were tested using thick Perspex encapsulation following initial priming doses. The Diamonex material gave an interesting, yet unfavourable, response. The two films shown in the figure, Dx200-1 and Dx200-2, are of the same thickness and subsequently could be observed for reproducible behaviour of films from the same manufacturer and type. Films responded similarly but with different leakage current levels. The response of the initial dose showed a sharp increase in both detectors. This overshoot indicated a brief detrapping of shallow energy levels upon excitation in an applied electric field. The overshoot is still present and constant during successive irradiations but less pronounced, which suggests detrapping effects at different energy levels. Once irradiation ceased, leakage currents show long decay times whose currents are  $\gg 0$ .

Figure 5.9 shows the response for Diamond Materials films. For dose rates of 200 and 250 MU min<sup>-1</sup>, the DM200 and DM400 films stabilized with rise times of  $\leq 2$  s. Both films also showed fall times  $\leq 2$  s, which is encouraging for use in modulated beams as many films reported in the literature exhibit longer fall times. However, the DM200 film again showed non-zero leakage currents ( $\sim 10$  pA) for up to 10 s following irradiation. Still, it achieved photocurrent to leakage current ratios of  $> 200:1$  as recommended by the IAEA [254] for reference standard dosimeters. The DM100 film exhibited a higher sensitivity, but its saw tooth-like behaviour indicated a large charge trapping population in the material that results in an unfavourably slow response.

In Figure 5.10, the E6SCPL and E6SCP2 films differed in response despite being the same films but with different surface polishing finishes. At dose rates of 200 and 250 MU min<sup>-1</sup>, the E6SCPL and E6SCP2 films displayed negligible leakage currents and had rise times of  $\leq 2$  and 7 s, respectively. Just like DM200 and DM400, both E6 films gave fall times of

$\leq 2$  s, which is a favourable characteristic for the dosimetry of conformal techniques such as IMRT.

An important characteristic is detector sensitivity, usually given in units of nC Gy<sup>-1</sup>. Although no exact threshold is set in the literature, sensitivity must be sufficient to measure low doses. Sensitivity is also expected to be stable after large doses for long-term use. In the case for diamond, its radiation hardness has been reported to be  $> 10^5$  Gy [32], which would allow for long-term usage with a stable response after priming.

Sensitivities varied over the range of material examined, which are summarized in Table 5.2. The highest sensitivities were observed in the single crystal material. An average sensitivity of 230 nC Gy<sup>-1</sup> (or specific sensitivity of 586 nC Gy<sup>-1</sup> mm<sup>-3</sup>) for the E6SCP2 material compares well to other studies investigating CVD diamond detectors, e.g. [10,152,159,163,256], PTW commercial detectors, e.g. [257,258] and commercial Si diode dosimeters, e.g. [259]. In particular, PTW states that the sensitivities of their natural diamond detectors are between 50–500 nC Gy<sup>-1</sup> with sensitive volumes between 1–6 mm<sup>3</sup>. High sensitivity was attributed to a low concentration of sample defects and/or a favourable concentration of dopants such as nitrogen that allow for high charge collection efficiency as well as low leakage currents. Sufficient sensitivity levels were found using this diamond detector configuration, but only E6SCPL and E6SCP2 appear to be suitable for more advanced techniques where short, intense pulses of radiation are used. The Type Ib material E6SCIb showed erratic behaviour and was therefore unusable for other measurements. However, it is interesting that, had the Type Ib film stabilized at 60 nA, the estimated sensitivity would be 1,870 nC Gy<sup>-1</sup>. Note that too high a sensitivity can be a disadvantage as in the case of the E6SCIb or even the E6SCP2 film; electrometers like the 2570/1 Farmer electrometer have charge or current collection limits, which is the reason why, in our methods, repeatable measurements were kept to smaller doses while investigating these films. In future work, highly sensitive detectors might include a divider that would reduce the current being measured by an electrometer such as the Farmer.

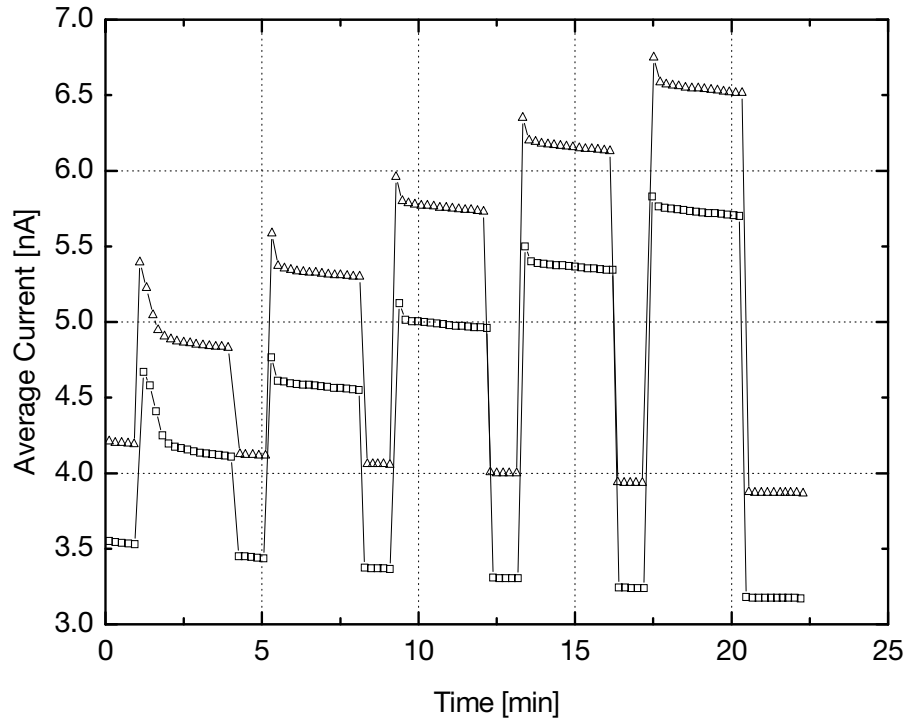


Figure 5.8. Priming response using dose rates of 50, 100, 150, 200 and 250 MU min<sup>-1</sup> for Dx200-1 ( $\Delta$ , top) and Dx200-2 ( $\square$ , bottom).

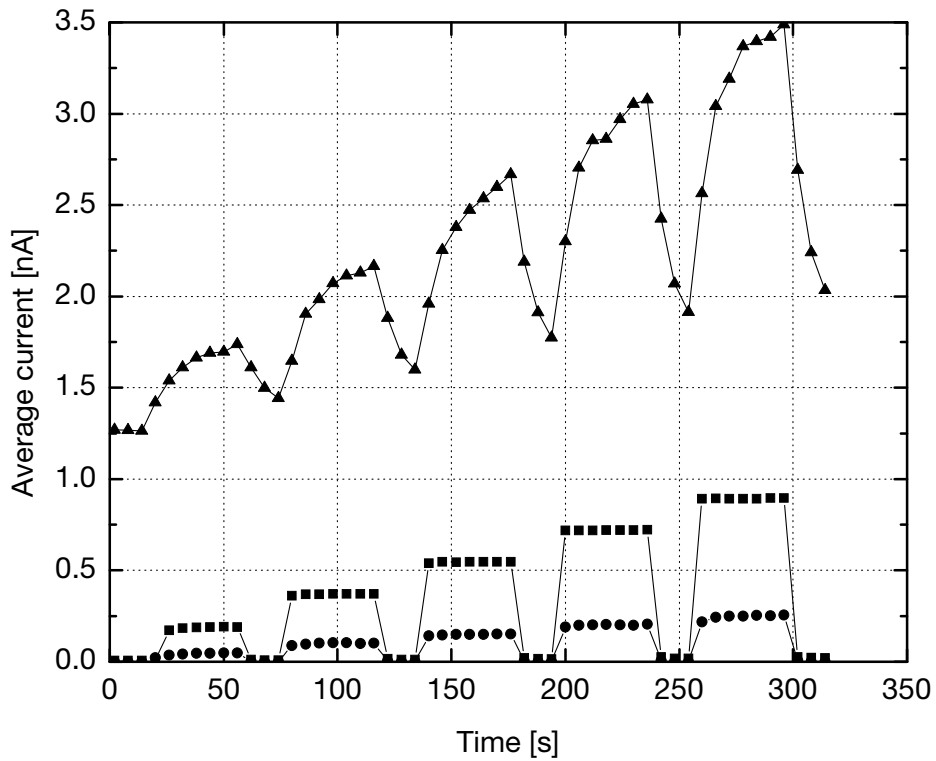
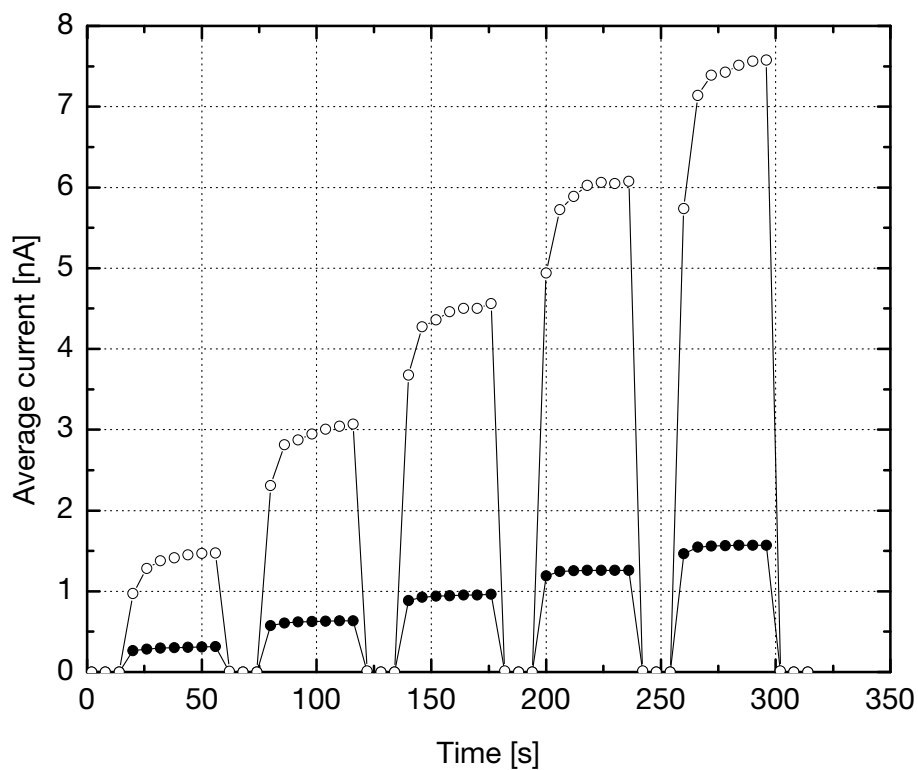


Figure 5.9. Response to dose rates of 50, 100, 150, 200 and 250 MU min<sup>-1</sup> (from left to right) for DM100 ( $\blacktriangle$ ), DM200 ( $\blacksquare$ ) and DM400 ( $\bullet$ ).



**Figure 5.10.** Response to dose rates of 50, 100, 150, 200 and 250  $\text{MU min}^{-1}$  (from left to right) for E6SCPL (●) and E6SCP2 (○).

**Table 5.2.** Summary of sensitivity data for several diamond films.

Material	Sensitivity	
	$[\text{nC Gy}^{-1}]$	$[\text{nC Gy}^{-1} \text{mm}^{-3}]$
Dx100	4.1	13.0
Dx200-1	4.6	7.34
DM100	-	-
DM200	26.1	41.5
DM400	7.7	6.09
E6SCIb	-	-
E6SCPL	47.7	121
E6SCP2	230	586
PTW*	50-500	9-500

\* Cited from the literature for comparison [11].

## 5.5 Dose Rate Dependence

The material properties of diamond can have an effect on the variation of detector response with dose rate. The relationship between conductivity  $\sigma$  induced in an insulating material and absorbed dose rate  $\dot{D}$  is expressed as

$$\sigma \propto \dot{D}^{\Delta}, \quad (5.1)$$

as described by Fowler [285,286] where usually  $0.5 < \Delta < 1$ . In an electron trap-free material,  $\Delta = 0.5$ . If traps in the material have the same capture cross section, then  $0.5 < \Delta < 1$ . Material with a uniform or quasi-uniform trap distribution in the forbidden energy gap region (between the valence and conduction bands) gives  $\Delta \approx 1$ .  $\Delta$  can be  $> 1$  if traps have differing capture cross sections. As electrical conductivity  $\sigma$  is proportional to current  $I$  at a constant bias, dose rate dependence was therefore calculated using

$$I = I_0 + k\dot{D}^{\Delta}, \quad (5.2)$$

where a power law regression is used with fitting parameters  $k$  and  $\Delta$  to test for linearity and  $I_0$  was either measured and/or set to 0 for comparison<sup>9</sup>. Dose rates were obtained by varying the pulse repetition rate of the linear accelerator via user settings.

Dependence on dose rate was investigated using accelerator dose rates of 50, 100, 150, 200 and 250 MU min<sup>-1</sup> at 248 V using the Farmer electrometer. Figures 5.11–5.13 show photocurrent  $I_{ph}$  ( $I_{ph} = \text{measured current } I_{meas} - \text{measured leakage current } I_{leakage}$ ) as a function of dose rate for (a) Dx100 and Dx200, (b) DM100, DM200 and DM400 and (c) E6SCP1 and E6SCP2. Photocurrents were allowed to stabilize before measurements were averaged. Doses used were no more than  $\sim 1.3$  Gy.

The  $\Delta$  values for Diamonex films Dx100 and Dx200 were found to be within the predicted range but  $< 1$  as expected for this quality of material. See Figure 5.11. However,  $\Delta$  values were found to be highly sensitive to the magnitude of  $I_{leakage}$  that was subtracted to deduce  $I_{ph}$ . For example, adding a linear shift of 20 pA to the Dx100 data changed  $\Delta$  from 0.61 to 1.00.

The polycrystalline Diamond Materials films varied from 0.91 to 1.02 despite their identical quality and surface finish as shown in Figure 5.12. The difference may then be due to different applied fields [ $V \mu\text{m}^{-1}$ ] as they were all tested at 248 V but are 100, 200 and

---

<sup>9</sup> Fitting parameter  $k$  indeed has units that balance the equation [157,285,286].

400  $\mu\text{m}$  thick. It would be interesting in the future to test these films of different thicknesses with the same applied field. Similarly, the same film (thickness) with different applied voltages also has different applied fields, which can have an affect on  $\Delta$  as reported in the literature [255,261] and is investigated in Chapter 6 [167]. As shown in Figure 5.13, the two single crystal E6 films were linear with  $\Delta$  values of 0.99 and 1.00 for the PL and P2 films, respectively. The data suggests that these films contain uniform or quasi-uniform trap distributions and would require minimal or no correction for dose rate nonlinearity. Aside from the Diamonex films studied here, the films in Table 5.3 compare well with the literature. Detectors studies in the literature have reported most  $\Delta$  values from 0.90 to 1.00. Table 5.4 lists the range of values by basic type of material.

An additional study of dose rate dependence as a function of a fixed dose (and not stabilized photocurrent), which was performed on a selected film, is presented in Section 7.3.

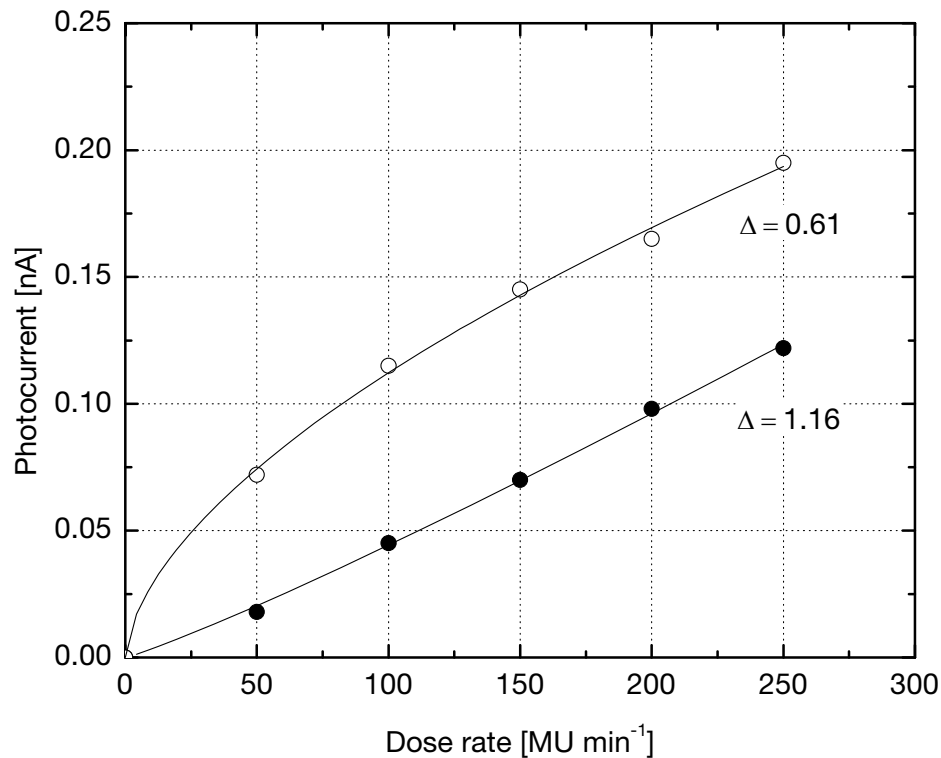


**Figure 5.11.** Photocurrent vs. dose rate for Dx100 (●) and Dx200-1 (○). Films are shown with power law curve fits.

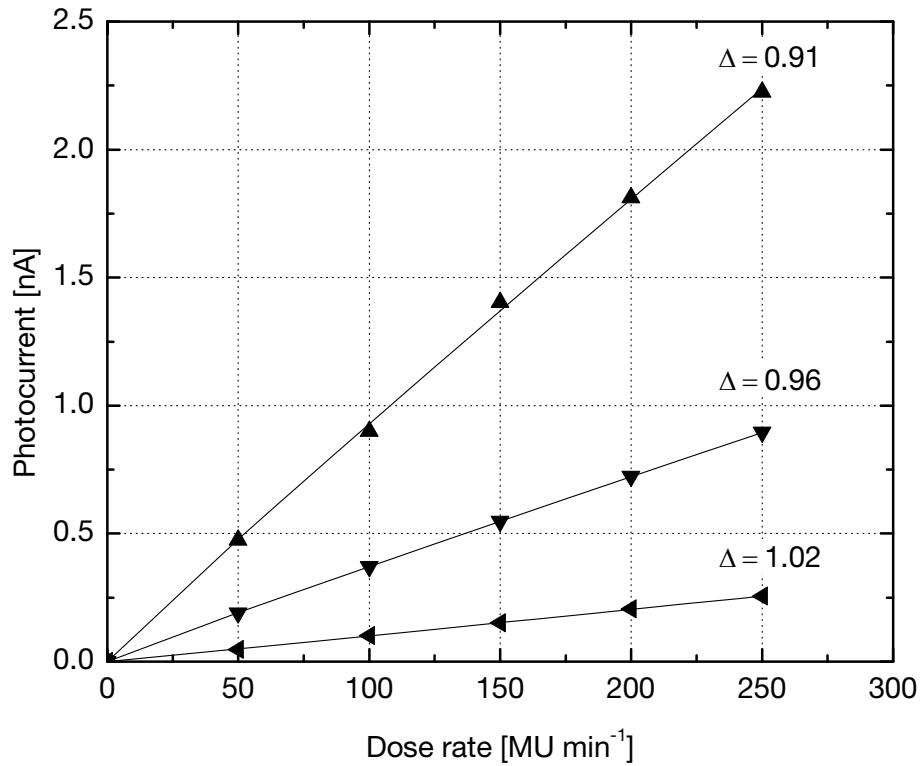


**Figure 5.12.** Photocurrent vs. dose rate for DM100 (▲), DM200 (▼) and DM400 (◄). Films are shown with power law curve fits.

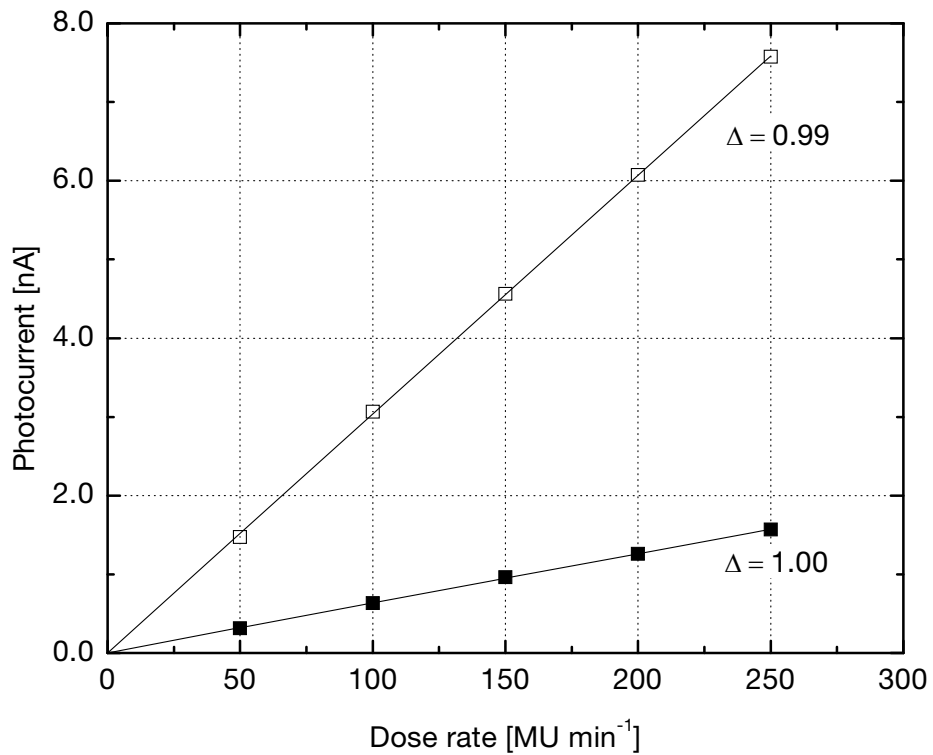


**Figure 5.13.** Photocurrent vs. dose rate for E6SCP2 (□) and E6SCPL (■). Films are shown with power law curve fits.



**Table 5.3.** Summary of curve fitting data for dependence on dose rate.

Material	$\Delta$
Dx100	$1.16 \pm 0.05$
Dx200-1	$0.61 \pm 0.02$
DM100*	$0.91 \pm 0.10$
DM200	$0.96 \pm 0.00$
DM400	$1.02 \pm 0.01$
E6SCPL	$0.99 \pm 0.01$
E6SCP2	$1.00 \pm 0.01$

\* Estimate

**Table 5.4.** Comparison of reported  $\Delta$  for different types of material.

Material	$\Delta$	Ref.
HPHT	0.49 – 0.97	[21,22]
Natural gem	0.92 – 1.00	[140,144,145,147,152,158,159,262,263]
CVD	0.86 – 1.07	[27,159,255,261,262,264-266]

## 5.6 Directional Dependence

An important characteristic of a dosimeter is having a response that is independent of its orientation with respect to a source of radiation. To determine directional dependence, the detectors were rotated every  $45^\circ$  to change the incident angle of radiation. The  $0^\circ$  position corresponds to the typical face-on irradiation of the detector. Data were collected by measuring stabilized current response as a function of eight different angles for dose rates of 50 and 250  $\text{MU min}^{-1}$ . Data were plotted for two dose rates to observe any inconsistencies during a series of measurements. The resulting data were then normalized to the datum taken at  $360^\circ$ , the measurement taken after one full rotation. The initial measurement at  $0^\circ$  was found to be sometimes low for all detectors and so normalizing data to the second measurement at the  $0^\circ$  position after one full rotation was found to be more reliable in this case. Inconsistencies were due to priming effects, which are studied in more detail in Chapter 7.

Directional dependence was plotted for several films as shown in Figures 5.14–5.17. Overall, minimal dependence and the most consistent response were seen in the E6 films. Data outliers were observed and removed from the plots due to either insufficient priming,

which created a reduction in sensitivity, or a physical obstruction such as couch support that impeded detector response. The Dx200 detector in Figure 5.14 had a physical obstruction at the 135° angle (couch); the same was seen with the E6SCP2 film at the 315° angle in Figure 5.16. When data outliers were removed from this analysis, dependence on incident angle was  $\pm 2$ ,  $\pm 4$ ,  $\pm 4$ ,  $\pm 1$  and  $\pm 1\%$  for Dx200, DM200, DM400, E6SCPL and E6SCP2, respectively. De Angelis *et al.* [158], Lambert *et al.* [142] and Westermarck *et al.* [267] have reported  $\pm 1.5\%$  for PTW detectors, even though some perceive that directional dependence of diamond detectors is considered negligible [7]. Other prototype detectors with their own unique encapsulation and device geometry have reported 1.5–2.0% for a synthetic diamond [43,268].

Improvements to minimize directional dependence may still be made by optimizing device encapsulation and electric contact thickness as reported in Monte Carlo simulations by Górká *et al.* [43,269], and is also being explored in our diamond detector research group by Baluti *et al.* [44].

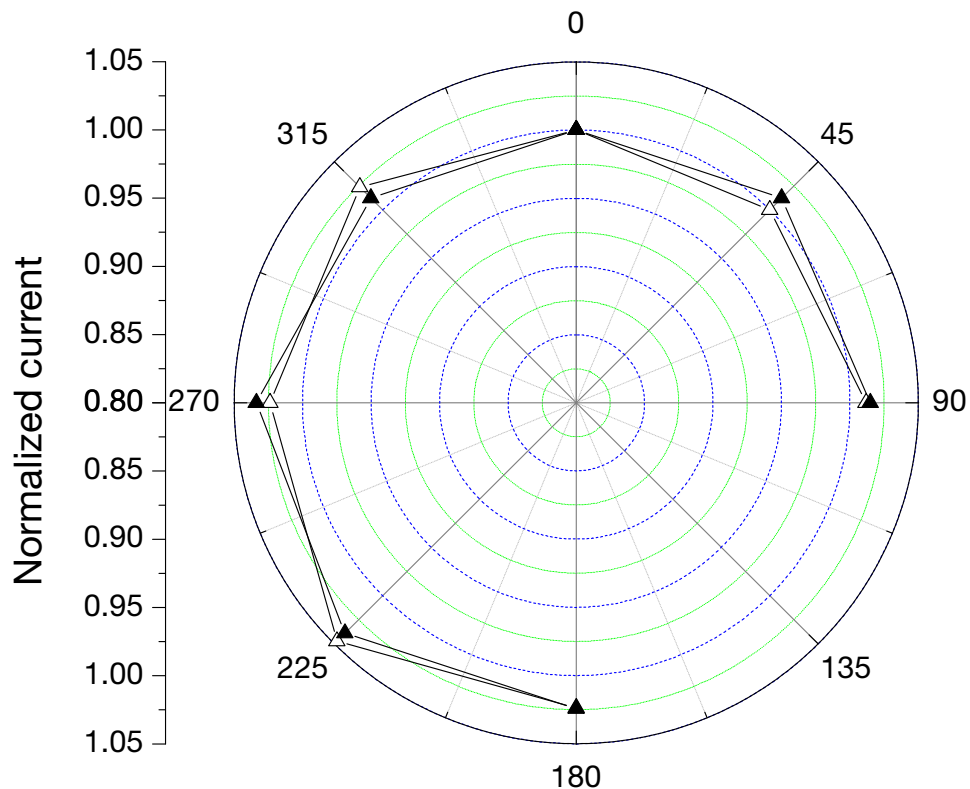


**Figure 5.14.** Variation in current vs. incident angle of irradiation for the Dx200 film for ( $\Delta$ ) 50 and ( $\blacktriangle$ ) 250 MU min<sup>-1</sup>.

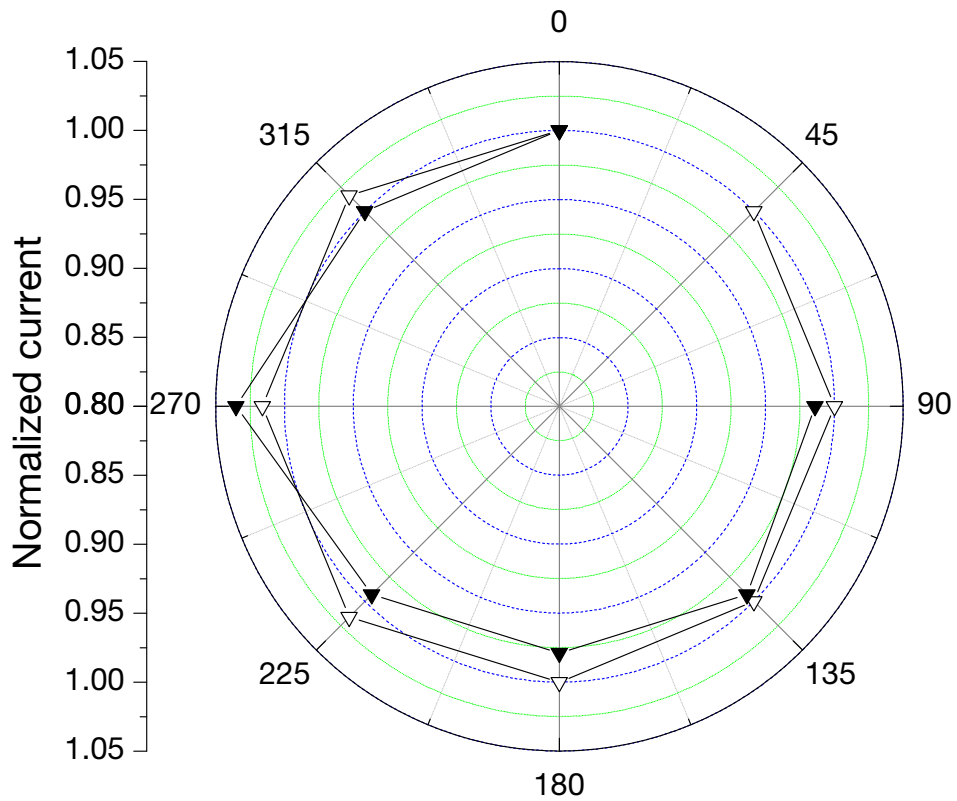


**Figure 5.15.** Variation in current vs. incident angle of irradiation for the DM400 film for (▽) 50 and (▼) 250 MU min<sup>-1</sup>.

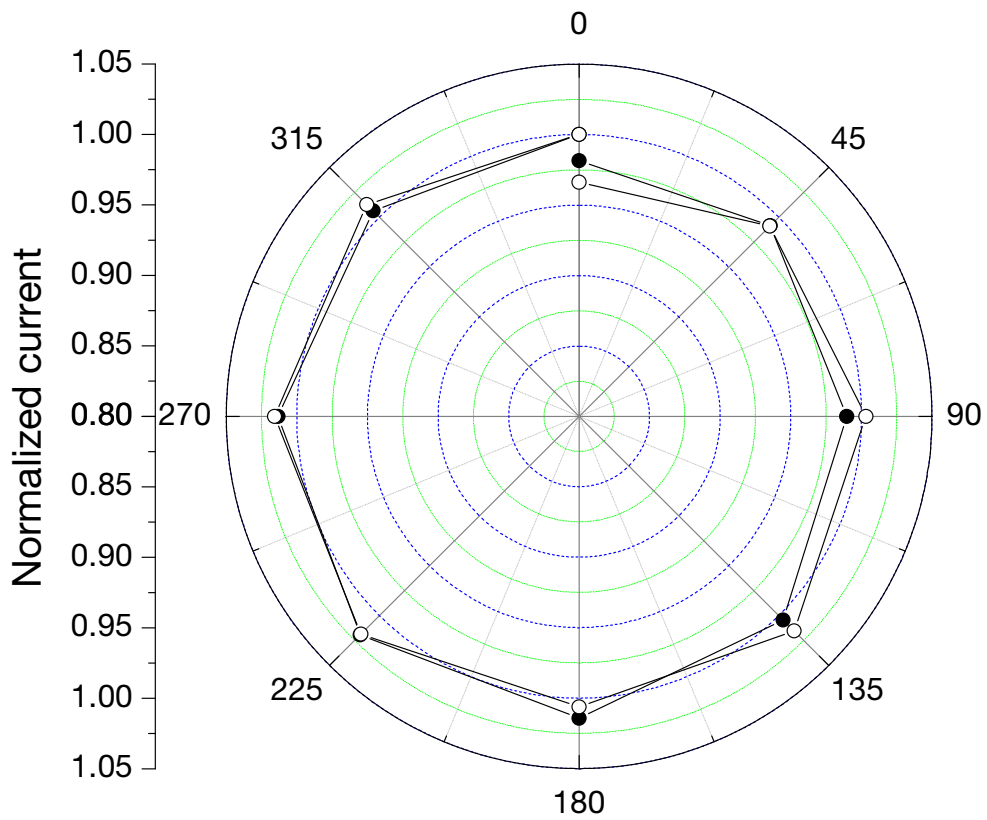


**Figure 5.16.** Variation in current vs. incident angle of irradiation for the E6SCPL film for (○) 50 and (●) 250 MU min<sup>-1</sup>.

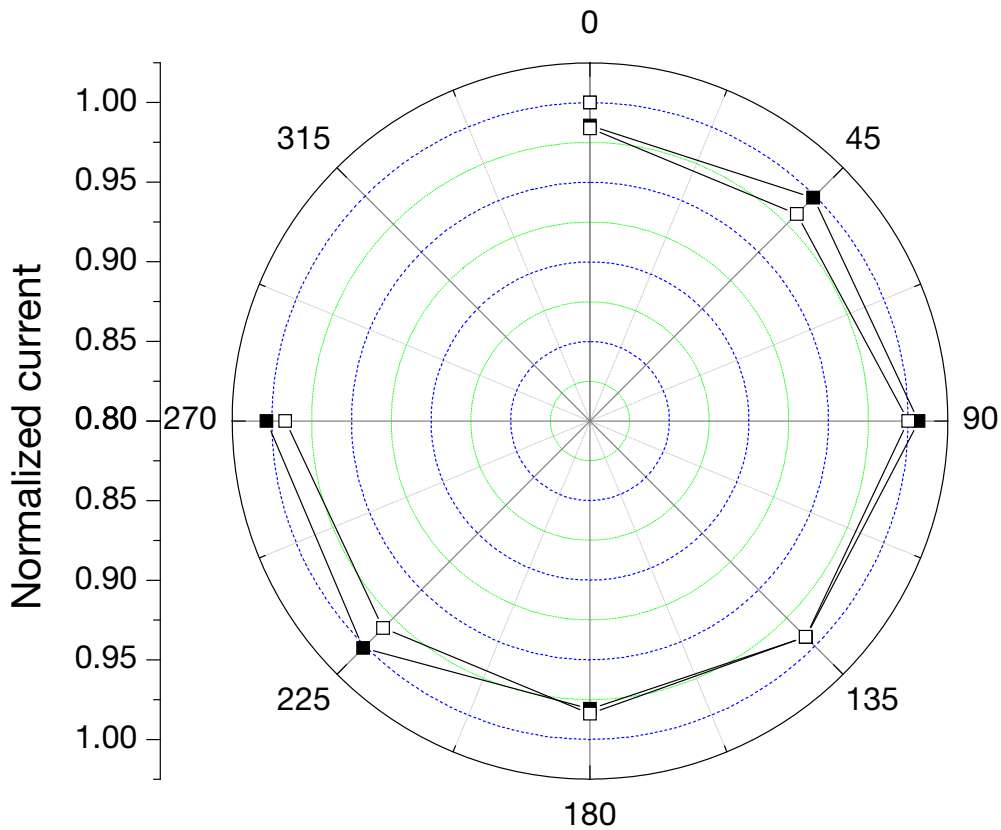


**Figure 5.17.** Variation in current vs. incident angle of irradiation for the E6SCP2 film for (□) 50 and (■) 250 MU min<sup>-1</sup>.

## 5.7 Concluding Remarks

This chapter presented the first set of irradiation measurements using 6 MV x-rays to analyze the overall performance of 11 diamond films that were commercially available from three manufacturers. Detectors were irradiated with a small dose to observe their “un-primed” responses. Detectors were then selected to receive a priming dose until currents stabilized and then irradiated further to investigate rise times, fall times, sensitivity, dose rate dependence and directional dependence. The response characteristics differed due to quality of the crystal as well as film thickness, with sensitive volumes from 0.31–1.26 mm<sup>3</sup>.

The low quality polycrystalline Diamonex material is considered unsuitable for dosimetric applications due to its lack of stable leakage current and photocurrent as well as priming doses much greater than acceptable or practical levels. Measurement of characteristics such as dose rate dependence was therefore sensitive to levels of leakage current, which made it susceptible to large uncertainties. The lack of a strong first-order Raman peak as described in Section 4.2 suggests that this material may not be suitable for dosimetry due to a high concentration of imperfections or impurities. Graphitic phases along grain boundaries may

increase conductivity [42], which helps explain the observed high leakage currents. Grain boundaries trap and scatter charge carriers, and have an effect on charge collection distance [287].

Some of the high quality polycrystalline diamond from Diamond Materials had favourable characteristics. The 200 and 400- $\mu\text{m}$  thick films from Diamond Materials are potential candidates for dosimetry due to their near-zero leakage current, low priming doses, quick rise times and good sensitivity. Both films also had very similar Raman spectra. DM200, however, had longer decay times following irradiation and so may hinder its use for applications such as IMRT. The 100- $\mu\text{m}$  film (DM100) did not share these favourable characteristics, which may be due to differences in crystalline quality as seen in the Raman spectra. Specifically, DM100 spectrum did not contain the same peaks that indicate N concentrations in the sample as the other two Diamond Materials films. The filling of traps in DM100 was relatively slow with respect to other films in this study, but also had no noticeable Raman peaks other than the diamond Raman line.

The single crystal CVD Element Six films E6SCPL and E6SCP2 exhibited suitable characteristics for dosimetry. Both showed near-zero leakage currents ( $< 1.25 \text{ pA}$ ), low priming doses ( $< 2$  and  $< 10 \text{ Gy}$ , respectively), low rise times ( $< 2$  and  $7 \text{ s}$ , respectively) and fall times ( $< 2 \text{ s}$ ), good sensitivity ( $47.7$  and  $230 \text{ nC Gy}^{-1}$ , respectively) and were weakly dependent on dose rate ( $\Delta = 0.99$  and  $1.00$ , respectively) and directional dependence ( $\pm 1\%$ ). Differences in the E6SCPL and E6SCP2 may be due to slight differences in N concentration. A study by Descamps *et al.* [245] showed that a difference in 20 ppm reduced sensitivity by over two orders of magnitude but helped minimize some priming effects. Because the E6SCP2 film had favourable characteristics for dosimetry including the highest sensitivity, it was selected for further analyses in the following chapters. Similarities in Raman spectra between DM200, DM400, E6SCPL and E6SCP2 also support their similarities in detector response. The single crystal HPHT film (E6SC1b) was tested for comparison but was too sensitive for the parameters set for this investigation.

Although some detectors were filled with dental wax, no differences could be attributed to the presence of the wax. Differences between DM200 (with wax) and DM400 (without wax), for instance, may be due to differences in applied field. Differences between E6SCPL (with wax) and E6SCP2 (without wax) may be due to differences in material quality and surface polishing. A systemic analysis of these differences will be addressed in future work.

The focus of the following chapter was to determine an optimal operating voltage for the E6SCP2 detector using conventional instrumentation.



## 6. Operating Voltage

---

Following the experiments presented in Chapter 5, a detector using a single crystal diamond film (E6SCP2) was selected for detailed analyses. In addition to having no apparent detrimental levels of impurities, this detector was chosen for its favourable response, such as low leakage current, minimal angular dependence and relatively low cost. This chapter details an analysis to determine an optimal operating voltage.

As reviewed in Chapter 2, an obstacle towards a realizable synthetic diamond detector has been mitigating or eliminating unwanted behaviour due to defects, e.g. [50-52]. The well known pumping or priming effect, e.g. [29,50,52,168,288,289], is a way to counteract defects or impurities to improve performance, e.g. to stabilize sensitivity, although it must be done routinely. Other problems may also originate from interface phenomena and device encapsulation [59,60]. Defects and device design not only limit capability but also introduce uncertainties when selecting parameters for optimizing device operation. One such parameter for optimizing detector performance is the selection of an appropriate bias voltage.

Previous diamond detector studies have reported various operating voltages chosen for experiments in radiotherapy, ranging anywhere from 0 V [47] to 1000 V ( $\sim 4.75 \text{ V } \mu\text{m}^{-1}$ ) [42]. Although diamond can withstand electric fields up to  $100 \text{ V } \mu\text{m}^{-1}$  [74,290], the application of such high fields in clinical dosimetry seems unnecessary, and, more importantly, limited by instrumentation. For example, voltage supplies of clinical electrometers used for radiotherapy dosimetry typically range from  $\pm 250$  to  $\pm 400$  V. Some authors have reported how or why a particular electric field was selected, using criteria such as optimizing sensitivity vs. leakage current or stability [42,48,49,52,131,149,289]. Studies have also focused upon polarity effects to determine corresponding correction factors, e.g. [25], including charge collection efficiency due to defects [291]. Correcting for polarity is routine when calibrating ion chambers or other dosimeters [279].

The aim of this study was to determine an optimal operating voltage of the E6SCP2 diamond detector. This included investigations on how changes in applied electric field affect detector performance, and determined whether an optimal operating voltage setting could be

found within the limits of available dosimetry equipment. Performance as a function of voltage was evaluated by investigating current-voltage characteristics, response dynamics, sensitivity and dependence on dose and dose rate.

## 6.1 Experimental Details

Data were acquired using two different instruments, which depended on the type of analysis being performed. One instrument used was a Farmer electrometer. As described in Section 3.2.3, the voltages available with this instrument were full, half, quarter and eighth divisions of approx.  $\pm 250$  V; actual settings were measured as  $\pm 248.0$ ,  $\pm 125.0$ ,  $\pm 62.5$  and  $\pm 30.8$  V. Unless stated otherwise, current measurements using this electrometer were integrated over 4-s intervals with a 2-s gap between them as performed in Chapter 5.

The Keithley electrometer [260] was used as a high-voltage source ( $\pm 210$  V) and to measure detector current over time. Section 3.2.3 describes details pertaining to data acquisition and hardware related to this instrument.

Irradiation measurements were performed using the setup in Section 3.5; this gave outputs of  $100 \text{ MU} = 0.77 \text{ Gy}$  and typical dose rates of  $250 \text{ MU min}^{-1} = 1.95 \text{ Gy min}^{-1}$ . The gantry of the linear accelerator was set at the default  $0^\circ$  angle. The SAD = 100 cm, SSD = 90 cm and depth  $z = 10$  cm. Unless stated otherwise, the detector was primed or pre-irradiated with a dose of 10 Gy as performed in Chapter 5. Any differences or changes in magnitude or behaviour of priming with respect to operating voltage were not addressed in this study, although one set of measurements showed that the difference in priming dose between 62.5 V and 248.0 V was identical.

## 6.2 Current-Voltage Characteristics

The detector was tested for leakage current using the Keithley electrometer by performing a voltage sweep from 0 to 200 V in 25 V increments, where an average of 10 measurements was taken at each step following a hold time of 90 s. The resulting I-V data were fit to a power law curve  $y = mx^b$  ( $R^2 = 0.9994$ ) with an exponent of 0.65 as shown in Figure 6.1. Leakage currents of  $1.40 \pm 0.02$  and  $2.20 \pm 0.02$  pA were observed at biases of 100 and 200 V, respectively; these values correspond to instantaneous resistances of  $7.1 \times 10^{13}$  and  $9.1 \times 10^{13} \Omega$ , respectively.



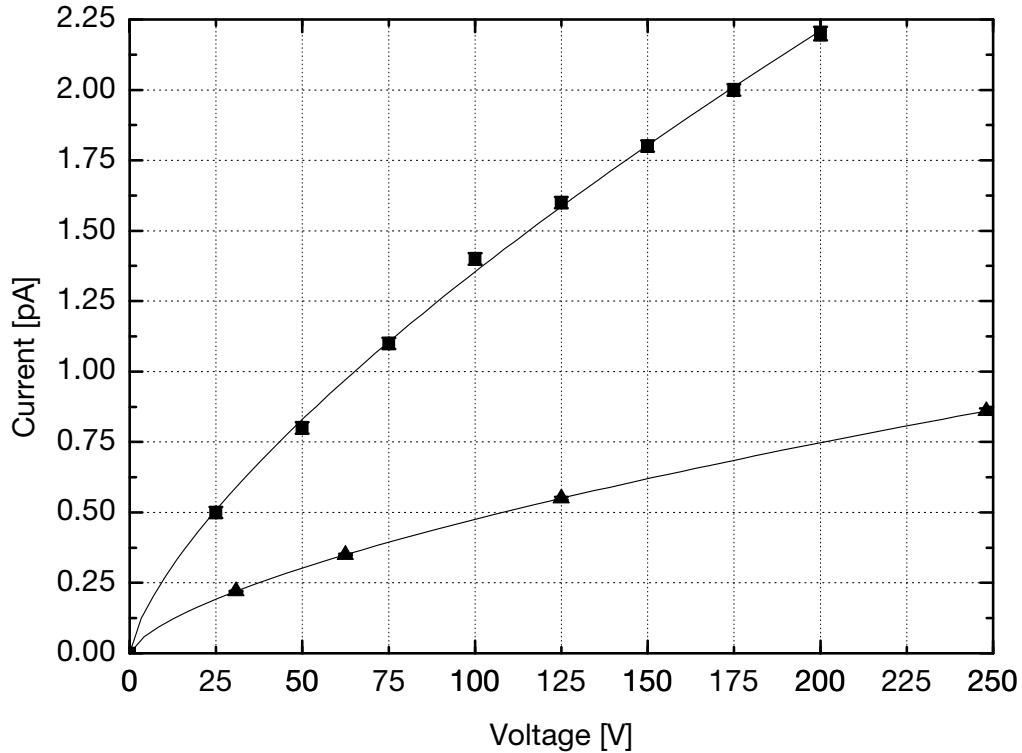


**Figure 6.1.** Leakage current vs. operating voltage for the E6SCP2 detector using the Keithley (■) and Farmer (▲) electrometers. Data are represented with error bars (obscured by data points) as  $I_{\text{avg}} \pm \sigma$ . The lines are power law fits to the data as described in the text.

Leakage current was also measured using the Farmer electrometer following irradiations by way of averaging charge over a particular time interval to observe any short or long-term variability over time or cumulative dose. See Figure 6.1. Immediately after irradiations, currents fell quickly below the detection limit of the electrometer when integrating charge over 4-s intervals, indicating currents of less than 1.25 pA at 248.0 V. At end of irradiation experiments, a more accurate measurement of leakage current was found by averaging total charge over 60-s intervals. Measurements averaged 0.22, 0.35, 0.55 and 0.86 pA at 30.8, 62.5, 125.0 and 248.0 V, respectively. The data were also fit to a power law curve ( $R^2 = 1$ ) with an exponent of 0.65.

Leakage currents were negligible for all voltage settings tested and compared well with previous studies, e.g. [26,49,50,164,292,293]. Time dependence in leakage current was observed when initially applying a voltage, which was expected as charge distributions consequently settled in the material, but its magnitude was still negligible. The small difference in detectable leakage current measured at high voltages between the two

electrometers (e.g. 2.2 pA at 200 V using the Keithley electrometer, 0.86 pA at 248.0 V for the Farmer electrometer) may be due to the zeroing function on the latter. The absence of significant leakage current is encouraging, as it eliminates some corrections needed following irradiations, hence a quicker and more direct evaluation of dose. High photocurrent to leakage current ratios (presented in the next section) were found to be favourable for detector performance, and were up to an order of magnitude higher than other single crystal diamond detector studies reported elsewhere [49]. A good ratio was associated with high resistivity and was attributed to an absence of graphitic impurities in the sample [227]. This is an advantage of single crystal diamond over polycrystalline diamond. Low leakage currents allow for higher voltages, which in turn can improve charge collection efficiency.

### 6.3 Response Dynamics

To observe the temporal response in photocurrent as a function of operating voltage, the Farmer electrometer was used to estimate response dynamics such as rise and fall times and stability. Measurements were repeated using all available (positive) voltage settings of 30.8, 62.5, 125.0 and 248.0 V at nominal dose rates of 50, 100, 150, 200 and 250 MU min<sup>-1</sup>. Measurements were taken to ensure that the response to irradiation was observed over a time interval where all responses had stabilized as shown in Figure 6.2. Three consecutive measurements were taken to evaluate leakage current both before and after irradiation.

Rise and fall times were calculated by calculating the amount of time it took a signal to cross the 10% and 90% thresholds of the calculated mean of stabilized current (see Table 6.1). Ideally, rise and fall times of the response current should be near zero. Overall, as accelerator dose rates increased, rise times fell. However, an increase in voltage resulted in an increase in rise times. Response times were best at 62.5 V, with rise times of 2 s for 100, 150, 200 and 250 MU min<sup>-1</sup>. Responses following irradiation were much faster: all 20 fall time measurements were < 2 s, or below the detectable limits with the equipment used in this study.

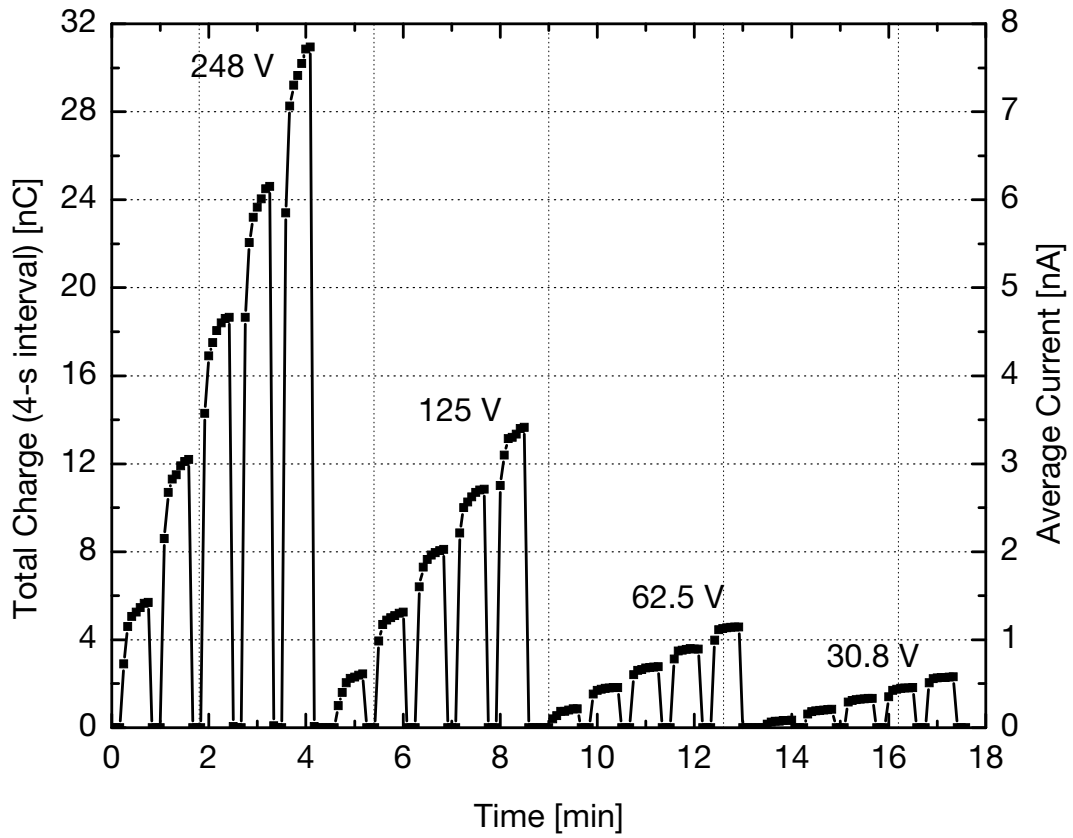


**Figure 6.2.** Total charge over 4-s intervals for output rates of 50, 100, 150, 200 and 250 MU  $\text{min}^{-1}$  (left to right) for 248, 125, 62.5 and 30.8 V.

**Table 6.1.** Rise time estimates for different voltages and dose rates [s].

Voltage [V]	Rate [MU $\text{min}^{-1}$ ]				
	50	100	150	200	250
248	14	7	7	7	7
125	14	7	7	4	4
62.5	14	2	2	2	2
30.8	21	10	5	2	2

Measuring rise and fall times was necessary to see how fast the detector could respond to different fluence rates over the given voltage range. An interesting result was that the quickest response on average was observed at 62.5 V for dose rates of 100 MU min<sup>-1</sup> and above. The resulting rise time of 2 s would potentially make this lower voltage the best of the available Farmer electrometer voltages for measuring dynamic beams, e.g. IMRT [48,294]. This also implies that using an electrometer with voltage settings above 248 V for such applications would not necessarily be appropriate for this or other similar detectors. Note that for modern applications that use higher dose rates ( $\geq 600$  MU min<sup>-1</sup>), low dose rate rise times could be ignored. Some encouraging results were the short fall (decay) times of  $< 2$  s. Note that in a recent study [48], fall times of a single crystal diamond detector and a PTW natural diamond detector were observed to be 0.78 and 1.58 s, respectively, which compare well to the fall times measured in this study. Their reported rise times also compare well with respect to the 2 s times at 62.5 V reported here, with 1.29 and 2.08 s for the single crystal and PTW detectors, respectively.

Overall, the time it took photocurrents to reach  $\sim 100\%$  from 90% improved with decreasing voltage. Estimates using the Farmer electrometer showed that photocurrent stabilized after  $\sim 30$  s for rates of 150 MU min<sup>-1</sup> and above for all voltages, and was stable after  $\sim 24$  s for rates of 200 and 250 MU min<sup>-1</sup> for 62.5 V. After signals stabilized, a ratio of photocurrent to leakage current was calculated. At a rate of 200 MU min<sup>-1</sup>, ratios of 2100, 2600, 5000 and 7200 were calculated at biases of 30.8, 62.5, 125.0 and 248.0 V, respectively. These ratios were well over the recommended value of 200 according to IAEA recommendations for reference dosimeters used in radiotherapy [283] as well as more demanding requirements set by authors assessing single crystal diamond detectors for IMRT applications [48,49,156].

Results showed that improvements in stabilizing times at higher dose rates could be found at a relatively lower voltage (62.5 V). Settling times may be partly due to the time needed for accelerator beam current to reach a steady-state as reported elsewhere [42], but most likely dominated by the release of charge from shallow energy levels at room temperature due to lattice defects as noted in literature [26,45,50,51,149,245,295]. No “overshoot” of the initial response was observed in this study as reported in some diamond in Chapter 5 and elsewhere [51,52,295], due to the use of low applied fields (up to 0.50 V  $\mu\text{m}^{-1}$ ) and high quality diamond. The resulting settling times and their effect in the dosimetry of dynamic beams will be tested in more detail in future work.

Short-term precision is a basic characteristic of any dosimetry system. Generally referred to as repeatability, it is defined as the “closeness of the agreement between the results of successive measurements of the same measure and carried out under the same conditions of measurement” [296]. To examine the repeatability of the E6SCP2 detector, several experiments were conducted to measure the repeatability of a specified dose for all available positive voltage settings. In each experiment, the detector was irradiated 5 times at 250 MU min<sup>-1</sup>. Repeatability R was then calculated as the percentage ratio of the standard deviation  $\sigma_q$  to the mean collected charge  $\mu_q$  [48]:

$$R = \frac{\sigma_q}{\mu_q} \cdot 100\%. \quad (6.1)$$

Improved repeatability was found at lower voltages. For example, repeatability of measuring total charge over 4-s intervals for 62.5 and 248.0 V were 0.1 and 0.4%, respectively; 1-s intervals were 0.2 and 0.4%, respectively. However, for 10-s intervals repeatability was 0.2% using all four voltage settings. No trend in the relative instability of the detector current using the Keithley electrometer was observed. These results show that repeatability may be optimized at a particular voltage and still meet the requirements for a secondary standard dosimetry system of < 0.5% [283]; the long-term stability (reproducibility) of an ion chamber of a secondary standard dosimetry system should also be < 0.5%. Adequate priming of the detector is then an important feature when using this diamond film.

Using the Keithley electrometer, current measurements displayed long decay times after irradiation ceased. Data acquisition using this instrument was found to be unreliable for measuring leakage currents during experiments most likely due to capacitance issues and instrument parameters required to detect photocurrent. Some authors using diamond detectors also report so-called side effects or decay times [49,52,297,298], and attribute them to thermal release of charge from shallow trap levels. In this study, it was determined that the decay (fall) times observed with this instrument were most likely due to instrumentation and cable issues and not due to diamond behaviour after comparing data from both electrometers.

## 6.4 Sensitivity

Sensitivity was found by calculating average current over five measurements using the Farmer electrometer after the beam and detector stabilized. See Figure 6.3. Sensitivities varied over the range of voltages tested, from about 14 to 235 nC Gy<sup>-1</sup> from 30.8 to 248.0 V, respectively. Aside from the observed data at 50 MU min<sup>-1</sup>, sensitivities fell within 2 nC Gy<sup>-1</sup>

over the range of dose rates and followed a linear trend from 62.5 to 248.0 V. At 62.5 V, sensitivity was weakly dependent on dose rate ( $\pm 1\%$ ).

Sensitivities indeed varied over the range of voltage tested. The highest sensitivities were observed at 248.0 V. At 248.0 V, an average sensitivity of  $235 \text{ nC Gy}^{-1}$  (or specific sensitivity of  $599 \text{ nC Gy}^{-1} \text{ mm}^{-3}$ ) compares well to other studies investigating CVD diamond detectors e.g. [26,144,149,158,299], commercial PTW detectors e.g. [289,300] and commercial Si diode dosimeters e.g. [301]. High sensitivity was attributed to a low concentration of sample defects and/or a favourable concentration of dopants such as nitrogen that allow for high charge collection efficiency as well as low leakage currents. Sufficient sensitivity levels were found using this diamond detector configuration within the voltage range of the Farmer electrometer and especially at 248.0 V. Even at 62.5 V, such levels are believed favourable for some applications in IMRT where small deliveries of monitor units are used, but further studies with respect to these complex fields are required.

Detector sensitivity was also compared while reversing bias polarity as illustrated in Figure 6.4. Sensitivity was determined this time at fixed rates of 50 and 250  $\text{MU min}^{-1}$  for 248.0, 125.0, 62.5, 30.8,  $-30.8$ ,  $-62.5$ ,  $-125.0$  and  $-248.0$  V. Applying a negative voltage gave a more-linear response down to 0 V, but reduced sensitivity by almost 25% at 248.0 V and 250  $\text{MU min}^{-1}$ . At 250  $\text{MU min}^{-1}$ , 62.5 V gave nearly the same sensitivity regardless of polarity (37 and 38  $\text{nC Gy}^{-1}$  for a positive and negative bias, respectively.)

It is common to perform certain calibrations for ion chambers and dosimeters to correct for polarity effects and determine charge collection efficiencies [279]. Dependence on bias polarity in this study may have been due to device design such as electrode material and encapsulation as reported in detailed studies of ionization chambers [25,302-305]. Other authors note that a change in response due to polarity is due to heterogeneity in the growth direction [219]. The data suggests that the electron trap populations may therefore be quite similar regardless of the direction of the applied field at 62.5 V. Correction factors due to polarity could be found for this detector, given that this quantity is found to be independent of other influencing quantities.

Reproducibility (or long-term precision) of the detector, along with its instrumentation, in terms of sensitivity over a period of two months in which this study took place varied by 1.2% (1 $\sigma$ ).

Note that due to functional limitations of the Farmer electrometer, individual measurements of charge were limited to 204.75 nC. Using a smaller applied field e.g. 62.5 V

with a sensitivity of  $37 \text{ nC Gy}^{-1}$  would therefore allow for a single measurement of charge up to  $\sim 5.5 \text{ Gy}$  versus  $\sim 0.87 \text{ Gy}$  for  $248 \text{ V}$ .

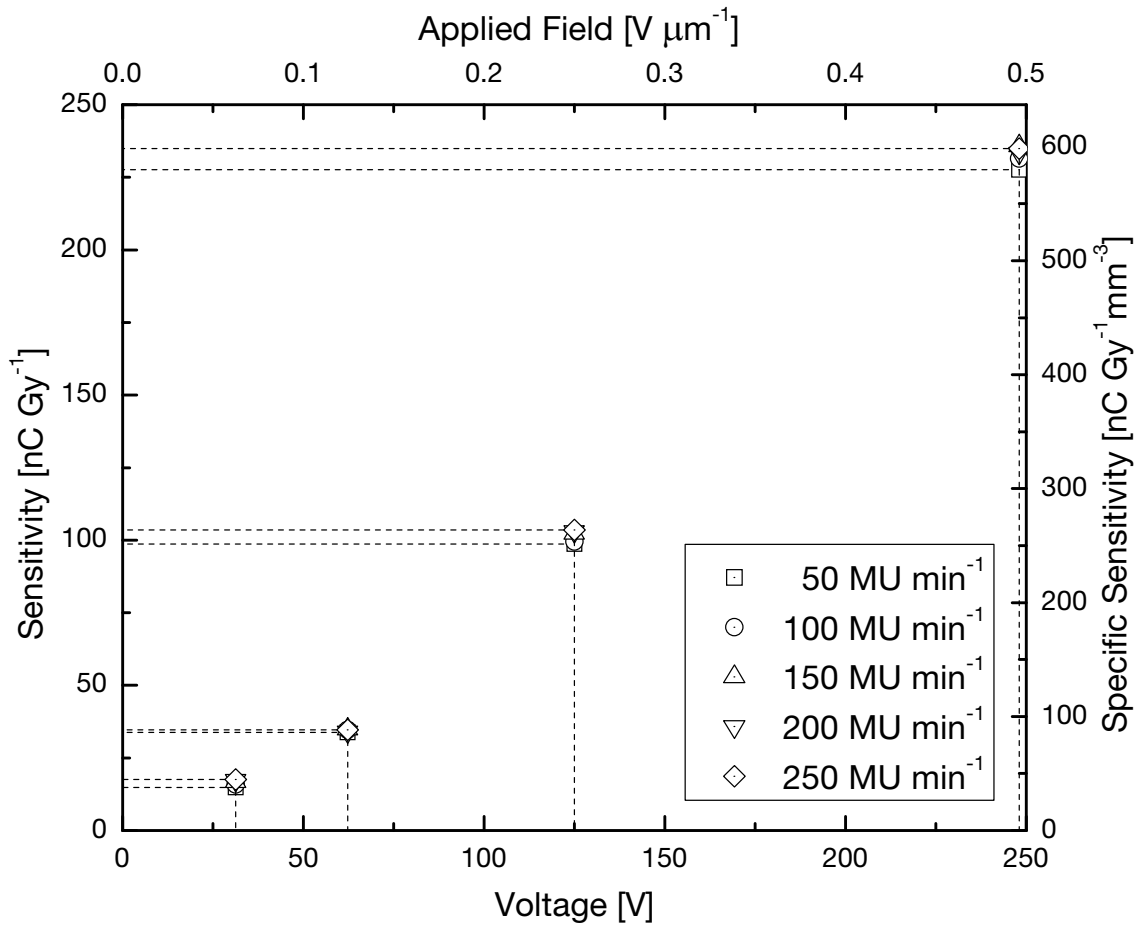


**Figure 6.3.** Sensitivity vs. operating voltage over the available ranges of positive voltages and nominal dose rates. Horizontal lines illustrate the range of sensitivities within one group.

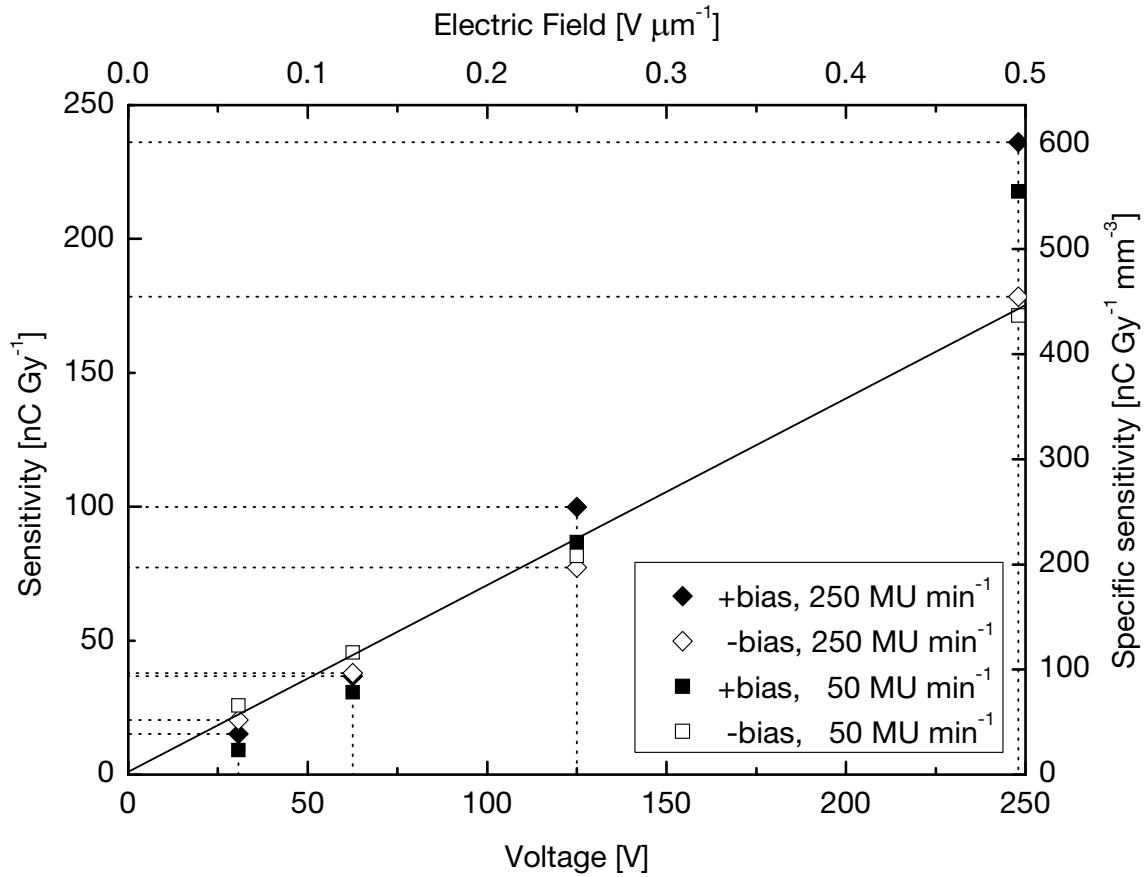


**Figure 6.4.** Sensitivity vs. absolute voltage. A straight line is drawn for comparison. Horizontal lines illustrate the difference in sensitivity when polarity is reversed when measuring delivery rates of  $250 \text{ MU min}^{-1}$ .

## 6.5 Dependence on Dose and Dose Rate

The detector was tested for dose and dose rate dependence over the available range of (positive) voltages. Dose dependence was evaluated by measuring charge over a range of 0–7.7 Gy using the Keithley electrometer. Figure 6.5 illustrates three such examples for 100, 150 and 200 V. Ideally, a linear relationship should occur between charge and dose. Overall, dose dependence was found to be linear for 100, 150 and 200 V from 0.77–7.7 Gy. Specifically, the  $R^2$  parameter of the linear best fit was found to be 0.9999 and 1 for ranges of 0–7.7 and 0.77–7.7 Gy, respectively, for all voltages tested. Repeatability of data e.g. at 0.77 Gy were 1.0, 1.2 and 4.0% for 100, 150 and 200 V, respectively ( $n = 5$ ), which was higher than when the E6SCP2 detector was used with the Farmer electrometer.



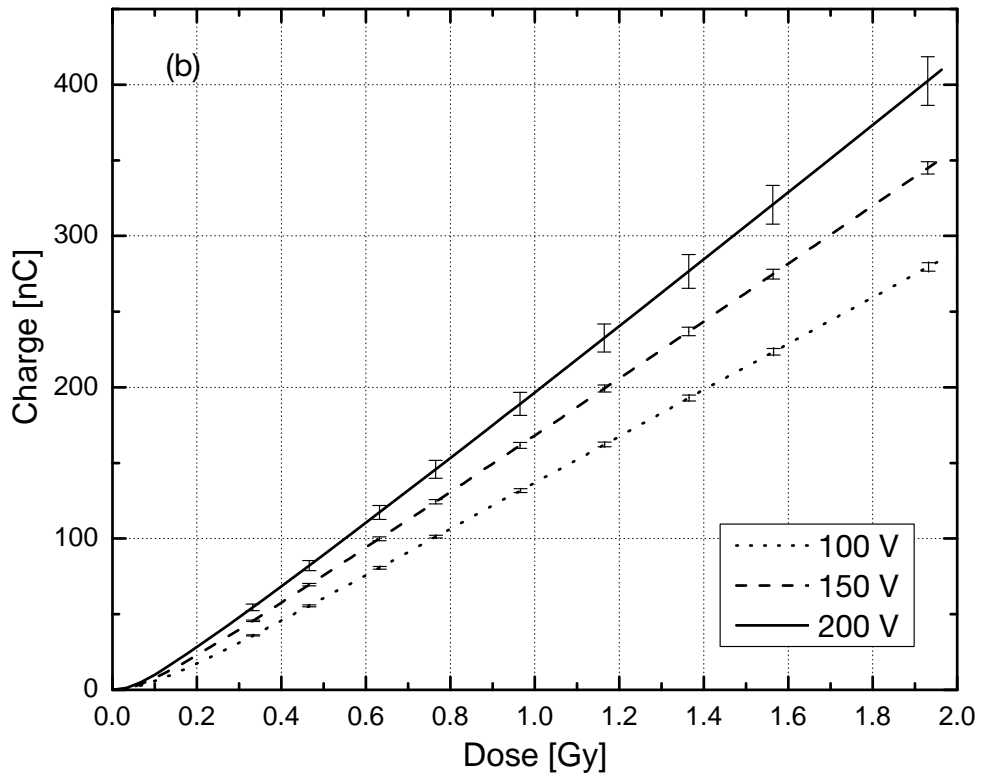
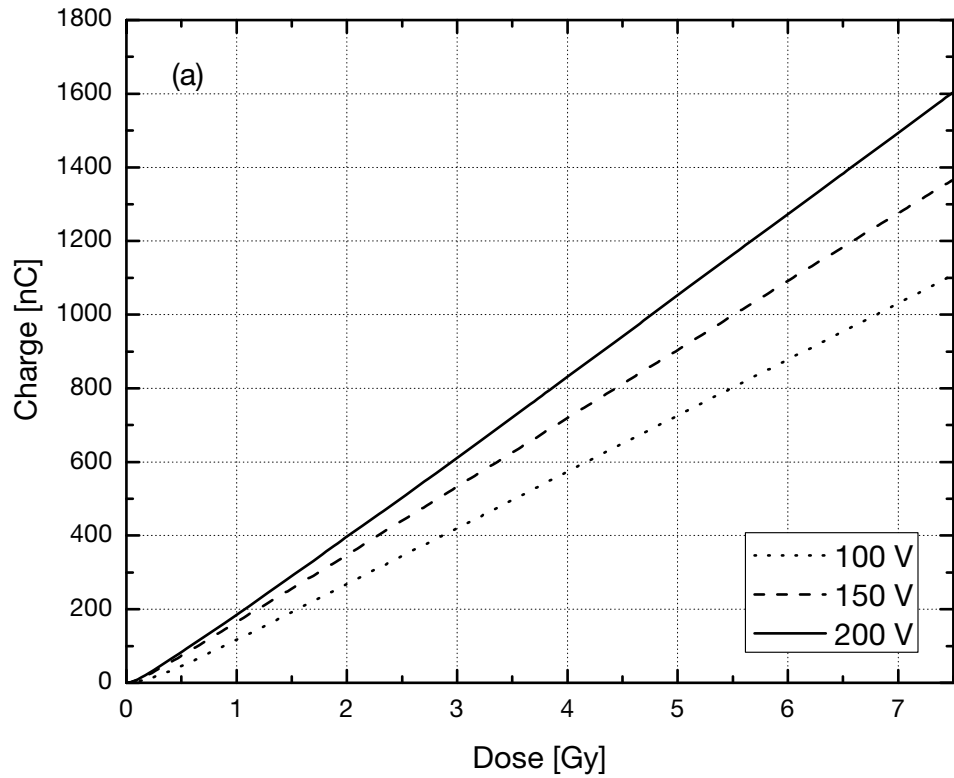


**Figure 6.5.** Charge vs. dose using a dose rate of  $1.95 \text{ Gy min}^{-1}$  at 100, 150 and 200 V over (a) 0–7.7 Gy and (b) 0–1.95 Gy. Lines represent hundreds of data points. Error bars are only shown at several chosen intervals for clarity.

Dependence on dose for this detector was linear for all of the available voltages tested. A saturation (rise) time of at least 2 s existed for all measurements, and so a slight nonlinear relationship between charge and dose was expected for doses under 1 Gy as noted in the literature [157]. Consequently, any improvement in the rise time (i.e. a quicker response) will improve dose linearity. In addition, the relationship between dose and total charge will most likely change favourably with higher dose rates, especially small doses delivered expeditiously with modern techniques such as IMRT.

Dose rate dependence was investigated over all available accelerator dose rates and all four available positive voltage settings of the Farmer electrometer as shown in Figure 6.6. Dependence on dose rate was calculated by using the fitting function Eq. (5.2) to test for linearity as described in Section 5.4, where a power law regression is used to test for linearity [285,286]; here, leakage current  $I_0$  from Eq. (5.2) was allowed to vary. Dose rates were obtained by varying the pulse repetition rate settings of the accelerator via the user console. Errors bars were not plotted, as uncertainties were small compared to current values. Repeatability of data were between 0.40 and 0.60% ( $n = 10$ ). The corresponding  $\Delta$  and square of the sample correlation coefficient  $R$  values are given in Table 6.2. Three of the four  $\Delta$  values were within  $1\sigma$  of unity. Note in Figure 6.6 that a nonlinear relationship between voltage and photocurrent, which is the same trend observed in Figure 6.3.

When investigating dose rate, a slight decrease in  $\Delta$  was observed by increasing voltage. This was in contrast to a previous study by Fidanzio *et al.* [292], which reported an improvement in dose rate linearity with increasing bias voltage, and where unity was reached when their detector was biased at  $6 \text{ V } \mu\text{m}^{-1}$ , an order of magnitude higher than the attainable field used in this study ( $0.5 \text{ V } \mu\text{m}^{-1}$ ). In addition, De Angelis *et al.* reported a 7% increase in  $\Delta$  when applying a voltage from 100 to 1 000 V ( $0.2$  to  $2 \text{ V } \mu\text{m}^{-1}$ ) [294]. Most studies of either PTW natural diamond or CVD diamond detectors report  $0.86 < \Delta < 1$ , e.g. [149,153,292,294,306,307], and as high as 1.07 [45], outside the typical range following Fowler theory [285]. In this study,  $\Delta$  values calculated for 30.8, 62.5 and 125.0 V came within  $1\sigma$  of unity. The error in  $\Delta$  values reported in this study may be due to measuring a slow response at low doses and dose rates as well as using only 5 data points. A future study would benefit from a wider range of dose rates.

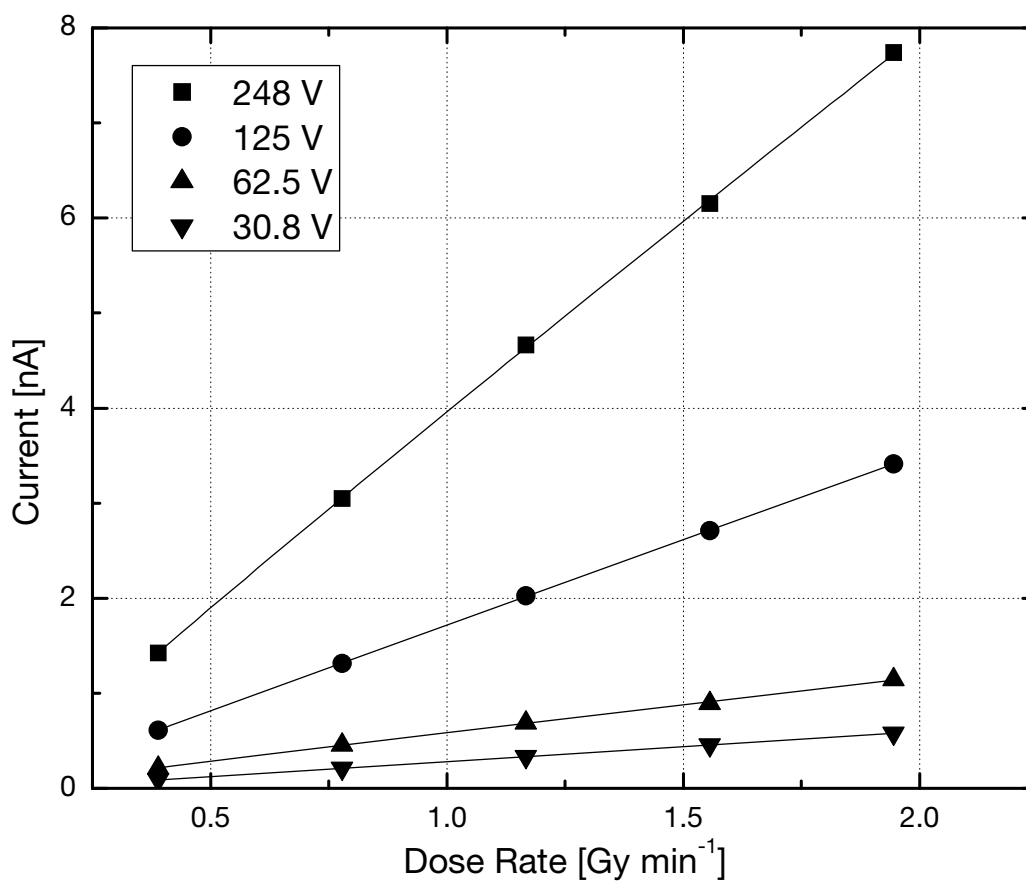


**Figure 6.6.** Photocurrent vs. dose rate for 30.8, 62.5, 125 and 248 V.

**Table 6.2.** Summary of fitting parameters  $\Delta$  and  $R^2$  for dose rate dependence.

V	$\Delta$	$R^2$
248.0	$0.95 \pm 0.03$	0.9999
125.0	$0.99 \pm 0.01$	1
62.5	$0.95 \pm 0.08$	0.9992
30.8	$1.01 \pm 0.02$	1

## 6.6 Concluding Remarks

To clarify, a summary of the results is listed in Table 6.3.

**Table 6.3.** Summary of findings for the operating voltage analysis.

Criterion	Finding
Leakage current	Negligible for all voltages tested ( $< 2.5 \text{ pA}$ )
Rise time	Best at 62.5 V: 2 s for 100, 150, 200 and 250 $\text{MU min}^{-1}$
Fall time	$< 1 \text{ s}$ for all voltages tested
Sensitivity	Sufficient for voltages $\geq 62.5 \text{ V}$ ( $\geq 37 \text{ nC Gy}^{-1}$ )
Polarity	62.5 V most consistent; (–) polarity more linear over voltages tested; corrections would be required for either (+) or (–) voltage settings
Dose dependence	No preferred voltage (100, 150 and 200 V); $R^2 = 1$ for 0.77–7.7 Gy
Dose rate dependence	No preferred voltage (30.8, 62.5, 125.0 and 248.0 V); corrections would be required as all $\Delta \neq 1$

An x-ray detector fabricated from commercially available single crystal CVD diamond film was used to investigate how changes in an applied field affected detector response, and determined whether an optimal operating voltage could be realized within the limits of conventional instrumentation used in radiation therapy. After investigating several dosimetric characteristics, the results of this study indicate a preference towards using 62.5 V due to its minimal rise time yet sufficient sensitivity, which was only weakly dependent on polarity. At this voltage, a much wider range of dose based on charge may also be recorded with the Farmer electrometer than at higher voltages where higher sensitivities are obtained. It may be tempting or even useful to use the highest voltage setting for either electrometer (or even higher with others), but this may result in limiting the use of this detector to a specific application where the temporal response is not important.

Magnitude as well as direction of the applied field had a considerable effect on detector behaviour. Leakage current was negligible during tests using a typical clinical dosimetry setup, reducing the use of correction factors and sources of error. One area of improvement will be further reducing the observed rise time and time to stability, which is critical to the success of diamond detectors as pinpoint chambers in complex fields; this shall be addressed in future work. Correction factors may be used to adjust for polarity, dose and dose rate dependence, although this is not ideal.

Experiments investigating the E6SCP2 detector for clinical use, e.g. tissue maximum ratios, off-axis beam profiles and small fields, are presented and discussed in the next chapter.

# 7. Clinical Investigations

---

In Chapter 5, a single crystal diamond detector (E6SCP2) was selected as a candidate for more detailed clinical analyses due to favourable response characteristics. In Chapter 6, the E6SCP2 detector was used to investigate how changes in applied electric field affected detector response and determined a preferred operating voltage within the limits of a conventional electrometer used in radiotherapy [167]. In this chapter, the same detector was used to evaluate some of its clinical advantages and limitations. This includes a closer look at repeatability and dose rate dependence, as well as comparing output factors, percent depth dose and off-axis profiles with an ion chamber or Si diode detector. Because the temporal response of the detector was not important for the following measurements, a voltage setting of 248 V was selected for high sensitivity.

## 7.1 Setup

The thin Perspex set-up in Section 3.5.3 was used for the following experiments. Details regarding source-to-surface distance (SSD), source-to-detector distance (SDD), measurement at depth  $z$ , dose rates, etc. are described in each section. A voltage setting of 248 V was used for the following experiments using the Farmer electrometer. A priming dose of  $\sim 10$  Gy was given before each experiment. Unless noted otherwise, the detector was oriented in the face-on position.

## 7.2 Repeatability

Repeatability was first calculated in Chapter 6 to observe any trend in short-term fluctuations of the E6SCP2 detector as a function of operating voltage. Here, the repeatability of the detector was examined more closely over several experiments. Repeatability  $R$  was calculated as the percentage ratio of the standard deviation  $\sigma_q$  to the mean collected charge  $\mu_q$  as defined in Eq. (6.1). A dose of 0.77 Gy (100 MU) was chosen so that total charge could be collected within one measurement and is a standard dose used in reference dosimetry for this setup.

The first set of measurements involved varying the target dose to evaluate detector resolution of dose. Total charge was measured 10 times for machine output rates of 98, 99, 100, 101 and 102 MU, with ~30 s between each set of doses and ~6 s between measurements as shown in Figure 7.1. Figure 7.2 illustrates an improvement by excluding the first measurement of each set. Dose values separated by a single MU (0.77 cGy) were statistically distinguishable using a student's t-test ( $P < 0.01$ ). Repeatability was found to be 1.0-1.5% and 0.4-0.6% for each set of measurements before and after excluding the first measurement, respectively; the improved repeatability compares well with the literature [48,60,156,294]. When the first measurement in a sequence is excluded to stabilize detector response, the average response meets IAEA requirements that call for the short and long-term stability of a secondary standard dosimeter to be  $< 0.5\%$  [254]. Each data point was then plotted in Figure 7.3 to illustrate this comparison as well as overall sensitivity within this range of dose. Górka *et al.* excluded the first measurement in their calculations of detector response due to stability but did not quantify the improvement [60].

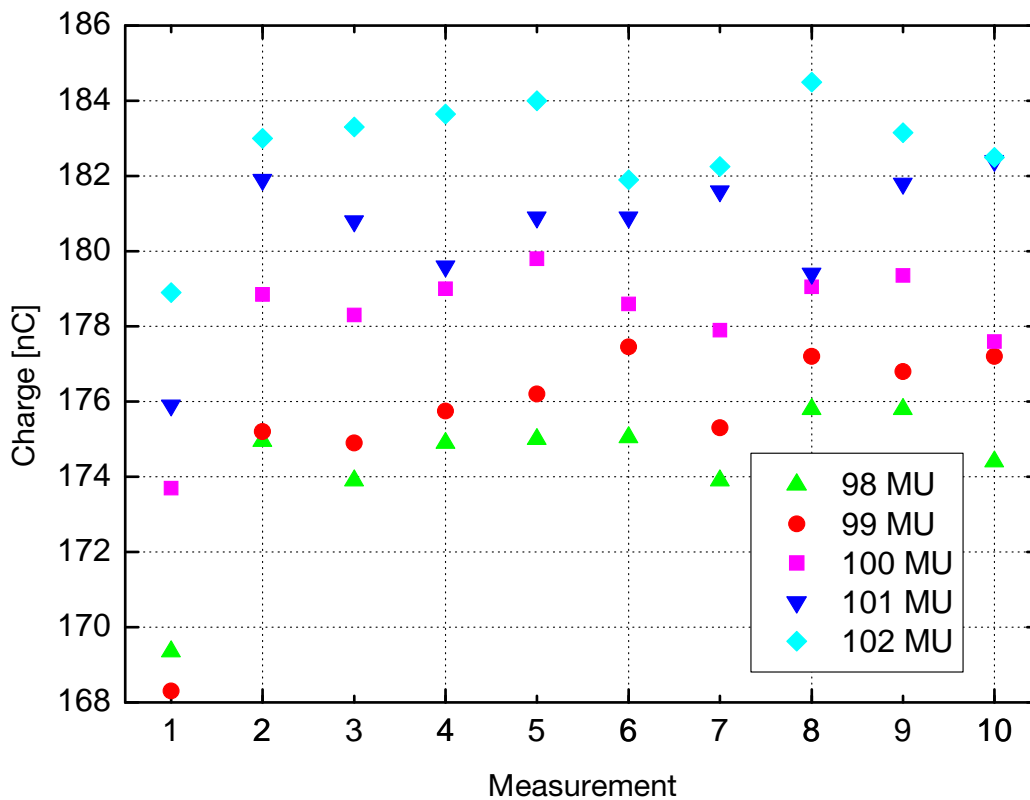


**Figure 7.1.** Total charge per fixed dose measurements of 98, 99, 100, 101 and 102 MU.

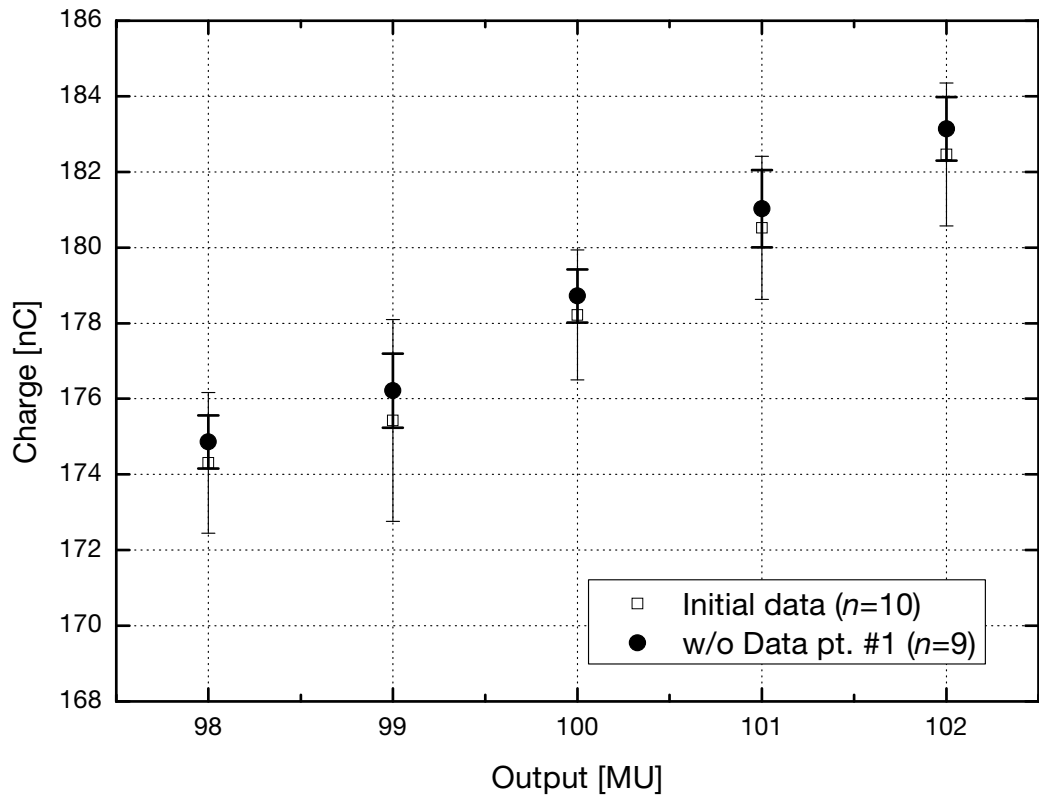


**Figure 7.2.** Total charge per fixed output measurement. Error bars are plotted for  $n = 9$  (●, thick bars) and  $n = 10$  (□, thin bars).

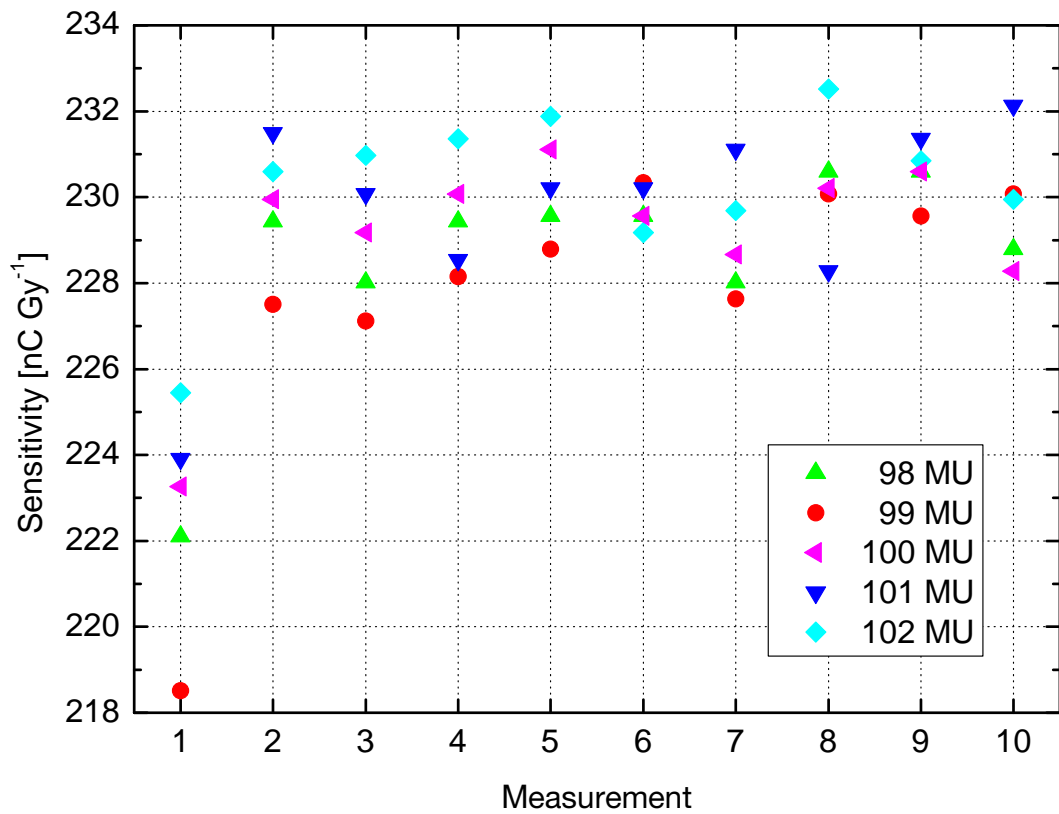


**Figure 7.3.** Sensitivity per fixed dose measurement.

It is known that trapped electrons in shallow defects of diamond are released at a probability  $1 - e^{-t/\tau}$ , where  $\tau$  is the detrapping time constant, as described in Chapter 2 [101,104]. Here, a set of measurements was performed to illustrate and quantify the reduction in sensitivity between individual measurements due to this trapping mechanism. The experiment involved measuring total charge for fixed doses of 0.77 Gy (100 MU) but then varying the time interval between measurements. Time intervals varied from 6 to 120 s as shown in Figure 7.4. The best curve fit, assuming an exponential release of charge over time, was a second-order exponential fit with an  $R^2 = 0.997$  and  $\tau$  values of 4.3 and 62.0, which was plotted to the data. The fit gave a sensitivity that stabilized to  $\sim 210 \text{ nC Gy}^{-1}$  for long time intervals, or an 8.5% relative reduction in sensitivity over the tested range. Regardless of the time between irradiation measurements, repeatability of charge was consistent as long as time intervals between irradiations were held fixed.

The data agrees with the literature that this material, albeit high-quality single crystal CVD diamond, contains defects that lead to detrapping of charge in the bulk material due to thermal effects near room temperature [101,104,308]. This detrapping phenomenon reduces short-term sensitivity as reported by other authors investigating CVD diamond [60,159,294,295]. Fitting the data at first with a first-order exponential fit gave an  $R^2 = 0.954$  with a  $\tau$  value of 23.0. The second-order exponential fit suggests that there were at least two primary and active but unstable trapping populations or energy levels that released charge at different rates [295].



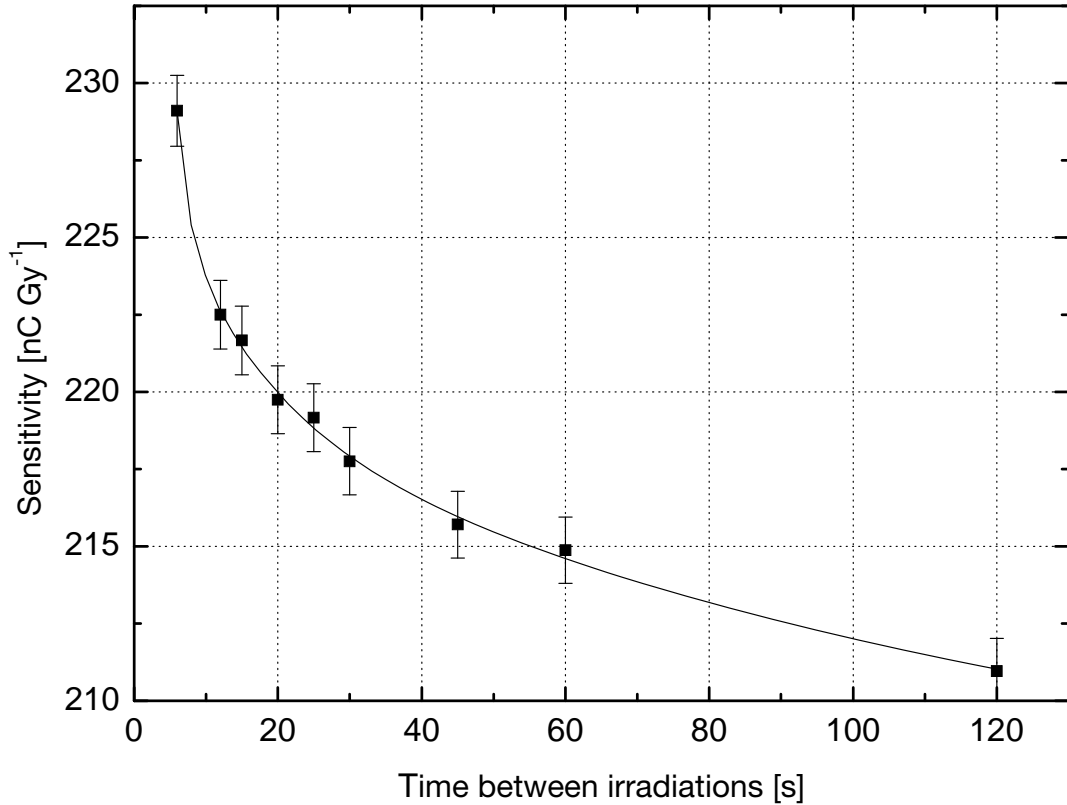


**Figure 7.4.** Sensitivity vs. time intervals between irradiations. An exponential curve fit is plotted.

Although quality has improved, trapping mechanisms were still identified in single crystal CVD diamond. Improvements in the growth process may still be needed to reduce the amount of defects in the material to mitigate the impact on device sensitivity. There have also been studies that aim to improve detection response following synthesis. A few reports in the literature suggest making improvements via neutron irradiation [309] or an increase in temperature of the sensitive volume [51,295]. Using a lower voltage as shown in Chapter 6 may reduce the effects of detrapping following irradiation, but this will also reduce sensitivity. Further experiments could be performed focusing on the effects of an applied electric field on defect populations as well as the presence of a magnetic field, whose effects have been observed in radiation monitoring for the BABAR experiment at Stanford [298].

For assurance of stability for clinical applications, this detector would require a priming dose to initially fill shallow and deep trapping levels and then a short priming dose any time the detector was not irradiated over a time interval that resulted in an unacceptable increase in the variability of the detector response.

### 7.3 Dose Rate Dependence: Fixed Dose Analysis

In Section 5.5, dose rate dependence was investigated using the relationship between conductivity, and therefore induced current, with dose rate [285]. However, most studies in the literature, including those carried out in Chapters 5 and 6, either allow the current to stabilize or do not report if a fixed dose was used. Ideally, the dosimeter reading  $m$  should be linearly proportional to the dosimetric quantity  $q$ ; for dose rate, the response of a dosimetry system  $m/q$  at two different dose rates should remain constant [174]. Here, dependence on dose rate was examined by measuring total charge for a fixed dose as a function of dose rate.

A dose of 0.77 Gy was repeated 5 times at nominal dose rates of 50, 100, 150, 200 and 250 MU min<sup>-1</sup> as shown in Figure 7.5. Error bars show average uncertainties. To predict a trend in the data, a first-order exponential curve fit to the data reveals that sensitivities converge at  $\sim 230$  nC Gy<sup>-1</sup>, the same sensitivity found in Section 5.4. In addition, when inspecting measured charge over a range of 100 MU min<sup>-1</sup> along the x-axis, the standard deviation of charge drops below an extrapolated 0.60% at dose rates  $\geq 450$  MU min<sup>-1</sup>. One can extrapolate dose response and hence sensitivity to vary by 0.60, 0.10 and 0.00% at 450, 600 and 1,000 MU min<sup>-1</sup>. Therefore, minimal correction would be needed for dose rate when using this detector in regions where dose rates are expected to be  $> 3.5$  Gy min<sup>-1</sup> using the given parameters and setup. This is a favourable result if the response of diamond detectors is required to be reproducible within 0.50% when used in modern conformal treatments that use higher dose rates.

Average current was calculated using the above data and then plotted against dose rate in Figure 7.6 to calculate dependence on dose rate. Error bars are shown in the figure, and were small compared to measured current values. Using curve fitting Eq. (5.2) gave a  $\Delta$  value of 0.92, which was reasonable but less than the ideal value of 1.00 found in Section 5.5 where a dose of  $\sim 1.3$  Gy at 250 MU min<sup>-1</sup> (1.95 Gy min<sup>-1</sup>) was used to stabilize currents. Many studies in the literature report using the Fowler relationship to evaluate the dose rate dependence for diamond but do not use or report a fixed dose. Some early studies [29,136], however, point out that the *instantaneous* value of  $\Delta$  decreases with increasing dose rate; this agrees with the theory for conductivity induced in insulating materials [285], which explains the trend in Figure 7.5. Therefore, it is important to analyze any variation in dose rate dependence. Note that this  $\Delta$  value is therefore valid for the range of dose rates studied only (0–1.95 Gy min<sup>-1</sup>). Subsequent experiments in this chapter used a  $\Delta$  value of 0.92 to correct data after clinical measurements.

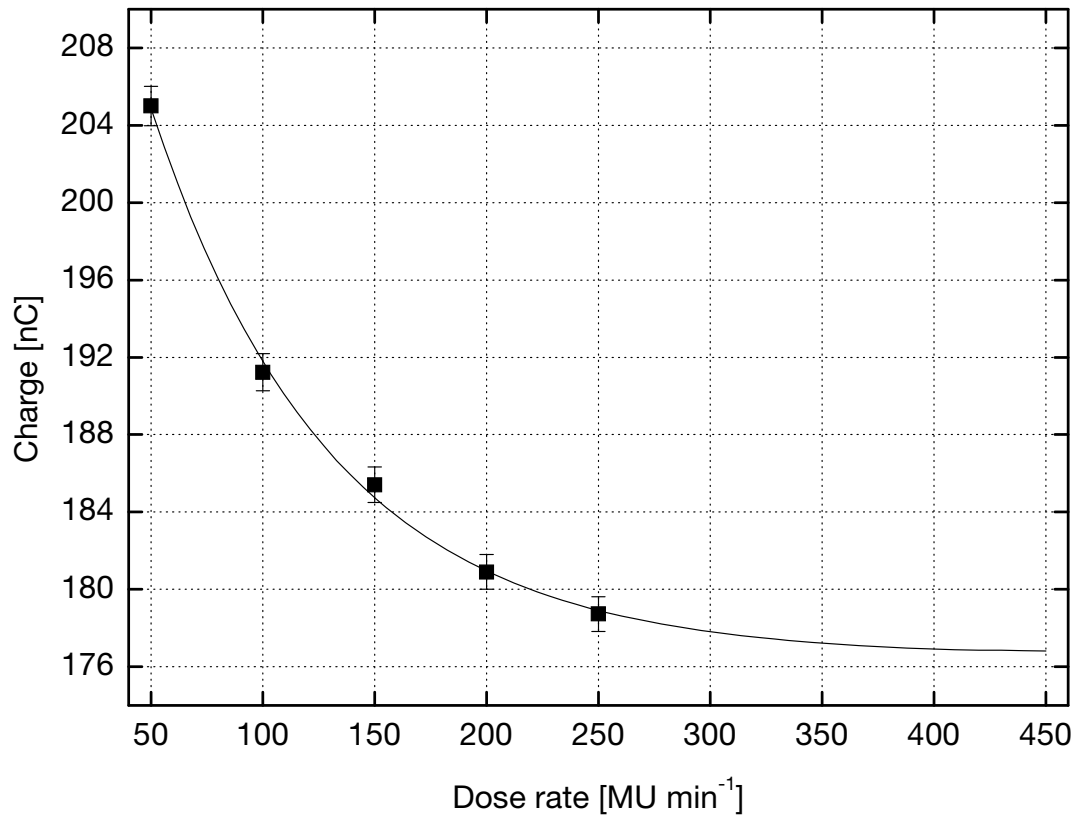


Figure 7.5. Total charge from a fixed dose of 0.77 Gy vs. dose rate.

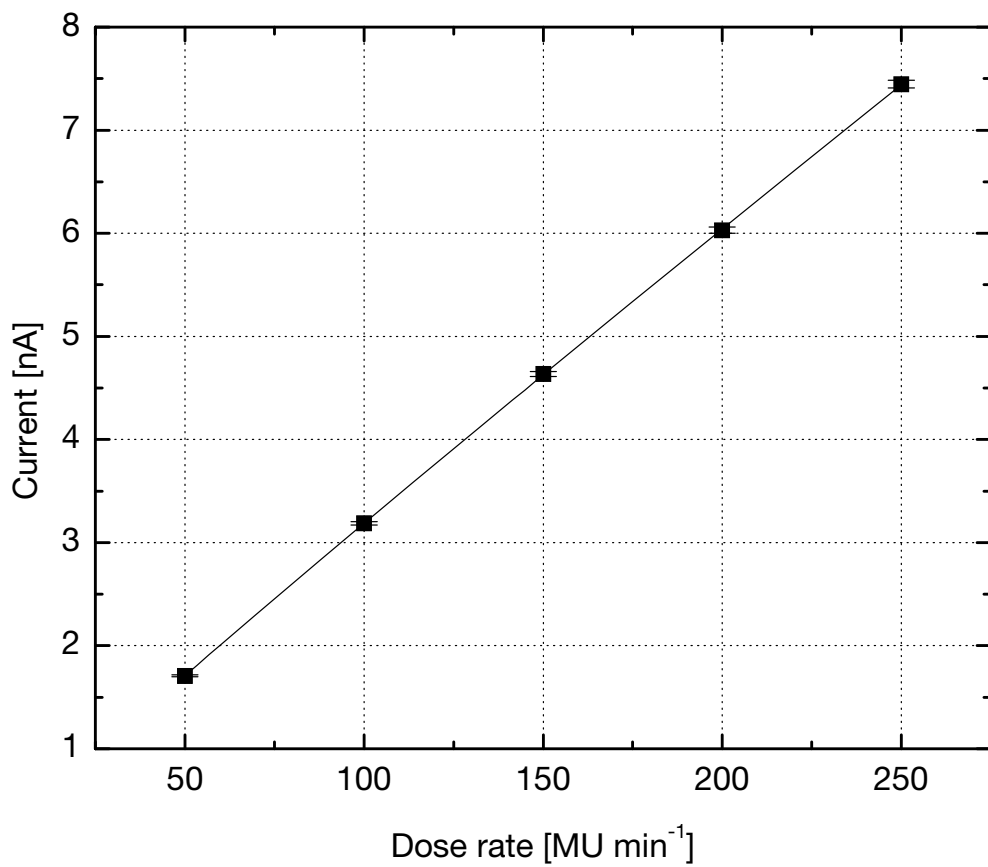


Figure 7.6. Average current vs. dose rate using fixed doses of 0.77 Gy.

## 7.4 Tissue Phantom Ratios

Several methods exist to calculate the relative absorbed dose to a patient, which include percent depth dose (PDD), tissue-air ratio (TAR), tissue-phantom ratio (TPR) and tissue-maximum ratio (TMR) [173,174]. PDD is dependent on SSD, which makes it unsuitable for isocentric techniques [173]. The use of TAR eliminates this problem but its use is limited to measurements in air. TPR and TMR were introduced to overcome limitations of TAR and were used in this project to compare dosimeter response as a function of depth.

The tissue-phantom ratio is defined as the ratio of the dose at a point Q on the central axis of a phantom at depth  $z$  to a dose at point  $Q_{\text{ref}}$  in a phantom at reference depth  $z_{\text{ref}}$  [174]:

$$\text{TPR}(z, A_Q, hv) = \left[ \frac{D_Q}{D_{Q_{\text{ref}}}} \right], \quad (7.1)$$

where  $A_Q$  is the field size at point Q and  $hv$  is the photon beam energy. A correction factor  $1/\Delta$  was used following measurements to compensate for dose rate dependence [292]. A special case of TPR is the tissue-maximum ratio, where the reference depth  $z_{\text{ref}}$  is equal to the maximum depth  $z_{\text{max}}$ :

$$\text{TMR}(z, A_Q, hv) = \left[ \frac{D_Q}{D_{Q_{\text{max}}}} \right]. \quad (7.2)$$

TPR data for the E6SCP2 detector was converted to TMR data, which could then be compared to TMR reference data for clinical dosimetry measured using a Farmer 0.6 cc ion chamber (PTW, Freiburg, Germany) [277]. A  $\Delta$  value of 0.92 found by the method in Section 7.6 was used. To perform these measurements, the couch height was held fixed to give an SDD = 100 cm and then slabs of Solid Water were added to increase measurement depth  $z$ . Measurements of 0.77 Gy were repeated 5 times at each depth with  $R < 0.70\%$ , where the first measurement was excluded as described in Section 7.2.

The TMR comparison is illustrated in Figure 7.7. Following a correction for dose rate dependence, the E6SCP2 detector agrees with the ion chamber to within 0.75%. Previous investigations also report similar comparisons between diamond detectors and ion chambers where both detectors are in good agreement once dose rate corrections are made for diamond [47,137,153,310]; a higher response for diamond is due to dose rate dependence, which originates from an inhomogeneous trap distribution [285].

Future work with this or similar (and preferably thinner) diamond detectors should include measuring PDD or TPR for small fields  $< 4 \times 4 \text{ cm}^2$ , where PTW natural diamond detectors have already been shown to be more accurate than other traditional dosimetry methods and ion chambers inadequate [148]. These values could then be compared to an analytical model proposed by Sauer *et al.*, as little data for such small fields exists in the literature [311].

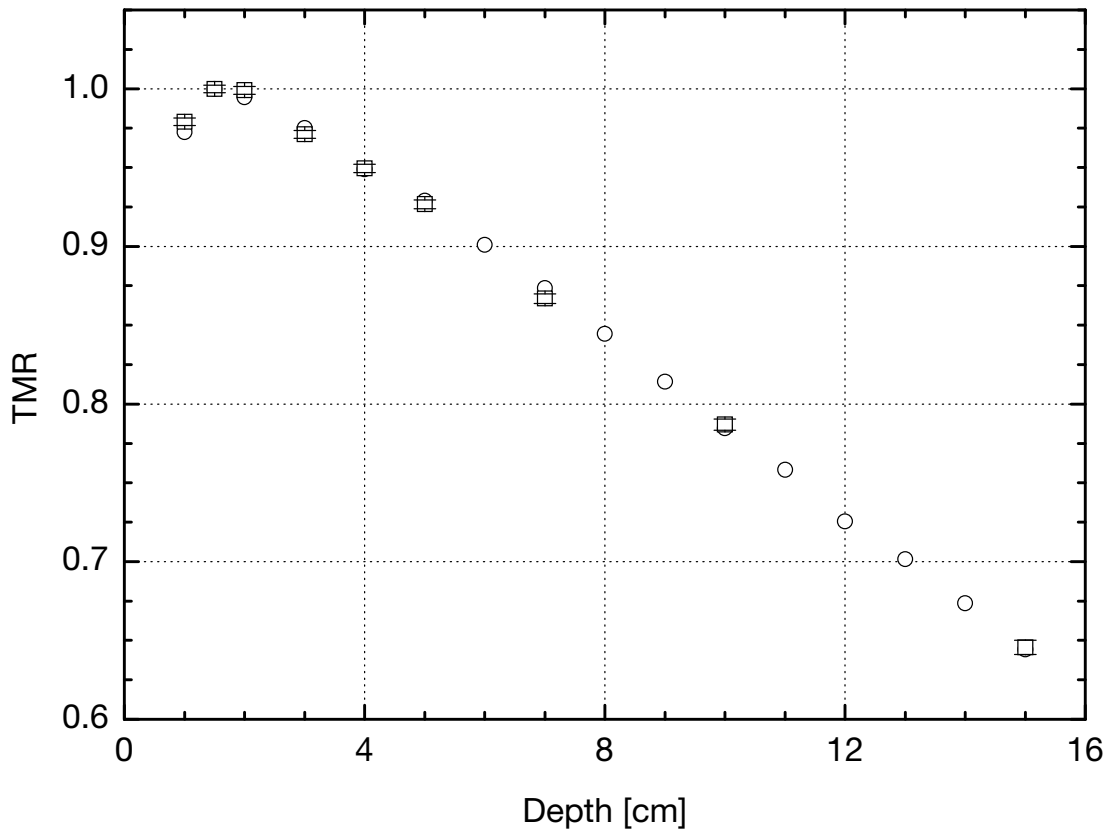


**Figure 7.7.** Tissue-maximum ratios for E6SCP2 (□) with error bars and a Farmer ion chamber (○).

## 7.5 Output Factors

A relative dose factor or machine output factor (OF) is a radiation treatment parameter for external beam radiotherapy, which is a method used to account for variations in collimator and phantom scatter with field size. OFs are defined as the ratio of the dose at a point P in a phantom for field size  $A$ ,  $D_p(A, b)$ , to a dose at point P in a phantom for a  $10 \times 10 \text{ cm}^2$  field,  $D_p(10, b)$  [174]:

$$\text{OF}(A, bv) = \left[ \frac{D_p(z_{\text{max}}, A, f, bv)}{D_p(z_{\text{max}}, 10, f, bv)} \right], \quad (7.3)$$

where  $z_{\text{max}}$  is the measurement depth at maximum dose,  $f$  is the SSD and  $bv$  is the beam energy. Again, a correction factor  $1/\Delta$  was used as a measurement correction factor to compensate for dose rate dependence [292] as in the previous section.

The E6SCP2 detector in the “edge-on” configuration (lateral width = 0.5 mm) was used to measure OFs and was compared to reference data using a 0.125 cc PTW waterproof thimble ion chamber [312]. The detectors were placed at isocenter (SAD = 100 cm). To avoid electron contamination of the photon beam at shallow depths, data were measured at a reference depth of  $z = 10$  cm then corrected to the depth of maximum dose,  $z_{\text{max}} = 1.5$  cm, using TMR reference data. Fixed doses of 0.59 Gy (75 MU) were used to measure detector response for each field size; a smaller dose was used at the time for convenience but did not affect repeatability of the data ( $n = 4$ ,  $R < 0.50\%$ ). OF data were compared to existing reference data at several field sizes, from  $15 \times 15$  cm<sup>2</sup> down to  $3 \times 3$  cm<sup>2</sup>. To compare with the literature, field sizes were measured with the E6SCP2 detector down to  $0.6 \times 0.6$  cm<sup>2</sup>. Output factor measurements of both detectors were fit with the following rational function, which was used as a best fit by the radiation oncology physics group at the hospital to normalize OF data:

$$\frac{a + bs}{1 + cs + ds^2}, \quad (7.4)$$

where  $s$  represents field size and  $a$ ,  $b$ ,  $c$  and  $d$  are fitting parameters. Data were then normalized using the best fit functions to a  $10 \times 10$  cm<sup>2</sup> field as shown in Figure 7.8.

Following corrections for dose rate dependence, OF values matched well from  $3 \times 3$  to  $10 \times 10$  cm<sup>2</sup> field sizes. Agreement between dosimeter measurements was within 1.3%. The E6SCP2 output factor value of 0.66 for a  $1 \times 1$  cm<sup>2</sup> field also matched the datum point to within 1% plotted by Laub and Wong [147] and Sauer and Wilbert [313] (extrapolated) in their analyses of output factors. A recent paper by Manolopoulos *et al.* compared two diamond detectors with a novel Si diode array but used different setup parameters [314].

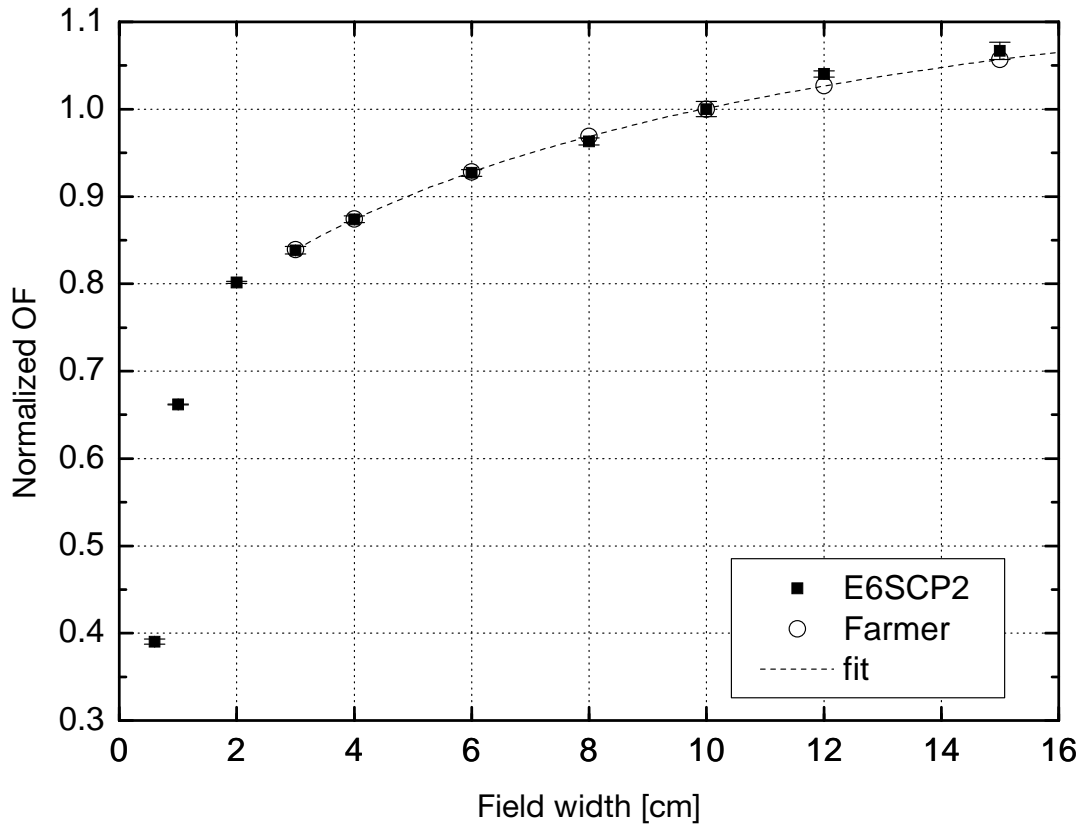


**Figure 7.8.** Comparison of Output Factors for E6SCP2 (■, with error bars) and a Farmer ion chamber (○). A best fit line for normalization is shown.

OFs are difficult to measure for small fields due to a lack of electron equilibrium and high dose gradients, and differences are seen when comparing OF data in fields  $< 3 \times 3 \text{ cm}^2$  [13]. Reports have compared (natural) diamond, diode, pinpoint or ion chambers and Monte Carlo simulations of small fields using different methods, e.g. [13,17,23,150,315,316], with the literature recently reviewed by Sauer and Wilbert [313]. These studies conclude that spatial resolution, composition and density of the detector are generally the most important factors for measurements in small fields. Natural diamond was found to be potentially suitable for output factor measurements for small fields because of its high spatial resolution and near-tissue equivalence, which minimizes perturbation effects due to stopping power ratios between diamond and water [13,147]. However, detector construction and contact material had an effect on sensitivity due to energy dependence [294,313]

Examining detector construction and different electrode materials is an area of future research for our research group, where electrode materials and thicknesses via Monte Carlo simulations are being explored. Preliminary Monte Carlo investigations have found that

electrode material as a function of atomic number (e.g. Ag, Al and Au) has an effect in both the face-on and edge-on configurations of the device.

## 7.6 Beam Profiles

Beam profile measurements are used in addition to central axis dose distributions to extend the calculation of dose to two and three dimensions. A beam profile consists of the umbral region, where the beam is not affected by collimators, and the penumbral region, where the field is indeed affected by collimators. The region of significance in this investigation is the penumbra, where changes in dose fall steeply with increasing distance from the central axis. This region is especially important for small fields, and so a detector with good spatial resolution is preferred to measure dose.

An off-axis ratio (OAR) was used to measure dose perpendicular to the central beam axis at a reference depth  $z_{\text{ref}}$  which may be defined as the ratio of total charge of the detector response at an off-axis point to the total charge on the central axis at the same depth. Dose at any point along the beam profile can then be found using the depth dose at the central axis and OARs. Dose at a point  $D(z_{\text{ref}}, x, y)$  can be defined as [187]:

$$D(z_{\text{ref}}, f, s, x, y) = OAR(z_{\text{ref}}, f, s, x, y) \times \left[ \frac{\%D(z_{\text{ref}}, f, s, 0, 0)}{100} \times D(z_{\text{max}}, f, s, 0, 0) \right], \quad (7.5)$$

where the expression in brackets represents the absorbed dose to a point  $z$  on the central axis, which is derived from the definition of percentage depth dose  $\%D(z_{\text{ref}}, f, s, 0, 0)$ .

The E6SCP2 detector was compared to available reference data from a Scanditronix p-type Si diode detector [10] of a  $10 \times 10 \text{ cm}^2$  field size at SDD = 100 cm at a  $z_{\text{ref}} = 10 \text{ cm}$ . Measurements were performed with the diamond detector in the “face-on” and “edge-on” orientations to compare spatial resolutions of 1 and 0.5 mm, respectively. Five measurements were repeated at each step in field size; the first measurement was ignored as in the previous section. Fixed doses of 0.77 Gy were used for convenience. The OARs for diamond responses were corrected for dose rate dependence. Penumbral widths were compared, which were defined as the distance measured horizontally across the profile width between the 80%–20% dose levels. Uncertainty in the diamond detector measurements were 1%.

The profile comparison is shown in Figure 7.9. According to the volume effect, widths in the penumbral region will increase with a decrease in spatial resolution of the detector. Hence, a larger sensitive volume will give a rounding of the profile shape. Penumbral widths



were 6.8, 5.3 and 5.8 mm for the E6SCP2 face-on, edge-on and diode face-on orientations. Similarities are seen in the beam profiles of the E6SCP2 in the face-on orientation and the diode detector, as both have the same lateral spatial resolution. The penumbral width for the edge-on diamond was smaller due to the volume effect [147]; the face-on diamond width was larger than the diode due to larger interval spacing of measurements. A higher shoulder in the penumbral region for the edge-on diamond measurements was observed as reported in other studies using the same orientations with respect to other, larger volume detectors [23,148]. Full-width at half-maximum (FWHM) measurements, which measure the width of the beam, of the E6SCP2 face-on, diode and E6SCP2 edge-on detector responses were 109.2, 108.8 and 108.0 mm, respectively. Differences here are due to interval spacing, but overall these measurements show that the FWHM beam width at depth will not quite match the geometric field width in question due to the nature of lateral electron disequilibrium in the absorbing medium at a given depth.

A  $1 \times 1 \text{ cm}^2$  beam profile was also measured in 0.2 cm increments using the diamond detector in the edge-on orientation. Other detectors were not available for comparison, but measurements were compared to results from the literature; the setup parameters of SSD = 100 cm and  $z = 1.5 \text{ cm}$  matched those used by Laub and Wong in an investigation of the volume effect of detectors [147]. The resulting profile over the full width of the beam is shown in Figure 7.10. The 80%–20% width of the penumbra was found to be 0.44 cm and the FWHM of the curve was 1.0 cm. In their study, the mean values of the area under the curve of  $1 \times 1 \text{ cm}^2$  profiles of several detectors were compared. This was performed by normalizing the profile curves to 0.68 and integrating a Gaussian fit function to the profile data. The mean value determined here was 0.66, which appears to be within 1% to the value plotted in their study. The few studies in the literature that measure small beam profiles with PTW diamond detectors use different setup parameters or different small field sizes [23,147,310]. To the author's knowledge, no other studies have published measurements that have attempted using CVD diamond in small fields.

The sandwich-type configuration of the detector geometry (electrode-detector material-electrode) allows for measurements with better spatial resolution than most other detectors used for profile measurements. Thicknesses of PTW diamond detectors reported by the manufacturer range from 0.1–0.4 mm, which has already been shown to give better spatial resolution in steep dose gradients than conventional dosimeters, e.g. ion chambers, and are comparable to p-type diode detectors. Measuring the actual penumbra of small fields is vital to clinical dose measurements as it may lead to non-negligible systematic errors and incorrect

conclusions in treatment planning. Given the high sensitivity of single crystal CVD diamond, experiments could be performed with diamond film thicknesses  $< 100 \mu\text{m}$  to further analyze the effect of dose measurements on the finite size of a detector.

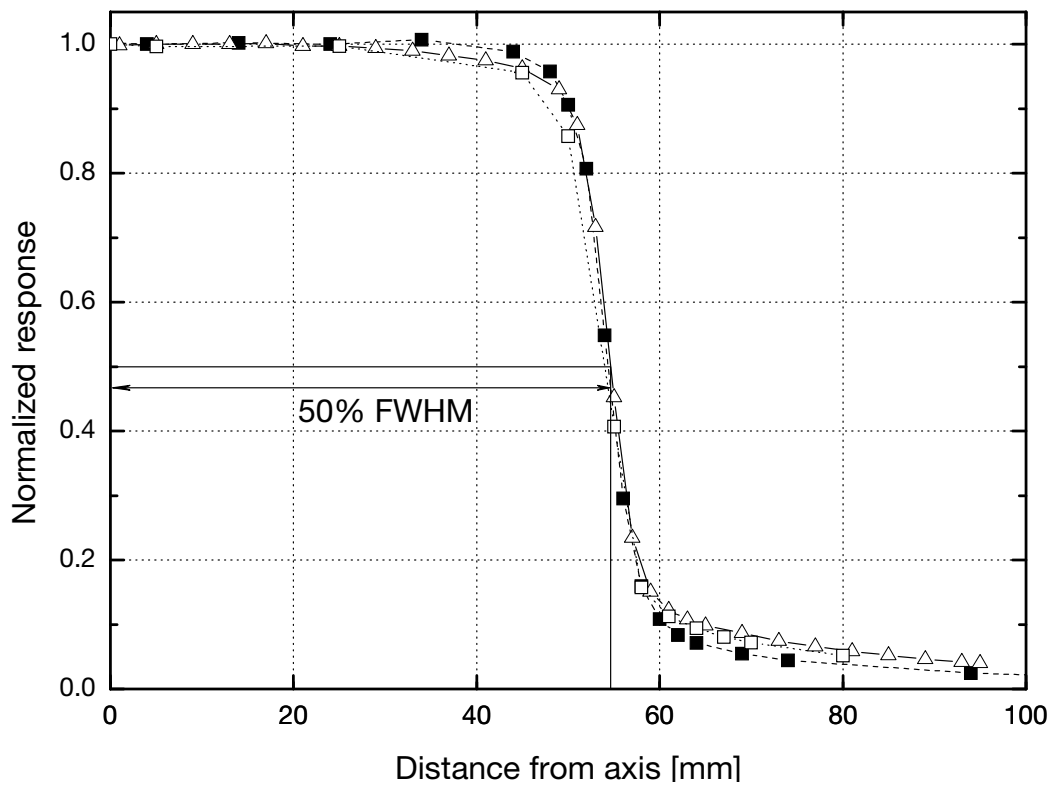


**Figure 7.9.** Off axis profile comparison at 10 cm depth for E6SCP2 detector in the face-on (□) and edge-on (■) orientations and a diode detector (Δ).

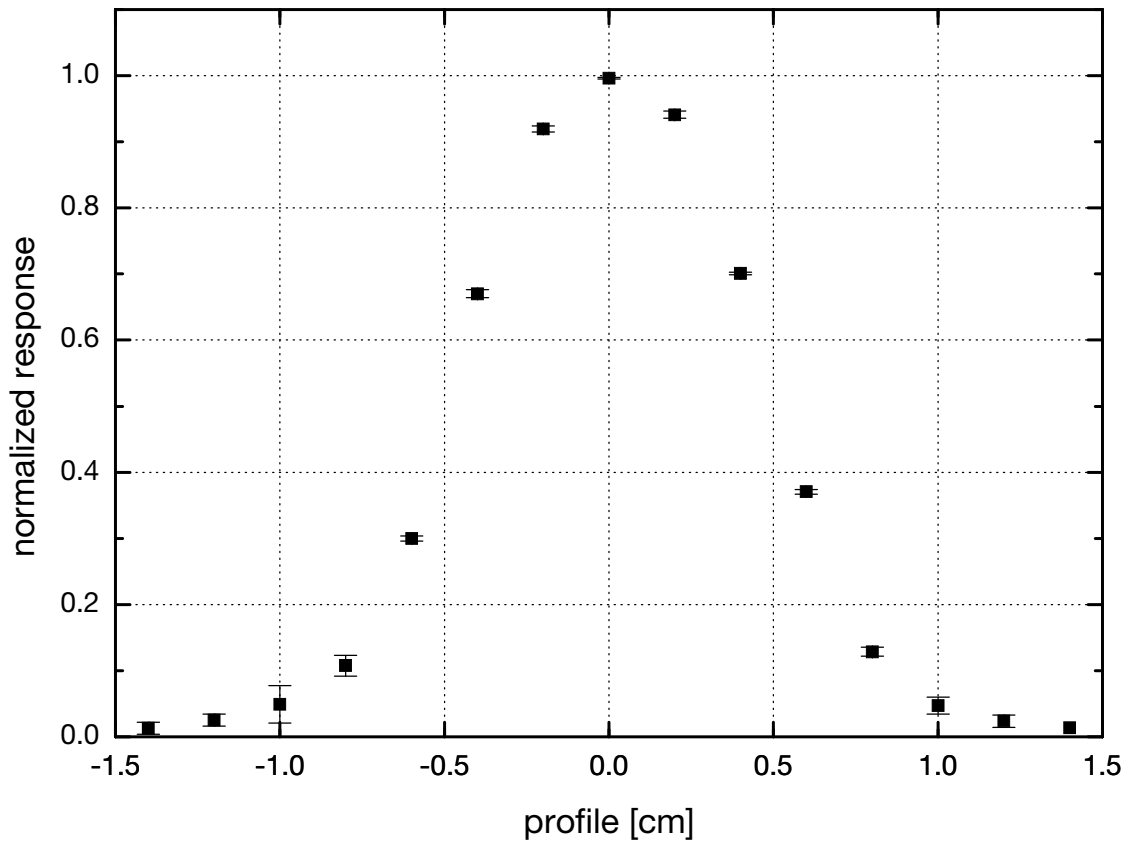


**Figure 7.10.** Off axis profile for a  $1 \times 1 \text{ cm}^2$  using the E6SCP2 detector in the edge-on orientation.

## 7.7 Concluding Remarks

A single crystal CVD diamond detector was tested under clinical conditions to evaluate its suitability for radiotherapy dosimetry of 6 MV photon beams. A closer look at repeatability showed that attention must be paid to a short-term loss in sensitivity due to charge detrapping effects following irradiation. Therefore, this detector would require a short priming dose any time it was not irradiated over a time interval that resulted in an unacceptable increase in the variability of response. Fixed-dose experiments looking at resolution in sensitivity showed that this detector under the given conditions could statistically distinguish between dose values separated by a single MU (0.77 cGy). When a fixed dose of 0.77 Gy was delivered at nominal available dose rates, dependence on dose rate was observed in contrast to the method used in previous chapters where stabilized currents with doses of  $\sim 1.3 \text{ Gy}$  were used. The correction factor  $\Delta$  may then vary with cumulative dose as well as range of dose rates used for calculation. Clinical dosimetric measurements were then performed to evaluate relative absorbed dose in a phantom. Response with diamond has

advantages over other dosimeters due to its tissue-equivalence and high sensitivity that make it a strong candidate for measuring dose in small fields and in high dose gradients where similar stopping power ratios, energy absorption coefficients, spatial resolution and small sensitive volumes are required. Using the diamond in the edge-on orientation also reduces perturbation of the beam due to its sandwich configuration and 150 nm Ag contacts for a more accurate dose determination.

It is not known how much correction factors differ between individual detectors that use single crystal or other commercially available CVD diamond films. The behaviour of PTW diamond detectors have been shown to differ due to variation in material properties [150]. It then becomes necessary to characterize a particular detector due to differences between dosimetric properties measured locally and those reported by PTW. Future work should involve testing multiple films from the same manufactured batch of single crystal films to deduce variability and reproducibility.

# 8. Conclusions and Future Work

---

## 8.1 Conclusions

The aim of this thesis was to investigate the suitability of commercially-available single crystal and polycrystalline CVD diamond films that had not been studied previously for use in radiotherapy dosimetry. Diamond films were characterized before a selection was packaged as prototype detectors for dosimetry. Following preliminary investigations, a single crystal CVD diamond detector was selected for detailed analyses that included a study of operating voltage and measurements under clinically relevant conditions.

Material characterization using spectrophotometry, Raman spectroscopy and bulk conductivity analyses were conducted to characterize each film as well as make correlations between material quality and detector response. Response characteristics varied due to relative differences in film quality as well as applied electric field. Understanding material quality is critical to improve the response capabilities of diamond detectors for radiotherapy applications. Waterproofing the detector could also be done so that it could be tested in water phantom dosimetry.

Prototype detectors were successfully designed and constructed to investigate the dosimetric response of diamond films under clinical conditions. The detectors were designed to minimize fluence perturbations, and so that they could be used with existing conventional dosimetry instrumentation. Thin Perspex encapsulation was used in the final design so that these detectors could be used in a Solid Water phantom to make comparisons with other dosimeters.

The polycrystalline diamond films purchased from Diamonex were considered unsuitable for dosimetric applications due to their lack of stability, low sensitivity, high leakage currents and high priming dose. Polycrystalline diamond films such as these are relatively inexpensive but do not exhibit qualities necessary for sustained irradiation that are expected of diamond. These diamonds were opaque and through Raman spectroscopy showed weak diamond abundances and high relative concentrations of impurities.

The 200 and 400- $\mu\text{m}$  thick films (DM200 and DM400) from Diamond Materials were potential candidates for further dosimetric analysis due to their near-zero leakage current, low priming doses, quick rise times and good sensitivity with small sensitive volumes. Material analyses showed a combination of high-quality diamond and low levels of nitrogen impurities that gave a favourable response. The DM200 film would be advantageous for off-axis beam profile measurements where high spatial resolution is required, as it is 40% thinner than the Element Six detectors. However, DM200 had longer decay times following irradiation that may hinder its use for dosimetry in dynamic beams where a quick response is required. Although comparable in response with the E6SCPL and E6SCP2 films, the DM200 film was 2–3 times more expensive. The 100- $\mu\text{m}$  film (DM100) was not suitable for dosimetry, which appeared to be due to differences in crystalline quality and higher levels of impurities based on material analyses.

The Element Six single crystal CVD films that were either polished (E6SCP2) or polished and lapped (E6SCPL) exhibited suitable characteristics for dosimetry. Similarly to the DM films, material analyses showed a combination of high-quality diamond and low levels of nitrogen impurities that proved to give a favourable response. At 248 V, both showed negligible leakage currents ( $< 1.25 \text{ pA}$ ), low priming doses ( $< 10 \text{ Gy}$ ), low rise times (7 and 2 s, respectively) and fall times ( $< 2 \text{ s}$ ), good sensitivity (230 and  $47.7 \text{ nC Gy}^{-1}$ , respectively) and were weakly dependent on dose rate and directional dependence ( $\pm 1\%$ ). The sensitive volumes were small ( $0.39 \text{ mm}^3$ ). Because the E6SCP2 film also showed the highest sensitivity, it was considered a candidate for further analyses.

The E6SCP2 detector was used to investigate how changes in an applied electric field affected detector response, and determined whether an optimal operating voltage could be realized within the parameters of conventional instrumentation used in radiation therapy. After investigating several dosimetric characteristics, the results of this study indicate a preference towards using 62.5 V ( $0.125 \text{ V } \mu\text{m}^{-1}$ ) due to its minimal rise time (2 s) and fall time ( $< 2 \text{ s}$ ) yet sufficient sensitivity ( $37 \text{ nC Gy}^{-1}$ ), which was also only weakly dependent on polarity. Photocurrent to leakage current ratios at all voltages tested ( $> 2100:1$ ) exceeded requirements set by IAEA for reference dosimeters in radiotherapy dosimetry (200:1) as well as more strict requirements by authors evaluating diamond detectors for IMRT (1000:1). To the author's knowledge, this was the first study for CVD diamond detectors in which operating voltage was analyzed to optimize for temporal response as required for modulated beams.

Investigations with the E6SCP2 detector were then performed in more clinically relevant conditions including small fields. Repeatability experiments showed a short-term loss in sensitivity due to charge detrapping effects following irradiation, which can be modelled. This detector would therefore require a short priming dose to stabilize the response if time between irradiations creates an unacceptable variation in response. Long-term stability of the detector was 1%. Experiments that investigated resolution in response showed that, under the given conditions, this detector could statistically distinguish between dose values separated by a single MU, which corresponded to 0.77 cGy. Dose rate dependence was observed when using short, fixed doses in contrast to a method used in previous chapters and the literature where stabilized currents and higher doses were used. Although not ideal, correction factors can therefore be used. Depth dose measurements using this detector compared well with other dosimeters. Using this diamond film in the edge-on orientation reduced perturbation of the beam due to its sandwich configuration and thin 150 nm Ag contacts. Comparisons of initial measurements with values in the literature indicate encouraging results for fields sizes  $< 4 \times 4 \text{ cm}^2$ , but further measurements and comparisons with Monte Carlo calculations are required. The dosimetric properties of this detector are likely to improve with higher dose rates.

Investigations have shown that the E6SCP2 diamond detector is suitable for routine dosimetry with conventional radiotherapy instrumentation, and was constructed with a total materials cost of  $< \text{NZ}\$200$ .

## 8.2 Future Work

The success of materials research and detector technologies has made diamond a viable option for radiotherapy dosimetry. Although progress has been made to make IMRT and small field dosimetry with diamond a possibility, more research to test and improve CVD diamond detectors for such applications is still required.

Access to oncology facilities changed over the course of this project due to the commissioning of linear accelerators. Although the literature has shown that these detectors have negligible or no energy dependence, future work could be performed using other machines with different beam qualities and higher dose rates. The next step for the E6SCP2 detector and other future candidates is to test their suitability in IMRT fields.

As diamond films in this project were acquired from commercial manufacturers, multiple detectors using the same type of film and packaging could be tested and compared for reproducibility.

An important response characteristic for these detectors was rise time. Future work to improve rise times other than optimising operating voltage could involve material characterization and addressing impurities and defects in the material, looking at differences in crystal size and their dynamics on conductivity, and using ion implantation and neutron irradiation to alter and create preferential electronic properties.

Detector optimization and interface phenomena are also interesting areas of research. Future investigations in our group include Monte Carlo calculations and experimental measurements to test different electrode materials, geometries and thicknesses, especially those low in atomic number  $Z$  to minimize fluence perturbations; this includes using a guard ring to make use of the triaxial connection on these detectors to collimate the applied electric field. Studies in film thickness, e.g. using film  $< 100 \mu\text{m}$  thick, could also be performed to test the limits of spatial resolution with diamond films for radiotherapy dosimetry. An “all carbon” detector would be ideal, which would involve graphitic contacts and cables. Future work in our group is looking at effective ways to graphitize the surface of diamond films.

The use of CVD film as a thermoluminescent dosimeter (TLD) is also a possibility. Our group is currently looking at comparing the TL properties of LiF dosimeters with single crystal and electronic quality polycrystalline CVD films analyzed in this project (E6SCPL, E6SCP2, E6EL200 and E6EL500).

Many characteristics of CVD diamond detectors already match or surpass those of PTW natural diamond detectors, including dose linearity, dose rate dependence, directional dependence, sensitivity, and sensitive volume. For future work, a direct comparison between the E6SCP2 detector and a PTW diamond detector would make clear how well this single crystal CVD diamond film compares against the natural diamonds used for radiotherapy dosimetry. Widespread commercialization of a diamond detector may be possible as CVD diamonds have the potential to be produced at higher qualities, have reproducible properties and at a lower cost than their natural counterparts.



# Bibliography

---

- [1] Garcia, M, Jemal, A, Ward, EM, Center, MM, Hao, Y, Siegel, RL & Thun, MJ, *Global Cancer Facts & Figures 2007*, American Cancer Society, Atlanta. 2007).
- [2] Delaney, G, Jacob, S, Featherstone, C & Barton, M, "The role of radiotherapy in cancer treatment," *Cancer*, vol. 104, no. 6, pp. 1129-37 (2005).
- [3] Ballas, LK, Elkin, EB, Schrag, D, Minsky, BD & Bach, PB, "Radiation therapy facilities in the United States," *International Journal of Radiation Oncology Biology Physics*, vol. 66, no. 4, pp. 1204-11 (2006).
- [4] Hall, EJ, "Intensity-modulated radiation therapy, protons, and the risk of second cancers," *International Journal of Radiation Oncology Biology Physics*, vol. 65, no. 1, pp. 1-7 (2006).
- [5] Bucci, MK, Bevan, A & Roach, M, "Advances in radiation therapy: conventional to 3D, to IMRT, to 4D, and beyond," *CA: A Cancer Journal for Clinicians*, vol. 55, no. 2, pp. 117-34 (2005).
- [6] Keall, P, "4-dimensional computed tomography imaging and treatment planning," *Seminars in Radiation Oncology*, vol. 14, pp. 81-90 (2004).
- [7] Das, IJ, Ding, GX & Ahnesjo, A, "Small fields: Nonequilibrium radiation dosimetry," *Medical Physics*, vol. 35, no. 1, pp. 206-15 (2008).
- [8] Paliwal, B & Tewatia, D, "Advances in radiation therapy dosimetry," *Journal of Medical Physics*, vol. 34, no. 3, pp. 108-16 (2009).
- [9] Ibbott, G, Ma, CM, Rogers, DWO, Seltzer, SM & Williamson, JF, "Anniversary Paper: Fifty years of AAPM involvement in radiation dosimetry," *Medical Physics*, vol. 35, no. 4, pp. 1418-27 (2008).
- [10] *Detectors | Dosimetry*, Iba Dosimetry (Scanditronix Wellhofer GmbH). Retrieved Dec. 17, 2009 2009, from <http://www.iba-dosimetry.com/complete-solutions/radiotherapy/relative-dosimetry/detectors>.
- [11] *PTW: Dosimetry Systems and Ionization Chambers for Radiation Measurement*, Physikalisch-Technische Werkstätten (PTW) GmbH, Freiburg. Retrieved 25 Apr 2009, from <http://www.ptw.de>.

- [12] *RADCAL: Accu-Family Instruments*. Retrieved 27 Dec 2009, from <http://www.radcal.com/accufamily.html>.
- [13] Haryanto, F, Fippel, M, Laub, W, Dohm, O & Nusslin, F, "Investigation of photon beam output factors for conformal radiation therapy—Monte Carlo simulations and measurements," *Physics in Medicine and Biology*, no. 11, p. N133 (2002).
- [14] McKerracher, C & Thwaites, DI, "Assessment of new small-field detectors against standard-field detectors for practical stereotactic beam data acquisition," *Physics in Medicine and Biology*, no. 9, p. 2143 (1999).
- [15] McKerracher, C & Thwaites, DI, "Notes on the construction of solid-state detectors," *Radiotherapy and Oncology*, vol. 79, no. 3, pp. 348-51 (2006).
- [16] Bouchard, H & Seuntjens, J, "Ionization chamber-based reference dosimetry of intensity modulated radiation beams," *Medical Physics*, vol. 31, no. 9, pp. 2454-65 (2004).
- [17] Martens, C, Wagter, CD & Neve, WD, "The value of the PinPoint ion chamber for characterization of small field segments used in intensity-modulated radiotherapy," *Physics in Medicine and Biology*, no. 9, p. 2519 (2000).
- [18] Das, IJ, Downes, MB, Kassae, A & Tochner, Z, "Choice of Radiation Detector in Dosimetry of Stereotactic Radiosurgery-Radiotherapy," *Journal of Radiosurgery*, vol. 3, no. 4, pp. 177-86 (2000).
- [19] Pappas, E, Maris, TG, Papadakis, A, Zacharopoulou, F, Damilakis, J, Papanikolaou, N & Gourtsoyiannis, N, "Experimental determination of the effect of detector size on profile measurements in narrow photon beams," *Medical Physics*, vol. 33, no. 10, pp. 3700-10 (2006).
- [20] Pappas, E, Maris, TG, Zacharopoulou, F, Papadakis, A, Manolopoulos, S, Green, S & Wojnecki, C, "Small SRS photon field profile dosimetry performed using a PinPoint air ion chamber, a diamond detector, a novel silicon-diode array (DOSI), and polymer gel dosimetry. Analysis and intercomparison," *Medical Physics*, vol. 35, no. 10, pp. 4640-8 (2008).
- [21] Pappas, E, Petrokokkinos, L, Angelopoulos, A, Maris, TG, Kozicki, M, Dalezios, I & Kouloulis, V, "Relative output factor measurements of a 5 mm diameter radiosurgical photon beam using polymer gel dosimetry," *Medical Physics*, vol. 32, no. 6, pp. 1513-20 (2005).
- [22] Letourneau, D, Pouliot, J & Roy, R, "Miniature scintillating detector for small field radiation therapy," *Medical Physics*, vol. 26, no. 12, pp. 2555-61 (1999).
- [23] Westermarck, M, Arndt, J, Nilsson, B & Brahme, A, "Comparative dosimetry in narrow high-energy photon beams," *Physics in Medicine and Biology*, no. 3, p. 685 (2000).

- [24] Mack, A, Mack, G, Wetz, D, Scheib, SG, Bottcher, HD & Seifert, V, "High precision film dosimetry with GAFCHROMIC[sup [registered sign]] films for quality assurance especially when using small fields," *Medical Physics*, vol. 30, no. 9, pp. 2399-409 (2003).
- [25] Stasi, M, Baiotto, B, Barboni, G & Scielzo, G, "The behavior of several microionization chambers in small intensity modulated radiotherapy fields," *Medical Physics*, vol. 31, no. 10, pp. 2792-5 (2004).
- [26] De Angelis, C, Bucciolini, M, Casati, M, Løvik, I, Bruzzi, M, Lagomarsino, S, Sciortino, S & Onori, S, "Improvements in CVD diamond properties for radiotherapy dosimetry," *Radiation Protection Dosimetry*, vol. 120, no. 1-4, pp. 38-42 (2006).
- [27] Cotty, WF, "Diamond as a Pinpoint Radiation Counter," *Nature*, vol. 177, no. 4519, pp. 1075-6 (1956).
- [28] Kozlov, SF, Belcarz, E, Hage-Ali, M, Stuck, R & Siffert, P, "Diamond nuclear radiation detectors," *Nuclear Instruments and Methods*, vol. 117, no. 1, pp. 277-83 (1974).
- [29] Plansky, B, "Evaluation of diamond radiation doseimeters," *Physics in Medicine and Biology*, no. 3, p. 519 (1980).
- [30] Burgemeister, EA, "Dosimetry with a diamond operating as a resistor," *Physics in Medicine and Biology*, vol. 26, no. 2, pp. 269-75 (1981).
- [31] Yoder, MN, "Semiconducting Diamond Technology," *Naval Resarch Reviews*, vol. 39, p. 27 (1987).
- [32] Butler, JE, Cheesman, A & Ashfold, MNR, "Recent Progress in the Understanding of CVD Growth of Diamond," in *CVD Diamonds for Electronic Devices and Sensors*, pp. 103-24(2009).
- [33] Butler, JE, Mankelevich, YA, Cheesman, A, Jie, M & Ashfold, MNR, "Understanding the chemical vapor deposition of diamond: recent progress," *Journal of Physics: Condensed Matter*, no. 36, p. 364201 (2009).
- [34] Wooldridge, DE, Ahearn, AJ & Burton, JA, "Conductivity Pulses Induced in Diamond by Alpha-Particles," *Physical Review*, vol. 71, no. 12, p. 913 (1947).
- [35] Curtiss, LF & Brown, BW, "Diamond as a Gamma-Ray Counter," *Physical Review*, vol. 72, no. 7, p. 643 (1947).
- [36] Vatnitsky, S & Jarvinen, H, "Application of a natural diamond detector for the measurement of relative dose distributions in radiotherapy," *Physics in Medicine and Biology*, vol. 38, pp. 173-8 (1993).

- [37] Keddy, RJ, Nam, TL & Burns, RC, "The detection of ionizing radiations by natural and synthetic diamond crystals and their application as dosimeters in biological environments," *Carbon*, vol. 26, no. 3, pp. 345-56 (1988).
- [38] Khrunov, VS, Martynov, SS, Vatnitsky, SM, Ermakov, IA, Chervjakov, AM, Karlin, DL, Fominych, VI & Tarbeyev, YV, "Diamond Detectors in Relative Dosimetry of Photon, Electron and Proton Radition Fields," *Radiation Protection Dosimetry*, vol. 33, no. 1-4, pp. 155-7 (1990).
- [39] Marczevska, B, Kupriyanov, I, Pal'yanov, Y, Nowak, T, Olko, P, Rebisz, M & Waligórski, MPR, "A study of radiation dosimeters based on synthetic HPHT diamond," *Diamond and Related Materials*, vol. 16, no. 2, pp. 191-5 (2007).
- [40] Marczevska, B, Nowak, T, Olko, P, Gajewski, W, Pal'yanov, Y, Kupriyanov, I & Waligórski, MPR, "Synthetic diamonds as active detectors of ionising radiation," *Diamond and Related Materials*, vol. 13, no. 4-8, pp. 918-22 (2004).
- [41] Cuttone, G, Azario, L, Barone Tonghi, L, Borchi, E, Boscarino, D, Bruzzi, M, Bucciolini, M, Cirrone, GAP, De Angelis, C, Della Mea, G, *et al.*, "The CANDIDO project: development of a CVD diamond dosimeter for applications in radiotherapy," *Nuclear Physics B - Proceedings Supplements*, vol. 78, no. 1-3, pp. 587-91 (1999).
- [42] Bruzzi, M, Bucciolini, M, Cirrone, GAP, Cuttone, G, Mazzocchi, S, Pirolo, S & Sciortino, S, "Characterisation of CVD diamond dosimeters in on-line configuration," *Nuclear Instruments and Methods in Physics Research Section A: Accelerators, Spectrometers, Detectors and Associated Equipment*, vol. 454, no. 1, pp. 142-6 (2000).
- [43] Manfredotti, C, Lo Giudice, A, Ricciardi, C, Paolini, C, Massa, E, Fizzotti, F & Vittone, E, "CVD diamond microdosimeters," *Nuclear Instruments and Methods in Physics Research Section A: Accelerators, Spectrometers, Detectors and Associated Equipment*, vol. 458, no. 1-2, pp. 360-4 (2001).
- [44] Whitehead, AJ, Airey, R, Buttar, CM, Conway, J, Hill, G, Ramkumar, S, Scarsbrook, GA, Sussmann, RS & Walker, S, "CVD diamond for medical dosimetry applications," *Nuclear Instruments and Methods in Physics Research Section A: Accelerators, Spectrometers, Detectors and Associated Equipment*, vol. 460, no. 1, pp. 20-6 (2001).
- [45] Balducci, A, Garino, Y, Giudice, AL, Manfredotti, C, Marinelli, M, Pucella, G & Verona-Rinati, G, "Radiological X-ray dosimetry with single crystal CVD diamond detectors," *Diamond and Related Materials*, vol. 15, no. 4-8, pp. 797-801 (2006).
- [46] Garino, Y, Lo Giudice, A, Manfredotti, C, Marinelli, M, Milani, E, Tucciarone, A & Verona-Rinati, G, "Performances of homoepitaxial single crystal diamond in diagnostic x-ray dosimetry," *Applied Physics Letters*, vol. 88, no. 15, pp. 151901-3 (2006).
- [47] Almaviva, S, Marinelli, M, Milani, E, Tucciarone, A, Verona-Rinati, G, Consorti, R, Petrucci, A, De Notaristefani, F & Ciancaglioni, I, "Synthetic single crystal diamond

- diodes for radiotherapy dosimetry," *Nuclear Instruments and Methods in Physics Research Section A: Accelerators, Spectrometers, Detectors and Associated Equipment*, vol. 594, no. 2, pp. 273-7 (2008).
- [48] Descamps, C, Tromson, D, Tranchant, N, Isambert, A, Bridier, A, De Angelis, C, Onori, S, Bucciolini, M & Bergonzo, P, "Clinical studies of optimised single crystal and polycrystalline diamonds for radiotherapy dosimetry," *Radiation Measurements*, vol. 43, no. 2-6, pp. 933-8 (2008).
- [49] Tranchant, N, Tromson, D, Descamps, C, Isambert, A, Hamrita, H, Bergonzo, P & Nesladek, M, "High mobility single crystal diamond detectors for dosimetry: Application to radiotherapy," *Diamond and Related Materials*, vol. 17, no. 7-10, pp. 1297-301 (2008).
- [50] Guerrero, MJ, Tromson, D, Rebisz, M, Mer, C, Bazin, B & Bergonzo, P, "Requirements for synthetic diamond devices for radiotherapy dosimetry applications," *Diamond and Related Materials*, vol. 13, no. 11-12, pp. 2046-51 (2004).
- [51] Guerrero, MJ, Tromson, D, Descamps, C & Bergonzo, P, "Recent improvements on the use of CVD diamond ionisation chambers for radiotherapy applications," *Diamond and Related Materials*, vol. 15, no. 4-8, pp. 811-4 (2006).
- [52] Bergonzo, P, Tromson, D, Descamps, C, Hamrita, H, Mer, C, Tranchant, N & Nesladek, M, "Improving diamond detectors: A device case," *Diamond and Related Materials*, vol. 16, no. 4-7, pp. 1038-43 (2007).
- [53] Lambert, GD & Klevenhagen, SC, "Penetration of backscattered electrons in polystyrene for energies between 1 and 25 MeV," *Physics in Medicine and Biology*, vol. 27, pp. 721-5 (1982).
- [54] Rikner, G & Grusell, E, "General specifications for silicon semiconductors for use in radiation dosimetry," *Physics in Medicine and Biology*, no. 9, p. 1109 (1987).
- [55] Grusell, E & Rikner, G, "Radiation Damage Induced Dose Rate Non-Linearity in an N-Type Silicon Detector," *Acta Oncologica*, vol. 23, no. 6, pp. 465 - 9 (1984).
- [56] Verhaegen, F, "Interface perturbation effects in high-energy electron beams," *Physics in Medicine and Biology*, vol. 48, no. 6, pp. 687-705 (2003).
- [57] Dutreix, J & Bernard, M, "Dosimetry at interfaces for high energy X and gamma rays," *British Journal of Radiology*, vol. 39, no. 459, p. 205 (1966).
- [58] Das, IJ, Khan, FM & Gerbi, BJ, "Interface dose perturbation as a measure of megavoltage photon beam energy," *Medical Physics*, vol. 15, p. 78 (1988).
- [59] Górká, B, Nilsson, B, Fernandez-Varea, JM, Svensson, R & Brahme, A, "Influence of electrodes on the photon energy deposition in CVD-diamond dosimeters studied with

- the Monte Carlo code PENELOPE," *Physics in Medicine and Biology*, no. 15, pp. 3607-23 (2006).
- [60] Górká, B, Nilsson, B, Svensson, R, Brahme, A, Ascarelli, P, Trucchi, DM, Conte, G & Kalish, R, "Design and characterization of a tissue-equivalent CVD-diamond detector for clinical dosimetry in high-energy photon beams," *Physica Medica*, vol. 24, no. 3, pp. 159-68 (2008).
- [61] Baluti, F, *Monte Carlo simulation of Chemical Vapour Deposition Diamond Detector*, M.Sc. Thesis, University of Canterbury. 2009).
- [62] *CRC Handbook of Chemistry and Physics*, 89th edn, CRC press, Boca Raton.(2009).
- [63] Prelas, MA, Popovici, G & Bigelow, LK, *Handbook of industrial diamonds and diamond films*, CRC Press.(1997).
- [64] Zaitsev, AM, *Optical properties of diamond: a data handbook*, Springer.(2001).
- [65] Yoder, MN, "Diamond Properties and Applications," in *Diamond Films and Coatings: Development, Properties, and Applications*(1993).
- [66] Sze, SM & Ng, KK, *Physics of semiconductor devices*, Wiley India Pvt. Ltd.(2008).
- [67] Morkoc, H, Strite, S, Gao, GB, Lin, ME, Sverdlov, B & Burns, M, "Large band gap SiC, III V nitride, and II VI ZnSe based semiconductor device technologies," *Journal of Applied Physics*, vol. 76, p. 1363 (1994).
- [68] Streetman, BG & Banerjee, S, *Solid State Electronic Devices*, 5th edn, Prentice Hall.(2000).
- [69] Isberg, J, Hammersberg, J, Johansson, E, Wikstrom, T, Twitchen, DJ, Whitehead, AJ, Coe, SE & Scarsbrook, GA, "High Carrier Mobility in Single-Crystal Plasma-Deposited Diamond," *Science*, vol. 297, no. 5587, pp. 1670-2 (2002).
- [70] Mainwood, A, "Recent developments of diamond detectors for particles and UV radiation," *Semiconductor Science and Technology*, no. 9, p. R55 (2000).
- [71] Sque, S, *Structure of Diamond - Steve Sque, University of Exeter*, from <http://newton.ex.ac.uk/research/qsystems/people/sque/diamond/structure/>.
- [72] Bragg, WL, "The Structure of Some Crystals as Indicated by Their Diffraction of X-rays," *Proceedings of the Royal Society of London. Series A, Containing Papers of a Mathematical and Physical Character*, vol. 89, no. 610, pp. 248-77 (1913).
- [73] Bernal, JD, "The Structure of Graphite," *Proceedings of the Royal Society of London. Series A, Containing Papers of a Mathematical and Physical Character*, vol. 106, no. 740, pp. 749-73 (1924).

- [74] Davis, RF, *Diamond Films and Coatings*.(1993).
- [75] Bragg, WH & Bragg, WL, "The structure of the diamond," *Proceedings of the Royal Society of London. Series A, Containing Papers of a Mathematical and Physical Character*, vol. 89, no. 610, pp. 277-91 (1913).
- [76] Bundy, FP, Hall, HT, Strong, HM & Wentorf, RH, "Man-made diamonds," *Nature*, vol. 176, no. 9, pp. 51-5 (1955).
- [77] Bovenkerk, HP, Bundy, FP, Chrenko, RM, Codella, PJ, Strong, HM & Wentorf, RH, "Errors in diamond synthesis," *Nature*, vol. 365, no. 6441, p. 19 (1993).
- [78] Spear, KE & Dismukes, JP, *Synthetic Diamond: Emerging CVD Science and Technology*, Wiley-Interscience.(1994).
- [79] Fedoseev, DV, Varnin, VP & Deryagin, BV, "Synthesis of Diamond in Its Thermodynamic Metastability Region," *Russian Chemical Reviews*, no. 5, p. 435 (1984).
- [80] Koizumi, S, Nebel, C & Nesladek, M, *Physics and Applications of CVD Diamond*, Wiley-VCH.(2008).
- [81] Sussmann, RS, *CVD Diamond for Electronic Devices and Sensors*, J. Wiley.(2009).
- [82] Alison, M, Mark, EN & Marshall, S, "Science's gem: diamond science 2009," *Journal of Physics: Condensed Matter*, no. 36, p. 360301 (2009).
- [83] Balmer, RS, Brandon, JR, Clewes, SL, Dhillon, HK, Dodson, JM, Friel, I, Inglis, PN, Madgwick, TD, Markham, ML, Mollart, TP, *et al.*, "Chemical vapour deposition synthetic diamond: materials, technology and applications," *Journal of Physics: Condensed Matter*, no. 36, p. 364221 (2009).
- [84] Das, IJ, "Diamond Detector," in DWO Rogers & JE Cygler (eds), *Clinical Dosimetry Measurements in Radiotherapy*, Medical Physics Publishing, Madison, p. 1112(2009).
- [85] Goodwin, DG & Butler, JE, "Theory of diamond chemical vapor deposition," *Handbook of Industrial Diamonds and Diamond Films*, pp. 527–81 (1997).
- [86] Butler, JE & Woodin, RL, "Thin film diamond growth mechanisms," *Philosophical Transactions of the Royal Society A: Mathematical, Physical and Engineering Sciences*, vol. 342, pp. 209- (1993).
- [87] Van Heerden, PJ, "The Crystal Counter, A New Instrument in Nuclear Physics (Utrecht thesis)," *NV Noord-Hollandsche Uitgevers Maatschappij* (1945).
- [88] Ahearn, AJ, "Conductivity Induced in Diamond by Alpha-Particle Bombardment and Its Variation among Specimens," *Physical Review*, vol. 73, no. 9, p. 1113 (1948).

- [89] Champion, FC, "Electrical Counting Properties of Diamonds," *Proceedings of the Physical Society. Section B*, no. 7, p. 465 (1952).
- [90] Stratton, K & Champion, FC, "Electrical Counting Response of Two Large Diamonds under Beta-Irradiation," *Proceedings of the Physical Society. Section B*, no. 7, p. 473 (1952).
- [91] Trott, NG, "Variations in the  $\hat{I}^2$  -particle Counting Properties of Diamond," *Proceedings of the Royal Society of London. Series A, Mathematical and Physical Sciences*, vol. 220, no. 1143, pp. 498-513 (1953).
- [92] Champion, FC & Wright, SB, "Diamond Conduction Counters with Small Electrode Separations," *Proceedings of the Physical Society*, no. 3, p. 385 (1959).
- [93] Champion, FC, "Symposium on Solid State Conductivity II. Recent Experiments with Crystal Counters," *Physics in Medicine and Biology*, no. 4, p. 334 (1960).
- [94] Garlick, GFJ, "Symposium on Solid State Conductivity I. Radiation-induced Conductivity," *Physics in Medicine and Biology*, no. 4, p. 325 (1960).
- [95] Prior, JR & Champion, FC, "Electroluminescence in Diamond," *Proceedings of the Physical Society*, no. 4, p. 849 (1962).
- [96] Clark, CD, Dean, PJ & Harris, PV, "Intrinsic Edge Absorption in Diamond," *Proceedings of the Royal Society of London. Series A, Mathematical and Physical Sciences*, vol. 277, no. 1370, pp. 312-29 (1964).
- [97] Champion, FC & Kennedy, PJ, "The counting properties of diamond under ionizing radiation," in R Berman (ed.), *Physical Properties of Diamond*, Oxford, Clarendon(1965).
- [98] Champion, FC & Roy, RR, "The Scattering of Fast  $\beta$ -particles through Large Angles by Nitrogen Nuclei," *Proceedings of the Physical Society*, no. 6, p. 532 (1948).
- [99] Hofstadter, R, "Remarks on Diamond Crystal Counters," *Physical Review*, vol. 73, no. 6, p. 631 (1948).
- [100] Lonsdale, K, "Remarks on Diamond Crystal Counters," *Physical Review*, vol. 73, no. 12, p. 1467 (1948).
- [101] McKay, KG, "Electron Bombardment Conductivity in Diamond," *Physical Review*, vol. 74, no. 11, p. 1606 (1948).
- [102] Chynoweth, AG, "Removal of Space-charge in Diamond Crystal Counters," *Physical Review*, vol. 76, no. 2, p. 310 (1949).
- [103] Newton, RR, "Space Charge Effects in Bombardment Conductivity through Diamond," *Physical Review*, vol. 75, no. 2, p. 234 (1949).



- [104] McKay, KG, "Electron Bombardment Conductivity in Diamond. Part II," *Physical Review*, vol. 77, no. 6, p. 816 (1950).
- [105] Freeman, GP & van der Velden, HA, "An Explanation of Differences in Counting Properties among Diamond Specimens," *Physical Review*, vol. 84, no. 5, p. 1050 (1951).
- [106] Bose, DN & Henisch, HK, "Radiation dosimetry by current glow in diamond," *Solid-State Electronics*, vol. 11, no. 3, pp. 273-8 (1968).
- [107] Canali, C, Gatti, E, Kozlov, SF, Manfredi, PF, Manfredotti, C, Nava, F & Quirini, A, "Electrical properties and performances of natural diamond nuclear radiation detectors," *Nuclear Instruments and Methods*, vol. 160, no. 1, pp. 73-7 (1979).
- [108] De Blasi, C, Galassini, S, Micocci, G, Ruggiero, L, Tepore, A, Nava, F, Manfredotti, C & Kozlov, SF, "Hole trapping levels in natural diamond nuclear detectors," *Nuclear Instruments and Methods*, vol. 163, no. 1, pp. 121-4 (1979).
- [109] Konorova, EA & Kozlov, SF, "Nuclear radiation detector made of diamond," *Sov. Phys.-Semiconductors*, vol. 4, no. 10, pp. 1600-5 (1970).
- [110] Kozlov, SF, Stuck, R, Hage-Ali, M & Siffert, P, "Preparation and characteristics of natural diamond nuclear radiation detectors," *Ieee Transactions on Nuclear Science*, vol. 22, no. 1, pp. 160-70 (1975).
- [111] Kozlov, SF, Konorova, EA, Kuznetsov, YA, Salikov, YA, Redko, VI, Grinberg, VR & Meilman, ML, "Diamond Dosimeter for X-Ray and  $\gamma$ -Radiation," *Ieee Transactions on Nuclear Science*, vol. 24, no. 1, pp. 235-7 (1977).
- [112] Vavilov, VS, Guseva, MI, Konorova, EA, Krasnopevtsev, VV, Sergienko, VF & Tutov, VV, "Semiconducting diamonds produced by ion bombardment," *Soviet Physics-Solid State*, vol. 8, pp. 1560-1 (1966).
- [113] RD42 - *Development of Diamond Tracking Detectors for High Luminosity Experiments at the LHC*. Retrieved 29 Apr 2009, from [http://graybook.cern.ch/programmes/experiments/r\\_d/RD42.html](http://graybook.cern.ch/programmes/experiments/r_d/RD42.html).
- [114] Gorisek, A, "Commissioning and first operational experience of the ATLAS Beam Conditions and Loss Monitors based on pCVD diamond sensors," *Nuclear Instruments and Methods in Physics Research Section A: Accelerators, Spectrometers, Detectors and Associated Equipment*, vol. In Press, Accepted Manuscript (2009).
- [115] Adam, W, Bauer, C, Berdermann, E, Bergonzo, P, Bogani, F, Borchini, E, Brambilla, A, Bruzzi, M, Colledani, C, Conway, J, *et al.*, "The first bump-bonded pixel detectors on CVD diamond," *Nuclear Instruments and Methods in Physics Research Section A: Accelerators, Spectrometers, Detectors and Associated Equipment*, vol. 436, no. 3, pp. 326-35 (1999).

- [116] Bauer, C, Baumann, I, Colledani, C, Conway, J, Delpierre, P, Djama, F, Dulinski, W, Fallou, A, Gan, KK, Gilmore, RS, *et al.*, "Recent results from the RD42 Diamond Detector Collaboration," *Nuclear Instruments and Methods in Physics Research Section A: Accelerators, Spectrometers, Detectors and Associated Equipment*, vol. 383, no. 1, pp. 64-74 (1996).
- [117] Friedl, M, Adam, W, Bauer, C, Berdermann, E, Bergonzo, P, Bogani, F, Borchhi, E, Brambilla, A, Bruzzi, M, Colledani, C, *et al.*, "CVD diamond detectors for ionizing radiation," *Nuclear Instruments and Methods in Physics Research Section A: Accelerators, Spectrometers, Detectors and Associated Equipment*, vol. 435, no. 1-2, pp. 194-201 (1999).
- [118] Krammer, M, Adam, W, Bauer, C, Berdermann, E, Bogani, F, Borchhi, E, Bruzzi, M, Colledani, C, Conway, J, Dabrowski, W, *et al.*, "Status of diamond particle detectors," *Nuclear Instruments and Methods in Physics Research Section A: Accelerators, Spectrometers, Detectors and Associated Equipment*, vol. 418, no. 1, pp. 196-202 (1998).
- [119] Adam, W, Berdermann, E, Bergonzo, P, de Boer, W, Bogani, F, Borchhi, E, Brambilla, A, Bruzzi, M, Colledani, C, Conway, J, *et al.*, "The development of diamond tracking detectors for the LHC," *Nuclear Instruments and Methods in Physics Research Section A: Accelerators, Spectrometers, Detectors and Associated Equipment*, vol. 514, no. 1-3, pp. 79-86 (2003).
- [120] Adam, W, de Boer, W, Borchhi, E, Bruzzi, M, Colledani, C, D'Angelo, P, Dabrowski, V, Dulinski, W, van Eijk, B, Eremin, V, *et al.*, "Radiation hard diamond sensors for future tracking applications," *Nuclear Instruments and Methods in Physics Research Section A: Accelerators, Spectrometers, Detectors and Associated Equipment*, vol. 565, no. 1, pp. 278-83 (2006).
- [121] Bergonzo, P, Brambilla, A, Tromson, D, Mer, C, Hordequin, C, Guizard, B, Foulon, F, Solé, VA & Gauthier, C, "Diamond as a tool for synchrotron radiation monitoring: beam position, profile, and temporal distribution," *Diamond & Related Materials*, vol. 9, no. 3-6, pp. 960-4 (2000).
- [122] Bergonzo, P, Brambilla, A, Tromson, D, Mer, C, Guizard, B, Foulon, F & Amosov, V, "CVD diamond for radiation detection devices," *Diamond & Related Materials*, vol. 10, no. 3-7, pp. 631-8 (2001).
- [123] Bergonzo, P, Brambilla, A, Tromson, D, Mer, C, Guizard, B & Foulon, F, "Diamond devices as characterisation tools for novel photon sources," *Applied Surface Science*, vol. 154, pp. 179-85 (2000).
- [124] Morse, J, Salomé, M, Berdermann, E, Pomorski, M, Cunningham, W & Grant, J, "Single crystal CVD diamond as an X-ray beam monitor," *Diamond and Related Materials*, vol. 16, no. 4-7, pp. 1049-52 (2007).
- [125] Bergonzo, P, Tromson, D & Mer, C, "CVD diamond-based semi-transparent beam-position monitors for synchrotron beamlines: preliminary studies and device

- developments at CEA/Saclay," *Journal of Synchrotron Radiation*, vol. 13, no. 2, pp. 151-8 (2006).
- [126] *NoRHDia web-page*, 2009, from <http://www-norhdia.gsi.de/>.
- [127] Burgemeister, EA, "Radiation detectors made from diamond," *Physica*, vol. 111B, pp. 319-20 (1981).
- [128] Burgemeister, EA & Schouten, W, "The Construction of a Diamond Detector for Ionising Radiation," *Radiation Protection Dosimetry*, vol. 6, no. 1-4, pp. 145-8 (1983).
- [129] Schouten, W, Schipper, J & Burgemeister, EA, 'Some Applications of Diamond Detectors in Clinical Dosimetry'. 1983).
- [130] Nam, TL, Keddy, RJ & Burns, RC, "Synthetic diamonds as in vivo radiation detectors," *Medical Physics*, vol. 14, p. 596 (1987).
- [131] Rodriguez, M, Griffin, S, DeWerd, L & Jeraj, R, "Characterization of the ADII-33 diamond detector," *Medical Physics*, vol. 34, pp. 215-20 (2007).
- [132] Bjork, P, Knoos, T & Nilsson, P, "Comparative dosimetry of diode and diamond detectors in electron beams for intraoperative radiation therapy," *Medical Physics*, vol. 27, no. 11, pp. 2580-8 (2000).
- [133] Mobit, PN & Sandison, G, A., "A Monte Carlo comparison of the response of the PTW-diamond and the TL-diamond detectors in megavoltage photon beams," *Medical Physics*, vol. 26, no. 11, pp. 2503-7 (1999).
- [134] Lambert, J, Nakano, T, Law, S, Elsey, J, McKenzie, DR & Suchowerska, N, "In vivo dosimeters for HDR brachytherapy: A comparison of a diamond detector, MOSFET, TLD, and scintillation detector," *Medical Physics*, vol. 34, no. 5, pp. 1759-65 (2007).
- [135] Heydarian, M, Hoban, PW, Beckham, WA, Borchardt, IM & Beddoe, AH, "Evaluation of a PTW diamond detector for electron beam measurements," *Physics in Medicine and Biology*, no. 8, p. 1035 (1993).
- [136] Hoban, PW, Heydarian, M, Beckham, WA & Beddoe, AH, "Dose rate dependence of a PTW diamond detector in the dosimetry of a 6 MV photon beam," *Physics in Medicine and Biology*, no. 8, p. 1219 (1994).
- [137] Laub, WU, Kaulich, TW & Nusslin, F, "A diamond detector in the dosimetry of high-energy electron and photon beams," *Physics in Medicine and Biology*, vol. 44, no. 9, pp. 2183-92 (1999).
- [138] Wolfram, UL, Theodor, WK & Fridtjof, N, "A diamond detector in the dosimetry of high-energy electron and photon beams," *Physics in Medicine and Biology*, no. 9, p. 2183 (1999).

- [139] Fidanzio, A, Luigi, A, Roberto, M, Aniello, R & Angelo, P, "PTW-diamond detector: Dose rate and particle type dependence," *Medical Physics*, vol. 27, no. 11, pp. 2589-93 (2000).
- [140] Angelis, CD, Onori, S, Pacilio, M, Cirrone, GAP, Cuttone, G, Raffaele, L, Bucciolini, M & Mazzocchi, S, "An investigation of the operating characteristics of two PTW diamond detectors in photon and electron beams," *Medical Physics*, vol. 29, no. 2, pp. 248-54 (2002).
- [141] Barnett, E, Mackenzie, M & Fallone, B, "Characterization of a PTW type 60003 diamond detector for clinical dosimetry with potential for IMRT point measurements," *Medical Physics*, vol. 30, no. 7, pp. 1943- (2003).
- [142] Schwedas, M, Scheithauer, M, Wiezorek, T & Wendt, TG, "Strahlenphysikalische Einflussgrößen bei der Dosimetrie mit verschiedenen Detektortypen," *Zeitschrift für Medizinische Physik*, vol. 17, no. 3, pp. 172-9 (2007).
- [143] Mazal, A, Delacroix, S, Bridier, A, Daures, J, Dolo, JM, Nauraye, C, Ferrand, R, Cosgrave, V & Habrand, JL, "Relative and absolute dosimetry of protontherapy beams," *Radiotherapy and Oncology*, vol. 37, pp. S43-S (1995).
- [144] Fidanzio, A, Azario, L, Angelis, CD, Pacilio, M, Onori, S, Kacperek, A & Piermattei, A, "A correction method for diamond detector signal dependence with proton energy," *Medical Physics*, vol. 29, no. 5, pp. 669-75 (2002).
- [145] Onori, S, Angelis, CD, Fattibene, P, Pacilio, M, Petetti, E, Azario, L, Miceli, R, Piermattei, A, Tonghi, LB, Cuttone, G, *et al.*, "Dosimetric characterization of silicon and diamond detectors in low-energy proton beams," *Physics in Medicine and Biology*, no. 10, p. 3045 (2000).
- [146] Pacilio, M, Angelis, CD, Onori, S, Azario, L, Fidanzio, A, Miceli, R, Piermattei, A & Kacperek, A, "Characteristics of silicon and diamond detectors in a 60 MeV proton beam," *Physics in Medicine and Biology*, no. 8, p. N107 (2002).
- [147] Laub, WU & Wong, T, "The volume effect of detectors in the dosimetry of small fields used in IMRT," *Medical Physics*, vol. 30, p. 341 (2003).
- [148] Heydarian, M, Hoban, PW & Beddoe, AH, "A comparison of dosimetry techniques in stereotactic radiosurgery," *Physics in Medicine and Biology*, no. 1, p. 93 (1996).
- [149] Bucciolini, M, Borchini, E, Bruzzi, M, Casati, M, Cirrone, P, Cuttone, G, De Angelis, C, Lovik, I, Onori, S & Raffaele, L, "Diamond dosimetry: Outcomes of the CANDIDO and CONRAD INFN projects," *Nuclear Instruments and Methods in Physics Research Section A: Accelerators, Spectrometers, Detectors and Associated Equipment*, vol. 552, no. 1, pp. 189-96 (2005).
- [150] De Angelis, C, Onori, S, Pacilio, M, Cirrone, GAP, Cuttone, G, Raffaele, L, Bucciolini, M & Mazzocchi, S, "An investigation of the operating characteristics of two PTW

- diamond detectors in photon and electron beams," *Medical Physics*, vol. 29, p. 248 (2002).
- [151] *Private communication*, PTW, Nov 6 2008.
- [152] Rustgi, SN, "Application of a diamond detector to brachytherapy dosimetry," *Physics in Medicine and Biology*, vol. 43, no. 8, pp. 2085-94 (1998).
- [153] Laub, WU, Kaulich, TW & Nusslin, F, "Energy and dose rate dependence of a diamond detector in the dosimetry of 4-25 MV photon beams," *Medical Physics*, vol. 24, no. 4, pp. 535-6 (1997).
- [154] *Dosimeters*, MAESTRO. Retrieved 15 Dec 2008, from <http://www.maestro-research.org/dosimeters.htm>.
- [155] Talamonti, C, Bucciolini, M, Marrazzo, L, Menichelli, D, Bruzzi, M, Cirrone, GAP, Cuttone, G & LoJacono, P, "Dosimetric characterization with 62 MeV protons of a silicon-segmented detector for 2D dose verifications in radiotherapy," *Nuclear Instruments and Methods in Physics Research Section A: Accelerators, Spectrometers, Detectors and Associated Equipment*, vol. 596, no. 1, pp. 126-30 (2008).
- [156] Tromson, D, Descamps, C, Tranchant, N, Bergonzo, P, Nesladek, M & Isambert, A, "Investigations of high mobility single crystal chemical vapor deposition diamond for radiotherapy photon beam monitoring," *Journal of Applied Physics*, vol. 103, no. 5, p. 054512 (2008).
- [157] Bruzzi, M, "Diamond Radiation Sensors for Radiotherapy," in RS Sussmann (ed.), *CVD Diamond for Electronic Devices and Sensors*, pp. 185-206(2009).
- [158] Cirrone, G, Cuttone, G, Lo Nigro, S, Mongelli, V, Raffaele, L & Sabini, M, "Dosimetric characterization of CVD diamonds in photon, electron and proton beams," *Nuclear Physics B - Proceedings Supplements*, vol. 150, pp. 330-3 (2006).
- [159] Cirrone, GAP, Cuttone, G, Lo Nigro, S, Mongelli, V, Raffaele, L, Sabini, MG, Valastro, L, Bucciolini, M & Onori, S, "Dosimetric characterization of CVD diamonds irradiated with 62 MeV proton beams," *Nuclear Instruments and Methods in Physics Research Section A: Accelerators, Spectrometers, Detectors and Associated Equipment*, vol. 552, no. 1-2, pp. 197-202 (2005).
- [160] Cirrone, GAP, Cuttone, G, Rafaele, L, Sabini, MG, De Angelis, C, Onori, S, Pacilio, M, Bucciolini, M, Bruzzi, M & Sciortino, S, "Natural and CVD type diamond detectors as dosimeters in hadrontherapy applications," *Nuclear Physics B - Proceedings Supplements*, vol. 125, pp. 179-83 (2003).
- [161] Vatnitsky, SM, Miller, DW, Moyers, MF, Levy, RP, Schulte, RW, Slater, JD & Slater, JM, "Dosimetry techniques for narrow proton beam radiosurgery," *Physics in Medicine and Biology*, no. 11, p. 2789 (1999).

- [162] Almaviva, S, Marinelli, M, Milani, E, Prestopino, G, Tucciarone, A, Verona, C, Veronarinati, G, Angelone, M & Pillon, M, "Improved performance in synthetic diamond neutron detectors : Application to boron neutron capture therapy," *Nuclear Instruments and Methods in Physics Research Section A: Accelerators, Spectrometers, Detectors and Associated Equipment*, vol. In Press, Accepted Manuscript (2009).
- [163] Angelone, M, Marinelli, M, Milani, E, Tucciarone, A, Pillon, M, Pucella, G & Veronarinati, G, "Neutron detection and dosimetry using polycrystalline CVD diamond detectors with high collection efficiency," *Radiation Protection Dosimetry*, vol. 120, no. 1-4, pp. 345-8 (2006).
- [164] Rebisz, M, Martemiyarov, A, Berdermann, E, Pomorski, M, Marczewska, B & Voss, B, "Synthetic diamonds for heavy-ion therapy dosimetry," *Diamond and Related Materials*, vol. 15, no. 4-8, pp. 822-6 (2006).
- [165] Rebisz, M, Voss, B, Heinz, A, Usenko, E & Pomorski, M, "CVD diamond dosimeters for heavy ion beams," *Diamond and Related Materials*, vol. 16, no. 4-7, pp. 1070-3 (2007).
- [166] Rebisz, M & Voss, B, "The response of thermally stimulated luminescence in CVD diamonds to heavy charged particles," *Radiation Measurements*, vol. 42, no. 4-5, pp. 628-31 (2007).
- [167] Betzel, GT, Lansley, SP, Baluti, F, Reinisch, L & Meyer, J, "Operating parameters of CVD diamond detectors for radiation dosimetry," *Nuclear Instruments and Methods in Physics Research Section A: Accelerators, Spectrometers, Detectors and Associated Equipment*, vol. In Press, Accepted Manuscript (2009).
- [168] Lansley, SP, G.T. Betzel, F. Baluti, J. Lydon & L. Reinisch, 'Suitability of Synthetic Diamond Films for X-ray Dosimetry Applications', *Proceedings of the 2008 Conference on Optoelectronic and Microelectronic Materials and Devices (COMMAD'08)*, IEEE, Sydney, Australia, pp. 34-7. 2008).
- [169] Almaviva, S, Ciancaglioni, I, Consorti, R, De Notaristefani, F, Manfredotti, C, Marinelli, M, Milani, E, Petrucci, A, Prestopino, G, Verona, C, *et al.*, "Synthetic single crystal diamond dosimeters for intensity modulated radiation therapy applications," *Nuclear Instruments and Methods in Physics Research Section A: Accelerators, Spectrometers, Detectors and Associated Equipment*, vol. In Press, Accepted Manuscript (2009).
- [170] Lansley, SP, G.T. Betzel, F. Baluti, L. Reinisch & J. Meyer, "Investigation of the suitability of commercially-available CVD diamond for megavoltage x-ray dosimetry," *Nuclear Instruments and Methods in Physics Research Section A: Accelerators, Spectrometers, Detectors and Associated Equipment*, vol. 607, no. 3, pp. 659-67 (2009).
- [171] Attix, FH, *Introduction to radiological physics and radiation dosimetry*, Wiley-Interscience.(1986).
- [172] Attix, FH, Roesch, WC & Tochilin, E, *Radiation Dosimetry*, 2nd edn, Academic Press New York.(1966-1969).

- [173] Khan, FM, *The Physics of Radiation Therapy*, 3rd edn, Lippincott Williams & Wilkins, Philadelphia.(2003).
- [174] Podgorsak, EB, *Review of radiation oncology physics: a handbook for teachers and students*, Educational Reports Series: April. 2003).
- [175] Kleinknecht, K, *Detectors for particle radiation*, Cambridge University Press, Cambridge.(1998).
- [176] Mayles, P, Nahum, AE & Rosenwald, JC, *Handbook of radiotherapy physics: theory and practice*, Taylor & Francis.(2007).
- [177] Mainwood, A, "Point Defects, Impurities and Doping," in *CVD Diamond for Electronic Devices and Sensors*, J. Wiley, pp. 49-63(2009).
- [178] Bruzzi, M, Hartjes, F, Lagomarsino, S, Menichelli, D, Mersi, S, Miglio, S, Scaringella, M & Sciortino, S, "Defect analysis of a diamond particle detector by means of photoconductivity and thermal spectroscopy characterization," *physica status solidi (a)*, vol. 199, no. 1, pp. 138-44 (2003).
- [179] Kalish, R, Uzan-Saguy, C, Philosoph, B, Richter, V & Prawer, S, "Loss of electrical conductivity in boron-doped diamond due to ion-induced damage," *Applied Physics Letters*, vol. 70, no. 8, pp. 999-1001 (1997).
- [180] Benabdesselam, M, Iacconi, P, Briand, D, Lapraz, D, Gheeraert, E & Deneuille, A, "Characterisation by thermoluminescence of boron doped polycrystalline diamond films," *Diamond and Related Materials*, vol. 9, no. 1, pp. 56-60 (2000).
- [181] Gonçalves, JAN, Sandonato, GM, Meléndrez, R, Chernov, V, Pedroza-Montero, M, De la Rosa, E, Rodríguez, RA, Salas, P & Barboza-Flores, M, "OSL and TL dosimeter characterization of boron doped CVD diamond films," *Optical Materials*, vol. 27, no. 7, pp. 1231-4 (2005).
- [182] Descamps, C, Tromson, D, Guerrero, MJ, Mer, C, Rzepka, E, Nesladek, M & Bergonzo, P, "Nitrogen-doped diamond: Thermoluminescence and dosimetric applications," *Diamond and Related Materials*, vol. 15, no. 4-8, pp. 833-7 (2006).
- [183] Secroun, A, Tallaire, A, Achard, J, Civrac, G, Schneider, H & Gicquel, A, 'Photoconductive properties of lightly N-doped single crystal CVD diamond films', *17th European Conference on Diamond, Diamond-Like Materials, Carbon Nanotubes, Nitrides and Silicon Carbide*, Estoril, PORTUGAL, pp. 953-7. 2006).
- [184] Barboza-Flores, M, Gastélum, S, Cruz-Zaragoza, E, Meléndrez, R, Chernov, V, Pedroza-Montero, M & Favalli, A, "Thermoluminescence properties of undoped and nitrogen-doped CVD diamond exposed to gamma radiation," *Radiation Measurements*, vol. 43, no. 2-6, pp. 379-82 (2008).

- [185] Trajkov, E, Praver, S & Spizzirri, P, "The effect of ion implantation on thermally stimulated currents in polycrystalline CVD diamond," *Diamond and Related Materials*, vol. 12, no. 10-11, pp. 1738-43 (2003).
- [186] Avigal, Y, Richter, V, Fizgeer, B, Saguy, C & Kalish, R, "The nature of ion-implanted contacts to polycrystalline diamond films," *Diamond and Related Materials*, vol. 13, no. 9, pp. 1674-9 (2004).
- [187] Metcalfe, P, Kron, T, Hoban, P & Paliwal, B, *The physics of radiotherapy X-rays from linear accelerators*, Medical Physics Pub.(1997).
- [188] *Determination of Absorbed Dose in a Patient Irradiated by Beams of X or Gamma Rays in Radiotherapy*, Washington D.C. 1976).
- [189] *Report 33: Radiation Quantities and Units*, ICRU (International Commission on Radiation, Units and Measurements). 1980).
- [190] *Report 60: Fundamental Quantities and Units for Ionizing Radiation*, ICRU (International Commission on Radiation, Units and Measurements). 1998).
- [191] Jordan, K, 'Recent advances in non gel tissue equivalent dosimeters', in *4th International Conference on Radiotherapy Gel Dosimetry*, vol. 56. Institute of Physics Publishing, pp. 132-41.(2009).
- [192] Agostinelli, S, Garelli, S, Piergentili, M & Foppiano, F, "Response to high-energy photons of PTW31014 PinPoint ion chamber with a central aluminum electrode," *Medical Physics*, vol. 35, p. 3293 (2008).
- [193] Mack, A, Scheib, SG, Major, J, Gianolini, S, Pazmandi, G, Feist, H, Czempiel, H & Kreiner, H-J, "Precision dosimetry for narrow photon beams used in radiosurgery--- Determination of Gamma Knife[sup [registered sign]] output factors," *Medical Physics*, vol. 29, no. 9, pp. 2080-9 (2002).
- [194] Scherf, C, Peter, C, Moog, J, Licher, J, Kara, E, Zink, K, Rödel, C & Ramm, U, "Silicon Diodes as an Alternative to Diamond Detectors for Depth Dose Curves and Profile Measurements of Photon and Electron Radiation," *Strahlentherapie und Onkologie*, vol. 185, no. 8, pp. 530-6 (2009).
- [195] Rosenfeld, AB, Lerch, MLF, Kron, T, Brauer-Krisch, E, Bravin, A, Holmes-Siedle, A & Allen, BJ, "Feasibility study of online high-spatial-resolution MOSFET dosimetry in static and pulsed x-ray radiation fields," *Ieee Transactions on Nuclear Science*, vol. 48, no. 6, pp. 2061-8 (2001).
- [196] Chuang, CF, Verhey, LJ & Xia, P, "Investigation of the use of MOSFET for clinical IMRT dosimetric verification," *Medical Physics*, vol. 29, no. 6, pp. 1109-15 (2002).



- [197] Rowbottom, CG & Jaffray, DA, "Characteristics and performance of a micro-MOSFET: An "imageable" dosimeter for image-guided radiotherapy," *Medical Physics*, vol. 31, no. 3, pp. 609-15 (2004).
- [198] Butson, MJ, Rozenfeld, A, Mathur, JN, Carolan, M, Wong, TPY & Metcalfe, PE, "A new radiotherapy surface dose detector: The MOSFET," *Medical Physics*, vol. 23, no. 5, pp. 655-8 (1996).
- [199] B. Rosenfeld, A, "MOSFET Dosimetry on Modern Radiation Oncology Modalities," *Radiation Protection Dosimetry*, vol. 101, no. 1-4, pp. 393-8 (2002).
- [200] Zilio, VO, Joneja, OP, Popowski, Y, Rosenfeld, A & Chawla, R, "Absolute depth-dose-rate measurements for an <sup>192</sup>Ir HDR brachytherapy source in water using MOSFET detectors," *Medical Physics-New York-Institute of Physics*, vol. 33, no. 6, pp. 1532-9 (2006).
- [201] Beddar, AS, Mackie, TR & Attix, FH, "Water-equivalent plastic scintillation detectors for high-energy beam dosimetry: I. Physical characteristics and theoretical considerations," *Physics in Medicine and Biology*, vol. 37, pp. 1883-900 (1992).
- [202] Beddar, AS, Mackie, TR & Attix, FH, "Water-equivalent plastic scintillation detectors for high-energy beam dosimetry: II. Properties and measurements," *Physics in Medicine and Biology*, vol. 37, pp. 1901-13 (1992).
- [203] Beddar, AS, "Water equivalent plastic scintillation detectors in radiation therapy," *Radiation Protection Dosimetry*, vol. 120, no. 1-4, pp. 1-6 (2006).
- [204] Archambault, L, Arsenault, J, Gingras, L, Beddar, AS, Roy, R & Beaulieu, L, "Plastic scintillation dosimetry: Optimal selection of scintillating fibers and scintillators," *Medical Physics*, vol. 32, p. 2271 (2005).
- [205] Archambault, L, Beddar, AS, Gingras, L, Roy, R & Beaulieu, L, "Measurement accuracy and Cerenkov removal for high performance, high spatial resolution scintillation dosimetry," *Medical Physics*, vol. 33, p. 128 (2006).
- [206] Archambault, L, Briere, T, Poenisch, F, Beaulieu, L & Beddar, S, 'MO-FF-A1-04: Toward a True Real-Time in Vivo Dosimetry System Using Plastic Scintillators', 6 edn, AAPM, pp. 2709-. (2009).
- [207] Jang, K, Cho, D, Shin, S, Yoo, W, Seo, J, Lee, B, Kim, S, Moon, J, Cho, Y-H & Park, B, "Characterization of a scintillating fiber-optic dosimeter for photon beam therapy," *Optical Review*, vol. 16, no. 3, pp. 383-6 (2009).
- [208] *Diamonex - A Leading Supplier of DLC Coatings and CVD Diamond Products*, DIAMONEX Products. Retrieved 19 Jun 2009, from [http://www.diamonex.com/products\\_CVD.htm](http://www.diamonex.com/products_CVD.htm).

- [209] *Diamond Materials: Advanced diamond technology*, Diamond Materials GmbH. Retrieved Dec. 24, 2009, from [http://www.diamond-materials.de/index\\_en.htm](http://www.diamond-materials.de/index_en.htm).
- [210] *Element Six*, Element Six Ltd. Retrieved 25 Apr 2009, from <http://www.e6.com>.
- [211] *Single Crystal Diamond Plate*, Element Six. Retrieved 25 Apr 2009, from <http://www.e6cvd.com/cvd/page.jsp?pageid=1003>.
- [212] *Synthetic CVD Diamond Products from Element Six*, Element Six Ltd., from [www.e6cvd.com](http://www.e6cvd.com).
- [213] Alvarez, J, Kleider, JP, Bergonzo, P, Tromson, D, Snidero, E & Mer, C, "Study of deep defects in polycrystalline CVD diamond from thermally stimulated current and below-gap photocurrent experiments," *Diamond and Related Materials*, vol. 12, no. 3-7, pp. 546-9 (2003).
- [214] Gonon, P, Deneuville, A, Fontaine, F & Gheeraert, E, "ELECTRICAL-CONDUCTION AND DEEP LEVELS IN POLYCRYSTALLINE DIAMOND FILMS," *Journal of Applied Physics*, vol. 78, no. 11, pp. 6633-8 (1995).
- [215] Manfredotti, C, Vittone, E, Fizzotti, F, Giudice, AL & Paolini, C, "Effects of light on the [']primed' state of CVD diamond nuclear detectors," *Diamond and Related Materials*, vol. 11, no. 3-6, pp. 446-50 (2002).
- [216] Brescia, R, Sio, AD, Donato, MG, Faggio, G, Messina, G, Pace, E, Pucella, G, Santangelo, S, Sternschulte, H & Rinati, GV, "Photoconductive properties of single-crystal CVD diamond," *physica status solidi (a)*, vol. 199, no. 1, pp. 113-8 (2003).
- [217] Lansley, SP, Betzel, GT, Baluti, F, Reinisch, L & Meyer, J, "Investigation of the suitability of commercially available CVD diamond for megavoltage X-ray dosimetry," *Nuclear Inst. and Methods in Physics Research, A*, vol. 607, no. 3, pp. 659-67 (2009).
- [218] Pospisil, J, Novak, R, Sopko, B, Spevacek, V, Hlidek, P, Matejka, P, Mackova, A, Cejnarova, A, Juha, L & Krasa, J, "Thermoluminescence of CVD diamond films used in photon dosimetry," *physica status solidi (a)*, vol. 185, no. 1, pp. 195-202 (2001).
- [219] Wang, L, Liu, J, Lou, Y, Su, Q, Shi, W & Xia, Y, "Effects of the polarity of bias voltage on the electrical performance of the diamond film detectors," *Materials Letters*, vol. 61, no. 21, pp. 4238-41 (2007).
- [220] Benabdesselam, M, Iacconi, P, Butler, JE & Nigoul, JM, "TL characterisation of a CVD diamond wafer for ionising radiation dosimetry," *Diamond and Related Materials*, vol. 12, no. 10, pp. 1750-4 (2003).
- [221] Benabdesselam, M, Serrano, B, Iacconi, P, Wrobel, F, Lapraz, D, Herault, J & Butler, JE, "Thermoluminescence properties of CVD diamond for clinical dosimetry use," *Radiation Protection Dosimetry*, vol. 120, no. 1-4, pp. 87-90 (2006).

- [222] Vittone, E, Ricciardi, C, Lo Giudice, A, Fizzotti, F, Manfredotti, C, Egeni, G & Rudello, V, "Micro-IBICC and micro-IL analyses of CVD diamond microdosimeters," *Nuclear Instruments and Methods in Physics Research Section B: Beam Interactions with Materials and Atoms*, vol. 181, no. 1-4, pp. 349-53 (2001).
- [223] Manfredotti, C, Lo Giudice, A, Vittone, E, Fizzotti, F, Garino, Y & Pace, E, "Memory effects in CVD diamond," *Diamond and Related Materials*, vol. 15, no. 9, pp. 1467-71 (2006).
- [224] Breese, MBH, Sellin, PJ, Alves, LC, Knights, AP, Sussmann, RS & Whitehead, AJ, "Imaging of charge transport properties in polycrystalline CVD diamond using IBIC and IBIL microscopy," *Nuclear Inst. and Methods in Physics Research, B*, vol. 181, no. 1-4, pp. 219-24 (2001).
- [225] Bacci, T, Borchi, E, Bruzzi, M, Santoro, M & Sciortino, S, "Correlation between material properties and leakage currents in CVD diamond films deposited by DC plasma glow discharge," *Materials Science & Engineering, B: Solid-State Materials for Advanced Technology*, vol. 47, no. 1, pp. 54-63 (1997).
- [226] Sellin, PJ, Breese, MBH, Knights, AP, Alves, LC, Sussmann, RS & Whitehead, AJ, "Imaging of charge transport in polycrystalline diamond using ion-beam-induced charge microscopy," *Applied Physics Letters*, vol. 77, p. 913 (2000).
- [227] Trucchi, DM, Cappelli, E, Conte, G, Mattei, G, Gramaccioni, C & Ascarelli, P, "The influence of grain-boundaries on the electronic performance of CVD diamond films," *Diamond and Related Materials*, vol. 14, no. 3-7, pp. 575-9 (2005).
- [228] Barnard, AS, *The Diamond Formula: Diamond Synthesis: A Gemmological Perspective*, Butterworth-Heinemann Ltd.(2000).
- [229] Nesládek, M, ek, Mv & Stals, LM, "Defect-Induced Optical Absorption in CVD Diamond Films," *physica status solidi (a)*, vol. 154, no. 1, pp. 283-303 (1996).
- [230] Mollart, TP, Lewis, KL, Pickles, CSJ & Wort, CJH, "Factors affecting the optical performance of CVD diamond infrared optics," *Semiconductor Science and Technology*, no. 3, p. S117 (2003).
- [231] Woods, GS, Van Wyk, JA & Collins, AT, "The nitrogen content of type Ib synthetic diamond," *Philosophical Magazine Part B*, vol. 62, no. 6, pp. 589-95 (1990).
- [232] *UV-Visible Spectrophotometer - Cintra 404*, GBC Scientific Equipment. Retrieved 29 Apr 2009, from <http://www.gbcsce.com/products/uv/c40.asp>.
- [233] Long, DA, *The Raman Effect: A Unified Treatment of the Theory of Raman Scattering by Molecules*, Wiley.(2002).

- [234] Colthup, NB, Daly, LH & Wiberley, SE, *Introduction to infrared and Raman spectroscopy*, Academic press New York.(1990).
- [235] Schrader, B & Bougeard, D, *Infrared and Raman spectroscopy: methods and applications*, VCH Weinheim.(1995).
- [236] Gardiner, D, Graves, P & Bowley, H, *Practical Raman Spectroscopy*, Springer-Verlag, New York.(1989).
- [237] Knight, DS & White, WB, "Characterization of diamond films by Raman spectroscopy," *Journal of Materials Research*, vol. 4, no. 2, pp. 385-93 (1989).
- [238] Bachmann, PK, Bausen, HD, Lade, H, Leers, D, Wiechert, DU & Herres, N, "Raman and X-ray studies of polycrystalline CVD diamond films," *Diamond and Related Materials*, vol. 3, no. 11, pp. 1308-14 (1994).
- [239] Bormett, RW, Asher, SA, Witowski, RE, Partlow, WD, Lizewski, R & Pettit, F, "Ultraviolet Raman spectroscopy characterizes chemical vapor deposition diamond film growth and oxidation," *Journal of Applied Physics*, vol. 77, p. 5916 (1995).
- [240] Leeds, SM, Davis, TJ, May, PW, Pickard, CDO & Ashfold, MNR, "Use of different excitation wavelengths for the analysis of CVD diamond by laser Raman spectroscopy," *Diamond and Related Materials*, vol. 7, no. 2-5, pp. 233-7 (1998).
- [241] May, PW, Smith, JA & Rosser, KN, "785 nm Raman spectroscopy of CVD diamond films," *Diamond & Related Materials*, vol. 17, no. 2, pp. 199-203 (2008).
- [242] Shroder, RE, Nemanich, RJ & Glass, JT, "Analysis of the composite structures in diamond thin films by Raman spectroscopy," *Physical Review B*, vol. 41, no. 6, pp. 3738-45 (1990).
- [243] Wagner, J, Wild, C & Koidl, P, "Resonance effects in Raman scattering from polycrystalline diamond films," *Applied Physics Letters*, vol. 59, p. 779 (1991).
- [244] Yoshikawa, M, Katagiri, G, Ishida, H, Ishitani, A, Ono, M & Matsumura, K, "Characterization of crystalline quality of diamond films by Raman spectroscopy," *Applied Physics Letters*, vol. 55, p. 2608 (1989).
- [245] Descamps, C, Tromson, D, Mer, C, Nesladek, M, Bergonzo, P & Benabdesselam, M, "Synthetic diamond devices for radio-oncology applications," *physica status solidi (a)*, vol. 203, no. 12, pp. 3161-6 (2006).
- [246] Assiamah, M, Nam, TL & Keddy, RJ, "A synthetic diamond probe for low-energy X-ray dose measurements," *Applied Radiation and Isotopes* vol. 65, no. 5, pp. 545-52 (2007).

- [247] *Coherent Inc.: Innova 90C*, Coherent Inc., from <http://www.coherent.com/Lasers/index.cfm?fuseaction=show.page&ID=355&loc=834&title=Innova%2090C>.
- [248] Evans, DA, Roberts, OR, Williams, GT, Vearey-Roberts, AR, Bain, F, Evans, S, Langstaff, DP & Twitchen, DJ, "Diamond–metal contacts: interface barriers and real-time characterization," *Journal of Physics: Condensed Matter*, vol. 21, no. 364223, p. 364223 (2009).
- [249] Allers, L & Mainwood, A, "Surface vacancies in CVD diamond," *Diamond and Related Materials*, vol. 7, no. 2-5, pp. 261-5 (1998).
- [250] Ciancaglioni, I, Spaziani, F, Rossi, MC, Conte, G, Kononenko, V & Ralchenko, V, "Diamond microstrip detector for deep UV imaging," *Diamond and Related Materials*, vol. 14, no. 3-7, pp. 526-30 (2005).
- [251] Bergonzo, P, Barrett, R, Hainaut, O, Tromson, D, Mer, C & Guizard, B, "Imaging of the sensitivity in detector grade polycrystalline diamonds using micro-focused X-ray beams," *Diamond and Related Materials*, vol. 11, no. 3-6, pp. 418-22 (2006).
- [252] Han, S, Wagner, RS, Joseph, J, Plano, MA & Moyer, MD, "Chemical vapor deposited diamond radiation detectors for ultrahigh radiation dose-rate measurements: Response to subnanosecond, 16-MeV electron pulses," *Review of Scientific Instruments*, vol. 66, no. 12, pp. 5516-21 (1995).
- [253] Pace, E, Pini, A, Corti, G, Bogani, F, Vinattieri, A, Pickles, CSJ & Sussmann, R, "CVD diamond optics for ultraviolet," *Diamond and Related Materials*, vol. 10, no. 3-7, pp. 736-43 (2001).
- [254] Lohstroh, A, Selfin, PJ, Boroumand, F & Morse, J, 'High gain observed in X-ray induced currents in synthetic single crystal diamonds', *12th Hasselt Diamond Workshop 2007 (SBDD XII)*, Diepenbeek-Hasselt, BELGIUM, pp. 3011-6. 2007).
- [255] *Agilent | Overview: Semiconductor Parameter Analyzer Series*, Agilent Technologies, Inc., from <http://www.home.agilent.com/agilent/product.jsp?nid=-34117.0.00&cc=US&lc=eng>.
- [256] *2570/1 Farmer Dosemeter*, Thermo Scientific. Retrieved 25 Apr 2009, from <http://www.thermo.com/com/cda/product/detail/0,1055,19647,00.html>.
- [257] *Pomona Electronics 5218 Connector*, Pomona Electronics. Retrieved 1 Jul 2008, from [http://www.pomonaelectronics.com/pdf/d\\_ai\\_5218\\_2\\_03.pdf](http://www.pomonaelectronics.com/pdf/d_ai_5218_2_03.pdf).
- [258] *Amphenol RF*, Amphenol RF - Global RF Solutions. Retrieved 19 Jun 2009, from <http://drawings.amphenolrf.com/pdf/183.pdf>.

- [259] *Belden - 50 Ohm Triax*, Belden Inc., from <https://edeskv2.belden.com/Products/index.cfm?event=showproductdetail&partid=2544>.
- [260] *Model 6430 Sub-Femtoamp Remote SourceMeter*, Keithley Instruments Inc. Retrieved 25 Apr 2009, from <http://www.keithley.com/products/currentvoltage/?mn=6430>.
- [261] *LabVIEW*, National Instruments. Retrieved 25 Apr 2009, from <http://www.ni.com/labview/>.
- [262] Lansley, SP, *Diamond Photodetectors for Deep Ultra-Violet Applications*, University of London. (2001).
- [263] *Wet Etching Recipes of Metals and Semiconductors*, Department of Electrical and Computer Engineering, Brigham Young University. Retrieved 29 Apr 2009, from [http://www.ee.byu.edu/cleanroom/wet\\_etch.phtml](http://www.ee.byu.edu/cleanroom/wet_etch.phtml).
- [264] Walker, P & Tarn, WH, *CRC handbook of metal etchants*, CRC Press Boca Raton.(1991).
- [265] *INFICON Thin Film Deposition Controllers and Monitors*, Inficon, from <http://www.inficonthinfilmdeposition.com/en/index.html>.
- [266] Sze, SM, *VLSI technology*, McGraw-Hill New York.(1983).
- [267] *Auto 500 Sputtering Systems for Research and Development*, BOC Edwards, from [www.edwards.co.il/catalog/14/140103.pdf](http://www.edwards.co.il/catalog/14/140103.pdf).
- [268] *Cadsoft Online: Home of the E.A.G.L.E. Layout Editor*, Cadsoft Computer, Inc. Retrieved 29 Apr 2009, from <http://www.cadsoftusa.com/>.
- [269] *Pomona Electronics 5219 Bulkhead Receptacle*, Pomona Electronics. Retrieved 19 Jun 2009, from [http://www.pomonaelectronics.com/pdf/d5219\\_1\\_01.pdf](http://www.pomonaelectronics.com/pdf/d5219_1_01.pdf).
- [270] *RS New Zealand | World Leading Distributor of Electronics, Electromechanical and Industrial Components*  
RS New Zealand. Retrieved Apr 29 2009, from <http://newzealand.rs-online.com/web/home.html>.
- [271] *Precision DC Current, Voltage, and Resistance Measurements*, 6th edn, Keithley Instruments Inc., USA.(2004).
- [272] *Acrylic Sheet & Perspex*, Lucite International, Southampton, from <http://www.lucite.com/perspex.asp>.
- [273] Orton, CG, "Clear Perspex Dosimetry," *Physics in Medicine and Biology*, no. 3, p. 377 (1966).

- [274] *Dental Laboratory Materials, Dental Laboratory Equipment, Dental Technology, etc.*, Metrodent, Huddersfield, Yorkshire, UK, from <http://www.metrodent.com/content/ukdental.htm>.
- [275] *Varian Clinac Medical Linear Accelerators*, Varian Medical Systems. Retrieved 25 Apr 2009, from [http://www.varian.com/us/oncology/radiation\\_oncology/clinac/](http://www.varian.com/us/oncology/radiation_oncology/clinac/).
- [276] Karzmark, CJ, Nunan, CS & Tanabe, E, "Medical electron accelerators," *McGraw-Hill* (1993).
- [277] *PTW: Farmer Ionization Chambers*, from [http://www.ptw.de/farmer\\_chambers0.html](http://www.ptw.de/farmer_chambers0.html).
- [278] *Radiation Oncology: Gammex 457 Standard Grade Solid Water*, from <http://www.gammex.com/n-portfolio/detail.asp?id=254&category=Radiation+Oncology&name=Gammex+457+Standard+Grade+Solid+Water>.
- [279] IAEA, *Absorbed Dose Determination in External Beam Radiotherapy: An International Code of Practice for Dosimetry based on Standards of Absorbed Dose to Water*, Technical Report Series No. 398, Vienna. 2006).
- [280] Thomaz, MF & Davies, G, "The decay time of N<sub>3</sub> luminescence in natural diamond," *Proceedings of the Royal Society of London. Series A, Mathematical and Physical Sciences*, vol. 362, no. 1710, pp. 405-19 (1978).
- [281] Kaneko, JH, Tanaka, T, Imai, T, Tanimura, Y, Katagiri, M, Nishitani, T, Takeuchi, H, Sawamura, T & Iida, T, "Radiation detector made of a diamond single crystal grown by a chemical vapor deposition method," *Nuclear Instruments and Methods in Physics Research Section A: Accelerators, Spectrometers, Detectors and Associated Equipment*, vol. 505, no. 1-2, pp. 187-90 (2003).
- [282] McCreery, RL, *Raman Spectroscopy for Chemical Analysis*, Wiley-Interscience.(2005).
- [283] IAEA, *Calibration of Dosimeters Used in Radiotherapy*, Technical Report Series No. 374, Vienna, 374. 1994).
- [284] Herrick, RJ, *DC/AC circuits and electronics: principles and applications*, Thomson Delmar Learning, New York.(2003).
- [285] Fowler, J, "Solid State Electrical Conductivity Dosimeters," in F Attix, W Roesch, E Tochilin & G Hine (eds), *Radiation dosimetry*, vol. 2, Academic Press, New York, pp. 290-324(1966).
- [286] Fowler, JF, "X-Ray Induced Conductivity in Insulating Materials," *Proceedings of the Royal Society of London. Series A, Mathematical and Physical Sciences*, vol. 236, no. 1207, pp. 464-80 (1956).

- [287] Collins, AT, "Detectors for UV and Far UV Radiation," in RS Sussmann (ed.), *CVD Diamond for Electronic Devices and Sensors*, pp. 165-83(2009).
- [288] Keddy, RJ, Nam, TL & Burns, RC, "Synthetic diamonds as ionisation chamber radiation detectors in biological environments," *Physics in Medicine and Biology*, vol. 32, no. 6, pp. 751-9 (1987).
- [289] Fidanzio, A, Azario, L, Venanzi, C, Pinzari, F & Piermattei, A, "Production and testing of a synthetic diamond film radiation dosimeter for radiotherapy," *Nuclear Instruments and Methods in Physics Research Section A: Accelerators, Spectrometers, Detectors and Associated Equipment*, vol. 479, no. 2-3, pp. 661-7 (2002).
- [290] Yoder, MN, *Diamond and Diamond-like Films and Coatings*, New York: Plenum Press.(1991).
- [291] Balducci, A, Marco, M, Milani, E, Morgada, ME, Pucella, G, Rodriguez, G, Tucciarone, A, Verona-Rinati, G, Angelone, M & Pillon, M, "Distribution of electrically active defects in chemical vapor deposition diamond: Model and measurement," *Applied Physics Letters*, vol. 86, no. 2, pp. 022108-10 (2005).
- [292] Fidanzio, A, Azario, L, Kalish, R, Avigal, Y, Conte, G, Ascarelli, P & Piermattei, A, "A preliminary dosimetric characterization of chemical vapor deposition diamond detector prototypes in photon and electron radiotherapy beams," *Medical Physics*, vol. 32, no. 2, pp. 389-95 (2005).
- [293] Fidanzio, A, Azario, L, Viola, P, Ascarelli, P, Cappelli, E, Conte, G & Piermattei, A, "Photon and electron beam dosimetry with a CVD diamond detector," *Nuclear Instruments and Methods in Physics Research Section A: Accelerators, Spectrometers, Detectors and Associated Equipment*, vol. 524, no. 1-3, pp. 115-23 (2004).
- [294] De Angelis, C, Casati, M, Bruzzi, M, Onori, S & Bucciolini, M, "Present limitations of CVD diamond detectors for IMRT applications," *Nuclear Instruments and Methods in Physics Research Section A: Accelerators, Spectrometers, Detectors and Associated Equipment*, vol. 583, no. 1, pp. 195-203 (2007).
- [295] Guerrero, MJ, Tromson, D, Bergonzo, P & Barrett, R, "Investigation of defects in CVD diamond: Influence for radiotherapy applications," *Nuclear Instruments and Methods in Physics Research Section A: Accelerators, Spectrometers, Detectors and Associated Equipment*, vol. 552, no. 1-2, pp. 105-11 (2005).
- [296] "Definitions and Glossary of Terms," *JOURNAL OF THE ICRU*, vol. 6, no. 2, pp. 39-41 (2006).
- [297] Bruinsma, M, Burchat, P, Edwards, AJ, Kagan, H, Kass, R, Kirkby, D & Petersen, BA, "CVD Diamonds in the BaBar Radiation Monitoring System," *Nuclear Physics B - Proceedings Supplements*, vol. 150, pp. 164-7 (2006).



- [298] Edwards, AJ, Bruinsma, M, Burchat, P, Kagan, H, Kass, R, Kirkby, D, Petersen, BA & Pulliam, T, "Radiation monitoring with CVD diamonds in BABAR," *Nuclear Instruments and Methods in Physics Research Section A: Accelerators, Spectrometers, Detectors and Associated Equipment*, vol. 552, no. 1-2, pp. 176-82 (2005).
- [299] Buttar, C, Conway, J, Meyfarth, R, Scarsbrook, G, Sellin, P & Whitehead, A, "CVD diamond detectors as dosimeters for radiotherapy," *Nuclear Instruments and Methods in Physics Research Section A: Accelerators, Spectrometers, Detectors and Associated Equipment*, vol. 392, no. 1, pp. 281-4 (1997).
- [300] Hoban, PW, Heydarian, M, Beckham, WA & Beddoe, AH, "DOSE-RATE DEPENDENCE OF A PTW DIAMOND DETECTOR IN THE DOSIMETRY OF A 6 MV PHOTON-BEAM," *Physics in Medicine and Biology*, vol. 39, no. 8, pp. 1219-29 (1994).
- [301] Pini, S, Bruzzi, M, Bucciolini, M, Borchi, E, Lagomarsino, S, Menichelli, D, Miglio, S, Nava, F & Sciortino, S, "High-bandgap semiconductor dosimeters for radiotherapy applications," *Nuclear Instruments and Methods in Physics Research Section A: Accelerators, Spectrometers, Detectors and Associated Equipment*, vol. 514, no. 1-3, pp. 135-40 (2003).
- [302] Helene, A & Jean-Claude, R, "Polarity effect for various ionization chambers with multiple irradiation conditions in electron beams," *Medical Physics*, vol. 18, no. 1, pp. 67-72 (1991).
- [303] Gerbi, B, J. & Khan, F, M., "The polarity effect for commercially available plane-parallel ionization chambers," *Medical Physics*, vol. 14, no. 2, pp. 210-5 (1987).
- [304] Kron, T, McNiven, A, Witruk, B, Kenny, M & Battista, J, "An Experimental Study of Recombination and Polarity Effect in a Set of Customized Plane Parallel Ionization Chambers," *Australasian Physical & Engineering Sciences in Medicine*, vol. 29, no. 4, pp. 291-8 (2006).
- [305] Chester, RR, Kelly, MS & Adrian, LO, "Ionization chamber, electrometer, linear accelerator, field size, and energy dependence of the polarity effect in electron dosimetry," *Medical Physics*, vol. 26, no. 2, pp. 214-9 (1999).
- [306] Bruzzi, M, Bucciolini, M, Casati, M, DeAngelis, C, Lagomarsino, S, Løvik, I, Onori, S & Sciortino, S, "CVD diamond particle detectors used as on-line dosimeters in clinical radiotherapy," *Nuclear Instruments and Methods in Physics Research Section A: Accelerators, Spectrometers, Detectors and Associated Equipment*, vol. 518, no. 1-2, pp. 421-2 (2004).
- [307] Bruzzi, M, Bucciolini, M, Nava, F, Pini, S & Russo, S, "Advanced materials in radiation dosimetry," *Nuclear Instruments and Methods in Physics Research Section A: Accelerators, Spectrometers, Detectors and Associated Equipment*, vol. 485, no. 1-2, pp. 172-7 (2002).
- [308] Balducci, A, Chiorboli, M, Donato, MG, Faggio, G, Marinelli, M, Messina, G, Milani, E, Potenza, R, Prestopino, G & Santangelo, S, "Analysis of trapping–detrapping defects

in high quality single crystal diamond films grown by Chemical Vapor Deposition," *Diamond and Related Materials*, vol. 15, no. 11-12, pp. 1878-81 (2006).

- [309] Bruzzi, M, Menichelli, D, Pini, S, Bucciolini, M, Mólnar, J & Fenyvesi, A, "Improvement of the dosimetric properties of chemical-vapor-deposited diamond films by neutron irradiation," *Applied Physics Letters*, vol. 81, p. 298 (2002).
- [310] Bucciolini, M, Buonamici, FB, Mazzocchi, S, Angelis, CD, Onori, S & Cirrone, GAP, "Diamond detector versus silicon diode and ion chamber in photon beams of different energy and field size," *Medical Physics*, vol. 30, no. 8, pp. 2149-54 (2003).
- [311] Sauer, O, A. & Wilbert, J, "Functional representation of tissue phantom ratios for photon fields," *Medical Physics*, vol. 36, no. 12, pp. 5444-50 (2009).
- [312] *PTW Semiflex chamber*, Physikalisch-Technische Werkstätten (PTW) GmbH. Retrieved 23 Dec 2009 2009, from [http://www.rpdinc.com/html/ptw\\_semiflex\\_chamber.html](http://www.rpdinc.com/html/ptw_semiflex_chamber.html).
- [313] Sauer, O & Wilbert, J, "Measurement of output factors for small photon beams," *Medical Physics*, vol. 34, no. 6, pp. 1983-8 (2007).
- [314] Manolopoulos, S, Wojnecki, C, Hugtenburg, R, Sidek, MAJ, Chalmers, G, Heyes, G & Green, S, "Small field measurements with a novel silicon position sensitive diode array," *Physics in Medicine and Biology*, no. 3, p. 485 (2009).
- [315] Verhaegen, F, Das, IJ & Palmans, H, "Monte Carlo dosimetry study of a 6 MV stereotactic radiosurgery unit," *Physics in Medicine and Biology*, no. 10, p. 2755 (1998).
- [316] Francescon, P, Cora, S & Cavedon, C, "Total scatter factors of small beams: A multidetector and Monte Carlo study," *Medical Physics*, vol. 35, no. 2, pp. 504-13 (2008).

# Appendix A : Surface preparation procedures

---

Degrease reagents:

Acetone

2-propanol (isopropanol, IPA)

Deionized water

The degreasing procedure (at room temperature)

Transfer sample to acetone

Transfer sample to 2-propanol

Transfer sample to Deionized water

Blow dry with nitrogen

Acid bath reagents:

Concentrated hydrochloric acid (c-HCl)

Concentrated nitric acid (c-HNO<sub>3</sub>)

Deionized (DI) water

Acid bath procedure:

1. Prepare etching solution (which consists of a mixture of c-HCl and c-HNO<sub>3</sub>.)
2. Transfer sample to etching solution
3. Heat solution to required temperature (if necessary.)
4. Transfer the sample to DI water.
5. Remove sample from DI water and blow dry with nitrogen.

**Table A.1.** List of material and wet etchants.

Material	Concentration	Etchant
Aluminium	1 : 1 : 1	HNO <sub>3</sub> : HCl : H <sub>2</sub> O
Gold	3 : 1	HNO <sub>3</sub> : HCl
Silver	1 : 1 : 1	HNO <sub>3</sub> : HCl : H <sub>2</sub> O
Silver epoxy	3 : 1 : 10	HNO <sub>3</sub> : HCl : H <sub>2</sub> O

Etching solutions were typically heated to 35 °C.

# Appendix B : Encapsulation Drawings

---

These drawings detail the corresponding drawings of the Perspex material used for detector encapsulation. Dimensions are given in mm.

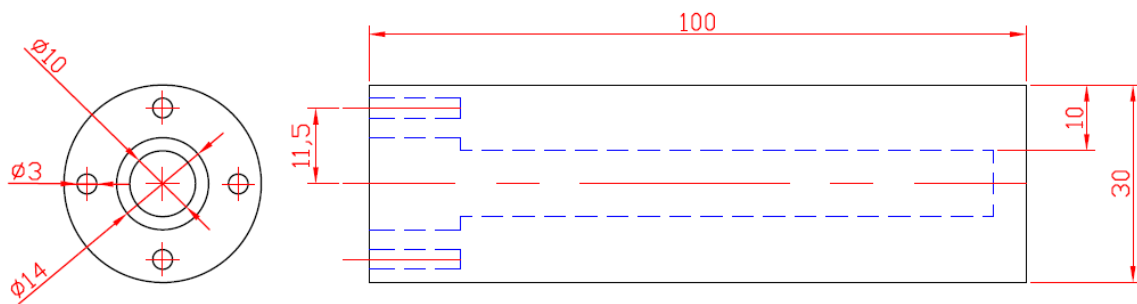


**Figure B.1.** Drawing of the thick Perspex encapsulation.

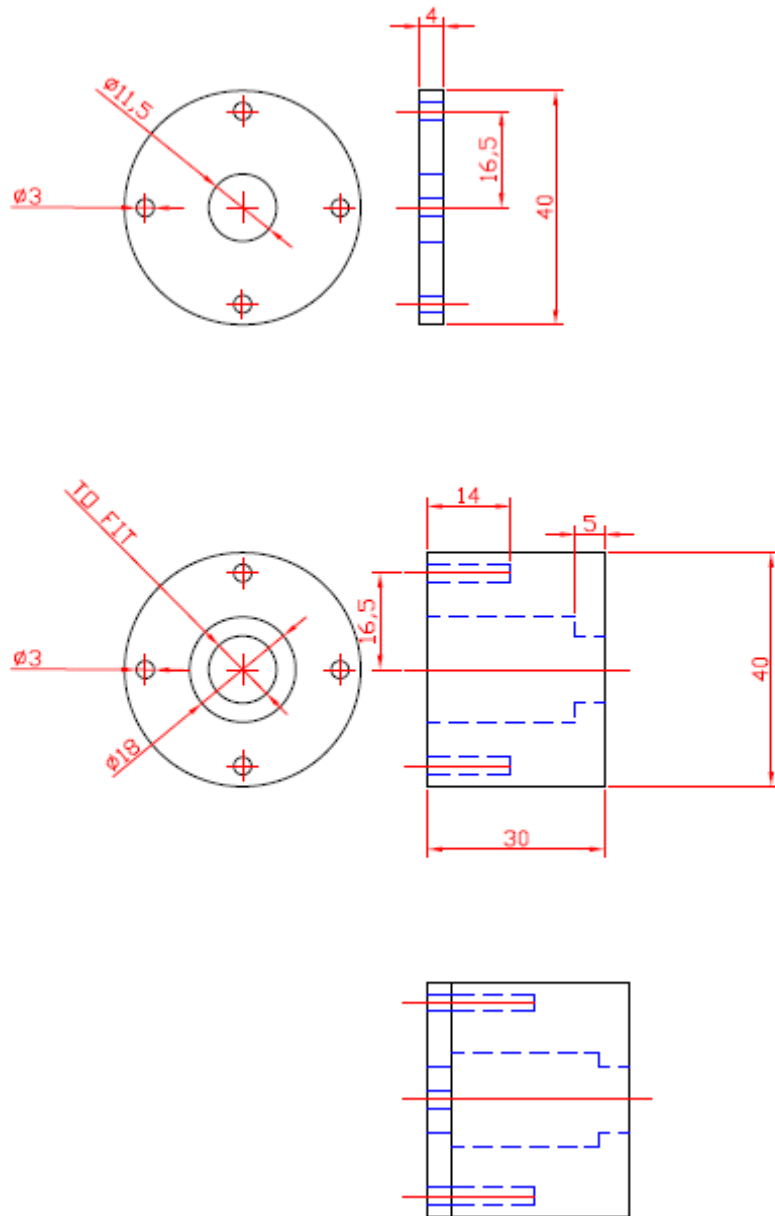


**Figure B.2.** Drawing of the thick Perspex encapsulation mid-section.

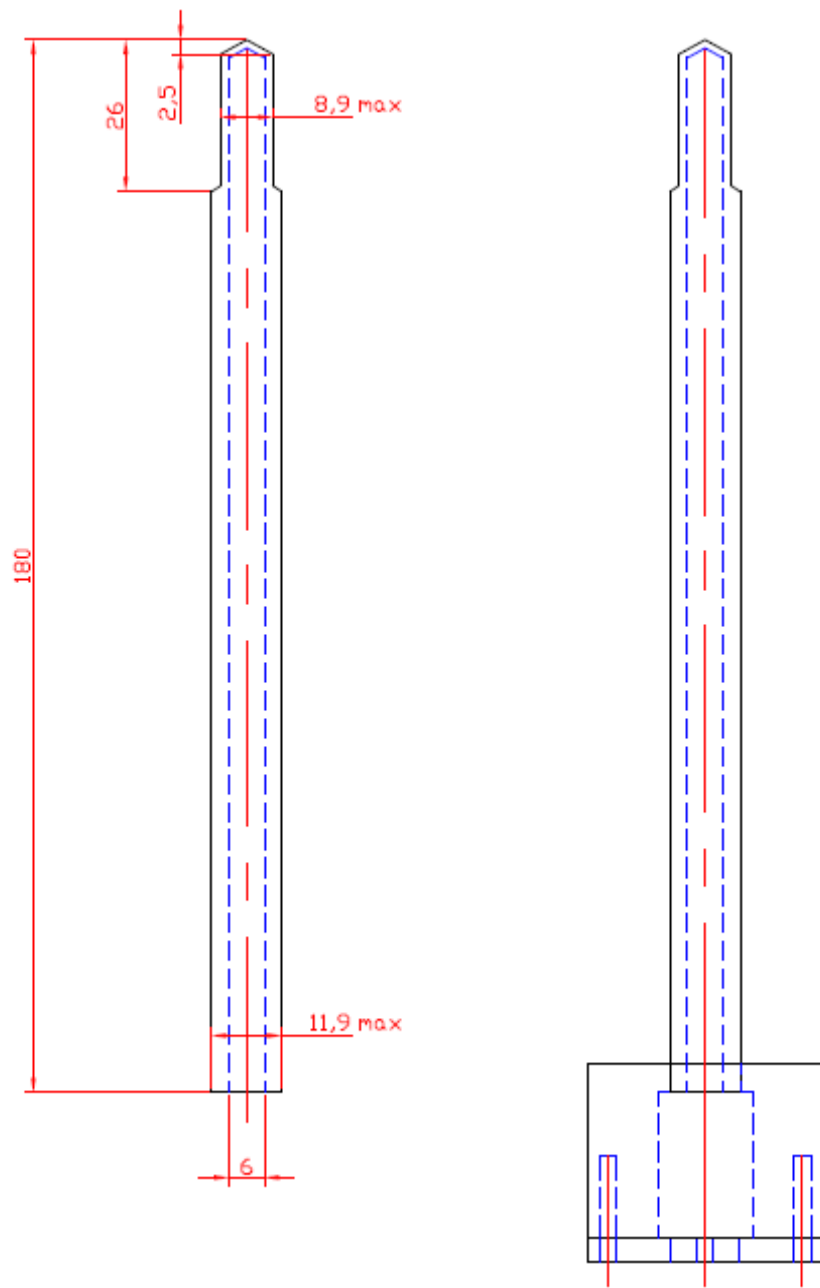


**Figure B.3.** Drawing of the thin Perspex encapsulation sleeve.





# Appendix C : Raman spectra – other films

---

Listed here are Raman spectra of diamond films that were not packaged for irradiation studies in this thesis, but may be used for future work.

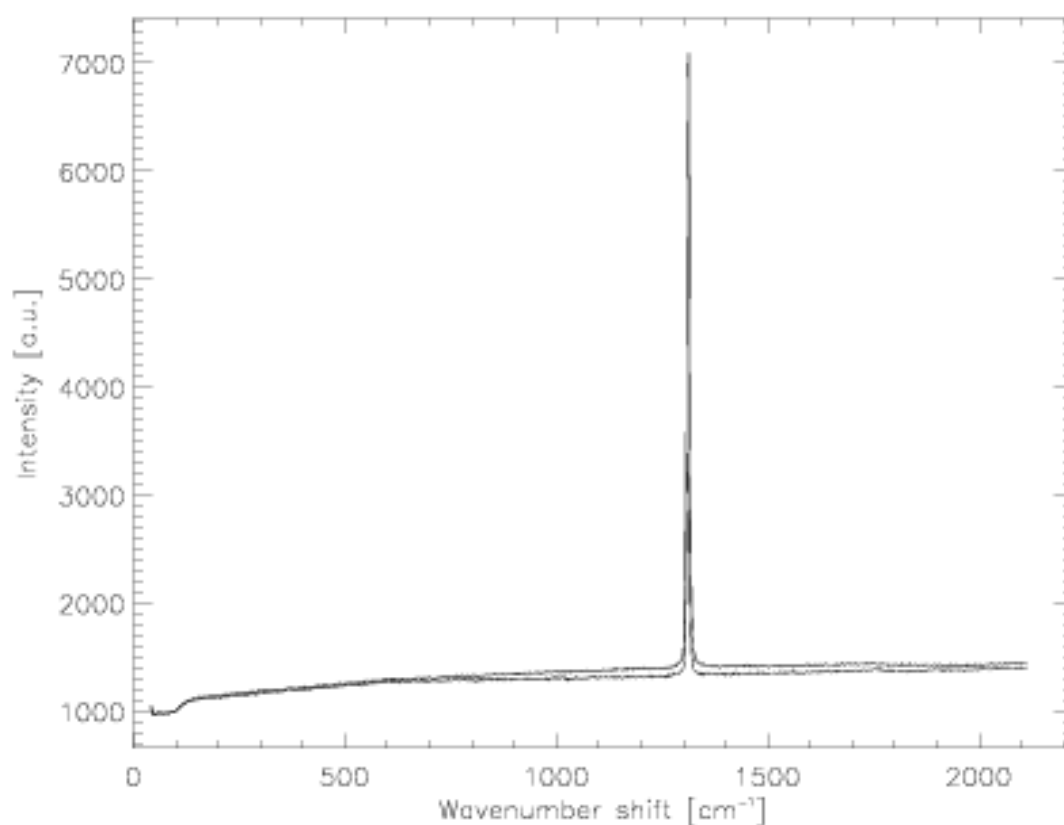


**Figure C.1.** Raman spectra for two E6 Diafilm samples.

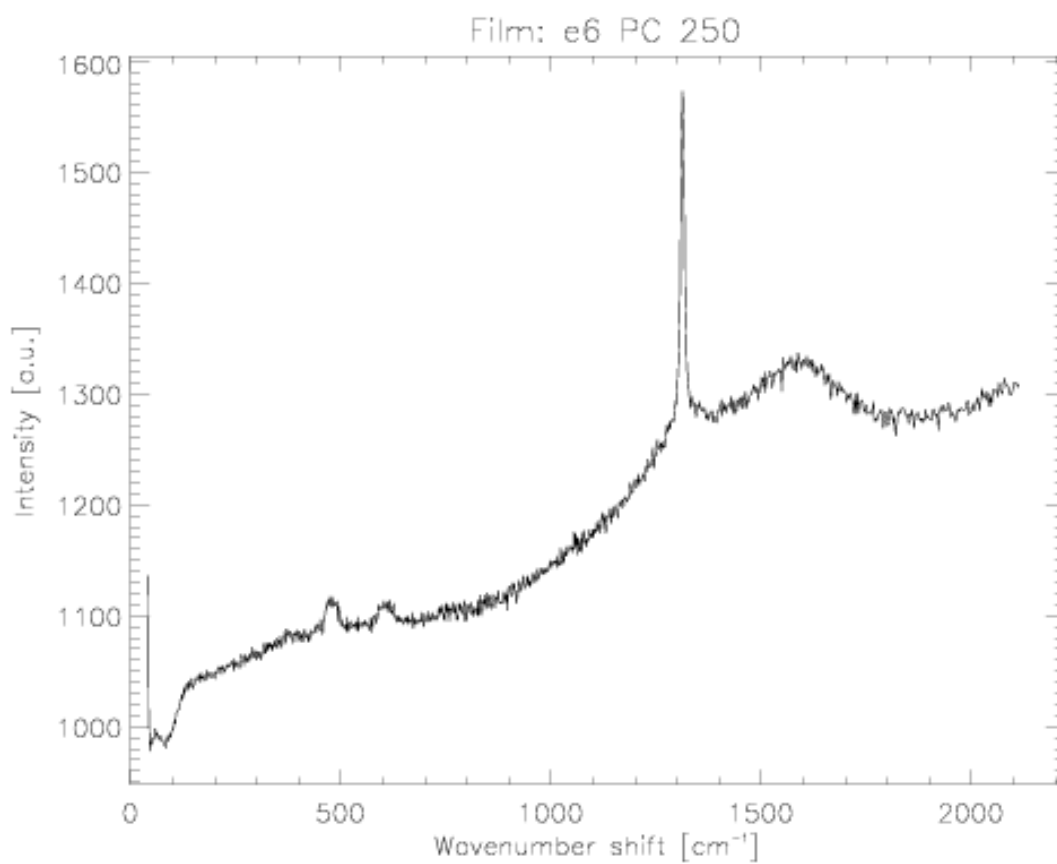
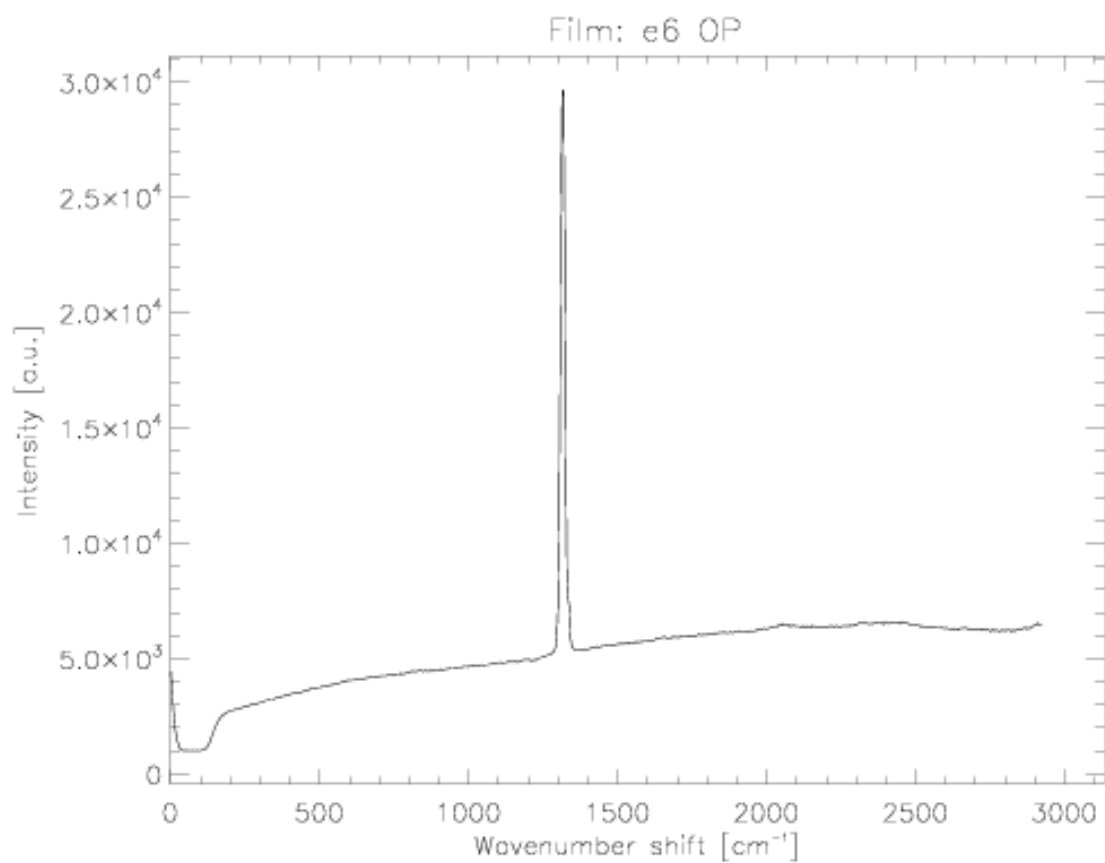


**Figure C.2.** Raman spectra for (a) E6OP and (b) E6PC250.

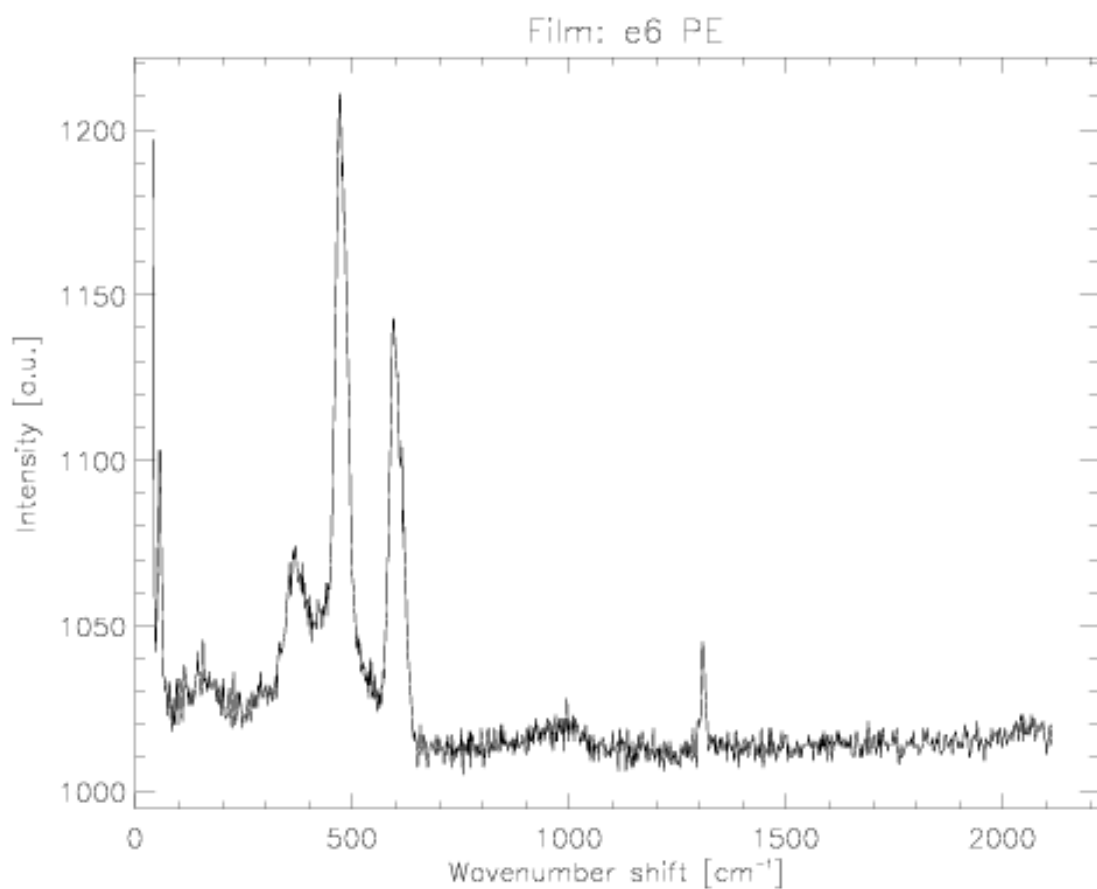
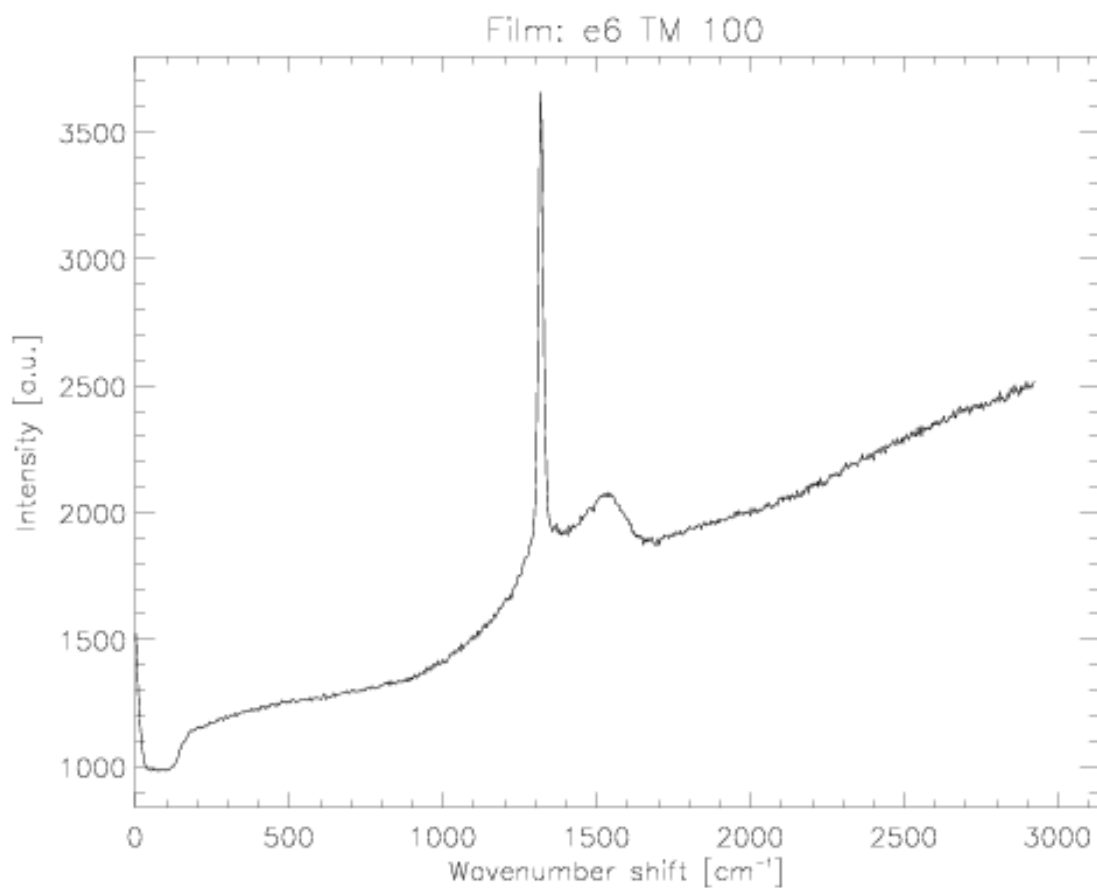


**Figure C.3.** Raman spectra (a) E6TM100 and (b) E6PE.



# Appendix D : List of Papers

---

Work from this thesis has contributed to the following papers:

2010

- **Betzel, G.T.**, S.P. Lansley, F. Baluti, L. Reinisch & J. Meyer, “Operating parameters of CVD diamond detectors for radiation dosimetry,” *Nuclear Instruments and Methods in Physics Research: Section A* 614, 130 (2010).

2009

- **Betzel, G.T.**, S.P. Lansley, F. Baluti, L. Reinisch & J. Meyer, “Operating Parameters of a Novel CVD Diamond Detector for X-ray Dosimetry,” *Proceedings of the 2009 American Association of Physicists in Medicine Annual Meeting, Houston, TX, Medical Physics* 36, 2603 (2009).
- **Betzel, G.T.**, “Operating Parameters of a Novel CVD Diamond Detector for X-ray Dosimetry,” *Department of Physics and Astronomy Annual Conference, University of Canterbury, Christchurch, New Zealand* (2009).
- Lansley, S.P., **G.T. Betzel**, F. Baluti, L. Reinisch & J. Meyer, “Comparison of commercially-available CVD diamond for 6 MV x-ray detection”, *Nuclear Instruments and Methods in Physics Research: Section A* 607, 659 (2009).
- Lansley, S.P., **G.T. Betzel**, F. Baluti, L. Reinisch & J. Meyer, “CVD Diamond X-ray Detectors for Radiotherapy Dosimetry”, *Proceedings of the 8<sup>th</sup> Annual IEEE Sensors Conference, Christchurch, New Zealand*, in press (2009).
- Lansley, S.P., **G.T. Betzel**, F. Baluti, L. Reinisch & J. Meyer, “Prototype X-ray Detectors Based on CVD Diamond”, *Proceedings of the IEEE Nuclear Science Symposium and Medical Imaging Conference, Orlando, FL* (2009).
- Baluti, F., J. Meyer, **G.T. Betzel**, S.P. Lansley & J.M. Lydon, “Preliminary Investigation of Monte Carlo Parameters in the Design of the 100  $\mu\text{m}$  Thick CVD Diamond Detector,” *Proceedings of the 2009 Engineering and Physical Sciences in Medicine and Australian Biomedical Engineering Conference, Canberra, Australia,, Australasian Physical and Engineering Sciences in Medicine*, in press (2009).

2008

- **Betzel, G.T.**, S.P. Lansley, F. Baluti, J.M. Lydon, & L. Reinisch, “Suitability of Synthetic Diamond Films as X-ray Detectors for Clinical Applications”, *Proceedings of the 2008 Engineering and Physical Sciences in Medicine and Australian Biomedical Engineering Conference, Christchurch, New Zealand, Australasian Physical and Engineering Sciences in Medicine* 31, 420-421 (2008).
- **Betzel, G.T.**, S.P. Lansley, F. Baluti, J.M. Lydon, & L. Reinisch, “Suitability of Synthetic Diamond Films for Radiotherapy Dosimetry,” *Proceedings of the 2008 American Association of Physicists in Medicine Annual Meeting, Houston, TX, Medical Physics* 35, 2788-2788 (2008).

- **Betzel, G.T.**, “Suitability of Synthetic Diamond Films as X-ray Detectors for Clinical Applications,” *Department of Physics and Astronomy Annual Conference, University of Canterbury, Christchurch, New Zealand* (2008).
- Lansley, S.P., **G.T. Betzel**, F. Baluti, J.M. Lydon & L. Reinisch, “Suitability of Synthetic Diamond Films for X-ray Dosimetry Applications,” *Proceedings of DIAMOND 2008, Diamond and Related Materials*, in press (2008).
- Lansley, S.P., **G.T. Betzel**, F. Baluti, J.M. Lydon, & L. Reinisch, “Diamond Radiation Detectors: A Viable Option for Dosimetry?” *Proceedings of the 2008 Engineering and Physical Sciences in Medicine and Australian Biomedical Engineering Conference, Christchurch, New Zealand, Australasian Physical and Engineering Sciences in Medicine* 31, 419-420 (2008).
- Lansley, S.P., **G.T. Betzel**, F. Baluti, J. Lydon & L. Reinisch, “Suitability of Synthetic Diamond Films for X-ray Dosimetry Applications”, *Conference on Optoelectronic and Microelectronic Materials and Devices, COMMAD 2008. Sydney, Australia. 34 - 37*, doi: 10.1109/COMMAD.2008.4802086 (2008).
- Baluti, F., J. Meyer, **G.T. Betzel**, S.P. Lansley & J.M. Lydon, “Preliminary Investigation of Monte Carlo Parameters in the Design of the 100  $\mu\text{m}$  Thick CVD Diamond Detector,” *Proceedings of the 2008 Engineering and Physical Sciences in Medicine and Australian Biomedical Engineering Conference, Christchurch, New Zealand, Australasian Physical and Engineering Sciences in Medicine* 31, 392-393 (2008).

2007

- **Betzel, G.T.**, S.P. Lansley, F. Baluti & L. Reinisch, “Synthetic Diamonds for Radiotherapy Dosimetry,” *Proceedings of the 2007 New Zealand Physics and Engineering in Medicine Annual Conference (Australasian College of Physical Scientists and Engineers in Medicine, New Zealand Branch), Wellington, New Zealand*, 30-31 (2007).
- **Betzel, G.T.**, “Synthetic Diamonds for Radiotherapy Dosimetry,” *Department of Physics and Astronomy Annual Conference, University of Canterbury, Christchurch, New Zealand* (2007).